Identifying Pilot Model Parameters for an Initial Handling Qualities Assessment

By

Neil Cameron, B.Eng.

Thesis submitted to the faculty of Engineering, University of Glasgow, for the Degree of Doctor of Philosophy. All aspects of the work herein are original in context except where indicated.

This Thesis is based on research conducted between October 1998 and December 2001 at the Departments of Aerospace and Electrical Engineering, University of Glasgow

Abstract

It is desirable to make an assessment of likely handling qualities to identify any deficiencies in a helicopter control system at an early stage in the design process before an expensive and potentially dangerous prototype is constructed. Inverse simulation offers a modelling technique that can be used for generating the data needed for such an assessment. Inverse simulation differs from conventional forward simulation in that the vehicle flight path is the input and the state and control time histories required for the task are generated. The inverse algorithm however, does not account for the pilot contribution to the flight data, thus the work herein demonstrates a method whereby this can be achieved.

To incorporate pilot effect into the Helinv generated data, the latter is applied as the command signal to the Man-Machine Control System (MMCS), which is a closed loop system encompassing the helicopter vehicle dynamics and a model of the pilot known as the Precision Pilot Model (PPM). The PPM Human Equalisation Characteristics (HEC) are determined via a constrained optimisation technique and the pilot effect is added in the system output. Validation of this technique is achieved through a case study whereby several operators, with different levels of experience, pilot a reduced order Puma helicopter model through a predefined mission task in a flight simulator constructed during the project. The equalisation characteristics are then determined for each pilot and compared with those generated using Helinv. A handling qualities assessment is presented for both sets of results and conclusions concerning the validity of Helinv with additional pilot effect finally drawn.

Acknowledgements

I would like to thank my supervisors Dr. Douglas Thomson and Prof. David Murray-Smith for the opportunity to undertake this work and for their patient guidance throughout its course. I would also like to express my gratitude to the inhabitants of the Flight Dynamics Laboratory for the endless questioning they endured and many unmemorable Friday nights! This gratitude also extends to the rest of the Aerospace Engineering and Electronics & Electrical Engineering departments who over the past years have motivated and given encouragement to make it to the end of the project. For fear of omitting to mention any of the countless people I am indebted to, I have deliberately not stated any! however thanks to everyone within the departments, SRS, halls, as well as those who date back to the beginning of my university career.

Special thanks must go to Aileen who, having endured many pilot and helicopter modelling discussions, is probably more relieved to see the end of this work than anybody else. However, without her encouragement, none of which would have been possible. Finally, I would like to dedicate this thesis to my parents.

Contents

Chapter 10 Research Conclusions

Nomenclature

General

$\underline{a}$	general translation acceleration vector
a_0	main rotor blade lift curve slope
a_{cg}	acceleration of aircraft centre of gravity
$\underline{a}_{hub/bl}$	translation acceleration vector of the main rotor hub in blade axis
a_z	heave axis acceleration
b	number of blades in main rotor
c	main rotor blade chord
d	drag of blade element per unit span
e	error signal
$\underline{e}$	error vector
eR	flap hinge offset
$e^{-\tau s}$	pure time delay
f_c	constraint vector
f_y, f_z	components of aerodynamic force per unit span on a blade element
g	acceleration due to gravity
g_{0tr0}, g_{0tr1}	tail rotor collective blade angle gearing constants
g_{1c0}, g_{1c1}	lateral cyclic stick-blade angle gearing constants
g_{1s0}, g_{1s1}	longitudinal cyclic stick-blade angle gearing constants
g_{c0}, g_{c1}	collective gearing constants
g_{cc0}, g_{cc1}	collective lever-lateral cyclic gearing constants
g_{ct0}	pedal/collective lever-tail rotor run gearing constant
g_{sc0}, g_{sc1}	collective lever-longitudinal cyclic gearing constants

g_{TR}	main/tail rotor gearing constant
h_r	height of main rotor hub above fuselage reference point
$\underline{i}_{sub}$, $\underline{j}_{sub}$, $\underline{k}_{sub}$	unit vectors describing current axis set (denoted by subscript)
k_{1s}, k_{1c}	feed forward gains
k_3	tail rotor delta 3 angle
k_g	accelerometer feedback gain
k_p, k_ϕ	feedback gains in roll axis control system
k_q, k_θ	feedback gains in pitch axis control system
k_r, k_ψ	feedback gains in yaw axis control system
l	lift of blade element per unit span
m	aircraft mass
m_0	blade mass per unit span
m_b	blade mass
m_β	blade mass moment
n_β	blade inertia number
p, q, r	roll, pitch and yaw rates as a perturbation from trim
$\dot{p}, \dot{q}, \dot{r}$	roll, pitch and yaw accelerations as a perturbation from trim
p_{pk}	peak roll rate
r_b	distance from main rotor hub to a point on the rotor blade
$\bar{r}_b$	normalised radial blade position
s	main rotor solidity
t	time at any point in mission task
t_m	time taken to complete mission task
$\underline{u}$, $\underline{y}$	state space input and output vectors
u, v, w	aircraft velocity components as a perturbation from trim
$\dot{u}, \dot{v}, \dot{w}$	aircraft acceleration components as a perturbation from trim
v_c	constrained lateral velocity
v_{cg}	velocity of aircraft centre of gravity
$\underline{v}_{hub/bl}$	translation velocity vector of the main rotor hub in blade axis
$\underline{x}$	state vector
x_o	boundary conditions
$\underline{x}_1$	vector of strongly controlled states

$\underline{x_2}$	vector of unconstrained states
x_{cg}	centre of gravity position forward of fuselage reference point
x_i	man machine control system input
x_o	man machine control system output
y_{max}	maximum lateral translation in mission task
$\boldsymbol{A}$	system matrix
$\boldsymbol{A}_c$	helicopter constrained system matrix
$\boldsymbol{B}$	state space control matrix
$\boldsymbol{B}_c$	constrained control matrix
$\boldsymbol{C}$	output matrix
$\boldsymbol{D}$	direct matrix
D_s	pilot reaction time
I_R	inertia of the whole rotor system
I_{xx}, I_{yy}, I_{zz}	aircraft roll, pitch and yaw moments of inertia in body axis
I_{xz}	product of inertia in body axes
I_β	blade flapping moment of inertia
K	sampled data model pilot gain
K_P	human operator gain
K_β	torsional spring stiffness
L, M, N	aircraft external aerodynamic moments
N_β	blade inertia number
P, Q, R	roll, pitch and yaw rates
P_e, Q_e, R_e	trim roll, pitch and yaw rates
Q_p	pilot attack
Q_E	engine torque
Q_{mr}, Q_{tr}, Q_{tr}	main and tail rotor torque and transmission
Q_ϕ	roll attitude quickness
R	length of rotor blade
$R(s)$	human operator remnant
T_i	lag time constant
T_l	lead time constant
T_n	neuromuscular time delay
U, V, W	aircraft velocity components

U_e, V_e, W_e	aircraft trim velocity components
U_P	perpendicular airflow over blade
$\overline{U}_P$	normalised perpendicular airflow over blade
U_T	tangential airflow over blade
$\overline{U}_T$	normalised tangential airflow over blade
V_f	total aircraft velocity
W	nominal rotor speed
X, Y, Z	aircraft external aerodynamic forces
X_e, Y_e, Z_e	components of distance translation in earth axis
$\dot{X}_e, \dot{Y}_e, \dot{Z}_e$	components of velocity translation in earth axis
X_u, X_p, etc.	X force derivatives
Y_c(s)	crossover model system transfer function
Y_{ol}	open loop crossover transfer function
$Y_H(s)$	helicopter transfer function
$Y_P(s)$	helicopter pilot transfer function (Precision Pilot Model)
Y_u, Y_p, etc.	Y force derivatives
Z_u, Z_p, etc.	Z force derivatives

Greek Symbols

α	aircraft angle of attack
α_{bl}	angle of attack of blade element
β	aircraft side slip
β_0	trimmed aircraft side slip
β_d	differential coning angle
δ	blade profile drag coefficient of main rotor
ϕ, θ, ψ	roll, pitch and yaw attitudes as a perturbation from trim
γ_s	rotor shaft angle
λ_β	normalised flap frequency
η_{1s}, η_{1c}	longitudinal and lateral stick positions
η_{1s0}, η_{1c0}	reference longitudinal and lateral stick positions

η_c, η_p	pilots collective lever and pedal displacement
η_{ct}	tail rotor control run variable
$\dot{\eta}_{pk}$	peak stick displacement derivative between zero crossings
θ_0	main rotor collective pitch angle perturbation from trim
θ_{0tr}	tail rotor collective pitch angle perturbation from trim
θ_{1s}, θ_{1c}	longitudinal and lateral cyclic perturbations from trim
θ_e	engine torque
ρ	air density
τ	time delay constant
τ_{c1}, τ_{c2}	longitudinal and lateral cyclic actuator time constants
τ_{c3}, τ_{c4}	main and tail rotor collective actuator time constants
$\underline{\omega}$	rotational velocity vector
ω_c	crossover frequency
ψ_h	heading adjustable by the pilot
ΔL, ΔM, ΔN	aircraft aerodynamic moments as a perturbation from trim
ΔX, ΔY, ΔZ	aircraft aerodynamic forces as a perturbation from trim
$\Delta\phi$	change in roll attitude between zero crossings
$\Delta\eta$	change in net stick displacement between zero crossings
Φ, Θ, Ψ	roll, pitch and yaw attitudes
Φ_e, Θ_e, Ψ_e	trim roll, pitch and yaw attitudes
Θ_0, Θ_{0tr}	main and tail rotor collectives
Θ_{1s}, Θ_{1c}	longitudinal and lateral cyclic
Ω	angular velocity of the main rotor
Ω_{idle}	idle angular velocity of the main rotor

Subscripts

bl	blade axis
cg	centre of gravity
e	earth fixed axis
bod	body axis

f	fuselage
fn	fin
hub	hub axis set
mr	main rotor
tp	tail plane
tr	tail rotor
tr/bl	tail rotor blade axis
tr/h	tail rotor hub axis
TR	torque

Abbreviations

2D	two dimensional
3D	three dimensional
cg	centre of gravity
ADS	aeronautical design standard
AFCS	automatic flight control system
DVE	degraded visual environment
GLUT	graphics libraries utility toolkit
GVE	good visual environment
HEC	human equalisation characteristics
Helinv	helicopter inverse simulation
HGS	helicopter generic simulation
HQR	handling qualities ratings
MMCS	man-machine control system
MTE	mission task element
NOE	nap-of-the-earth
OpenGL	open graphics libraries
PC	personal computer
PPM	precision pilot model
SQP	sequential quadratic programming
USE	useable cue environment

Chapter 1

Introduction, Main Aim and Objectives

1.1 Introduction

Handling qualities ratings (HQR) were developed in the late 1960s as a means of quantifying the static and dynamic stability of fixed wing aircraft. Engineers attempted to measure the vehicle handling qualities subjectively by developing scales and measurement techniques to describe the perceived pilot workload. The static and dynamic stability of the helicopter also clearly influences the design and design process of the aircraft. As such, it is prudent to investigate the vehicle handling qualities and identify any major deficiencies before an expensive and potentially dangerous prototype is built for flight test trials.

Cooper & Harper (1969) developed what is now the most widely recognised subjective handling qualities rating scale, which is illustrated in Figure 1.1. This scale, with the aid of the questionnaire in Figure 1.2, represents the decision process made by the pilot based on task perception. The scale spans three levels where the desired handling qualities are represented by a Level 1 rating, where little or no compensation is required by the pilot. Level 2 is acceptable only in emergency situations or a degraded visual environment, while a Level 3 rating suggests that the pilot cannot maintain the desired performance with a realisable workload. The questionnaire made available to the pilot after the flight test aids the pilot in determining the Handling Qualities Rating (HQR). However, additional comments by the pilot are required in order to further assess and understand the decision process involved in returning a rating. The rating returned by the pilot depends not only on personal opinion but the

nature of the task and the conditions it is to be performed under. Clearly the Cooper-Harper scale is not a definitive measure of the handling qualities, but merely a measure of the pilot's perception of the vehicle's ability to perform a task. As a result, increasingly objective handling quality assessment techniques have been sought after, one of which is described by Padfield (1996).

Padfield (1996) provides a quantitative method for assessing rotorcraft handling qualities by first considering whether the vehicle, performing a predefined task, exhibits the required Level 1 handling qualities characteristics. This is achieved by defining specific Mission Task Elements, where a MTE is defined as

"An element of a mission that can be treated as a handling qualities task"

This definition has significant ramifications for a rotorcraft handling qualities assessment. For example a helicopter operating close to the ground (nap-of-the-earth NOE) can be described as performing a series of tasks that may be defined and piloted as an individual task, enabling a handling qualities assessment for each individual MTE that defines the overall manoeuvre. The ratings described by ADS-33D (1994), and more recently ADS-33E (1996) also consider that the atmospheric conditions are not always constant, thus a different rating scale is applied in a Good Visual Environment (GVE) than is applied in a Degraded Visual Environment (DVE).

The handling qualities assessment is carried out in two stages. First the flight data is subjected to an attitude quickness assessment to determine whether the helicopter, performing a predefined mission task achieves the required Level 1 attitude quickness rating. This is an objective method of determining whether the combination of vehicle and predefined task are suitable for a handling qualities assessment and can be directly related to the widely recognised subjective Cooper & Harper handling qualities scale. When it has been determined that the flight data describes a Level 1 attitude quickness and is appropriate for use in a handling qualities assessment, the pilot workload, which provides an insight into the handling qualities, can be calculated using a parameter called pilot attack.

1.2 Thesis Main Aim

Any deficiencies in the helicopter system will inevitably present themselves during flight test trials although this is not without risk to the aircraft and more importantly, the pilot. Therefore, from the manufacturers' perspective, it is advantageous to simulate the aircraft during the initial stages of the design process, enabling a handling qualities assessment to identify any such deficiencies. Ordinarily designers have flight simulators available throughout an aircraft's design based on a non-linear helicopter model, where many also incorporate motion cues such as a moving base to further improve realism. However, designing and performing a set of experiments in a 'full' flight simulator can be expensive both financially and time wise. Two PC based simulation techniques are therefore proposed to aid the designer in an initial handling qualities assessment, allowing the designer to adapt the helicopter model so that different vehicle configurations may be considered. The first is conventional forward simulation, where the pilot applies the control inputs that regulate the helicopter open (or even closed) loop response to a set of control inputs as illustrated in Figure 1.3. The second, inverse simulation, demonstrated in Figure 1.4, derives the state and control time histories necessary to follow a predefined flight path. In order for these simulation techniques to be fully representative, they must include the complete control system, which includes the human operator (pilot) and the vehicle, otherwise known as the Man-Machine Control System (MMCS) illustrated in Figure 1.5, where the pilot model acts to reduce the error. Clearly, pilot effect is incorporated in the time histories recorded from an open loop, forward simulation scenario, for example, the data recorded from a flight simulator, because the human operator is required to apply the control inputs which regulate the helicopter states.

To accurately replicate the open loop (forward simulation) man-machine system using inverse simulation however, the pilot effect must still be integrated into the recorded flight data because the inverse algorithm does not employ a pilot model. The work undertaken throughout this project addresses this problem and demonstrates a method whereby pilot effect can be successfully integrated into the inverse simulation output for improved data realism. The proposed method for applying the pilot effect to the inverse simulation output as documented by Leacock (2000), is to first apply a primary state parameter, for example the attitude angle ϕ, as the command signal $x_i(t)$

of the MMCS. The model depicted in Figure 1.5, then operates by comparing the system output $x_o(t)$ with the system input $x_i(t)$ and presents the resulting error $e(t)$ to the pilot model. The pilot model then attempts to minimise this error by optimising its human equalisation characteristics (HEC) provided an appropriate pilot model has been selected, outputting the control time history $\eta(t)$. This output is the same as the control output $\eta(t)$ from the inverse algorithm, however the pilot effect has now been incorporated into the control time history. $\eta(t)$ is then passed to the vehicle dynamics and the 'vehicle state plus pilot effect' $x_o(t)$ output. The whole process is repeated for a prescribed range of pilot characteristics until the combination producing the minimum error $e(t)$ is found. The output $x_o(t)$ consists of the input and additional pilot effect and as a result is representative of the complete MMCS, allowing a valid handling qualities analysis to be performed.

The question why is it necessary to assess helicopter handling qualities early in the design process and how pilot effect can be incorporated into the validated inverse simulation algorithm is to be the basis of this thesis. The main aim can therefore be summarised as the thesis title

"Identifying pilot model parameters for an initial handling qualities assessment"

The main aim and title have been carefully worded to reflect that the work aims to present a method whereby 'improved data realism' of the inverse simulation output is achieved. Although the work centres on helicopter handling qualities assessment, focus is actually on developing a desktop tool enabling this analysis. Handling qualities therefore are only included in the thesis to provide the reader with an overall understanding of the project and the design process to which it is aimed.

Before further discussing each aspect of the work and the objective of each chapter, the author would like to make clear that although many of the principles considered herein are well established in the engineering community, each topic considered has been used or adapted to meet specific requirements in order to create a 'desktop' tool for analysing helicopter handling qualities which is entirely unique. The technique offered presents a method whereby no expensive and hazardous flight test trials are

required early in the design process for an initial handling qualities assessment. The user can simply select a nap-of-the-earth (NOE) task to be flown and calculate the pilot effect on the vehicle response by determining the pilot characteristics. In order to create this handling qualities assessment tool the step-by-step process of describing each chapter begins with an introduction relating the relevant issues to helicopter handling qualities and finishes with a thesis overview.

1.3 Objectives

1.3.1 Selection of an Appropriate Helicopter Pilot Model

The human operator, who applies control inputs to influence the vehicle response, is clearly an integral part of the helicopter system. It is therefore essential to model the pilot, in conjunction with the vehicle dynamics, to accurately represent the system [Hess & Zeyada (2001)]. Several types of model exist, from non-linear, quasi-linear, sampled data, optimal and adaptive pilot models. Each of these model types focuses on modelling specific behavioural or performance characteristics of the operator. Therefore, to select an appropriate model for this work, it is important to consider each model and ask whether or not it describes the pilot characteristics in a manner that is applicable to a handling qualities analysis [Hess (1987)]. This question is addressed in Chapter 3 by discussing each model type and considering how the selected model parameters can be calculated.

1.3.2 Vehicle Dynamics - Multiple Control Representation

It has been stated that it is of utmost importance to model the human operator correctly. However, the same is true of the system that the operator is controlling. If the model does not replicate the actual system under examination then any subsequent results will be wrong, thus invalid. The work introduces a non-linear Helicopter Generic Simulation (HGS) model and explains why this model hampers a flight dynamics investigation. Instead, a linear HGS version is proposed in which the state variables are calculated as a deviation from the trimmed reference condition, resulting

in a state space representation. The appropriate vehicle dynamic transfer function can then be selected depending on the mission task being performed and the most influential control input.

Helicopter control systems are complex where a combination of the four controls, longitudinal and lateral cyclic, main and tail rotor collective, is required to achieve even a simple manoeuvre. Likewise, when performing any task, a combination of all four control inputs is required and should be represented in the vehicle dynamics block of the MMCS accordingly, i.e. transfer functions relating the primary controlled state parameter to each of the control axes must be incorporated. The conventional transfer function representation of the vehicle dynamics does not allow for this, so a method whereby the full set of transfer functions is represented must be devised.

1.4 Development of a Linear Inverse Simulation Algorithm

The conventional approach to aircraft simulation is to develop a mathematical model of the vehicle then determine its response to a set of control inputs. Inverse simulation is essentially the opposite of this, generating the required state and control time histories for a prescribed flight path. The HELicopter INVerse simulation package Helinv, developed at the university of Glasgow by Thomson (1990), produces the ideal state and control time histories as the output because the inverse algorithm does not contain a pilot model. Thus to accurately model the MMCS, the pilot effect must be incorporated into the output. The results can then be validated via a handling qualities analysis by comparison with flight test data for the same MTE and vehicle.

Inverse simulation and its application to handling qualities assessments has been widely recognised, especially when considering rotorcraft performing NOE Mission Task Elements. The MTEs under consideration generally involve precise manoeuvring and positioning, thus lending themselves well to mathematical modelling. The inverse algorithm exists in two forms, one employing a numerical integration technique while the second applies a differentiation routine to solve a series of differential equations. The helicopter inverse simulation algorithm (Helinv) developed by Thomson (1990) employs a full, non-linear helicopter model which has

found applications in several studies such as offshore manoeuvring simulation Taylor (1995) and previous pilot workload studies such as Padfield et al (1994) and Leacock (2000). The inverse algorithm employs a full non-linear helicopter model called the Helicopter Generic Simulation (HGS) model, however a linear version of HGS exists and can also be applied to a linear inverse simulation algorithm [Thomson & Bradley (1990)].

The pilot in the MMCS was selected to be represented by a quasi-linear pilot model with zero remnant, where the inherently non-linear operator is represented by a linear model and a remnant added to represent the non-linearities. It was decided that because the MMCS was constructed from a linear helicopter model and a linear pilot model with zero remnant, linear inverse simulation should also be used for modelling consistency. This is not to say that it is unsatisfactory to apply a non-linear command signal such as that calculated from the non-linear Helinv model, only that linear modelling is considered in this thesis for consistent results. It was therefore necessary to construct a linear inverse algorithm using Matlab® code similar to that developed by Thomson & Bradley (1990). The model discussed in Chapter 5 considers a constrained side slip condition which to the author's knowledge has not previously been documented.

From the inverse simulation generated time histories, the dominant attitude parameter can be selected and applied as the command signal of the MMCS in conjunction with an appropriate vehicle model. The pilot model equalisation characteristics can then be estimated such that the chosen values result in the minimum possible error between the system command signal $x_i(t)$ and the output $x_o(t)$. Once this has been achieved the system output can be described as being the system input with added pilot effect. The two time histories (the MMCS input and output) may then be compared via an attitude quickness assessment considered in Chapter 2, which illustrates whether the task achieves the desired Level 1 handling qualities and the pilot effect on the attitude quickness parameters. Finally a pilot attack calculation is performed to determine the helicopter handing qualities.

As a result of the inverse simulation generated state and control time histories being 'ideal', the equalisation characteristics calculated from the selected pilot model are optimal, producing the minimum optimisation error achievable by any pilot. It is therefore important to compare the inverse simulation generated time histories for a given task with those recorded by a human operator piloting the same manoeuvre. Ideally this would take place with real flight test data, however if engineers wish to assess handling qualities at an early design stage, clearly flight test data is not available. Therefore, the only method currently available of analysing the time histories with additional pilot effect is to perform the task in a flight simulator.

1.5 Development of a Linear, Mission Programmable Flight Simulator

Examination of the adapted inverse simulation time histories requires real flight test data that already incorporates the pilot effect. This can be obtained through an open-loop forward simulation where the human operator attempts to pilot a predefined mission task. Although many PC based flight simulators are available commercially, none allowed the adaptation of these primary parameters to the extent required. As a result, a flight simulator has been developed which places emphasis on modelling exactly the same vehicle dynamics and mission task elements as described in the inverse simulation package.

1.6 Development of a Reduced Order Helicopter Model

The linear state space model, due to the cross coupling between the longitudinal and lateral dynamic helicopter modes, will be shown to prove difficult to pilot in the flight simulator for reasons discussed in Chapters 6 & 7. One solution to this problem is to consider reducing the order of the model by neglecting the states that do not adversely affect the longitudinal or lateral task under consideration. Also, this suggests that the less influential controls can also be neglected from the helicopter model.

It is then important to ensure that the selected reduced order model still accurately mimics the full system. This can be achieved not only by demonstrating that the

responses to a simple control input such as a step or a doublet are similar for the full and reduced order models, but that the reduced order model is still dynamically representative of the system. Each mode is therefore considered and if the remaining reduced order eigenvalues differ significantly from those representing the full system, that particular reduced order combination is discarded. The time histories generated from inverse simulation incorporating the reduced order model are validated and the helicopter model applied to the flight simulator to be flown by the human operators.

1.7 Comparison of Simulation with added Pilot Effect and Flight Test Data

When the state and control time histories have been obtained from the reduced order inverse algorithm and flight simulator for the same MTE, the data can be applied as the MMCS command signal and the pilot characteristics determined. This then allows a direct comparison of the pilot derived data with the inverse generated results. The optimum pilot characteristics are next incorporated into the pilot model and the pilot effect in turn, incorporated into the inverse data as the system output. Once this has been achieved, a handling qualities assessment can be performed on the two sets of data and the results compared.

1.8 Thesis Structure

The thesis begins with a handling qualities review, demonstrating how the attitude quickness parameter can be used to determine if a mission task displays the required Level 1 handling qualities rating. Helicopter pilot modelling is next introduced in Chapter 3, presenting various models such as the Precision Pilot Model and discussing how the model parameters can be estimated. As the work focuses on rotorcraft, it seemed appropriate to include a discussion on rotorcraft dynamics and helicopter modelling, therefore this discussion can be found in Chapter 4. Chapter 5 and Chapter 6 are concerned with the actual flight data generation that is to be used as the command signal for the man-Machine Control System. Chapter 5 considers inverse simulation and its linear version while Chapter 6 describes the flight simulator developed during the work. Helicopter modelling is again considered in Chapter 7,

however here a reduced order linear model is presented to reduce the complexity of the system, making the linear model operable in the helicopter flight simulator. Chapter 8 then considers a longitudinal flight test case where the mission task suitability to a handling qualities assessment is examined via the techniques considered in Chapter 2. This chapter also considers how the task is to be implemented in the flight simulator and the instructions given to the pilot on how to complete the task. The Human Equalisation Characteristics from the linear inverse simulation and also for each sortie were calculated for each pilot. The corresponding attitude quickness and pilot attack charts were then found and illustrated in Chapter 9. The recorded time histories are also displayed and discussed in Chapter 9 and conclusions finally drawn in chapter 10. The thesis also contains five appendices that are of relevance to the work but based on previous research. These are included primarily as an immediate source of reference for the reader.

Chapter 2

Helicopter Handling Qualities Assessment

2.1 Introduction

The following chapter introduces a subjective handling qualities assessment technique in the form of the Cooper & Harper scale and considers how this provides the basis for the development of a more rigorous assessment tool. This new 'objective' assessment tool functions in two distinct stages. Firstly an attitude quickness calculation is performed to ensure that the task is suitable for a handling qualities assessment. If a Level 1 rating is returned, a pilot attack calculation is carried out to determine the handling qualities.

It is accepted that the manoeuvre definition is critical to the handling qualities analysis. Therefore an attitude quickness calculation is performed on a 'smooth global polynomial' slalom, where the task is represented by one polynomial equation, and a 'piecewise polynomial' slalom, where a series of polynomial and linear equations are pieced together to represent the task, highlighting the characteristics of each task. Finally the pilot attack parameter is considered, which is primarily a measure of pilot workload as opposed to the vehicle performance driven attitude quickness rating. The term 'pilot attack' reiterates the importance of including a pilot model in the simulation derived data as the human operator, who applies the control inputs, may significantly alter the vehicle dynamics and response.

2.2 Handling Qualities

Padfield (1996) highlights the consequences of poor handling qualities in a discussion relating to an incident where the pilot lost control of a helicopter. He was only able to regain control when, after a series of violent manoeuvres, the helicopter self-righted. A modern definition of handling qualities involves two components, the first being the vehicle response to a control input and the other with the external environment such as weather conditions. The handling qualities definition however originated from Cooper & Harper (1969) as

"Those qualities or characteristics of an aircraft that govern the ease and precision with which a pilot is able to perform the tasks required in support of an aircraft role"

Handling qualities criteria were developed in association with fixed wing aircraft by documents such as Military Specification 8785 [Anon (1969)] and updated in Defence Standard 00-970 (1984), and considered only the static and dynamic stability of the aircraft. These formal documents attempted to quantify the system characteristics by defining the limits of acceptable and unacceptable modes. They however failed to include atmospheric effects, basing their analysis solely on the vehicle i.e. flying qualities. Flying qualities according to Key (1988) can be perceived as a subset of handling qualities, referring to the aircraft stability and control characteristics, whereas handling qualities also relates to the task, visual and physical environments. This ultimately means that any handling quality analysis is specific only to the vehicle and manoeuvre under examination. Although the author has adopted this terminology other authors do not embrace this definition. Padfield (1996) states that he sees no reason to relegate flying qualities to be a subset of handling qualities and does not make a distinction between the two terms.

At the time of publication of the military specifications, engineers attempted to develop appropriate handling quality scales and measurement techniques which captured the workload perceived by the pilot such as McDonnell (1968). The most widely recognised scale was the Cooper-Harper handling qualities scale [Cooper & Harper (1969)] as illustrated in Figure 1.1. The scale represents the decision process

made by the pilot based on their judgement of task performance, achieved and expected pilot workload. The decision tree is split into three main sections, each consisting of a range of pilot ratings.

- Level 1, Ratings 1→3 – The aircraft is satisfactory and requires minimal workload.
- Level 2, Ratings 4→6 – Rating 4 requires some compensation to achieve the desired performance or deficiencies warrant improvement. Ratings 5 or 6 require considerable to extensive compensation.
- Level 3, Ratings 7→9 – The pilot cannot achieve adequate performance from the aircraft with a tolerable workload.

The Cooper-Harper scale also includes a rating 10 indicating that the pilot loses control of the vehicle at some point during the manoeuvre. The minimum required standard in terms of pilot workload and task performance assessed using the Cooper-Harper scale is a Level 1 HQR throughout most of the operational flight envelope. Cooper & Harper (1969) also consider that although the Level 1 condition is satisfactory, it does not mean that the aircraft is perfect. It means that the aircraft is suitable for its intended use without further improvement. Level 2 is unsatisfactory but tolerable, where the aircraft adequate for the purpose required however improvements are desirable, whereas Level 3 describes an aircraft with major control deficiencies and is unacceptable. Clearly the HQR describes an aircraft's ability to perform a task. However, if the aircraft rating is described as unsatisfactory or inadequate (Level 2 or 3) there is no information available to examine the nature of the deficiencies. This is because the rating is essentially a summary of pilot opinion on the workload required to fly a task with a defined level of performance. For this reason many handling qualities assessments are accompanied by a pilot questionnaire which describes the flight test in detail. One such pilot questionnaire was developed by Howell & Charlton (1997) and can be seen in Figure 1.2.

Although the rating represents the handling qualities specific to the vehicle and manoeuvre, it is dependent on the perceived pilot workload and is derived by the pilot following the decision tree illustrated in the Cooper-Harper scale. The scale is

subjective and non-uniform, meaning that a pilot returning a rating of 6 does not necessarily have to work twice as hard as when a rating of 3 is returned. It is universally accepted that pilots should return ratings which are whole numbers, however in some circumstances this may not be appropriate. For example, a pilot may decide that a vehicle describes neither Level 1 or Level 2 HQR, thus a value of 3.5 is returned. In the case of several test pilots performing a manoeuvre, the individual ratings may be averaged and a whole number may not be returned. Caution must be exercised when averaging the ratings because if the spread of ratings returned by the individual pilot spans across the three rating levels, the pilots are most likely to be flying different tasks. If the manoeuvre is not well defined, different operators may interpret the instructions in a dissimilar manner. If this does occur the pilots are not likely to perform the same task and consequently a spread of HQRs occurs. When the returned ratings are only spread over two levels but are still reasonably similar, it can be assumed that the pilots have understood the task definition and the differences in ratings can be put down to differences in individual piloting techniques.

The Cooper-Harper scale does not give a strict definition of aircraft handling qualities. The scale represents only the pilot's opinion of how well the vehicle was able to perform the task, although the scale is still viewed as a good approximation to the vehicles handling qualities. Interest has been shown by many designers in developing modern handling quality assessments, such as techniques that can evaluate the vehicle characteristics using mathematical or simulation models. These are particularly beneficial in the field of rotorcraft as deficiencies may be identified in the system before the construction of an expensive prototype is undertaken.

Helicopters are being used to accomplish more and more tasks which can be as diverse as search and rescue, fire fighting or for military applications. Inevitably the demands placed on the pilot to complete the task, other than simply applying controls to manoeuvre the vehicle along the desired flight path, are also increasing. This is because the pilot must focus not only on the flight path, but also the other assigned tasks such as weapon deployment, which increase workload. Consequently good handling qualities are vital if missions are to be completed satisfactorily. This is especially true of the helicopter, as this type of vehicle is often required to fly NOE manoeuvres. The United Kingdom published a set of handling qualities standards (UK

Def Stan 00-970) [Anon (1984)] for rotorcraft design and airworthiness, but this proved to be overshadowed by the U.S. equivalent Aeronautical Design Standard (ADS) due to the volume of rotorcraft in America. Although the author is aware that the latest version ADS-33E (1996) was recently published, its predecessor ADS-33D (1994) is referred to throughout this thesis.

2.3 Aeronautical Design Standard ADS

The pilot flying a specific manoeuvre, determines the handling quality ratings described by the Cooper-Harper scale based on their judgement of task performance and pilot workload. It is important at this point to define task performance requirements when considering the manoeuvre as they are fundamental to the HQR. As considered in the previous section, ADS-33D (1994) is widely recognised as the most authoritative requirement document for helicopter handling qualities. The document defines a list of mission tasks which include descriptions of the manoeuvre and suggestions on how to conduct the flight test as considered in the following section. ADS-33D goes on to define the vehicle response required to achieve Level 1 or 2 handling qualities for each MTE performed in different environments with varying pilot attention levels. One of the main advancements made from this publication over its predecessor [MIL-H-8501 (1961)] is that there is no categorisation of aircraft into different size or role. The handling qualities are assessed solely on the helicopters ability to perform a MTE, emphasising the multi-role nature of the aircraft.

2.3.1 Mission Task Elements

ADS-33D defines a range of MTEs that can be used to assess helicopter handling qualities. The document details descriptions of how the manoeuvres should be flown and a set of guidelines as to how the task cues should be set up. It should be stressed that the task definition for a handling qualities assessment must be strictly adhered to by any rotorcraft acquired by the American armed forces. The requirements however may not be so rigorously applied to the rest of the world, as in Europe they are viewed

primarily as a set of guidelines open to interpretation. DERA for example, have found it beneficial to develop a variation on the slalom manoeuvre based on ADS-33D as described by Howell (1995).

Although the mission task definition may not appear to be related directly to the vehicle handling qualities, careful task selection and definition are fundamental to the assessment. For example, Padfield (1996) defines the importance of task selection to a handling qualities assessment as

"Task performance drives workload which drives pilot ratings"

The final important feature of the manoeuvre is that it must be reproducible. This is important because, in order to adequately assess handling qualities, the manoeuvre must be flown by a minimum of three pilots where at least two return the same rating. Evidently, if more pilots are used then a higher number must again return the same rating to validate the task. If this is not the case it is likely that the pilots misunderstood the exact mission requirements and the test should be redefined to eliminate any misinterpretation. Pausder & Von Grünhagen (1990) summarised the mission requirements for a successful handling qualities evaluation as being

- The task must be representative of the operational mission requirement
- The task must be reproducible by different pilots
- A low risk safety procedure must be adhered to for the flight test.

This definition reiterates the importance of a well defined and duplicable mission task which ADS-33D addresses, from which two of the definitions are now listed.

- Slalom *"Initiate the maneuver in level unaccelerated flight and lined up with the centreline of the test course. Perform a series of smooth turns at 152 (500ft) metre intervals (at least twice to each side of the course). The turns shall be at least 15.2 (50ft) metres from the centreline, with a maximum lateral error of 15.2 metres. The maneuver is to be accomplished below the reference altitude, 30.5*

(100ft) metres. Complete the maneuver on the centreline, in coordinated straight flight."

- Quick hop *"Start from a stabilised hover. In the GVE, rapidly increase power to approximately maximum, maintain altitude constant with pitch attitude, and hold collective constant during the acceleration to an airspeed of 50 knots. Upon reaching the target airspeed, initiate a deceleration by aggressively reducing the power and holding altitude constant with pitch attitude. In the DVE, accelerate to a groundspeed of at least 50 knots, and immediately decelerate to hover over a defined point. The maximum nose down attitude should occur immediately after initiating the maneuver and the peak nose up pitch attitude should occur just before reaching the final stabilised hover."*

Although ADS defines many more mission task elements such as the bob-up bob-down, pirouette, side step and hover turn, this work is not concerned with validating these tasks. It would therefore be inappropriate to attempt to define them all so the reader is referred to ADS-33D (1994) for further task definitions. Once the mission task has been selected, it is necessary to verify that the task is flown to an appropriate standard to enable a qualitative handling qualities assessment. This is achieved by ADS-33D with the introduction of a new parameter called the 'attitude quickness parameter' which is given further consideration in the following section.

2.3.2 Attitude Quickness

The attitude quickness parameter provides an objective means of deriving a rating, granting the analyst the ability to assess the open loop performance of the aircraft. The attitude quickness defines the behaviour of the helicopter in the pitch, roll and yaw axes, however, other techniques can be employed to determine the cross coupling characteristics [Padfield (1996)]. The attitude quickness parameters for pitch and roll are defined in ADS-33D (1994), in the changes in moderate amplitude attitude section as

"The attitude quickness parameter shall exceed the limits specified in Figure 2.1a & *Figure* 2.1b. *The required attitude changes shall be made as rapidly as possible from one steady attitude to another without significant reversals in the sign of the control input relative to the trim position"*

Figure 2.1a represents target acquisition and tracking manoeuvres for the roll axis while Figure 2.1b represents the roll attitude quickness for all other mission tasks. Before these plots can be clearly interpreted a definition of the attitude quickness is required. When applied to the roll axis this is

$$\text{Roll Attitude Quickness} = Q_{\phi} = \frac{p_{pk}}{\Delta\phi} \tag{2.1}$$

where p_{pk} is the peak roll rate encountered and $\Delta\phi$ is the coincident change in roll attitude occurring between zero crossings. Figures 2.1a & 2.1b then illustrate how the roll attitude quickness parameter can be plotted against the minimum attitude change on the roll attitude quickness chart to ascertain the handling qualities level for a particular flight test manoeuvre. It is worth recalling when examining these plots that the requirements for adequate control are Level 1, while Level 2 is acceptable only in emergency situations. The most appropriate method of demonstrating a roll attitude quickness chart is via an example, however, an appropriate mission task element must first be selected.

2.4 Flight Test Data Acquisition and Attitude Quickness Example

The final prerequisite according to Pausder & Von Grünhagen (1990) for the mission task is that the manoeuvre must be performed at a low risk status. In the case of a real flight test, this factor is strongly linked to a good manoeuvre definition. However, with the advances in technology, increasing amounts of flight test data are safely and cost effectively derived from flight simulators. Recently though, flight data for an aircraft performing a predefined manoeuvre can be obtained through Inverse Simulation. This topic in conjunction with manoeuvre modelling is considered in

detail in Chapter 5. However, to demonstrate the roll attitude quickness, the ADS-33D (1994) slalom mission task element has been modelled and applied to the Helinv algorithm to produce the manoeuvre time histories. The slalom manoeuvre was chosen as it is primarily a longitudinal tracking task, hence only p and ϕ are illustrated throughout the roll attitude quickness assessment, as the remaining state variables and controls are not required.

2.4.1 Mathematical Modelling of the ADS-33D Slalom Manoeuvre

Inverse Simulation can only be applied to specific mission task elements such as those defined in ADS-33D (1994) if the task can be represented mathematically. There are two techniques used at the University of Glasgow for defining flight test manoeuvres. The first uses a smooth global polynomial function [Thomson & Bradley (1996)] to represent the task whilst the other models individual sections of the task flight path with polynomial functions then concatenates them to represent the task [Leacock (2000)]. This section is concerned primarily with illustrating the difference between these two modelling techniques, using roll attitude quickness to demonstrate how the manoeuvre model effects the handling qualities, reinforcing the statement in Section 2.3 *"the manoeuvre definition is fundamental to the handling qualities assessment"*.

2.4.2 Smooth Global Polynomial Manoeuvre Definition

Thomson & Bradley (1997) developed a library of basic linear translational and turning manoeuvres, based on the mission task requirements specified by ADS-33D (1994). The first approach adopted was to fit a global polynomial function to the primary aircraft parameters by splitting the manoeuvre into its constituent parts to which specific mathematical boundary conditions can be rigorously applied. The boundary conditions for the smooth global polynomial slalom manoeuvre, which define the mission profile, are derived from the ADS-33D (1994) slalom recommendations stated in Section 2.3 and can be summarised as

- The helicopter initiates and terminates the task in a trimmed flight state on the manoeuvre centre line.
- When the maximum lateral distance is attained, the lateral velocity is zero.
- When crossing the manoeuvre centre line, the maximum velocity is attained.
- When the minimum lateral distance is reached, the lateral velocity is zero.

Using this set of boundary conditions for the slalom manoeuvre as depicted in Figure 2.2, the lateral distance translated throughout the manoeuvre can be represented by the global polynomial

$$y(t) = \left\{ 759s\left(\frac{t}{t_m}\right)^3 - 6220s\left(\frac{t}{t_m}\right)^4 + 21390s\left(\frac{t}{t_m}\right)^5 - 39291s\left(\frac{t}{t_m}\right)^6 \right.$$
$$\left. + 40353s\left(\frac{t}{t_m}\right)^7 - 21845s\left(\frac{t}{t_m}\right)^8 + 4855s\left(\frac{t}{t_m}\right)^9 \right\} y_{\max} \qquad (2.2)$$

where t_m is the time taken to perform the task, t is the time at any point during the manoeuvre and y_{max} is the maximum lateral distance. Figure 2.2 also illustrates the smooth nature of the flight path when the global approximation is applied. Thomson & Bradley (1997) found that this manoeuvre flight path model compared favourably with how the pilot flies the task in a real flight test.

2.4.3 Piecewise Polynomial Function Method

A second modelling technique called piecewise modelling can be applied to the ADS-33D (1994) slalom definition to generate the flight path. The piecewise model can be defined as either the flight path, velocity or acceleration required to perform the task then integrated or differentiated to give the unknown flight path, velocity or accelerations. This example defines the flight path by identifying five distinct sections in the slalom task. For the ADS-33D (1994) slalom, the five sections depicted in Figure 2.3 are

- A section that involves a rapid increase in the lateral distance from trimmed flight to a maximum distance after t_1 seconds, ensuring a roll angle of at least 25 degrees is attained.
- A constant lateral displacement section.
- A section in which the lateral distance is rapidly decreased to the maximum negative distance. The period required to achieve this is $2t_1$.
- A constant lateral displacement section.
- A section in which there is an increase in lateral displacement to zero.

The piecewise polynomial equations used to define the sections of the piecewise slalom task can be third, fifth or seventh order as considered by Leacock (2000). It is then important to realise that if specifying the flight path and then differentiating to ascertain the vehicle velocity and acceleration, the third order equation is not appropriate. This is because when it is differentiated twice, it describes a linear acceleration, which is uncharacteristic of the helicopter.

When the piecewise polynomial flight path in Figure 2.3 is compared with that generated using the smooth global polynomial function, a distinct difference is noticeable in the flight path. Therefore, the following section aims to determine which mathematical manoeuvre model is more suitable for a handling qualities analysis by calculating the attitude quickness parameters.

2.4.4 Attitude Quickness Calculation for the Two Slaloms

The purpose of comparing the two slalom manoeuvre models described previously is not to validate the modelling techniques as this has already been accomplished by Thomson & Bradley (1997). This exercise is simply to illustrate the modelling techniques, the method of calculating the roll attitude quickness parameters and how the model definition affects these parameters. In the following example the quickness parameters are calculated by hand to demonstrate how the calculation is performed, however, the actual technique is implemented using the Matlab® software package.

Both the global polynomial and piecewise polynomial manoeuvre flight paths have been applied to a linear inverse simulation algorithm and the state and control time histories calculated for the Puma helicopter flying at forty knots. The work presented in the thesis focuses on this helicopter and flight speed, thus it is prudent at this point to introduce the Puma helicopter depicted in Figure 2.4 with configuration data listed in Appendix *I*. Figure 2.5 illustrates the roll angle ϕ and roll rate p for the forty knot global polynomial slalom case derived using the inverse simulation technique. The plot illustrates how the manoeuvre is initiated by a pulse of lateral cyclic, causing in increase in the roll rate to p_{pk1}. Once p_{pk1} has been reached, lateral cyclic is reversed to force the helicopter to reduce its roll rate, then roll in the opposite direction. This process is continued until all slalom gates have been negotiated. The plot also shows the peak roll rate between zero crossings, then demonstrates how the change in roll angle between the zero crossings is calculated. Consider the first roll attitude quickness parameter, the change in roll angle $\Delta\phi_1$ and roll rate peak p_{pk1}, can be extracted from Figure 2.5 to give the first attitude quickness as

$$Q_{\phi 1} = \frac{p_{pk1}}{\Delta\phi_1} = \frac{-2.29}{-5.00} = 0.458 \tag{2.3}$$

Likewise, Figure 2.6 illustrates the corresponding roll and roll rate time histories for the piecewise slalom. Comparison of these plots with the polynomial manoeuvre time histories in Figure 2.5 clearly indicates the very different manner in which the task is performed, where the piecewise slalom requires much larger changes in roll angle than the polynomial task.

The remaining attitude parameters for the global polynomial slalom are calculated in the same manner as demonstrated in equation (2.3) and plotted on the attitude quickness chart in Figure 2.7. It should be noted here that at the end of the task, p does not reach zero, therefore only four quickness parameters are shown in Figure 2.7. If p did reach zero, a fifth parameter would be recorded at the end of the task. This chart shows that for the global polynomial slalom, none of the roll attitude parameters define Level 1 characteristics, suggesting that the manoeuvre definition is not suitable for use in a handling qualities assessment. Thomson & Bradley (1997) agree that this

flight path definition is representative of how the pilot flies the manoeuvre, however, the aggressive approach adopted by the ADS-33D (1994) slalom defined in Section 2.4.2 for attaining Level 1 handling qualities is not captured in the task definition. Leacock (2000) when performing a similar experimental analysis, also found that the polynomial definition was not suitable for a Lynx helicopter performing the same mission task because the roll attitude necessary to meet the desired performance requirements was not achieved. This unsuitability can be traced to the small and slow stick displacements required to pilot the helicopter through the global polynomial defined task. The control inputs for the piecewise polynomial task however, can be controlled by the manoeuvre designer such that sufficiently large and fast control inputs are required in order to follow the desired flight path, resulting in Level 1 attitude ratings.

The attitude quickness parameters for the piecewise defined slalom are calculated from the linear inverse simulation generated state and control time histories in Figure 2.6 using exactly the same technique as described previously. Again the calculation of the first attitude quickness parameter is demonstrated, where the change in roll angle $\Delta\phi_1$ and roll rate peak p_{pk1} can be extracted from Figure 2.6 to give

$$Q_{\phi 1} = \frac{p_{pk1}}{\Delta\phi_1} = \frac{-46.11}{-31.56} = 1.461 \tag{2.4}$$

The attitude quickness parameters are plotted on Figure 2.7 to enable a direct comparison with the global polynomial defined slalom. It is evident from the chart that approximately half the roll attitude quickness parameters for this manoeuvre are Level 1, while the remainder define Level 2 or Level 3 ratings. These results demonstrate that the piecewise polynomial manoeuvre definition is also unsuitable for use in a handling quality analysis. However, the attitude quickness assessment is only a measure of the task suitability to a handling qualities assessment, thus can only be used to validate the manoeuvre model for use in a handling qualities assessment. Another parameter is therefore introduced which is capable of identifying pilot workload based on the individual pilot, as opposed to the vehicle orientation.

2.5 Pilot Workload

As considered previously, the pilot flying a manoeuvre determines the handling qualities rating based on judgement of the task performance and pilot workload. Although it is evident that there are many contributing factors to the pilot workload, it has until recently been difficult to define. When performing a mission task, the pilot will adopt a control strategy which maximises his performance thus minimising the required workload. The workload is affected by outside influences such as the Useable Cue Environment (UCE). This parameter was introduced by ADS-33D (1994) to quantify the visual environment in which the pilot must work and can be defined in a similar manner to the attitude quickness assessment with 1 representing a Good Visual Environment (GVE) and 3 representing a Degraded Visual Environment (DVE). This was an important development in assessing handling qualities ratings as the pilot performing a manoeuvre in a DVE may return a level 2 HQR. When performing the manoeuvre in a GVE however, the same pilot may suggest Level 1 handling qualities. Although pilot workload has been difficult to define, Charlton et al (1998) identify three key components affecting the pilot workload

- Navigation – This is the least demanding exercise for the pilot as it requires large infrequent control inputs relating to a change in heading.
- Guidance – Concerned with following a path when performing a nap of the earth task. The pilot is required to apply control inputs which will allow the safe navigation of a task. Navigation is concerned with major path changes whereas guidance can be perceived as obstacle avoidance throughout the manoeuvre.
- Stabilisation – This is the most demanding workload component for the pilot, requiring frequent control inputs in order to maintain the preferred task attitude and altitude.

Additional sources of workload come from other tasks such as communication and in the case of military aircraft, activating and deploying weapons. These secondary tasks introduce the concept of 'divided attention' as considered again by the ADS-33 documents. This suggests that because pilot attention is frequently diverted to other tasks, it is assumed that the pilot is no longer able to perform the mission to the

highest standard. In the case of a co-pilot assisting the pilot, situations can arise where the task is not assigned to a specific crew member which again increases the pilot workload. Situations such as these can cause a spread in handling qualities ratings in conjunction with factors such as pilot fatigue. These can be compensated for in the handling qualities analysis by including a pilot calibration into the assessment.

2.6 Pilot Attack

Pilot workload is considered to consist of three main components, navigation, guidance and stabilisation. Although there is no specific definition of the workload it can be measured by a parameter called 'Pilot Attack', which is calculated in a similar way to the attitude quickness parameter as demonstrated by Charlton et al. (1998). Here however, focus is on the pilot stick displacement instead of roll attitude. The Pilot Attack parameter can be defined as

$$\text{Pilot Attack}\left(Q_p\right)=\frac{\dot{\eta}_{pk}}{\Delta\eta} \tag{2.5}$$

where $\dot{\eta}_{pk}$ is the peak value in the rate of change of stick displacement between zero crossings and $\Delta\eta$ is the corresponding change in the net stick displacement. As the task requires the pilot to apply control inputs, each stick displacement can be viewed as an element of pilot workload identifiable by associating an attack parameter to each peak or trough. The global and piecewise polynomial ADS-33D (1994) slaloms, flown at forty knots in a Puma, have again been chosen to illustrate this technique even though both task definitions do not exhibit Level 1 qualities. Figure 2.8 demonstrates the lateral cyclic control input and its derivative eta1cdot, which are required for determining the net stick displacement and the peak values in stick derivative respectively for the global polynomial slalom. Upon analysis of the stick displacement time history, it is evident that the pilot control action is characterised by a maximum stick rate and corresponding stick displacement, allowing the calculation of an aggression parameter or pilot attack. The corresponding stick and stick derivative time histories for the piecewise slalom are depicted in Figure 2.9

illustrating the much larger stick displacements required for the helicopter to follow the predefined flight path. The pilot attack parameters for both polynomial and piecewise slaloms are plotted on an attack chart in Figure 2.10 enabling a direct comparison between the two modelling techniques.

Padfield et al (1994) stipulate that the attack parameters representing a large net stick displacement are associated with vehicle navigation while the parameters with a small stick displacement and small attack parameter describe helicopter stabilisation. Finally the parameters with small stick displacement and high attack parameters are related to the control inputs required for guidance through the task. The attack chart illustrated in Figure 2.10 clearly shows that all the polynomial slalom attack parameters are gathered in the bottom left corner of the chart. This implies that the task does not require any large control inputs to change the vehicle heading through the task, only smaller faster inputs are required which relate to guidance and stabilisation. The more aggressive piecewise slalom which requires roll rates of up to two hundred degrees per second, as demonstrated in Figure 2.9, has a much wider spread of attack parameters however several of them are beyond the 100°/s boundary.

It has been shown that the slalom tasks analysed here are not suitable for a handling qualities assessment due to the unsuitable aggression levels of the task. This MTE, performed in a Puma helicopter at forty knots, is however still focused on in the following chapters while considering the MMCS and inverse simulation. A more appropriate task will be considered in Chapter 8 when the experiment set-up is presented.

2.7 Conclusions

An important handling qualities assessment technique is introduced from the ADS-33D (1994) document and Padfield et al (1994), consisting of two calculations. These are the attitude quickness calculation, which is derived from the vehicle states, and the pilot attack calculation, which can be calculated from the pilot control inputs and their derivatives. Handling qualities rating are influenced by the mission task definition which is demonstrated for the ADS-33D (1994). Tthe importance of correctly

representing the MTE by defining the task using smooth global polynomial and piecewise modelling techniques was also discussed.

The examples considered in this chapter, which were generated from the inverse simulation package, have not had the pilot effect incorporated into the state time histories. This problem is addressed in the following chapter where various pilot models are considered.

Chapter 3

Helicopter Pilot Modelling

3.1 Introduction

Chapter 3 focuses on human operator modelling and introduces a set of key variables which effect the pilots' ability to control the helicopter. The most influential key variable is the set of '*Task Variables*' encompassing the vehicle dynamics, the control input applied to the MMCS, the display technique adopted and finally the pilot model. The pilot model is arguably the most complex aspect of the MMCS to model as human operators perform at many levels, vary in adaptability and may be at different points on their learning curves.

The development of pilot modelling, from classical to modern control theory is introduced, focusing on the Precision Pilot Model (PPM) which was developed to aid in the understanding of handling qualities ratings. In conjunction with the appropriate helicopter model, the PPM can be used to determine a set of 'Optimum Human Equalisation Characteristics' for any system input which may then be used to aid the helicopter handling qualities assessment.

3.2 The Man-Machine Control System (MMCS)

Effective engineering design often requires physical situations to be mathematically modelled. However, as industrial and military systems become increasingly complex, greater demands are being placed on human operators when performing a task, thus

they become an integral part of the overall system. Sheridan (1985), through studies into pilot behaviour in aerospace systems, considers the necessity to incorporate a model of the human operator as an element in the control system. Also in the case of aircraft studies, Automatic Flight Control Systems (AFCS) have given the designers the power to shape the response of any aircraft. Fundamentally though, it is still the pilot who is required to apply the control inputs in response to changing situations and, as a result, a model of the human operator is essential to the successful development of an AFCS. Figure 3.1 illustrates how a pilot model and vehicle dynamics are applied in a feedback loop. The error information can be presented to the pilot for either a compensatory or pursuit display, where the man-machine interaction was described by Sutton (1990) as "*time varying with variable gain and non-linear*". Employing a method such as this, where the human operator can be modelled as a single element in the MMCS, allows an insight into both the human operator behaviour and the task. This modelling technique also permits the experiment to be duplicated which cannot be guaranteed when depending on a human operator to close the loop.

Although several pilot models exist, it is crucial to select a pilot model which yields information applicable to a handling qualities assessment. For this reason a summary of pilot modelling is presented, introducing a range of pilot models and discussing the suitability of each to assessing aircraft handling qualities.

3.3 Variables in the Man-Machine Control System

Before the pilot model and its associated characteristics are discussed, it is important to consider the four key variables effecting the pilots ability to control the vehicle according to McRuer and Jex (1967). The first of these four key sets is the '*environment*' external to the pilot. This set relates to the visual conditions such as the light conditions and visual environment, alongside physical factors such as temperature, vibration and loading on the vehicle. These environmental factors are superimposed on the pilot and are difficult to control, however, when applied to a flight simulator they can be easily constrained. The next set of variables is defined as '*operator centred*' and depend on operator training and other human characteristics

such as motivation and fatigue. This set of variables in conjunction with the '*procedural*' variables, encompass mission task instructions and practice, can be minimised by employing highly motivated and skilled operators to generate the command signal. Finally, the most important set of key variables are the *'task variables'*, comprising all the system inputs and controls which directly affect the pilot's control task. These parameters include the system input or command signal, the method used to display the information to the pilot, the controlled vehicle dynamics and finally the manipulator or pilot model which are now considered.

3.3.1 The Command Signal

The command signal or input for the MMCS would ordinarily be applied as real flight test data for a mission task such as the slalom manoeuvre. However, because flight test data is clearly not available at an early design stage, two aircraft simulation techniques have been employed to generate the required data. The first is to simulate the manoeuvre using the inverse simulation algorithm Helinv in both the non-linear and linear forms, which will be discussed in Chapter 5. Another method used to develop the relevant manoeuvre data was to perform the manoeuvre in a PC based flight simulator. Advances in computer technology have allowed designers to pilot and obtain information on numerous aircraft configurations, decreasing the potential risk involved in building an expensive test flight simulator or prototype at a later development stage. Helicopter models and tasks can be easily adjusted or even changed completely, depending on the design requirements and operational envelope. However, as a PC based flight simulator encompassing all the aspects required was not available commercially, a linear helicopter flight simulator was created as described in Chapter 6.

3.3.2 The Display

The MMCS display pictured in Figure 3.1 can be described as operating as either a compensatory or a pursuit tracking system, depending on how the information is input and displayed. A compensatory tracking task is one in which the output signal from

the system is fed back and compared with the input signal, resulting in an error which the operator is required to annul as demonstrated in Figure 3.2*a*. An example of a real compensatory system is the design of an aircraft glide-slope indicator, where the pilot attempts to reduce the error between the actual and the required glide-slope. It should be noted that the compensatory display provides relative information. When the operator is manually tracking a target, he cannot be certain if the displayed error is a result of his performance, target movement or a combination of both. In Pursuit tracking however, the human operator is presented with true information (both the input and output) from which he attempts to judge and account for the error [Wargo (1967)] as shown in Figure 3.2*b*.

Kreifeldt (1965) considers the application of the two display types, suggesting that a compensatory display type, such as that considered herein, is the only method in which the human input/output characteristics can be directly measured. Sheridan & Ferrell (1974) state that this is because the operators continuous linear characteristics can be deduced from the closed loop system frequency response characteristics, which is not the case for the pursuit display, as the human operator is then a two input, single output operator.

3.3.3 The Vehicle Dynamics

The linear equations of motion can be calculated from the full non-linear HGS model discussed in Chapter 5 [Thomson (1989)], and can be expressed in state space form as

$$\dot{\underline{x}} = \mathbf{A}\underline{x} + \mathbf{B}\underline{u} \tag{3.1}$$

where $\boldsymbol{A}$ and $\boldsymbol{B}$ are the system and control matrices respectively which contain the aerodynamic, relevant gravitational and velocity terms. The state vector $\underline{x}$ and the control vector $\underline{u}$ are again given by

$$\underline{x} = \begin{bmatrix} u & v & w & p & q & r & \phi & \theta & \psi & \Omega & \theta_e \end{bmatrix}^T \tag{3.2}$$

$$\underline{u} = \begin{bmatrix} \theta_0 & \theta_{1s} & \theta_{1c} & \theta_{0tr} \end{bmatrix}^T \tag{3.3}$$

The state and control matrices ***A*** and ***B*** can be evaluated for any reference trim state, allowing the transfer function corresponding to any combination of state and control to be established from

$$Y_H(s) = \frac{\underline{x}(s)}{\underline{u}(s)} = (sI - \mathbf{A})^{-1}\mathbf{B} \tag{3.4}$$

The vehicle transfer function relating the primary controlled variable to the control applied can then be implemented in the MMCS alongside the pilot model, which is used to determine the pilot behaviour for the given manoeuvre.

3.3.4 Pilot Modelling

The pilot model is the final task variable to be considered and also the focus of Chapter 3. Before further consideration is given to selecting an appropriate pilot model for the work, it is important to recollect the aims of this work and thus what information we require from the pilot model. As considered in the introductory chapter, the thesis aims to demonstrate how pilot effect can be incorporated into inverse simulation generated time histories for assessing helicopter handling qualities. A pilot model is therefore required which can provide an insight into what the operator does during the manoeuvre. This type of model is referred to as a behavioural model, where the control time history describes the behaviour of the human operator (i.e. what the human does), whereas a performance model describes how well the task was carried out.

The various approaches used to develop human operator control models can be directly related to the advances in classical and modern control engineering [Sutton (1990)]. These models can be split into the following types

- Quasi-linear or continuous describing function models.
- Sampled data and discrete models.
- Optimal control models.

- Adaptive models.
- Simulation and non-linear models.

Each type is now considered except non-linear models, as each element in the MMCS considered throughout this work is linear.

3.4 Quasi-Linear Pilot Modelling

The MMCS is inherently non-linear thus difficult to model. This complex problem was nevertheless solved previously by Tustin (1947) using a servomechanism theory to analyse gun control equipment. A summation of Tustins work was published by Wilde & Westcott (1962), showing that the quasi-linear system concept originally evolved from the observation that many non-linear systems have responses to simple control inputs that are similar to the responses of the equivalent linear system. It was observed that the system output contained higher frequencies than the input (a result uncharacteristic of a linear system), which Tustin called the 'remnant'. The basic quasi-linear Man-Machine Control System can be represented in block diagram form as shown in Figure 3.3, where the human operator is an integral part of the closed loop system performing a single axis tracking task. The model replicates the non-linear response by applying a control input to the equivalent linear system. The output of this system then has the additional remnant applied, which represents the difference between the actual and linearised model. Sutton (1990) defines this quasi-linear model of the human operator as being

"*The approximate linear model $Y_P(s)$ of a non-linear system which minimises the remnant R(s), where R(s) is the portion of the human operators control output that is not linearly correlated with the system input*"

The work herein considers the quasi-linear model without remnant, representing only systems in which the pilot behaves linearly. Although Tustin recognised that the human pilot could be modelled linearly with the addition of a remnant, the quasi-linear model he developed was very basic. His work however, paved the way for a

vast amount of research in this area resulting in the development of various pilot models, including sampled data, optimal and adaptive pilot models.

3.4.1 The Precision Pilot Model

Another such human operator model developed as a result of Tustin's work was the quasi-linear Precision Pilot Model (PPM), reviewed by McRuer and Krendel (1957), which models the response of a pilot performing a single axis tracking task. The model parameters are determined by minimising the mean square error between its response and actual human operator response, and can be described in the Laplace Domain as

$$Y_p(s) = K_p \frac{(1+T_l s)}{(1+T_i s)} \left\{ \frac{e^{-\tau s}}{1+T_n s} \right\} \tag{3.5}$$

where K_p is the '*Pilot Gain*' representing the pilot's ability to respond to an error in the amplitude of a controlled variable. T_l is the '*Lead Time Constant*' illustrating the pilot's ability to predict a control input and T_i is the '*Lag Time Constant*' which describes the ease with which the pilot executes the required control input. These three terms are collectively known as the '*Human Equalisation Characteristics*' (HEC). The remaining two terms on the right can be defined as the 'Inherent Human Limitations', where $e^{-\tau s}$ represents a '*Pure Time Delay* or *Transport Lag*' where τ is the time delay constant. This parameter can be described as the period between the decision to change a control input and the act itself. Finally T_n is the '*Neuromuscular lag Time Constant*' portraying the time taken to trigger the muscle from when the signal is sent from the brain. These human limitations can be considered constant for any pilot flying a single axis-tracking task, leaving only the equalisation characteristics to be determined. The HEC are specific to individual pilots, reflecting their skill and ability, whereas the inherent limitations may be considered uniform across a group of pilots.

The PPM is widely recognised as a standard pilot model and has found applications in handling qualities studies, pilot rating evaluation and analysis of aircraft dynamic behaviour. Sutton (1990) also considers the PPM and more specifically, discusses how the size of the remnant can be used to help assess the handling qualities of proposed aircraft designs in the longitudinal plane. This example suggests that when the operator was forced to behave in a non-linear manner, for example if the man-machine interface is unsuitable for the task or if the pilot is also required to perform secondary tasks, the handling qualities are poor or unacceptable (a further list of non-linear characteristics are listed by Kelley (1968) in Table 3.1). Consequently the remnant was found to vary between large and very large as illustrated in Figure 3.4. Conversely when the handling qualities were acceptable, the remnant was small and the pilot could be modelled linearly.

3.4.2 The Crossover Model

The crossover model is a remarkably simple two parameter model which operates in the same manner as the PPM, by trying to annul the error between the input and the system output. McRuer (1965) demonstrates this model to be of the form

$$Y_{ol}(s) = Y_P(s)Y_C(s) = \frac{\omega_c e^{-\tau s}}{s} \tag{3.6}$$

where $Y_P(s)$ is the human operator transfer function, $Y_C(s)$ the system transfer function, ω_c is the crossover frequency and τ is the effective time delay (the pure time delay and the neuromuscular lag). McRuer & Jex (1967) demonstrate that any given set of vehicle dynamics resemble the characteristics dictated by the primary rule of thumb, defined by Sutton (1990) as

"A rule of thumb due to Bode is that a system will be stable provided the slope of the Bode plot in the region of crossover is approximately –20dB"

meaning that the open loop characteristics in the region of crossover should resemble an integrator. Although the PPM and the crossover model can adequately match the

gain and phase characteristics of the pilot, Kelley (1968) composed a list of criticisms of quasi-linear modelling in relation to the actual human operators , which are listed in Table 3.1. As a result, in recent years, model designers have focused on developing models which provide an insight into what the pilot is actually doing, as described in the PPM human equalisation characteristics.

Table 3.1 Comparison of the Quasi-Linear Model With an Actual Human Operator (After Kelley (1968))(Reproduced From Sutton (1990))

Quasi-Linear Models	Actual Human Operators
Input Narrowness • Input has the same number of dimensions as output. • One display. • Assumes impoverished display format (compensatory or pursuit tracking).	• Input typically has more dimensions than multiple displays. • May use highly sophisticated multi-dimensional displays (contact analogue, predictor display or direct view of environment).
Lacks Internal Task Representation • Does not include any explicit representation of task or environment. • Cannot adapt to changes in task save through arbitrary parameter adjustments.	• Operation is virtually effected by understanding of task and environment. • Veridical changes in internal representation of task result in changed predictions, and hence, a different non-arbitrary form of adaptation.
Point-In-Time Limitation • Restricted to present error, fixed exponential weightings of past, and derivatives. • Cannot remember; can only summarise signals via integration (lag). • Cannot predict input or output; response is an arbitrary weighting of error, lead and lag terms.	• Response based on remembered past and predicted future. • Can remember, modify response, or change internal task representation in consequence of past experience. • Can predict; response can be formed and modified to minimise future (predicted) error. Can preview or anticipate input as well as predict output, and plan response based on both of these "excursions from present time".

3.5 Sampled Data Models

Sampled Data Systems were developed in response to the hypothesis set out by Craik (1947). Craik hypothesised that the human operator's output when performing a continuous tracking task, consisted of a series of step responses, each triggered approximately every 0.5 seconds. The first sampled data description was proposed by Ward (1958), but was criticised by Bekey (1962) because, in the words of Bekey

"Ward's study suffers from an almost complete lack of analytical work which makes quantitative evaluation of his model very difficult"

Bekey proposed a new sampled data model based on criticisms of the quasi-linear model limitations. The model, illustrated in Figure 3.5, shows the human operator to be modelled by a sample and hold element in conjunction with a quasi-linear model $Y_P(s)$. The plant dynamics, in this case represented by a gain term, thus the quasi-linear model was taken as

$$G_H s = \frac{Ke^{-D_s s}}{1 + T_n s} \tag{3.7}$$

where K is the model gain, D_s is the reaction time and T_n is the neuromuscular time constant. The input information, relayed to the operator's central nervous system, is supplied only once every T seconds and is controlled by the sampling switch. The human operator output, however, is continuous and therefore a 'data reconstruction' or 'hold' element must follow the sampler, which reconstructs the input on the information provided at the sampling points.

Sampled Data Models are a widely accepted description of the pilot behaviour. However, intermittent control input (Craiks theorem) unnecessarily increases model complexity. Benefits are however attained when employing this approach in adaptive pilot modelling.

3.6 Optimal Control Models

Quasi-linear modelling is limited in that it only applies to single-input single-output linear systems. Chen (1971) further criticises quasi-linear modelling for being restricted to describing the relationship between the input and output of the system. In sharp contrast with this, the state space structure of the linear optimal control operator allows the model to be applied to linear multi-variable systems which not only describe the input-output relationship, but also the internal structure of the system. This type of model is optimal with respect to a given performance index provided the

operator is experienced, well motivated and will always perform in an optimal manner.

The most famous optimal control model is that developed by Kleinman (1971) as illustrated in Figure 3.6, where the vehicle dynamics are represented in the standard state space form

$$\dot{\underline{x}} = \mathbf{A}\underline{x} + \mathbf{B}\underline{u} \tag{3.8}$$

The model operates via the controller reacting to an information display showing the state and control variables in the form of

$$\underline{y} = \mathbf{C}\underline{x} + \mathbf{D}\underline{u} \tag{3.9}$$

where $\boldsymbol{C}$ and $\boldsymbol{D}$ are time variant. The model can be split into four sections, the first being a perceptual model which injects noise to represent operator randomness (equivalent to the remnant in the quasi-linear model). Next an information processor in the form of a Kalman filter and a least squares predictor estimates the system variables. A set of optimal gains is then chosen to minimise the quadratic cost function [Grace (1992)]. Finally an output model accounting for the inherent limitations is included, where the 'desired' operator control signal and additional noise vector are subjected to a neuromuscular lag. The actual control signal is then applied to the vehicle dynamics.

The main problem with this type of model is that when the operator's limitations are described, a precise performance index must be specified. This can be overcome by solving the inverse optimal problem, where the control index and noise are selected to match the vehicle dynamics, neuromuscular lag and time delay. The solution however, is still only optimal in relation to the chosen performance index which the user must select, but may be sub-optimal in others. In addition, according to Sutton (1990), the model does not provide an insight into how the operator learns to behave as an optimal controller.

3.7 Adaptive Pilot Models

Very often situations arise which require the human operator to apply control inputs to adjust and maintain the stability of the system, which are referred to as 'pilot adaptability'. Figure 3.7 illustrates the main adaptive characteristics of the pilot according to Young (1969) and are now summarised.

- *Learning Adaptation and Task Adaptation* – As the human operator becomes more familiar with a system, they learn about the response characteristics, resulting in quicker detection of a problem. Nomoto (1977) suggests that learning adaptation, although closely linked to task adaptation, differs in that once an operator is trained in one system, they will be able to adapt to the handling qualities of another similar system much faster than a beginner will.
- *Input Adaptation* - This is when the operator is able to predict patterns in the control input. As the operator becomes more experienced through learning adaptation, they will be able to examine the previous input histories thus allowing them to anticipate the following input.
- *Controlled Element Adaptation* – This refers to the pilots' ability to change control strategies if and when the vehicle handling characteristics alter. Elkind, Kelly & Payne (1964) demonstrated the importance of this showing that the operator took a period of time to adapt to new system dynamics.
- *Programmed and Biological Adaptation* – This describes the pilot response to a changing situation, whereby the pilot reacts to the altered system by implementing a taught control strategy as opposed to learning or controlled element adaptation. Biological adaptation is closely linked to this, representing the heightened state of awareness of the operator after sensing a change in the system.

Although several adaptive pilot models have been developed, none of them incorporate all these adaptive characteristics. However a summary of these models follows.

The first adaptive control model developed was by Costello (1968) as depicted in Figure 3.8. The model consists of a quasi-linear model, which is operational when the

input signal is continuous and when discontinuous an open loop surge model is switched on instead. Phatak & Bekey (1969) criticised the failure to identify the decision-control logic adopted by the pilot. They attempted to achieve this when considering autopilot failures in a simulated roll axis hover mode by employing a supervisory algorithm as illustrated in Figure 3.9. They postulated that the operator remembers the maximum values of error and error rate before failure. A decision region is then selected as twice the maximum error rate, where anything outside this region represents system failure. Gilstad & Fu (1971) adopted a different 2D approach as illustrated in Figure 3.10, where the gain could vary on each control axis. An algorithm for calculating the gain adaptability, similar to that employed by Phatak & Bekey, but with more than two modes is then used to determine the total system gain. The next contributor to the adaptive pilot model work was Hess (1980), who again criticised quasi-linear and optimal control modelling for the lack of explanation of the operator dynamics. Hess developed the compensatory Structural Pilot Model illustrated in Figure 3.11, where the model is composed of a central nervous and a neuromuscular system model, with model parameters listed in Table 3.1 [Sutton (1990)].

Table 3.1 Typical Parameter Values for the Structural Pilot Model [Hess (1980)]

Plant Dynamics	K	K_1	K_2	K_3	K_4	p_1	ω_3	ω_4	τ_1	τ_2	ζ	ω_n
K	0	2.13	11.1	2	1	0.05	0.2	0.2	0.2	0.14	0.707	10
K/s	1	3.42	22.2	2	1	0.05	--	0.2	0.2	0.14	0.707	10
K/s^2	2	10.5	26.2	10	1	0.2	0.4	0.4	0.2	0.14	0.707	10

The adaptive Structural pilot is presented with the error on the display and internally generates a displayed error rate, which is processed through a pulsing logic transfer function. This is governed by the parameter p_1, representing the probability that the switch is in position 1. A further time delay τ_2 is then imposed to account for the time taken by the operator to process the display information. The signal is then processed by a second order neuromuscular delay, a remnant added, then presented to the vehicle dynamics block Y_C. Table 3.1 demonstrates the pilot model parameters which depend on the pilot's adaptability to the plant dynamics. For example, when the plant

transfer function is an integrator, K = 1, ω_3 is not applicable, therefore the transfer function reduces to a simple gain K_3. Also if ω_4 is much less than the crossover frequency, then the pilot acts as a pure gain.

Since the development of the Structural Model, Hess has applied it to many situations such as the development of a preview control model [Hess & Chan (1988)], assessing aircraft handling qualities [Hess (1987)], [Hess & Yousefpor (1992)] and even adapted it to contain motion cues [Hess (1990)].

3.8 Pilot Model Selection

This chapter has so far illustrated the wide variety of pilot models developed from servomechanism theory through to modern control theory. The task now is to choose a model that will provide the information required for this particular handling qualities study. As will be demonstrated in later chapters, the vehicle dynamics are linear, thus due to the 'small angle' rule, any mission task performed is restricted to being only a few seconds long. This means that the pilot characteristics can be assumed to be constant for the manoeuvre, therefore an evaluation of the manoeuvre as a whole is necessary so that the more complex adaptive pilot models are not required. Optimal control models have also been discarded for this study as they only guarantee the optimal pilot characteristics in relation to a performance index, where the theory does not aid the user in selecting such an index. This leaves sampled data models and quasi-linear modelling. Sutton (1990) however, reports that the operator intermittency still remains a theory and also overcomplicates the model. Quasi-linear modelling is therefore the final option. The PPM has been selected over the crossover model, as the latter does not give an insight into the pilot characteristics.

3.9 Application of the Precision Pilot Model

This type of quasi-linear model is not restricted to the case of an aircraft pilot. Again, Sutton (1990) refers on several occasions to how the PPM can be applied to a ships

helmsman to determine whether or not the helmsman performed in a linear fashion by analysing the remnant. For further background reading on the use of pilot models, Costello & Higgins (1966) composed a bibliography concerned specifically with modelling the human operator as an element in a control system.

3.9.1 Precision Pilot Model Parameter Estimation

As stated previously, the inherent human limitations can be considered constant for any given pilot, as obtained through observation from McRuer & Krendel (1974) and Pausder & Jordan (1976). The neuromuscular lag time constant is a parameter which can vary significantly as it depends on the dynamic characteristics of the limb in relation to the control strategy. However for the remainder of the work the neuromuscular lag time constant has been fixed at 0.1 seconds as observed by McRuer & Krendel (1974). The pure time delay was also found to vary depending on the tracking task being assessed. This was found to be of the order of 0.1 seconds and is modelled in the Laplace domain as a fourth order Padé approximation.

The counterbalancing equalisation characteristic variables, considered in Section 3.4.1, define the pilot response for the mission task. Therefore in order to determine the optimum pilot response for the manoeuvre, the optimum HEC must be determined. Sutton (1990) suggests that based on results found by Elkind (1956), the human operator gain is ordinarily between 0.1 and 1 second. He also noted that the ratio of gain to the operator lag time constant remained about 10 : 1. Finally the human operator lead constant, responsible for improving the tracking stability, varies between 0.1 and 2.5 seconds, although in extreme cases values of up to five seconds have been recorded by M^{c}Ruer and Krendel (1957). These boundary conditions can be used to determine the optimum HEC utilising a constrained optimisation technique considered in Chapter 8.

3.10 Conclusions

A review of pilot modelling is presented, ranging from classical servomechanism theory through to modern control theory. One such pilot model developed is the quasi-linear PPM, which simulates the behaviour of the inherently non-linear pilot with a combination of a linear pilot model plus a remnant. A low remnant indicates that the operator behaves in a linear fashion and conversely if a large remnant is required, the pilot is behaving non-linearly resulting in unacceptable handling qualities. Consideration has also been given on how to calculate PPM parameters, where the '*inherent human limitations*' can be considered to be constant for any pilot allowing the '*human equalisation characteristics*' to be determined by employing a constrained optimisation technique. The following chapters consider the remaining elements of the '*Task Variable*' set, the helicopter model and the command signal, where the system under analysis employs a compensatory display.

Chapter 4

Helicopter Modelling

4.1 Introduction

When simulating an aircraft, it is as important to model the vehicle dynamics as to represent the human operator. This chapter therefore focuses on the helicopter, discussing the fundamental differences between fixed wing and helicopter flight. Chapter 4 next considers the complex seven-degree of freedom helicopter model, which is incorporated in the non-linear Helicopter Generic Simulation (HGS).

Although the methods of solving non-linear equations computationally are well established and understood, it is not possible to derive meaningful analytical solutions from them. Flight Dynamics tends to use a more analytical approach to determine the stability characteristics of an aircraft, involving a simplified linearised helicopter model. This simplified approach also means that the equations are much easier to manipulate making any investigation much more convenient. Finally the chapter considers how the linear state space model can be applied to the MMCS as a transfer function, representing the relationship between any combination of states and controls.

4.2 The Basic Principles of Helicopter Flight

An appropriate starting point to this chapter is to consider the differences and complexity of the helicopter in relation to the fixed wing aircraft, where there are two

fundamental differences. Firstly, the helicopter possesses the ability to fly at low speeds and even to hover. As a result of these unique abilities, the helicopter is able to precisely follow a planned trajectory. This low speed and hover capability can only be achieved at the expense of payload and operating cost [Thomson & Bradley (1998)] as low speed flight implies that there is less lift from the aerodynamic surfaces, hence the maximum payload is considerably less than that of a fixed wing aircraft. Secondly, the helicopter is controlled in a manner very different to that of the fixed wing aircraft, due not just to the vehicle configuration, but also because of the complex cross-coupling between the longitudinal and lateral states.

4.2.1 Helicopter Control Principles

The basic method of varying the direction and speed of the helicopter is to vary the magnitude and direction of the main rotor thrust vector [Johnson (1980)]. This is achieved using any or a combination of up to three control inputs. The first control is the '*main rotor collective*', controlling the magnitude of the thrust vector and is denoted by θ_0. This collectively alters the pitch of all the rotor blades by means of a collective lever. The pilot is also able to control the pitch of each individual blade cyclically around a complete revolution by applying '*longitudinal cyclic pitch* θ_{1s}', by pushing the cyclic stick forwards. This causes the advancing blade to flap downwards while the retreating blade flaps upwards, producing the effect of tilting the main rotor forwards. The result of this rotor tilt is that the thrust vector is also tilted forward, pitching the helicopter nose down, while the component of the thrust vector on this axis allows accelerated flight. Similarly when '*lateral cyclic pitch* θ_{1c}' is applied by moving the cyclic stick to the side, the blade pitch on the opposite side of the rotor increases while the pitch on the other side decreases. The resulting rotor tilt causes the helicopter to bank or roll to the same side as the control stick displacement. These three controls determine the orientation of the main rotor. However, the increased torque transmitted to the main rotor by the engine, must be balanced by an opposing moment. This opposing moment is applied through a tail rotor via '*tail rotor collective* θ_{0tr}', controlled through pedal displacements altering the pitch of the blades. This control may also be used to adjust the heading Ψ of the helicopter, by

collectively increasing or decreasing the amount of pitch applied to the tail rotor blades in a similar manner to the main rotor collective.

In the case of the fixed wing aircraft, the longitudinal and lateral aircraft modes are controlled exclusively by the longitudinal and lateral aircraft controls respectively. In the case of the helicopter however, the main rotor collective and longitudinal cyclic influence 'primarily' the longitudinal helicopter modes which, in turn, are governed by the longitudinal and vertical velocities, pitch and pitch rates. The remaining two controls, lateral cyclic and tail rotor collective, therefore 'dominate' the lateral modes, which are governed by side velocity, roll and yaw headings and rates.

4.2.2 Control Requirements for Trimmed Forward Flight

One major drawback of the helicopter in relation to the fixed wing aircraft is the cross coupling between the longitudinal and lateral modes. This is best described when considering the control inputs required for transition from hover to accelerated flight, without changing altitude or heading [Thomson & Bradley (1997)]. First, longitudinal cyclic is applied to give the required acceleration, but as the main rotor is tilted forward, the thrust vector matching the weight of the aircraft is reduced. This can be compensated for by an increase in main rotor collective. However, as the blade pitching angle is increased, blade drag also increases, therefore to maintain rotor speed, the engine torque must be increased. As a result of the increased engine torque, an increase in tail rotor collective is thus required to maintain the required heading. Finally a change in lateral cyclic pitch is required to counteract the side force created by the increase in tailrotor collective.

This example of the control inputs required to simply accelerate a helicopter from hover, illustrates the complexity of the system as inputs in all four control axes are necessary. The pilot workload however, can be reduced by incorporating a flight control system that compensates for a control input by altering the existing control inputs through a series of mechanical linkages. This automatic flight control system (AFCS) is discussed in more detail in Chapter 6 and Appendix *II*, whereas the helicopter model in which the flight control system is applied is now considered.

4.3 Helicopter Generic Simulation (HGS)

Given the complexity of the helicopter, modelling it proves to be a challenging task. The comprehensive Helicopter Generic Simulation (HGS) model, which includes the rotor blade flapping as a state variable and the dynamics of the rotor induced flow, has been employed in the inverse simulation routine Helinv but also exists outwith this algorithm. The HGS model considered herein and as outlined by Thomson & Bradley (1998), contains simplified rotor dynamics where only the fuselage and rotorspeed degrees of freedom are incorporated. This assumption can be made by assuming that these effects (blade flapping and lag) occur instantaneously and can be calculated independently. The non-linear HGS model is described in full in Appendix *III* however, a brief overview is now presented.

With the assumption that only the fuselage and rotorspeed degrees of freedom are incorporated, the state vector becomes

$$\underline{x} = [U \quad V \quad W \quad P \quad Q \quad R \quad \Phi \quad \Theta \quad \Psi \quad \Omega \quad Q_E]^T \tag{4.1}$$

where U, V, W, are the components of transitional velocity relative to a body fixed frame of reference, P, Q, R, are the angular velocities about the body axes, Φ, Θ, Ψ, are the Euler angles relating the body axes to the earth axes, Ω is the angular velocity of the main rotor and Q_E is the engine torque. The control vector can then be written as

$$\underline{u} = [\Theta_0 \quad \Theta_{1s} \quad \Theta_{1c} \quad \Theta_{0tr}]^T \tag{4.2}$$

where the main rotor collective, longitudinal and lateral cyclic and tail rotor collective are the control inputs respectively. The fuselage can be considered to be symmetrical about the xz plane, therefore only the I_{xz} product of inertia term is required by the familiar Euler rigid body equations

$$\dot{U} = -(WQ - VR) + \frac{X}{m} - g\sin\Theta \tag{4.3a}$$

$$\dot{V} = -(UR - WP) + \frac{Y}{m} + g\cos\Theta\sin\Phi \tag{4.3b}$$

$$\dot{W} = -(VP - UQ) + \frac{Z}{m} + g\cos\Theta\cos\Phi \tag{4.3c}$$

$$I_{xx}\dot{P} = (I_{yy} - I_{zz})QR + I_{xz}(\dot{R} + PQ) + L \tag{4.3d}$$

$$I_{yy}\dot{Q} = (I_{zz} - I_{xx})RP + I_{xz}(R^2 + P^2) + M \tag{4.3e}$$

$$I_{zz}\dot{R} = (I_{xx} - I_{yy})PQ + I_{xz}(\dot{P} + QR) + N \tag{4.3f}$$

where m is the aircraft mass, I_{xx}, I_{yy} and I_{zz} are the moments of inertia and I_{xz} is the product of inertia. The rate of change of the attitude angles are related to the body axes angular velocities by the kinematic expressions

$$\dot{\Phi} = P + Q\sin\Phi\tan\Theta + R\cos\Phi\tan\Theta \tag{4.3g}$$

$$\dot{\Theta} = Q\cos\Phi - R\sin\Phi \tag{4.3h}$$

$$\dot{\Psi} = Q\sin\Phi\sec\Theta + R\cos\Phi\sec\Theta \tag{4.3i}$$

Finally the rotor speed governor equations as given by Padfield (1981) are

$$\dot{Q}_E = \frac{1}{\tau_{e_1}\tau_{e_2}}\left[-(\tau_{e_1} + \tau_{e_3})\dot{Q}_E - Q_E + K_3(\Omega - \Omega_{idle} + \tau_{e_2}\dot{\Omega})\right] \tag{4.3j}$$

$$\dot{\Omega} = \frac{(Q_E - Q_R - g_{TR}Q_{TR} - Qtr)}{I_R} + \dot{R} \tag{4.3k}$$

where $\tau_{e_1}, \tau_{e_2}, \tau_{e_3}, K_3$ are the time constants and gains of the governor, Ω_{idle} is the angular velocity of the rotor in idle, g_{TR} is the main/tail rotor gearing ratio, Q_R, Q_{TR}, Q_{tr}, are the torques required to drive the main rotor, tail rotor and transmission. Finally I_R is the effective inertia of the whole rotor system. These equations of motion are widely recognised for any rigid body, however, to present them in the form required by the inverse simulation algorithm, $\dot{P}$ and $\dot{R}$ must be eliminated from the right hand side of equation (4.3d) and equation (4.3f). This is achieved simply by

substituting (4.3f) into (4.3d) to give $\dot{P}$ and vice versa for $\dot{R}$, giving the following solutions

$$\dot{P} = \frac{I_{zz}L^* + I_{xz}N^*}{I_{xx}I_{zz} - I_{xz}^2} \qquad \dot{R} = \frac{I_{xx}N^* + I_{xz}L^*}{I_{xx}I_{zz} - I_{xz}^2}$$

where

$$L^* = \left(I_{yy} - I_{zz}\right)QR + I_{xz}PQ + L \qquad N^* = \left(I_{xx} - I_{yy}\right)PQ + I_{xz}QR + N$$

The non-linear equations of motion in equations (4.3) apply to all rigid bodies, not just the helicopter. The determining factors in the modelling of the vehicle are the external forces and moments *X*, *Y*, *Z*, *L*, *M*, *N*, where for example, the rolling moment L of the helicopter can be defined as

$$L = L_{mr} + L_{tr} + L_f + L_{tp} + L_{fin} \tag{4.4}$$

which includes components from the fuselage *f*, main and tail rotors *mr* and *tr* respectively, horizontal tail plane *tp* and the vertical fin *fn*. The HGS model is discussed by Thomson & Bradley (1997), therefore only a brief overview is presented here with a comprehensive review in Appendix *III*.

4.3.1 Summary of HGS Model

As considered previously, the non-linear equations are valid for all rigid bodies where the external forces and moments determine the vehicle being modelled. In the case of the helicopter, the external forces and moments on the fuselage are due entirely to aerodynamic loading and are calculated from look-up tables of appropriate wind tunnel data. The look-up tables give force and moment coefficients as functions of the incidence angles, the angle of attack α and sideslip β given by

$$\tan\alpha = \frac{W}{U} \qquad \sin\beta = \frac{V}{V_f} \qquad V_f = \sqrt{U^2 + V^2 + W^2}$$

where V_f is the velocity of the aircraft. The external forces and moments produced by the rotor are found by 'blade element theory' where the aerodynamic loads are found for individual blade elements, then summed across the blade span.

This complex helicopter model has been utilised in the non-linear inverse simulation algorithm and can also be used in a helicopter flight simulator. The differential equations can be solved numerically using a fourth order Runge-Kutta method to give the time histories of the state variables. The equations of motion are then solved simultaneously with the kinematic equations yielding the Euler angle time histories.

Although the non-linear equations are well established, it is not possible to derive meaningful analytical solutions from them. In order to determine the stability characteristics of an aircraft, it is advantageous to employ a simplified linear model. This type of model is much easier to manipulate and when incorporated into a helicopter flight simulator, will be easier to control and will also run in real time on a desktop PC.

4.4 The Linear HGS Model

The need to understand the flight dynamics of helicopters and why they are so difficult to build with natural stability, has led to extensive research into analytical methods that can predict different phenomenon. Most understanding of stability and control has come from simple theoretical approximations such as the linear HGS model, which is not only necessary in establishing aircraft stability characteristics, but also proves easier to employ and pilot in a flight simulator. The linear, six degree of freedom model is however not valid in all scenarios. It is only valid for small perturbations from trim [Houston & Caldwell (1984)].

The starting point for the linear model, which is applicable to all rigid bodies, is to understand that the aircraft states are calculated as deviations from the steady level flight state or 'trimmed flight'. This is achieved by considering the states to consist of two components

$$\begin{aligned} U &= U_e + u \quad V = V_e + v \quad W = W_e + w \\ P &= P_e + p \quad Q = Q_e + q \quad R = R_e + r \\ \Phi &= \Phi_e + \phi \quad \Theta = \Theta_e + \theta \quad \Psi = \Psi_e + \psi \end{aligned} \tag{4.5}$$

where the subscript e represents the reference trim state and the lower case denotes the perturbation from trim. The trim values remain constant in the following dynamic analysis where any change in the flight state is described as a perturbation from trim. The aerodynamic forces and moments are central to the linearisation process and can also be expressed as a trim value and deviation from trim where

$$\begin{aligned} X &= X_e + \Delta X \quad Y = Y_e + \Delta Y \quad Z = Z_e + \Delta Z \\ L &= L_e + \Delta L \quad M = M_e + \Delta M \quad N = N_e + \Delta N \end{aligned} \tag{4.6}$$

The linear trim condition can then be determined from the non-linear equations of motion by assuming that all accelerations and rates are zero and that any products of perturbations are small and therefore negligible. The resulting equations are then

$$m\dot{u} = -m\left(W_e q - V_e r\right) - mg\cos\Theta_e + \Delta X \tag{4.7a}$$

$$m\dot{v} = -m\left(U_e r - W_e p\right) + mg\left(\phi\cos\Theta_e \sin\Phi_e - \theta\sin\Theta_e \sin\Phi_e\right) + \Delta Y \tag{4.7b}$$

$$m\dot{w} = -m\left(V_e p - U_e q\right) - mg\left(\theta\sin\Theta_e \cos\Phi_e + \phi\sin\Phi_e \cos\Theta_e\right) + \Delta Z \tag{4.7c}$$

$$\Delta L = I_{xx}\dot{p} - I_{xz}\dot{r} \tag{4.7d}$$

$$\Delta M = I_{yy}\dot{q} \tag{4.7e}$$

$$\Delta N = I_{zz}\dot{r} - I_{xz}\dot{p} \tag{4.7f}$$

$$\dot{\theta} = q\cos\Phi_e - r\sin\Phi_e \tag{4.7g}$$

$$\dot{\phi} = p + q\sin\Phi_e \tan\Theta_e + r\cos\Phi_e \tan\Theta_e \tag{4.7h}$$

$$\dot{\psi} = r\cos\Phi_e \sec\Theta_e + q\sin\Phi_e \sec\Theta_e \tag{4.7i}$$

The aerodynamic force and moment perturbations from trim can be represented in the form of a Taylor series. The perturbations are expressed as a summation of the instantaneous values of the disturbance velocities, control angles and their time derivatives.

$$X = X_e + \left(\frac{\partial X}{\partial u}\right)_e u + \left(\frac{\partial X}{\partial \dot{u}}\right)_e \dot{u} + \left(\frac{\partial X}{\partial v}\right)_e v + \cdots\cdots + \left(\frac{\partial X}{\partial \theta_0}\right)_e \theta_0 + \cdots\cdots \qquad (4.8)$$

Equation (4.8) demonstrates this only for the aerodynamic moment X, however, all six forces and moments can be expanded in this manner, where again e denotes that the derivative should be calculated from trim. Clearly, with a full set of derivatives in all six equations, the equations may become difficult to manipulate. However, for a wide range of flight states the acceleration derivatives are small and may be neglected from the Taylor series. It is worth noting that this assumption is specific to the helicopter and that a different set of assumptions must be made for a fixed wing aircraft. For example, A.W. Babister (1980) demonstrates that in fixed wing aircraft, the derivative $\left(\frac{\partial M}{\partial \dot{w}}\right)_e$ is not negligible due to the lag in an up-gust reaching the tail-plane and therefore cannot be neglected from the equation. Other assumptions may be made for the fixed wing aircraft but are not considered here.

Finally the aerodynamic force and moment perturbations such as that considered in equation (4.8), can be substituted into equations (4.7) to give the linearised equations of motion which, when divided by the aircraft mass, gives the semi-normalised state derivatives as

$$X_u = \frac{1}{m}\left(\frac{\partial X}{\partial u}\right)_e \qquad X_v = \frac{1}{m}\left(\frac{\partial X}{\partial v}\right)_e \qquad X_{\theta_0} = \frac{1}{m}\left(\frac{\partial X}{\partial \theta_0}\right)_e \quad etc.$$

which can be expressed in the state space form

$$\dot{\underline{x}} = \boldsymbol{A}\underline{x} + \boldsymbol{B}\underline{u} \qquad (4.9)$$

where $\underline{x}$ and $\underline{\dot{x}}$ represent the state and differentiated state vectors and $\underline{u}$ is the control vector. $\boldsymbol{A}$ is the state matrix containing the stability derivatives which can be represented as

$$\boldsymbol{A}=\begin{bmatrix}\boldsymbol{A}_{11} & \boldsymbol{A}_{12}\\ \boldsymbol{A}_{21} & \boldsymbol{A}_{22}\end{bmatrix} \tag{4.10}$$

where

$$\mathbf{A}_{11}=\begin{bmatrix} X_u & X_w-Q_e & X_q-W_e & -g\cos\Theta_e\\ Z_u+Q_e & Z_w & Z_q+U_e & -g\cos\Phi_e\sin\Theta_e\\ M_u & M_w & M_q & 0\\ 0 & 0 & \cos\Phi_e & 0\end{bmatrix}$$

$$\mathbf{A}_{12}=\begin{bmatrix} X_v+R_e & X_p & 0 & X_r+V_e\\ Z_v-P_e & Z_p-V_e & -g\sin\Phi_e\cos\Theta_e & Z_r\\ M_v & M_p-\dfrac{2P_eI_{xz}+R_e\left(I_{xx}-I_{yy}\right)}{I_{yy}} & 0 & M_r+\dfrac{2R_eI_{xz}-P_e\left(I_{xx}-I_{zz}\right)}{I_{yy}}\\ 0 & 0 & -\Omega_a\cos\Theta_e & -\sin\Phi_e\end{bmatrix}$$

$$\mathbf{A}_{21}=\begin{bmatrix} Y_u-R_e & Y_w+P_e & Y_q & -g\sin\Phi_e\sin\Theta_e\\ L_u' & L_w' & L_q'+k_1P_e-k_2R_e & 0\\ 0 & 0 & \sin\Phi_e\tan\Theta_e & \Omega_a\sec\Theta_e\\ N_u' & N_w' & N_q'-k_1R_e-k_3P_e & 0\end{bmatrix}$$

$$\mathbf{A}_{22}=\begin{bmatrix} Y_v & Y_p+W_e & g\cos\Phi_e\cos\Theta_e & Y_r-U_e\\ L_v' & L_p'+k_1Q_e & 0 & L_r'-k_2Q_e\\ 0 & 1 & 0 & \cos\Phi_e\tan\Theta_e\\ N_v' & N_p'-k_3Q_e & 0 & N_r'-k_1Q_e\end{bmatrix} \tag{4.11}$$

where

$$L_p'=\frac{I_{zz}L_p}{I_{xx}I_{zz}-I_{xz}^2}+\frac{I_{xz}N_p}{I_{xx}I_{zz}-I_{xz}^2} \qquad N_r'=\frac{I_{xx}N_r}{I_{xx}I_{zz}-I_{xz}^2}+\frac{I_{xz}L_r}{I_{xx}I_{zz}-I_{xz}^2}$$

$$k_1=\frac{I_{xz}\left(I_{zz}+I_{xx}-I_{yy}\right)}{I_{xx}I_{zz}-I_{xz}^2} \qquad k_2=\frac{I_{zz}\left(I_{zz}-I_{yy}\right)+I_{xz}^2}{I_{xx}I_{zz}-I_{xz}^2} \qquad \frac{I_{xx}\left(I_{yy}-I_{xx}\right)+I_{xz}^2}{I_{xx}I_{zz}-I_{xz}^2}$$

Matrix $\boldsymbol{A_{11}}$ represents the longitudinal modes of motion, $\boldsymbol{A_{22}}$ represents the lateral derivatives, while matrices $\boldsymbol{A_{12}}$ and $\boldsymbol{A_{21}}$ represent the cross coupling between the longitudinal and lateral modes. This 'modal' separation is not necessary when assessing aircraft dynamics, but has been included to further highlight the cross coupling between the longitudinal and lateral helicopter modes. For the case of a fixed wing aircraft, the cross coupling derivatives would be zero, showing that the aircraft longitudinal and lateral modes are decoupled. However, this is not the case for the helicopter as these cross-coupling terms influence the vehicle modes, hence the handling qualities. Finally, $\boldsymbol{B}$ is the control matrix, composed of the control derivatives shown in Equation 4.12.

$$\mathbf{B} = \begin{bmatrix} X_{\theta_0} & X_{\theta_{1s}} & X_{\theta_{1c}} & X_{\theta_{0tr}} \\ Z_{\theta_0} & Z_{\theta_{1s}} & Z_{\theta_{1c}} & Z_{\theta_{0tr}} \\ M_{\theta_0} & M_{\theta_{1s}} & M_{\theta_{1c}} & M_{\theta_{0tr}} \\ 0 & 0 & 0 & 0 \\ Y_{\theta_0} & Y_{\theta_{1s}} & Y_{\theta_{1c}} & Y_{\theta_{0tr}} \\ M'_{\theta_0} & M'_{\theta_{1s}} & M'_{\theta_{1c}} & M'_{\theta_{0tr}} \\ 0 & 0 & 0 & 0 \\ N'_{\theta_0} & N'_{\theta_{1s}} & N'_{\theta_{1c}} & N'_{\theta_{0tr}} \end{bmatrix} \tag{4.12}$$

The heading ψ, which is a perturbation from trim, can be calculated independently from the linearised version of Equation (4.7i)

$$\dot{\psi} = r \tag{4.13}$$

The heading ψ has been neglected from the matrices, as the direction of the flight in the horizontal plane has no bearing on the aerodynamic forces and moments. However, it should be noted that the remaining attitude angles θ and ϕ, cannot be treated in such a way as any change from the trim condition influences the gravitational terms and hence the aerodynamic moments in Equations 4.7a, 4.7b & 4.7c.

4.4.1 The Stability Derivatives

The state and control matrices containing the stability derivatives illustrated in equations (4.9) & (4.10) can be applied not just to the helicopter but to any vehicle. However, assumptions can be made to further reduce the order of systems which are decoupled, such as fixed wing aircraft. The state and control matrices illustrated in Figures 4.1 & 4.2 show that for the helicopter, there are 36 stability derivatives and 24 control derivatives for which numerical values must be assigned. This can be achieved in one of three ways

- Wind tunnel tests
- Flight testing
- Analytical techniques

The correct derivation of these is essential to accurately represent the vehicle being modelled. This chapter however, is not concerned with the estimation of the derivatives via wind tunnel or flight testing methods, although Anon. AGARD (1991) comprehensively discusses these techniques. Instead the derivatives, calculated at the equilibrium state, are determined here by numerical differentiation of the non-linear equations as described by equation (4.14)

$$X_u = \frac{1}{m}\left(\frac{\partial X}{\partial u}\right)_e = \frac{1}{m}\frac{X(U_e + \delta u) - X(U_e - \delta u)}{2\delta u} \tag{4.14}$$

This numerical differentiation equation is explained when considering Figure 4.1, which illustrates the aerodynamic force X against the trim velocity U_e. The stability derivative X_u can be determined for a small change in trim velocity δu according to equation (4.14). It should be noted that all the state and control derivatives can be determined in this way but only one is illustrated here because there are one hundred and eight stability derivatives defined in exactly the same manner as considered by Padfield (1996) who discusses in detail some of their characteristics.

4.4.2 The Normal Modes of Motion

The stability and control derivatives contained in the linear equations of motion aid in the understanding of helicopter flight dynamics. Analysis of the model takes place by considering that for small deviations from trim, the helicopter model can be treated as a linear combination of normal modes. These modes can be determined from the system eigenvalues, which are calculated from the stability matrix A. The discussion so far has illustrated that many of the coupled longitudinal/lateral derivatives are strongly linked and have a major influence on the response characteristics. However, in the following discussion, the assumption that the modes are weakly coupled and can be treated in two distinctive sets, longitudinal and lateral, is made.

- *The Longitudinal Modes*

Phugoid Mode - This mode can be visualised in the form of a helicopter rotating about a virtual hinge. The distance from this virtual hinge to the cg of the helicopter determines the ratio of u to q in the mode eigenvector. Figure 4.2 shows this mode to be a naturally unstable (positive real part) oscillatory helicopter mode, which becomes increasingly less unstable as speed increases.

Pitch and Heave Modes – These modes, in a full non-linear helicopter, would ordinarily be subsidence modes [Padfield (1996)]. However, Figure 4.2 demonstrates that for the linear helicopter model, these two longitudinal modes are coupled, suggesting that this complex conjugate eigenvalue actually represents the pitch short period mode.

- *The Lateral Modes*

Spiral Mode – In the case of the Puma helicopter, as demonstrated in Figure 4.2, this is a slow stable mode, influencing only the heading and roll angles. The mode can be considered as a banked turn of increasing radius and without sideslip.

Roll – This is a fast, stable mode, which is strongly influenced by the roll damping L_p, where the helicopter rotates only about the x-axis.

Dutch Roll Mode – The final mode considered is arguably the most complex, consisting of a combination of sideslip, yaw and rolling motion. It tends to be stable. Occasionally however, the mode can be unstable creating severe handling problems, but the mode is generally characterised by the change in stability as illustrated in Figure 4.2. As the aircraft sideslips in one direction, it yaws in the other, maintaining an almost linear flight path. This motion then causes the helicopter to roll in the same direction as the yaw.

The helicopter handling qualities are strongly influenced by the stability of the normal modes [Padfield (1996)], where stability of the mode is determined by whether or not the real part of the eigenvalue is positive or negative (stable modes having a negative real eigenvalue). Emphasis will be placed on the handling qualities assessment in the following chapter, however, the final aspect of the helicopter model is now considered, which is to represent the vehicle dynamics in an appropriate form for the MMCS.

4.4.3 Transfer Function Representation of the Helicopter Model

Equation (4.9) represents the helicopter in state space form via a series of differential equations with constant stability and control derivatives, equations (4.11) & (4.12). Although this representation is extremely useful in determining the vehicle characteristics, the aim of this chapter is not only to present an overview of helicopter modelling, but also to restructure the model in a way that it can be used to represent the vehicle dynamics in the MMCS. This is achieved simply by taking the state space representation

$$\dot{\underline{x}} = \mathbf{A}\underline{x} + \mathbf{B}\underline{u}$$

and transforming it to the Laplace domain to give

4.6 Conclusions

This chapter has presented a brief overview of helicopter modelling. Starting with an illustration of the complexity and the cross coupling of the system by discussing the control inputs required to perform a simple task. The linear HGS model is presented, illustrating the steps required to manipulate the linear equations of motion into the convenient state space form, allowing the vehicle dynamic modes to be assessed by determining the eigenvalues of the state matrix.

The helicopter model can now be used in conjunction with the PPM considered in the previous chapter, to determine the HEC for a predefined task. Once this has been achieved in the inverse simulation case, the pilot effect can be added to the MMCS input to give the actual attitude time history. Clearly before this can happen the command signal for the MMCS must be generated as is considered in the following two chapters. Chapter 5 discusses how the helicopter can be simulated through inverse simulation, while Chapter 6 focuses on the forward simulation with the development of a helicopter flight simulator.

$$s\underline{x}(s) = \mathbf{A}\underline{x}(s) + \mathbf{B}\underline{u}(s)$$

Finally, rearranging to relate the state variables to the control inputs gives

$$(sI - \mathbf{A})\underline{x}(s) = \underline{u}(s)\mathbf{B}$$

$$\frac{\underline{x}(s)}{\underline{u}(s)} = (sI - \mathbf{A})^{-1}\mathbf{B} \tag{4.15}$$

This basic formula can be used to define transfer functions illustrating the relationships between the states and controls. The appropriate vehicle dynamic transfer function can then be chosen, depending on the mission task being performed and which control is most influential as considered by Pausder & Jordan (1976).

4.5 Multiple Control Axis Helicopter Model

Although the helicopter can be represented by the change in the primary attitude angle and the most influential control input, it does not give an accurate description of the vehicle dynamics if more than one control input is applied. In order to represent multiple control inputs in the linear MMCS, a minimum of two transfer functions are required in parallel. For example, if the slalom task previously considered is flown using a combination of only lateral cyclic θ_{1c} and tail rotor collective θ_{0tr}, the vehicle dynamics block $Y_H(s)$ of the MMCS can be represented as illustrated in Figure 4.3. $Y_{H1}(s)$ represents the relationship between the dominant attitude change, in this case the roll angle ϕ, and lateral cyclic. $Y_{H2}(s)$ therefore represents the transfer function relating ϕ to the tail rotor collective. Clearly, if all four control inputs are required during a task, then transfer functions representing all four controls must be included in the vehicle dynamics block.

Chapter 5

Inverse Simulation – Helinv

5.1 Introduction

The conventional approach to aircraft flight simulation is to develop a mathematical model of the vehicle, then determine its real time response to a set of control inputs applied by a pilot. However, very often simulation models are required to assess an aircraft's response to control inputs or examine its stability characteristics offline. This can be particularly difficult to achieve for a helicopter due to the unique operating requirements of the vehicle, such as performing precise tracking tasks. These NOE mission tasks are defined in the ADS-33 document series as single axis tracking tasks such as

Turn to Target – "*From a stabilized hover at an altitude of less than 20 ft, complete a 180 degrees turn. Turns shall be completed in both directions. The final heading tolerance should be based on a sight mounted on the rotorcraft, preferably the same sight to be used for operational missions.*"
Sidestep – "*Starting from a stabilised hover with the longitudinal axis of the rotorcraft oriented 90 degrees to a reference line marked on the ground, initiate a rapid and aggressive lateral acceleration, holding altitude constant with power. Hold target velocity for 5 seconds and then initiate an aggressive deceleration to hover at constant altitude. The peak bank angle during deceleration should occur just before the rotorcraft comes to a stop. Establish and maintain a stabilized hover for 5 seconds. Immediately repeat the maneuver in the opposite direction.*"

and can be readily described by mathematical functions. Inverse simulation is a technique that lends itself very well to solving this type of problem, as it generates the required state and control time histories for a given flight path. This chapter presents two methods of inverse simulation, the first containing a full non-linear helicopter model and the second involving a simplified linear version of the model. Emphasis will be placed on the linear inverse simulation technique for consistency as the remaining blocks in the MMCS are generated using linear algorithms.

5.2 Helicopter Inverse Simulation - Helinv

The Inverse Simulation package Helinv, developed at the University of Glasgow by Thomson (1990), can be used to predict a set of control inputs required to force a vehicle along a predefined flight path. By defining algebraically a mission task, the Helinv algorithm solves the equations of motion generating a unique time history of control inputs. This contrasts with conventional forward simulation, which determines the vehicle flight path for a given set of control inputs and can be expressed as the initial value problem

$$\dot{x} = f(x,u) \qquad x(0) = x_0 \tag{5.1}$$

$$y = g(x) \tag{5.2}$$

where x is the state vector, u is the control vector and y is the output vector. Equation (5.1) shows how the model predicts the vehicle response to a given set of control inputs. Inverse simulation differs from this technique in that a predetermined output vector y is used to calculate the required control time histories u. To demonstrate this method, a statement of the inverse problem can be formed first by differentiating equation (5.2) to give

$$\dot{y} = \frac{dg}{dx}\dot{x} = \frac{dg}{dx} f(x,u) \tag{5.3}$$

In the case where this equation is invertible with respect to u, it is possible to write

$$u = h(x, \dot{y}) \tag{5.4}$$

Substituting back into equation (5.1) gives

$$\dot{x} = f(x, h(x, \dot{y})) = F(x, \dot{y}) \tag{5.5}$$

Equations (5.4) & (5.5) represent a complete statement of the inverse problem with $\dot{y}$ as the input vector and u as the output vector. The input vector $\dot{y}$, required to initiate the algorithm, defines the manoeuvre geometry for which the vehicles cg must precisely follow. Each manoeuvre must be defined in terms of the earth fixed axes, giving the input the initial form

$$\dot{y} = \begin{bmatrix} \dot{x}_e & \dot{y}_e & \dot{z}_e \end{bmatrix}^T$$

Specifying these three initial constraints is sufficient only for determining the aircraft position along the flight path. Subsequently the aircraft is free to point in any direction. Considering the four helicopter controls it is clear that the longitudinal and lateral cyclic inceptors control the x and y directions, while the main rotor collective governs the heave axis. The remaining control is then the tail rotor collective and it follows that the aircraft heading angle ψ is a suitable constraint giving the input vector as

$$\dot{y} = \begin{bmatrix} \dot{x}_e & \dot{y}_e & \dot{z}_e & \dot{\psi} \end{bmatrix}^T$$

The input vector containing the heading constraint is best suited to longitudinal manoeuvres such as the Quick-Hop or lateral manoeuvres such as the side step where turning or a change of heading is not required. If a manoeuvre does require a change in heading, such as the turn to target, it is more convenient to define the fourth constraint in terms of side slip β.

$$\dot{y} = \begin{bmatrix} \dot{x}_e & \dot{y}_e & \dot{z}_e & \beta \end{bmatrix}^T$$

As the aim of this chapter is to show how inverse simulation can be used to generate the MMCS command signal and not the validation of the Helinv programme, a comprehensive discussion of the algorithm employed in Helinv is contained in Appendix *IV* and not the main text.

5.3 Helicopter Model

Like most complex inverse simulation models such as the Hess, Gao Wang algorithm [Hess, gao & Wang (1991)], Helinv is composed of two entities, the inverse algorithm and the helicopter model. The helicopter model applied in Helinv is known as Helicopter Generic Simulation (HGS), which employs a seven degree of freedom state vector alongside a conventional control vector

$$\underline{x} = \begin{bmatrix} U & V & W & P & Q & R & \Phi & \Theta & \Psi & \Omega & Q_E \end{bmatrix}^T \tag{5.6}$$

$$\underline{u} = \begin{bmatrix} \Theta_0 & \Theta_{1s} & \Theta_{1c} & \Theta_{0tr} \end{bmatrix}^T \tag{5.7}$$

where U, V, W are the axial velocities, P, Q, R the rotational velocities, Φ, Θ, Ψ the attitude angles, Ω is the engine rotorspeed and Q_E is the engine torque. The control vector in equation (5.7) represents the four helicopter controls, main rotor collective, longitudinal cyclic, lateral cyclic and tail rotor collective respectively.

Although the inverse simulation algorithm employs the complex non-linear HGS model, the HGS model was not developed specifically for this package. The helicopter model also exists outwith Helinv in non-linear and linear versions. The discussion so far has considered how the output from Helinv is dependent on the mission task geometry although the helicopter model must also be able to adequately model the vehicle response. A full review of the validated HGS model can be found in Appendix *III*. The aim of inverse simulation in this context is to correctly generate the state and control time histories using the HGS model. Therefore emphasis here has

been placed on mathematically defining manoeuvres as the mission task geometry determines the generated output vector.

5.4 Manoeuvre Modelling

The successful application of Helinv depends on the mission task model being representative of the actual task to be flown. A library of mission task elements exists in the form of the Aeronautical Design Standard ADS-33D (1994) published by the United States Army. The document suggests guidelines for performing single axis tracking tasks which can be applied to the development of a manoeuvre mathematical model. It should however be noted that although ADS-33D constitutes one of the most comprehensive and important rotorcraft handling qualities guidelines, it does not encompass all manoeuvres such as the Climb-turn contained in the Helinv mission task library, which is similar to the 'turn to target task', however a vertical repositioning is also required.

Figure 5.1 illustrates how the slalom manoeuvre, introduced in chapter 2, is to be flown with constrained heading (Ψ = 0). However the manoeuvre can also be executed by applying a different control strategy as considered in Figure 5.2, where the side slip (β = 0) is constrained instead of the heading. The task is then to replicate the flight path shown in Figure 5.1 and Figure 5.2 algebraically, allowing Helinv to determine the state and control time histories for the manoeuvre. This was achieved by Leacock (2000) by first assuming that the helicopter starts and finishes the manoeuvre in a fully trimmed flight state. The required flight path can then be split into various sections where the lateral translation is at a maximum or minimum and is expressed as a function of manoeuvre time t_m.

1. At the start of the manoeuvre lateral distance, velocity and acceleration are zero

$$t = 0 \qquad y = \dot{y} = \ddot{y} = 0$$

2. The minimum lateral distance is achieved when the lateral velocity is zero

$$t = \frac{1}{4} t_m \quad \dot{y} = 0 \quad y = y_{\min}$$

3. The maximum lateral distance is achieved when the lateral velocity is zero

$$t = \frac{3}{4} t_m \quad \dot{y} = 0 \quad y = y_{\max}$$

4. At the end of the manoeuvre lateral distance, velocity and acceleration are zero

$$t = t_m \qquad y = \dot{y} = \ddot{y} = 0$$

These boundary conditions can be used to develop a mathematical expression for the manoeuvre. In this case, as there are ten constraints, the resulting polynomial has the form

$$y(t) = \left\{ 759s\left(\frac{t}{t_m}\right)^3 - 6220s\left(\frac{t}{t_m}\right)^4 + 21390s\left(\frac{t}{t_m}\right)^5 - 39291s\left(\frac{t}{t_m}\right)^6 \right.$$
$$\left. + 40353s\left(\frac{t}{t_m}\right)^7 - 21845s\left(\frac{t}{t_m}\right)^8 + 4855s\left(\frac{t}{t_m}\right)^9 \right\} y_{\max} \qquad (5.8)$$

where t_m is the manoeuvre time and s is the maximum (negative as initial displacement here is to the left) lateral distance travelled in the manoeuvre. The ADS-33D slalom, as discussed, is to be performed over a distance of 608 metres with a lateral translation of ±15.2 metres. Clearly these geometric constraints determine the flight path and hence a change in speed will affect the manoeuvre time and not the flight path. Figure 5.2 illustrates the lateral displacement time histories for the forty and eighty knot cases, demonstrating the shorter period of time required to perform the task as the speed increases.

Once the flight path has been established, Helinv can be used to predict the control inputs required for the helicopter to precisely follow the flight path. Figures 5.4 & 5.5 present the Helinv generated state and control responses respectively for the Puma

helicopter model performing the ADS-33D slalom with constrained sideslip at forty and eighty knots. The first noticeable point from Figure 5.4 is that because this is a constrained side slip case, V does not change throughout the task. From this plot it is also clear that because the manoeuvre is a lateral one, the longitudinal variable time histories do not deviate significantly from their initial trimmed condition. Figure 5.5 demonstrates that in the forty knot case, only small changes in all four controls are required to successfully fly the task. This is especially true for the 'longitudinal' controls, main rotor collective and longitudinal cyclic. Figures 5.4 & 5.5 demonstrate that for this example, a change (decrease) in lateral cyclic produces the effect of tilting the main rotor to the left, resulting in the aircraft rolling to the left and a change in heading. This one control input also causes a decrease in altitude due to a reduction in lift produced, which is counterbalanced by an increase in main rotor collective (to maintain the correct altitude) and engine torque. The increased engine torque must then be balanced by an increase in tail rotor collective to maintain heading. When the required roll rate is achieved, the lateral cyclic input is reversed in order to maintain the correct aircraft heading. As this control input is applied, the main rotor collective is slowly reduced to its trim value then, when the blade is tilted in the opposite direction, more collective, engine torque and tail rotor collective are again required.

Analysis of the two flight speed time histories shows that because the higher speed manoeuvre is performed in a shorter time, the manoeuvre is flown in a much more aggressive manner. This requires larger control inputs which more than doubles the controlled roll angle Φ in relation to the forty knot case. It is also evident that the heading Ψ time history does not vary in magnitude over the flight speed range. This is because the vehicle is following the same flight path, the same heading profile is required over different periods of time for the various flight speeds.

As considered in section 5.2, Helinv can function in one of two ways, the first constraining sideslip and the second constraining the heading angle. Figures 5.6 & 5.7 depict the predicted state and control results for the constrained heading slalom compared with the constrained side slip slalom at forty knots. Although each constrains a different parameter, the remaining state responses are similar. It is noticeable however, that the constrained sideslip technique requires smaller control

inputs in order to perform the manoeuvre, suggesting that it would be an easier task for a pilot to perform than with constrained heading.

5.5 Linear Inverse Simulation

Linearisation as described in chapter 4, is a standard way of analysing the behaviour of nonlinear dynamic systems. The linearised equations of motion, when expressed in state space form, can be used to describe the unconstrained response of the helicopter to a series of control inputs. More significantly, this technique can be used to analyse aircraft stability and to derive the vehicle dynamics as a transfer function. The requirement here however, is that a statement of the inverse problem be formed by rewriting the linearised equations such that the state and control time histories can be determined for a predefined flight path. The linearised equations of motion can be expressed in state space form as

$$\dot{\underline{x}} = \boldsymbol{A}\underline{x} + \boldsymbol{B}\underline{u} \tag{5.9}$$

where $\boldsymbol{A}$ and $\boldsymbol{B}$ are the system and control matrices respectively which contain the aerodynamic and relevant gravitational and velocity terms. The state vector $\underline{x}$ and the control vector $\underline{u}$ are given by

$$\underline{x} = \begin{bmatrix} u & v & w & p & q & r & \phi & \theta \end{bmatrix}^T \tag{5.10}$$

$$\underline{u} = \begin{bmatrix} \theta_0 & \theta_{1s} & \theta_{1c} & \theta_{0tr} \end{bmatrix}^T \tag{5.11}$$

The first stage is then to split the state vector into those variables strongly influenced by the constraints and those that are unconstrained. It follows that as considered in section 5.2, the longitudinal and lateral cyclic control the x and y directions influencing u and v respectively, whereas the main rotor collective controlling the heave axis primarily influences w. Finally as the tail rotor strongly influences the heading ψ, the vector of constraint influenced states $\underline{x}_1$ and the vector of unconstrained states $\underline{x}_2$ are

$$\underline{x}_1 = \begin{bmatrix} u & v & w & r \end{bmatrix}^T \qquad \underline{x}_2 = \begin{bmatrix} p & q & \theta & \phi \end{bmatrix}^T \tag{5.12}$$

which can be written as

$$\begin{bmatrix} \dot{\underline{x}}_1 \\ \dot{\underline{x}}_2 \end{bmatrix} = \begin{bmatrix} \mathbf{A}_{11} & \mathbf{A}_{12} \\ \mathbf{A}_{21} & \mathbf{A}_{22} \end{bmatrix} \begin{bmatrix} \underline{x}_1 \\ \underline{x}_2 \end{bmatrix} + \begin{bmatrix} \mathbf{B}_1 \\ \mathbf{B}_2 \end{bmatrix} \begin{bmatrix} \underline{u} \end{bmatrix} \tag{5.13}$$

On expansion, Equation (5.13) gives

$$\dot{\underline{x}}_1 = \mathbf{A}_{11}\underline{x}_1 + \mathbf{A}_{12}\underline{x}_2 + \mathbf{B}_1\underline{u} \tag{5.14}$$

$$\dot{\underline{x}}_2 = \mathbf{A}_{21}\underline{x}_1 + \mathbf{A}_{22}\underline{x}_2 + \mathbf{B}_2\underline{u} \tag{5.15}$$

Solving equation (5.14) for the control vector assuming $\boldsymbol{B}_1$ to be non-singular

$$\underline{u} = \mathbf{B}_1^{-1}\left[\dot{\underline{x}}_1 - \mathbf{A}_{11}\underline{x}_1 - \mathbf{A}_{12}\underline{x}_2\right] \tag{5.16}$$

Substituting (5.16) into (5.15) allows the unconstrained states to be expressed in terms of the constraint influenced states

$$\dot{\underline{x}}_2 = \left[\mathbf{A}_{22} - \left(\mathbf{B}_2\mathbf{B}_1^{-1}\right)\mathbf{A}_{12}\right]\underline{x}_2 + \left[\left(\mathbf{A}_{21} - \left(\mathbf{B}_2\mathbf{B}_1^{-1}\right)\mathbf{A}_{11}\right)\underline{x}_1 + \left(\mathbf{B}_2\mathbf{B}_1^{-1}\right)\underline{x}_1\right] \tag{5.17}$$

The linear solution requires the unconstrained states $\underline{x}_2$ to be expressed in terms of the constraints $\underline{f}_c$. However the strongly influenced states $\underline{x}_1$ are a function of both $\underline{x}_2$ and $\underline{f}_c$ as is apparent on examination of the linearised Euler transformation

$$\begin{bmatrix} u \\ v \\ w \end{bmatrix} = \begin{bmatrix} L_{1_0} & L_{2_0} & L_{3_0} \\ M_{2_0} & M_{2_0} & M_{3_0} \\ N_{1_0} & N_{2_0} & N_{3_0} \end{bmatrix} \begin{bmatrix} \dot{x} \\ \dot{y} \\ \dot{z} \end{bmatrix} + \begin{bmatrix} L_{1_d} & L_{2_d} & L_{3_d} \\ M_{1_d} & M_{2_d} & M_{3_d} \\ N_{1_d} & N_{2_d} & N_{3_d} \end{bmatrix} \begin{bmatrix} \theta \\ \phi \\ \psi \end{bmatrix} \tag{5.18}$$

where the direction cosines are given by

$$L_1 = \cos\Theta\cos\Psi \qquad L_2 = \cos\Theta\sin\Psi \qquad L_3 = -\sin\Theta$$
$$M_1 \sin\Phi\sin\Theta\cos\Psi - \cos\Phi\sin\Psi \qquad M_2 = \sin\Phi\sin\Theta\sin\Psi + \cos\Phi\cos\Psi \qquad M_3 = \sin\Phi\cos\Psi$$
$$N_1 = \cos\Phi\sin\Theta\cos\Psi + \sin\Phi\sin\Psi \qquad N_2 = \cos\Phi\sin\Theta\sin\Psi - \sin\Phi\cos\Psi \qquad N_3\cos\Phi\cos\Theta$$

At this point it is important to note that the linear inverse simulation can be solved in one of two ways, depending on how the fourth constraint is specified. The first technique, discussed by Thomson and Bradley (1990), is to incorporate a yaw or heading constraint in conjunction with the flight path constraints. As this is a well documented routine, the algorithm has not been considered in the main text but can be found in Appendix *V*. Instead the second technique has been focused on, which is to specify constrained side slip given by

$$v = V\sin\beta \tag{5.19}$$

Linearising this yields the constrained sideslip velocity

$$v_c = V_0\beta\cos\beta_0 + V\sin\beta_0 \tag{5.20}$$

where v, V and β are all perturbation values and β_0 represents the trimmed side slip β. The linearised equations (5.9) are nowexpressed in terms of the constraint influenced states. Hence from equation (5.20) and the linearised Euler transformation in equation (5.18), the yaw velocity is given by the kinematic expression

$$\psi = \frac{1}{m_{3_d}}\left[v_c - \left(m_{1_0}\dot{x} + m_{2_0}\dot{y} + m_{3_0}\dot{z} + m_{1_d}\theta + m_{2_d}\phi\right)\right] \tag{5.21}$$

Substituting equation (5.21) back into the Euler transformation gives

$$\begin{bmatrix} u \\ v \\ w \end{bmatrix} = \begin{bmatrix} l_1^* & l_2^* & l_3^* \\ 0 & 0 & 0 \\ n_1^* & n_2^* & n_3^* \end{bmatrix}\begin{bmatrix} \dot{u} \\ \dot{v} \\ \dot{w} \end{bmatrix} + \begin{bmatrix} l_4^* & l_5^* \\ 0 & 0 \\ n_4^* & n_5^* \end{bmatrix}\begin{bmatrix} \theta \\ \phi \end{bmatrix} + \begin{bmatrix} l_6^* \\ 1 \\ l_6^* \end{bmatrix}\begin{bmatrix} v_c \end{bmatrix} \tag{5.22}$$

where

$$
\begin{aligned}
l_1^* &= l_{1_0} - m_{1_0} l_6^* & n_1^* &= n_{1_0} - m_{1_0} n_6^* \\
l_2^* &= l_{2_0} - m_{2_0} l_6^* & n_2^* &= n_{2_0} - m_{2_0} n_6^* \\
l_3^* &= l_{3_0} - m_{3_0} l_6^* & n_3^* &= n_{3_0} - m_{3_0} n_6^* \\
l_4^* &= l_{1_d} - m_{1_d} l_6^* & n_4^* &= n_{1_d} - m_{1_d} n_6^* \\
l_5^* &= l_{2_d} - m_{2_d} l_6^* & n_5^* &= n_{2_d} - m_{1_d} n_6^* \\
l_6^* &= \frac{l_{3_d}}{m_{3_d}} & n_6^* &= \frac{n_{3_d}}{m_{3_d}}
\end{aligned}
$$

The linearised transformation of earth fixed to body fixed axes accelerations are expressed as

$$
\begin{bmatrix} \dot{u} \\ \dot{v} \\ \dot{w} \end{bmatrix} = \begin{bmatrix} L_{1_0} & L_{2_0} & L_{3_0} \\ M_{2_0} & M_{2_0} & M_{3_0} \\ N_{1_0} & N_{2_0} & N_{3_0} \end{bmatrix} \begin{bmatrix} \ddot{x} \\ \ddot{y} \\ \ddot{z} \end{bmatrix} - \begin{bmatrix} W_e q - V_e r \\ U_e r - W_e p \\ V_e p - U_e q \end{bmatrix} \tag{A5.23}
$$

where the body fixed acceleration $\dot{v}$ can be rewritten as

$$
r = \frac{1}{U_e}\left(m_{1_0} \ddot{x} + m_{2_0} \ddot{y} + m_{3_0} \ddot{z} - \dot{v} + W_e p\right) \tag{5.24}
$$

Combining and rearranging (5.22) and (5.24) gives

$$
\underline{x}_1 = \mathbf{T}_1 \dot{\underline{f}}_c + \mathbf{T}_2 \underline{f}_c + \mathbf{T}_3 \underline{x}_2 \tag{5.25}
$$

where

$$\mathbf{T}_1 = \begin{bmatrix} 0 & 0 & 0 & 0 \\ 0 & 0 & 0 & 0 \\ 0 & 0 & 0 & 0 \\ m_{1_0}/U_e & m_{2_0}/U_e & m_{3_0}/U_e & -1/U_e \end{bmatrix} \quad \mathbf{T}_2 = \begin{bmatrix} l_1^* & l_2^* & l_3^* & l_6^* \\ 0 & 0 & 0 & 1 \\ n_1^* & n_2^* & n_3^* & n_6^* \\ 0 & 0 & 0 & 0 \end{bmatrix} \quad \mathbf{T}_3 = \begin{bmatrix} 0 & 0 & l_4^* & l_5^* \\ 0 & 0 & 0 & 0 \\ 0 & 0 & n_4^* & n_5^* \\ W_e/U_e & 0 & 0 & 0 \end{bmatrix}$$

Differentiating (5.24) gives the yaw rate acceleration

$$\dot{r} = \frac{1}{U_e}\left(m_{1_0}\ddot{x} + m_{2_0}\ddot{y} + m_{3_0}\ddot{z} - \ddot{v} + W_e\dot{p}\right) \tag{5.26}$$

Combining and rearranging equation (5.26) and the linearised transformation of earth-fixed to body-fixed axes accelerations in equation (A5.23) gives

$$\underline{\dot{x}}_1 = \mathbf{T}_1\underline{\ddot{f}}_c + \mathbf{T}_4\underline{\dot{x}}_2 + \mathbf{T}_5\underline{x}_2 + \mathbf{T}_6\underline{\dot{f}}_c \tag{5.27}$$

where

$$\mathbf{T}_4 = \begin{bmatrix} 0 & 0 & 0 & 0 \\ 0 & 0 & 0 & 0 \\ 0 & 0 & 0 & 0 \\ W_e/U_e & 0 & 0 & 0 \end{bmatrix} \quad \mathbf{T}_5 = \begin{bmatrix} W_eV_e/U_e & -W_e & 0 & 0 \\ 0 & 0 & 0 & 0 \\ -V_e & U_e & 0 & 0 \\ 0 & 0 & 0 & 0 \end{bmatrix} \quad \mathbf{T}_6 = \begin{bmatrix} l_7^* & l_8^* & l_9^* & -V_e/U_e \\ 0 & 0 & 0 & 1 \\ n_{1_0} & n_{2_0} & n_{3_0} & 0 \\ 0 & 0 & 0 & 0 \end{bmatrix}$$

$$l_7^* = l_{1_0} + \frac{m_{1_0}V_e}{U_e} \qquad l_8^* = l_{2_0} + \frac{m_{2_0}V_e}{U_e} \qquad l_9^* = l_{3_0} + \frac{m_{3_0}V_e}{U_e}$$

Equations (5.25) and (5.27) can be substituted into (5.17) giving

$$\begin{aligned} \underline{\dot{x}}_2 = &\left[I - \mathbf{B}_2\mathbf{B}_1^{-1}\mathbf{T}_4\right]^{-1}\left\{\mathbf{A}_{22} - \mathbf{B}_2\mathbf{B}_1^{-1}\left(A_{12} - \mathbf{T}_5\right) + \left(\mathbf{A}_{21} - \mathbf{B}_2\mathbf{B}_1^{-1}\mathbf{A}_{11}\right)\mathbf{T}_3\right\}\underline{x}_2 + \\ &\left[I - \mathbf{B}_2\mathbf{B}_1^{-1}\mathbf{T}_4\right]^{-1}\left\{\left[\mathbf{B}_2\mathbf{B}_1^{-1}\mathbf{T}_1\right]\underline{\ddot{f}}_c + \left[\left(\mathbf{A}_{21} - \mathbf{B}_2\mathbf{B}_1^{-1}\mathbf{A}_{11}\right)\mathbf{T}_1 + \mathbf{B}_2\mathbf{B}_1^{-1}\mathbf{T}_6\right]\underline{\dot{f}}_c\right\} + \\ &\left[I - \mathbf{B}_2\mathbf{B}_1^{-1}\mathbf{T}_4\right]^{-1}\left\{\left[\left(\mathbf{A}_{21} - \mathbf{B}_2\mathbf{B}_1^{-1}\mathbf{A}_{11}\right)\mathbf{T}_2\right]\underline{f}_c\right\} \end{aligned}$$

The unconstrained states are now expressed in terms of the constraints. This solution can be simplified to

$$\dot{\underline{x}}_2 = \mathbf{A}_c \underline{x}_2 + \mathbf{B}_c \underline{u}_c \tag{5.28}$$

where

$$\mathbf{A}_c = \left[I - \mathbf{B}_2\mathbf{B}_1^{-1}\mathbf{T}_4\right]^{-1}\left\{\mathbf{A}_{22} - \mathbf{B}_2\mathbf{B}_1^{-1}\left(\mathbf{A}_{12} - \mathbf{T}_5\right) + \left[\mathbf{A}_{21} - \mathbf{B}_2\mathbf{B}_1^{-1}\mathbf{A}_{11}\right]\mathbf{T}_3\right\}$$

$$\mathbf{B}_c = \begin{bmatrix} \left[I - \mathbf{B}_2\mathbf{B}_1^{-1}\mathbf{T}_4\right]^{-1}\mathbf{B}_2\mathbf{B}_1^{-1}\mathbf{T}_1 \\ \left[I - \mathbf{B}_2\mathbf{B}_1^{-1}\mathbf{T}_4\right]^{-1}\left(\left(\mathbf{A}_{21} - \mathbf{B}_2\mathbf{B}_1^{-1}\mathbf{A}_{11}\right)\mathbf{T}_1 + \mathbf{B}_2\mathbf{B}_1^{-1}\mathbf{T}_6\right) \\ \left[I - \mathbf{B}_2\mathbf{B}_1^{-1}\mathbf{T}_4\right]^{-1}\left(\mathbf{A}_{21} - \mathbf{B}_2\mathbf{B}_1^{-1}\mathbf{A}_{11}\right)\mathbf{T}_2 \end{bmatrix}^T$$

$$\underline{u}_c = \begin{bmatrix} \ddot{\underline{f}}_c \\ \dot{\underline{f}}_c \\ \underline{f}_c \end{bmatrix} \qquad \underline{f}_c = \begin{bmatrix} \dot{x} \\ \dot{y} \\ \dot{z} \\ v_c \end{bmatrix} \qquad \underline{x}_2 = \begin{bmatrix} p \\ q \\ \theta \\ \phi \end{bmatrix}$$

Once the unconstrained matrix $\underline{x}_2$ has been calculated, it can be substituted back into equation (5.25) to give the constrained parameter time histories $\underline{x}_1$. Finally, these results can be used to determine the control inputs from equation (5.16).

As the ADS-33D slalom was considered for the non-linear HGS Helinv algorithm, Figures 5.8 & 5.9 compare the nonlinear and linear Helinv state and control time histories for the forty knot constrained sideslip manoeuvre, performed by a Puma helicopter. Analysis of these plots shows that although the linear inverse simulation technique requires a greater roll angle (ϕ) and greater control inputs in all four control axes, overall the linear inverse simulation is a good approximation to the full non-linear algorithm. The oscillations and increases in control input can be explained when considering the stability characteristics of the aircraft. The constrained equation of motion in equation (5.28) contains the constrained system matrix A_c, allowing the dynamic properties of the constrained system to be calculated from its eigenvalues. Figure 5.10 shows the root locus plot of both modes. From the diagram, it is apparent

that over the low flight speed range, the eigenvalues and hence the period of oscillation are almost constant. One of the stable modes with period of 1.24 seconds represents the transient oscillation clearly seen in the longitudinal and lateral cyclic control inputs in Figure 5.9 and also the state variable p in Figure 5.8 with measured periods between 1.15 and 1.3 seconds. Even though measuring errors are apparent, the linear algorithm produces periods similar to the predicted values. The oscillatory control inputs are a result of the flight path being precisely followed by linear Helinv and, as considered by Bradley and Thomson (1990), pilots also display this oscillatory nature in their control strategies when attempting to perform a tracking task, but not to the same extent. This is because the pilot flies the manoeuvre within specified limits rather than following the exact flight path.

5.5.1 Validation of Helinv Algorithm

So far this chapter has considered the inverse simulation algorithm and validation of the linear simulation in relation to the non-linear model. However, if any meaningful information is to be produced, the inverse simulation must replicate the behaviour of the real helicopter. The conventional approach to this validation is simply to compare the Helinv output and the flight data for the same manoeuvre, speed and vehicle.

The manoeuvre considered in this chapter is the ADS-33D slalom single axis tracking task, performed in a Puma Helicopter. However, as there is no flight data readily available for this project meeting these criteria, reference is made to Thomson & Bradley (1997). This paper considers the validation of non-linear Helinv via the Quick-Hop manoeuvre performed in a Westland Lynx Helicopter. Figure 5.11 illustrates the comparison referred to between the actual flight data and the state and control time histories developed using inverse simulation for this manoeuvre. The plots demonstrate that the correct trend is being predicted in all controls, resulting in similar roll and pitch attitudes recorded from the flight test. These and other results, presented by Thomson & Bradley (1997), verify that the non-linear or linear inverse algorithm (as the linear algorithm has been proven in this chapter to replicate the non-linear system) can be used to predict the vehicle parameter time histories.

5.6 Conclusions

Flight testing is an expensive way of obtaining real flight data. However mission tasks can be easily simulated using the inverse simulation package Helinv if the mission task can be mathematically modelled. This chapter has considered one of many ADS-33D (1994) mission task elements, the slalom manoeuvre, and how Helinv can predict the 'ideal' state and control time histories for the manoeuvre. The following chapter presents the development of a helicopter flight simulator incorporating a linear HGS model for creating real or 'non-ideal' flight data to aid in a handling qualities assessment. As this programme and the vehicle dynamics block discussed in Chapter 6 are linear, it was necessary to generate a linear version of the inverse simulation technique for consistency. The linear version of Helinv operates using a numerical integration technique, described by Thomson and Bradley (1990), which calculates the deviation from steady level trimmed flight for the predefined manoeuvre geometry. This technique makes the common engineering assumption that any perturbations from trim are small, limiting the application of linear Helinv.

Chapter 6

Development of a Mission Programmable Flight Simulator

6.1 Introduction

Inverse simulation has been presented as a valuable tool for generating the ideal state and control time histories used as the command signal for the MMCS. Chapter 6 focuses on developing an alternative method for deriving actual pilot data, which can be used in a helicopter handling qualities assessment. This involves creating a real time helicopter flight simulator using Visual C/C++6, incorporating a flexible helicopter model with fully functional cockpit view and automatic flight control system. Finally, of equal importance, is the 3D environment in which the mission tasks are to be performed, which is translated and rotated around the stationary helicopter model, producing the effect of flight.

6.2 Desktop Flight Simulator Requirements

Using the PPM in conjunction with the MMCS to assess HQR, requires a mission task to be flown by numerous pilots in the same helicopter. The recorded flight data can then be applied to the MMCS as described in Chapter 2 to generate the optimum HEC. Inverse simulation, as discussed previously, is one method that can be applied to derive the input to the MMCS where the state and control time histories generated represent the ideal manoeuvre time history. Clearly, when the ideal manoeuvre time history is used as the command signal for the MMCS, the PPM will minimise the

error by calculating the optimum HEC. Other methods of attaining manoeuvre flight data must now be considered to compare with those generated from Helinv. Ideally, real flight test data would be used but as it is not available for this project, an alternative method of creating manoeuvre time histories, using a PC based flight simulator, is proposed.

Before a PC based flight simulator is selected in which to create the command signal by piloting a selected mission task, it must adhere to certain criteria which are essential for creating realistic flight data. These requirements are as follows:

- Operational Functionality – the main objective of developing a flight simulator is to obtain pilot data to be used as the input to the MMCS. Therefore, it is imperative that the state and control time histories are output to file during the flight. Although the manoeuvre may be correctly displayed in the 3D environment, the flight and recorded time histories only fully represent the manoeuvre flown by the pilot if the simulation runs in real time.
- Helicopter Model - A valid helicopter model must be incorporated which calculates the state and control time histories, where the operator is able to select a reference trim speed to perform the chosen mission task. Deviation from the trimmed flight condition can then be achieved by applying control inputs to the system via joystick. These control inputs can govern directly the control inputs or can be applied through an automatic flight control system (AFCS).
- 3D Environment – This is the 'world' viewed by the pilot from inside the stationary, fully functional helicopter cockpit. The 3D environment is where the mission task elements must be realised and manipulated to give the illusion of flight.

Although there are many PC based flight simulators available commercially, one that allowed access to the programme code, in order to change the surrounding environment, task and vehicle model was not available commercially at the time. Therefore the task of developing a mission programmable flight simulator was undertaken.

6.3 Development of a Mission Programmable Flight Simulator

Developing a real time helicopter flight simulator incorporating the elements described above is a complex and challenging task. Central to the simulator is the helicopter model describing the vehicle response to a control input. Attitude change and distance travelled by the helicopter are calculated, then used to manipulate a visual environment. As the requirements for creating the flight simulator are defined in the previous section, the helicopter model applied to obtain manoeuvre time histories is considered, followed by the construction of the three-dimensional environment and operator viewpoints.

6.3.1 Helicopter Model

As discussed in Chapter 5, the HGS model exists in a full non-linear version such as that employed in Helinv, but also in a simplified linear version. The flight simulator described herein incorporates the linearised six-degree of freedom HGS model, therefore it should be noted that the state and control vectors are calculated at a reference trim state. The linear model of a rigid aircraft is derived using the following assumptions at the trim condition

- There are no resultant accelerations on the aircraft.
- The aircraft has no angular velocity.
- The aircraft is assumed to be in symmetric flight.

It is also important to define the aircraft frame of reference. As illustrated in Figure 6.1 the body axis frame of reference is measured from the cg of the aircraft where

- The positive x-axis points along the nose of the vehicle.
- The positive y-axis points to the right.
- The z-axis points downwards.

The importance of defining this frame of reference will be demonstrated in Section 6.5 as the OpenGL® axis is not specified in the same manner.

The linear HGS model can be used to determine the helicopter dynamics by generating a state space representation of the vehicle dynamics about a reference trim condition

$$\dot{\underline{x}} = \mathbf{A}\underline{x} + \mathbf{B}\underline{u} \tag{6.1}$$

where the state and control vectors respectively are typically

$$\underline{x} = \begin{bmatrix} u & v & w & p & q & r & \phi & \theta & \psi \end{bmatrix}^T \tag{6.2}$$

$$\underline{u} = [\theta_0 \;\; \theta_{1s} \;\; \theta_{1c} \;\; \theta_{0tr}]^T \tag{6.3}$$

The state space representation shown in equation (6.1), can be integrated using a fourth order Runge-Kutta integration routine, as described by Teukolsky, Vetterling & Flannery (1994), to give the state variables as deviations from trim

$$\underline{x} = \int_{x_1}^{x_2} \dot{\underline{x}} dt \tag{6.4}$$

where the time interval (x_2-x_1) is the integration step size. This technique can be verified by comparison with the established fourth order Runge-Kutta integration routine of Matlab® (1992). The Matlab® results are generated by calculating the response of the vehicle to a control input. The plant transfer functions are determined from the familiar matrix manipulation of the state and control matrices

$$\frac{x(s)}{u_j(s)} = (sI - \mathbf{A})^{-1}\mathbf{B} \tag{6.5}$$

Equation (6.5) may be used to obtain the transfer function relating a control input to a state parameter. For example, the transfer function relating pitch attitude to lateral cyclic, for the Puma helicopter flying at forty knots, was found to be

$$\frac{\theta(s)}{\theta_{1c}(s)} = \frac{27.9s^6 + 60.2^5 + 97.5^4 + 74.3s^3 + 34.4s^2 + 5.3s + 3}{s^8 + 3.7s^7 + 7.1s^6 + 9.2s^5 + 7.3s^4 + 3.4s^3 + 0.7s^2 + 0.2s + 0.1} \tag{6.6}$$

The remaining thirty five transfer functions relating each state to each control input have not been presented here as this has been provided solely as an example. The reader is referred to Padfield (1996) for further reading. Figure 6.2 compares the state variables response to a one-degree step input in θ_{lc} at forty knots. The plots show that when the blade plane is 'tilted to the right (positive control input), the helicopter rolls to the right resulting in a lateral velocity component w. As a result of the blade plane changing, there is a decrease in lift thus the helicopter loses altitude (w decreases) and forward speed increases. Finally the pitch angle θ can be seen to remain almost unchanged. It is also clear from the plots and the discussion above that cross-coupling between the longitudinal and lateral modes exists due to the lateral control input influencing the longitudinal aircraft state variables. The agreement between the flight simulator and the validated Matlab® integration routines confirm that the helicopter model functions correctly.

6.3.1.1 Modal Analysis

The denominator of the helicopter transfer function in equation (6.6) can be further considered for a modal analysis as demonstrated in Section 4.4.2 and Figure 4.2. The eigenvalues can be determined by factorising the characteristic equation for the forty knot case to give

Roll = -1.5356 Spiral = -0.2308 Dutch Roll = -0.3375±1.2523i

Phugoid = 0.0455±0.27i Pitch and Heave = -0.6837±0.7382i

which are plotted in Figure 4.2. It is also possible to illustrate which state variables influence each mode through an eigenvector analysis which illustrates the cross-coupling between the longitudinal and lateral modes. For example, the spiral mode, which is a lateral mode, is strongly influenced by w and u. The longitudinal phugoid mode is represented by two complex eigenvalues, dominated by the longitudinal variables u and w, and the lateral parameters v, p and r. The cross-coupling between the two sets of state variables in the remaining modes, which is not presented here, also highlights the complex control nature of the aircraft.

6.3.1.2 Linear Euler Transformation

Once the state variables have been calculated, the final step is to convert from body axis velocities to earth axis velocities using the linearised Euler transformation

$$\begin{bmatrix} u \\ v \\ w \end{bmatrix} = \begin{bmatrix} l_{10} & l_{20} & l_{30} \\ m_{10} & m_{20} & m_{30} \\ n_{10} & n_{20} & n_{30} \end{bmatrix} \begin{bmatrix} \dot{x} \\ \dot{y} \\ \dot{z} \end{bmatrix} + \begin{bmatrix} l_1' & l_2' & l_3' \\ m_1' & m_2' & m_3' \\ n_1' & n_2' & n_3' \end{bmatrix} \begin{bmatrix} \theta \\ \phi \\ \psi \end{bmatrix} \tag{6.7}$$

where

$$\begin{aligned}
l_{10} &= \cos\Theta_e \cos\Psi_e \\
l_{20} &= \cos\Theta_e \sin\Psi_e \\
l_{30} &= -\sin\Theta_e \\
m_{10} &= \sin\Phi_e \sin\Theta_e \cos\Psi_e - \cos\Phi_e \sin\Psi_e \\
m_{20} &= \sin\Phi_e \sin\Theta_e \sin\Psi_e + \cos\Phi_e \cos\Psi_e \\
m_{30} &= \sin\Phi_e \cos\Theta_e \\
n_{10} &= \cos\Phi_e \sin\Theta_e \cos\Psi_e + \sin\Phi_e \sin\Psi_e \\
n_{20} &= \cos\Phi_e \sin\Theta_e \sin\Psi_e - \sin\Phi_e \cos\Psi_e \\
n_{30} &= \cos\Phi_e \cos\Theta_e
\end{aligned}$$

$$
\begin{aligned}
l_1' &= l_{30}\left(\dot{X}_e \cos\Psi_e + \dot{Y}_e \sin\Psi_e\right) - \dot{Z}_e \cos\Theta_e \\
l_2' &= 0 \\
l_3' &= -\dot{X}_e l_{20} + \dot{Y}_e l_{10} \\
m_1' &= m_{30}\left(\dot{X}_e \cos\Psi_e + \dot{Y}_e \sin\Psi_e\right) + \dot{Z}_e l_{30} \sin\Phi_e \\
m_2' &= \dot{X}_e n_{10} + \dot{Y}_e n_{20} + \dot{Z}_e n_{20} \\
m_3' &= -\dot{X}_e m_{20} + \dot{Y}_e m_{10} \\
n_1' &= n_{30}\left(\dot{X}_e \cos\Psi_e + \dot{Y}_e \sin\Psi_e\right) + \dot{Z}_e l_{30} \cos\Phi_e \\
n_2' &= -\left(\dot{X}_e m_{10} + \dot{Y}_e m_{20} + \dot{Z}_e m_{20}\right) \\
n_3' &= -\dot{X}_e n_{20} + \dot{Y}_e n_{10}
\end{aligned}
$$

Again the earth axis velocities can be integrated using the fourth order Runge-Kutta integration routine to give the earth axis translations. These are then updated to the screen with the attitude angles, producing the effect of flight. In addition to the linear HGS model, the simulator includes an Automatic Flight Control System (AFCS) which is designed to ease the pilot workload.

6.3.2 Automatic Flight Control System (AFCS)

Helicopters are inherently unstable vehicles and consequently employ a stabilising system or Automatic Flight Control System (AFCS). This is usually made up from Stability and Control Augmentation System (SCAS) functions, applied through a series of actuators and autopilot functions applied through parallel actuators.

The SCAS is initiated through pilot stick displacement, calculating the main and tail rotor deflection through a series of actuators and mechanical linkages as illustrated in Figures 6.4a & 6.4b. The cockpit controls are represented by displacements η, with appropriate subscripts where

$$0 \leq \eta \leq 1 \tag{6.8}$$

with the positive sense defined by a positive increase in the corresponding rotor blade angle. The stick displacements can be assigned to the control axis as considered later in Section 6.6, then applied to a series of actuators as described in Appendix *II*.

6.3.3 3D Environment

This section discusses the 3D environment incorporating the HGS model in which the human operator performs a mission task. Created using Visual C\C++6 and utilising the OpenGL® graphics Libraries, described by Woo, Neider, Davis & Shreiner (1999), the basic 3D environment employs the same frame of reference as OpenGL® to generate the buildings and cloud effect.

The starting point is to create a window in which the visual environment can be viewed. The OpenGL® libraries, however, contain only rendering commands and are designed to be independent of any window operating system. Consequently, it contains no commands for opening windows or external inputs from joystick or mouse. As it is essential to develop an interactive 3D environment for piloting mission task elements, a window must be created in which to view and interact with the surrounding environment. This can be achieved by incorporating the OpenGL® Utility Toolkit (GLUT), libraries as detailed by Kilgard (1996) which can be summarised as a window system independent toolkit, simplifying the implementation of OpenGL® on different windows systems.

The visual environment created using computer graphics is simply a 2D image of the 3D surroundings. To display the surroundings accurately, the environment must be drawn as if it is actually 3D and lying on a plane inside the computer. OpenGL® employs a fixed frame of reference as shown in Figure 6.5, which differs from the aircraft frame of reference and is as described below

- The positive x-axis points to the right.
- The positive y-axis points upwards.
- The negative z-axis points into the computer screen.

The 3D world is constructed as the inside of a cube about the origin, with pictures of clouds textured onto the four sides and top surfaces. A landscape image is also pasted to the bottom surface of the cube simulating the ground scenery. The backdrop has been enhanced from a 2D surface with cloud effect simply by adding 3D mountains

and buildings to portray an airport. This involves calculating the vertex co-ordinates of each object and joining them together using a series of coloured polygons or triangles. This technique can also be employed to represent the helicopter model as illustrated in Figure 6.6, to define the manoeuvre flight path as a series of gates using the 'line-loop' command. Once the visual environment in which the mission tasks are to be flown has been established, it is possible to consider the view from which the operator attempts to pilot the helicopter.

6.4 Aircraft View

For the helicopter flight simulator developed, the aircraft view has been fixed to the origin. The illusion of flight is then created by rotating the helicopter attitude angles about each axis. The earth axis velocities are then integrated, giving the distances travelled over each time step and translating each axis by the appropriate amount. The perception of flight could quite as easily have been created by holding the environment stationary and translating the camera view around the task. However, it was felt that the technique adopted is more representative of the task, as the position of the pilot relative to the cockpit does not change during the flight. This is evidently the case when considering the addition of a cockpit view. The pilot's view of the cockpit does not change throughout the flight, but if the cockpit were translated through the scenery, any attitude changes would have to be displayed as a rotation of the cockpit, altering the pilots visual perception of the display.

6.5 Cockpit View

As stated previously the cockpit is fixed to the 2D computer screen (i.e. constrained to be zero in the z-axis). The attitude angles and body axis velocities used to portray vehicle motion can also be relayed to the pilot in the cockpit via a series of five instruments:

- Artificial horizon.

- Airspeed indicator.
- Vertical airspeed indicator.
- Turn indicator.
- Compass.

These instruments are constructed individually by laying a series of geometric shapes, such as polygons and circles, on top of each other until the desired effect is achieved [Giltrap (1995)]. However, for this application it was found that because many circles were required to produce the instrumentation, the procedure was computationally expensive. Each instrument was therefore drawn outwith Visual C using a Paintshop programme Paintshop Pro 6 (1999). The instrumentation could then be textured onto the cockpit frame using the same technique employed to include the cloud effect. The instrument needles are then drawn at the origin, the appropriate rotations indicating the vehicle response performed and finally translated to their respective instruments. It is imperative that these operations are carried out in this order or they will not represent the correct flight state or appear in the correct place. It is important again at this point to note the differing frames of reference in OpenGL® (Figure 6.1) and the helicopter body axis (Figure 6.5) as the instrument needle rotations and translations are considered.

6.5.1 *Instrument Needle Rotation and Translation*

Any change in control input results in a change in vehicle response, hence the instrument needles must change accordingly to update the recalculated vehicle states to the pilot. Due to the fact that the fourth order Runge-Kutta integration routine calculates the state response to a control input as a deviation from trim, each instrument needle must be calibrated to show the trim condition then any changes added to the initial state. The needles and rotations required for each instrument are now addressed

- Airspeed indicator – This shows the forward velocity of the aircraft relative to the earth as no atmospheric model is included. Here the needle is simply a thick line,

drawn such that it points to zero on the indicator, then rotated about the z-axis to indicate the trim velocity $\dot{x}_e$. Any perturbations are added to the trim value at the beginning of each loop before the needle is rotated. The final step (for all needles but only discussed once) is to translate the needle, from where it is drawn at the origin, to the centre co-ordinate of the textured instrument.

- Vertical airspeed indicator – This needle is constructed using the same process as described above, indicating the vertical airspeed $\dot{z}_e$.
- Turn indicator – representing the roll attitude of the vehicle, the turn indicator needle is simply two perpendicular lines meeting at the origin. The needle can then be rotated by Φ_e degrees to show the roll angle at trim, with any perturbations then being added.
- Compass – In this case the needle is represented by the helicopter, where the initial heading is chosen to be North. The four headings drawn on the compass are then rotated about the stationary needle by the yaw angle ψ.
- Artificial horizon – This was the most difficult needle to model as a sphere comprising two colours was required. The effect was achieved by representing one eighth of a semicircle by a series of polygons, rotating the shape 45° about the y-axis seven times, then changing colour and rotating once about the z-axis. Finally the needle is rotated about the x, y, z axes by the trim and deviation from trim angles θ, ψ, ϕ respectively.

As considered throughout this chapter, the cockpit view or helicopter model are fixed to the stationary viewing window. The background environment is then rotated and translated around the operator viewpoint. The effect of roll, pitch and yaw about the z, x, y axes respectively is achieved via the same process described for rotating the artificial horizon, however, to update the distance travelled by the vehicle is more complex.

The trim velocities U_e, V_e, W_e are added to the perturbation velocities u, v, w, then multiplied by the time interval $(x_2 - x_1)$ to give the distance travelled each time step. This in turn, is the distance the flight simulator environment must be translated. As the programme calculates only the distance flown each time step, an accurate visual simulation is only achieved by storing the distance translated at the end of each loop

and adding on the next perturbation. Once this has been achieved, another critical test can be performed on the flight simulator.

6.6 Real Time Simulation

The model to date has considered the linear HGS model and the environment in which the user can perform a chosen mission task. One of the many flight simulator criteria discussed in Section 6.2 is that the simulator must run in real time. If the output data does not represent a real time simulation, then any relation with Helinv generated results for the same mission task will be invalid. Real time simulation can be achieved by relating a user defined fixed time increment in the fourth order Runge-Kutta integration routine to the computer clock. It was found in this case that the flight simulator was running faster than real time and therefore needed to be slowed down. This was realised by creating a subroutine which held the timer in a loop until a time step of 0.04 seconds had elapsed, then the timer released, the next set of calculations performed and the graphics updated.

Figure 6.7 shows a screen shot of the flight simulator being flown at the forty knot trim condition. As the helicopter is flying in trim the controls are also trimmed, therefore the pilot is not applying any control input. Clearly, if the pilot is to perform a tracking task in the flight simulator, control inputs are required to alter the state parameters accordingly. This interaction is achieved by assigning the controls to the various axes of a calibrated joystick.

6.7 Control Input

The control inputs necessary to vary the vehicle states are required to be implemented in a smooth and efficient manner. One method of applying control inputs is to assign the four controls to different keys on the keyboard. This means that each control can be applied only as a constant step, which is not representative of the real system. Hence an alternative method incorporating a joystick has been employed.

The joystick used is a 'Flightstick' consisting of three axes. The Longitudinal and lateral cyclic are controlled by stick position as illustrated in Figure 6.8. The stick range on the x and y axes are each calibrated from ±1000 and the control input range on each axis assigned to the stick positions. The *z*-axis, which is a dial, can be calibrated in a similar way and can be assigned to control either main or tail rotor collective directly or through the AFCS. When a mission task was flown in the flight simulator, it was found that there was a signal processing error in the joystick z-axis which resulted in a large momentary change in the control value. This is demonstrated in Figure 6.9, which illustrates the recorded tail rotor collective applied during the slalom task at forty knots compared with that generated using linear inverse simulation. The signalling fault in the data can be seen in the flight simulator recorded time history. Clearly, when a handling qualities analysis is undertaken and the pilot attack in the tail rotor axis is calculated. These spikes in the data will cause extremely large and unrepresentative pilot attack parameters to be calculated. This can be counteracted however by filtering the z-axis time history. As a result, all control time histories recorded from the z-axis of the joystick from the flight simulator are subjected to a filtering process to eliminate the spikes in the main or tail rotor collective time histories. This has been demonstrated in Figure 6.10, where the tail rotor collective from Figure 6.9 has been filtered. The plot illustrates that, although the spikes in the plot have been reduced, some still remain. The overall result however, is much more representative of the actual control inputs and thus applicable to a handling qualities analysis.

Evidently the three joystick axes cannot fully simulate four helicopter controls. Although this is a model limitation, the problem can be overcome when selecting the desired mission task. For example, if the chosen manoeuvre were a longitudinal tracking task, the main rotor collective would be assigned to the *z*-axis of the controller. However if a lateral task is chosen tail rotor collective is required instead. Another solution to the problem presents itself in the following chapter when reduced order modelling is introduced. As the constrained and unconstrained matrices presented in Chapter 5 must be square, reduced order modelling will ensure the required number of controls is manageable by the three-axis joystick.

6.8 Conclusions

By creating a PC based helicopter flight simulator, mission task elements can be flown by various pilots over a range of flight speeds in real time. The user can select the mission task and the trim flight speed at which they wish to perform. The flight simulator requirements have all been strictly adhered to and the written C code has been proven to function correctly by comparison with Matlab® generated results. Emphasis has been placed upon a linear helicopter model capable of reproducing the time histories predicted using Helinv, not creating a realistic, high fidelity visual environment and helicopter. This is again reinforced in the following chapter when considering reduced order modelling. Although model limitations have been stressed, the model has still proved to be valid for the task required i.e. deriving flight data for a mission task element flown by a human operator. Also considered, is that the joystick is capable of implementing only three of the four helicopter controls, however, this problem is addressed by considering reduced order modelling in the following chapter.

Chapter 7

Reduced Order Modelling of the Vehicle Dynamics

7.1 Introduction

Linear inverse simulation was shown in Chapter 5 to produce similar state and control time histories for predefined manoeuvres as the full non-linear system. The correlation between the two models enabled the development of a helicopter flight simulator containing a linear HGS model. It was found in Chapter 6 that although the helicopter model incorporated in the flight simulator was linear, it was still difficult to pilot because of the unstable vehicle dynamics. Due to this, and also because the human operator is limited by the graphics libraries to applying only three out of the four controls in any manoeuvre, Chapter 7 considers a technique to further simplify the vehicle dynamics by reducing the number of states in the linear model. Naturally it is essential that the reduced order model can accurately reproduce the state and control time histories predominant in the manoeuvre while still representing the initial vehicle dynamics. This can be examined by analysing and comparing the eigenvalues of the two systems, along with the system responses to various control inputs such as a doublet.

7.2 Derivation of a Reduced Order Model

The full linear helicopter model, incorporated in the flight simulator, has proven difficult to pilot, thus Chapter 7 presents a method that can be used for deriving

reduced order dynamics of a helicopter. Employing a reduced order model instead of the full system can alleviate some of the workload on the pilot during the manoeuvre by discarding the unwanted vehicle modes. The reduced order model must however be derived according to the mission task being modelled, from the linearised equations of motions, which can be expressed as

$$\dot{\underline{x}} = \mathbf{A}\underline{x} + \mathbf{B}\underline{u} \tag{7.1}$$

where $\boldsymbol{A}$ and $\boldsymbol{B}$ are the system and control matrices respectively which contain the aerodynamic, relevant gravitational and velocity terms. The state vector $\underline{x}$ and the control vector $\underline{u}$ are again given by

$$\underline{x} = \begin{bmatrix} u & v & w & p & q & r & \phi & \theta & \psi & \Omega & Q_e \end{bmatrix}^T \tag{7.2}$$

$$\underline{u} = \begin{bmatrix} \theta_0 & \theta_{1s} & \theta_{1c} & \theta_{0tr} \end{bmatrix}^T \tag{7.3}$$

A common simplification used in helicopter dynamics is to assume a constant rotor speed and engine torque, hence Ω and Q_e may be removed from equation (7.2) giving

$$\underline{x} = \begin{bmatrix} u & v & w & p & q & r & \phi & \theta & \psi \end{bmatrix}^T \tag{7.4}$$

This state matrix is the basis for the reduced order model and is independent of the manoeuvre. Before discussing the effect of the chosen manoeuvre on the selection of state parameters for the reduced order model, it is worth noting that in many linearised models, ψ can be determined independently by integrating the yaw rate r, Thus heading can be removed from the state matrix. Inverse simulation however, exists in two forms. The first requires the manoeuvre to be performed with constrained side slip and the second with constrained heading. The constrained side slip case does not require the yaw angle to be retained in the constraint vector and thus can be calculated as described previously. The constrained heading case does however require the yaw angle to be retained, as it is fundamental to the constrained inverse algorithm. For this reason the heading has been left in the state matrix until the inverse simulation technique is considered.

The state matrix in equation (7.4) is a combination of state parameters, dominant in either the longitudinal or lateral directions. To derive a reduced order model of the vehicle dynamics, the dominant state parameters must be found for that manoeuvre and separated from the others. In the case of a fixed wing aircraft, these could easily be separated into longitudinal and lateral terms, where the longitudinal states u, w, q, are controlled by the elevator and the longitudinal terms v, p, r, are influenced by rudder and aileron inputs. This separation is not so distinguishable for the helicopter due to the cross coupling between the longitudinal and lateral states.

The reduced order model for the manoeuvre must be dynamically representative of the full linear system or the reduced order model is invalid. Clearly the same reduced order model cannot be applied to different manoeuvres such as the slalom which is a lateral manoeuvre, and the longitudinal quick-hop. This is again because each of these manoeuvres has different dominant states. Including these same states for each manoeuvre would result in dominant parameters being neglected, or a model which was not dynamically representative of the original. The solution therefore is to derive a unique reduced order model, specific to each manoeuvre.

7.3 Reduced Order Modelling of the Vehicle Dynamics for the Slalom

Recall the definition of the slalom manoeuvre defined by the Aeronautical Design Standard ADS-33D (1994) in Chapter 5, as illustrated in Figure 5.1. The results presented, generated using Helinv and linear Helinv, concentrated on the forty and eighty knot velocities and therefore for consistency, the results and analysis presented in this chapter will be for the same cases.

An appropriate starting point in assessing the validity of the reduced order model is to determine the full system aircraft modes. This is achieved by determining the system eigenvalues from the state matrix A equation (7.1). Table 7.1 shows the full system eigenvalues and modes for the Puma helicopter flying at 40 knots.

Table 7.1 Modes and Eigenvalues for the 40 Knot Full and Reduced Order Linear Helicopter Models

	Eigenvalues		
Mode	**Full System** (states $u\ v\ w\ p\ q\ r\ \phi\ \theta$)	**Reduced A** (states $u\ v\ p\ r\ \phi$)	**Reduced B** (states $u\ v\ p\ r\ \phi$)
Phugoid	$0.042 \pm 0.267i$	-0.0177	----------
Spiral	-0.212	-0.18	-0.186
Dutch Roll	$-0.344 \pm 1.25i$	$-0.31 \pm 1.25i$	$-0.308 \pm 1.25i$
Short Period	$-0.683 \pm 0.596i$	----------	----------
Roll	-1.54	-1.77	-1.77

Close inspection of the table reveals that the eigenvalue, representing the longitudinal phugoid mode, shows the mode and therefore the helicopter to be unstable, with a period of approximately 23.5 seconds and a time to double amplitude of 1.6 seconds. Thus providing an insight into why the helicopter flight simulator became increasingly difficult to pilot as the manoeuvre progressed. However as the slalom manoeuvre is primarily a lateral one, assumptions can be made which further reduce the complexity of the dynamic system,

- It is assumed that the manoeuvre will be flown in a co-ordinated manner such that v is strongly controlled (constrained sideslip). It follows that ψ is no longer a degree of freedom and can be removed from the state vector.
- As the slalom is essentially a lateral/directional manoeuvre, it can be assumed that pitch excursions will be slow and of small magnitude, hence q and θ may be neglected.

- The slalom is performed at a constant height, therefore the change in vertical velocity w will be negligible.

Applying these assumptions to the linearised model reduces the state vector to

$$\underline{x} = \begin{bmatrix} u & v & p & r & \phi \end{bmatrix}^T \tag{7.5}$$

The eigenvalues are again determined for the reduced order system and are found in the column *Reduced A* in Table 7.1. Clearly the lateral modes (spiral, dutch roll and roll modes) are still representative of the full order system while the longitudinal short period mode has been discarded. Finally, the phugoid mode has visibly altered in magnitude and is no longer representative of the full system eigenvalue. One solution to this is to disregard the final longitudinal term u from the state vector eliminating the phugoid mode. This solution is reinforced when reconsidering the structure of the linear inverse simulation algorithm presented in Chapter 5. The model is constructed such that the vector of constraint influenced states $\underline{x}_1$ and the vector of unconstrained states $\underline{x}_2$ require square state matrices $\boldsymbol{A}_{11}$, $\boldsymbol{A}_{12}$, $\boldsymbol{A}_{21}$ and $\boldsymbol{A}_{22}$ of equal size in order perform the necessary matrix calculations. The reduced order model therefore must also contain square state matrices of equal size. Examination of the reduced order model shows that $\underline{x}_1$ currently is a *1x3* vector, while $\underline{x}_2$ is a *1x2* vector resulting in state matrices of varying magnitudes. As a result, matrix multiplication will not function correctly in the algorithm. Again, the solution is to further reduce the constrained vector by assuming that as the manoeuvre is to be flown at a constant speed, the deviation from trim in forward velocity u is zero, therefore this term may be discarded leaving the state matrix

$$\underline{x} = \begin{bmatrix} v & p & r & \phi \end{bmatrix}^T \tag{7.6}$$

which can be subdivided into the constrained and unconstrained vectors of equal size

$$\underline{x}_1 = \begin{bmatrix} v & r \end{bmatrix}^T \qquad \underline{x}_2 = \begin{bmatrix} p & \phi \end{bmatrix}^T \tag{7.7}$$

Reduced B in Table 7.1 shows the eigenvalues for this reduced order system from which favourable comparisons can be made with the full system lateral eigenvalues. From these comparisons it is also clear that the validated reduced order model for the slalom, has neglected the unstable phugoid mode. As a consequence, the reduced order linear flight simulator should prove to be easier to pilot through the manoeuvre.

7.4 Reduced Order Model of Control Inputs

The reduced order model of the vehicle dynamics for the ADS-33D slalom manoeuvre has provided a solution to another problem encountered in Chapter 6. Recall that the Open Graphics Libraries (OpenGL) allowed only three control inputs to be applied throughout any one manoeuvre without alterations to the graphics libraries. This is insufficient to adequately control the helicopter model which requires four control axes.

When the reduced order model is applied, the constrained and unconstrained state vectors must again be of equal size with square state matrices, therefore the control vector must also be reduced to the same magnitude due to the matrix algebra. The definition of the ADS-33D slalom and the assumptions discussed can again be used to determine which controls are not required in the reduced order model,

- The slalom is essentially a lateral/directional manoeuvre, it can be assumed that pitch excursions will be slow and of small magnitude, hence longitudinal cyclic θ_{1s} may be neglected.
- The slalom is performed at a constant height therefore the change in main rotor collective θ_0 will be negligible.

The control time histories presented in Chapter 5, Figure 5.9, for the slalom show good agreement with these assumptions in that the manoeuvre is performed primarily using lateral cyclic and tail rotor collective, where the remaining controls do not significantly deviate from their reference trim value. The vehicle dynamics model has been validated by assessing the vehicle modes and eigenvalues. The control input

assumptions, and analysis of the control time histories, are not enough to verify the control input requirements. The results can be verified simply by applying a control input to the two models and comparing the state response.

7.5 Reduced Order Model Response

The reduced order vehicle dynamics have been derived in state space format, where the system response to a control input can be simulated and compared with the full system response. This is achieved by utilising the Simulink toolbox contained in Matlab®, where the vehicle dynamics for the linear and reduced order cases are required to be applied as transfer functions. The state and control matrices $\boldsymbol{A}$ and $\boldsymbol{B}$ can be evaluated for any reference trim state, allowing the transfer function corresponding to any combination of state and control to be established from

$$Y_H(s) = \frac{\underline{x}(s)}{\underline{u}(s)} = (sI - \mathbf{A})^{-1}\mathbf{B} \tag{7.8}$$

The tracking task under examination is a lateral manoeuvre controlling primarily the change in roll angle ϕ, using lateral cyclic. Hence the corresponding transfer functions representing the full and reduced order systems respectively are as follows

$$\left(\frac{\phi}{\theta_{1c}}\right)_{full} = \frac{27.94s^6 + 60.16s^5 + 975s^4 + 74.29s^3 + 34.39s^2 + 5.25s + 2.99}{s^8 + 3.72s^7 + 7.12s^6 + 9.23s^5 + 7.26s^4 + 3.43s^3 + 0.72s^2 + 0.2.1s + 0.033}$$

$$\left(\frac{\phi}{\theta_{1c}}\right)_{reduced} = \frac{27.95s^2 + 28.12s + 47.65}{s^4 + 2.58s^3 + 3.20s^2 + 3.46s + 0.55} \tag{7.9}$$

These transfer functions portray the reduction in the complexity of the vehicle dynamics for this combination of states and controls and also for the remaining combinations which are not shown here. Before any conclusions are drawn about the validity of the reduced order model for this particular scenario, it would be useful to

consider the full linear system response to a doublet control input, such as that depicted in Figure 7.1 for a one degree doublet input in lateral cyclic. The positive one degree, stick displacement causes the helicopter to roll and yaw to the right, resulting in a lateral velocity component v. Due to the main rotor being 'tilted', lift is reduced causing the helicopter to pitch nose down, lose altitude and gain forward velocity. This figure illustrates the extent of the cross coupling of the helicopter, where a lateral cyclic input clearly influences the longitudinal parameters. These response plots help understand the necessity to neglect the state parameters which are not essential to the manoeuvre, which are ultimately responsible for triggering potentially unstable or unwanted aircraft modes.

When a one degree doublet input in longitudinal cyclic is applied to the full and reduced order systems, the responses are as illustrated in Figure 7.2. The plots illustrate only the response of the key variables for the slalom manoeuvre and not the discarded parameters such as u and q. As the manoeuvre is performed with constrained sideslip, v is also neglected from Figure 7.2 as this response to a control input in the actual manoeuvre will be constrained to zero. The reduced order system is clearly a good approximation of the full system in all the key variables, resulting only in a slight increase in magnitude of the reduced order model response, reinforcing the model validation. Further weight is added to this validation in Figure 7.3, where the reduced order system response is again compared with the full order model for a one degree doublet input in tail rotor collective. Here the reduced order model compares favourably with the full system, although again there is a slight loss in the magnitude of the response.

As the reduced order dynamics have been shown to be representative of the full system model, the reduced order state and control vectors can be applied to the linear inverse simulation algorithm and the helicopter flight simulator. The reduced state space representation employed in the flight simulator has been verified by the application of a doublet control input as described previously. However, the reduced order linear inverse simulation is still required to show that it will generate the same state and control time histories as the full system.

7.6 Reduced Order Linear Inverse Simulation

The flight simulator has been shown to be difficult to pilot due to the linear nature of the model and the inherent instabilities of the helicopter. A reduced order model compliant with the selected MTE is therefore employed, thus the same assumptions are applicable to the reduced order inverse simulation helicopter model as in the flight simulator. Recall that in Section 7.3 equation (7.7), the constrained ($\underline{x}_1$) and unconstrained ($\underline{x}_2$) state vectors for the slalom manoeuvre became

$$\underline{x}_1 = \begin{bmatrix} v & r \end{bmatrix}^T \qquad \underline{x}_2 = \begin{bmatrix} p & \phi \end{bmatrix}^T$$

Also from the assumption that the manoeuvre is performed at a constant speed and height, the control and constraint vectors respectively can be rewritten as

$$u = \begin{bmatrix} \theta_{1c} & \theta_{0tr} \end{bmatrix}^T \qquad f_c = \begin{bmatrix} \dot{y} & v_c \end{bmatrix}^T$$

When the vehicle dynamics have been recast from state space form to that required by linear inverse simulation, the same iteration process as described in Chapter 5 is applied to determine the state and control time histories for the predefined manoeuvre. Nevertheless, the equations incorporated in the algorithm are altered, hence the algorithm is described again for the constrained sideslip case.

Recall that from equations (5.16) & (5.18) the yaw velocity is given by the kinematic expression in equation (5.19). When the assumptions about the reduced order model are applied equation (5.19) becomes

$$\psi = \frac{1}{m_{3_d}} \left[v_c - m_{2_0} \dot{y} + m_{2_d} \phi \right] \tag{7.10}$$

which when substituted back into the linearised Euler transformation gives

$$v = v_c \tag{7.11}$$

From equation (A5.12) the body fixed acceleration can be recast to represent the yaw rate r, and when reduced can be written as

$$r = \frac{1}{U_e}\left[m_{2_0}\ddot{y} - \dot{v} + W_e p\right] \tag{7.12}$$

Combining and rearranging (7.11) and (7.12) gives

$$x_1 = \mathbf{T}_1\dot{f}_c + \mathbf{T}_2 f_c + \mathbf{T}_3 x_2 \tag{7.13}$$

Where

$$\mathbf{T}_1 = \begin{bmatrix} 0 & 0 \\ m_{2_0}/U_e & -1/U_e \end{bmatrix} \quad \mathbf{T}_2 = \begin{bmatrix} 0 & 1 \\ 0 & 0 \end{bmatrix} \quad \mathbf{T}_3 = \begin{bmatrix} 0 & 0 \\ W_e/U_e & 0 \end{bmatrix} \tag{7.14}$$

Differentiating equation (7.12) gives the yaw rate acceleration

$$\dot{r} = \frac{1}{U_e}\left[m_{2_0}\dddot{y} - \ddot{v} + W_e \dot{p}\right] \tag{7.15}$$

where $\dddot{y}$ and $\ddot{v}$ are the absolute accelerations and governing the rate of change of acceleration at the start and end of each section. Combining and rearranging equations (7.15) and the linearised transformation of earth fixed to body fixed axis lateral acceleration in equation (A5.12), gives

$$\dot{\underline{x}}_1 = \mathbf{T}_1\ddot{\underline{f}}_c + \mathbf{T}_4\dot{\underline{x}}_2 + \mathbf{T}_5\dot{\underline{f}}_c \tag{7.16}$$

where

$$\mathbf{T}_4 = \begin{bmatrix} 0 & 0 \\ W_e/U_e & 0 \end{bmatrix} \qquad \mathbf{T}_5 = \begin{bmatrix} 0 & 1 \\ 0 & 0 \end{bmatrix} \tag{7.17}$$

Substituting $\underline{x}_1$ in equation (7.1) and $\dot{\underline{x}}_1$ in (7.16) into equation (A5.7) allows the unconstrained states to be expressed in terms of the constraint influenced states. Finally the solution can be simplified to the desired form as shown in equation (A5.16) where the constrained state and control vectors are defined as

$$\mathbf{A}_c = \left[I - \mathbf{B}_2\mathbf{B}_1^{-1}\mathbf{T}_4\right]^{-1}\left\{\mathbf{A}_{22} - \mathbf{B}_2\mathbf{B}_1^{-1}\mathbf{A}_{12} + \left[\mathbf{A}_{21} - \mathbf{B}_2\mathbf{B}_1^{-1}\mathbf{A}_{11}\right]\mathbf{T}_3\right\}$$

$$\mathbf{B}_c = \begin{bmatrix} \left[I - \mathbf{B}_2\mathbf{B}_1^{-1}\mathbf{T}_4\right]^{-1}\mathbf{B}_2\mathbf{B}_1^{-1}\mathbf{T}_1 \\ \left[I - \mathbf{B}_2\mathbf{B}_1^{-1}\mathbf{T}_4\right]^{-1}\left(\left(\mathbf{A}_{21} - \mathbf{B}_2\mathbf{B}_1^{-1}\mathbf{A}_{11}\right)\mathbf{T}_1 + \mathbf{B}_2\mathbf{B}_1^{-1}\mathbf{T}_5\right) \\ \left[I - \mathbf{B}_2\mathbf{B}_1^{-1}\mathbf{T}_4\right]^{-1}\left(\mathbf{A}_{21} - \mathbf{B}_2\mathbf{B}_1^{-1}\mathbf{A}_{11}\right)\mathbf{T}_2 \end{bmatrix}^T$$

Once the reduced order linear algorithm is constructed for the ADS-33D slalom MTE, the state and control time histories can be found. Figure 7.4 illustrates these compared with the full linear model for the forty knot case. As the manoeuvre is performed in this case with constrained sideslip, v has been neglected from the plots, as this parameter does not deviate from its initial trim value. Figure 7.4 demonstrates that the predicted state parameters are almost identical to those generated from the full linear model. This is achieved by applying different control inputs as can be viewed in the η_{1c} and η_p plots, which is necessary in order to compensate for the longitudinal cyclic and main rotor collective inputs which are no longer applied.

Finally the damped oscillations contained in the control time histories, arising from the modes associated with the 'full' constrained state matrix are again considered, where the modes are calculated from the constrained matrix $\boldsymbol{A_C}$. Clearly the single constrained mode of the reduced order model exhibits a transient oscillation similar to one represented in the full linear model and on close inspection, the eigenvalue shows the mode to be of the same period, approximately 1.2 seconds. This reinforces the conclusion that the reduced order vehicle dynamics are still representative of the full system. Table 7.2 demonstrates the constrained mode eigenvalues for the full and reduced linear models at 40 knots and also for a higher speed case of 80 knots.

Table 7.2 Comparison of the Constrained State Matrix Modes at 40 & 80 Knots

Mode	Speed	Eigenvalue	Period	Damping
Mode 1	40kn Full	-0.053 ± 5.05i	1.244 secs	1.5 %
	40kn Reduced	-0.017±4.98i	1.262 secs	
	80kn Full	-0.062 ± 4.98i	1.262 secs	1.26 %
	80kn Reduced	-0.002±4.97i	1.264 secs	
Mode 2	40 knots	-0.101 ± 2.62i	2.398 secs	3.83 %
	80knots	-0.166 ± 2.73i	2.302 secs	6.07 %

These results demonstrate that even though the flight speed increases, the constrained modes do not deviate significantly from their low speed values. One noticeable point however is that in 'mode 2' for the full linear model (as this mode has been neglected in the reduced order system) the damping factor has almost doubled. This is also evident in Figure 7.5, which illustrates the slalom manoeuvre flown this time at 80 knots, where again the state parameters are almost exactly the same as calculated in Chapter 5 using the full linear and non-linear models. The control time histories are seen to exhibit the same constrained modes of the same period in the input, however, the plots show that they are not as prominent because the damping factor has increased, suggesting the mode becomes less influential as the manoeuvre speed increases.

7.7 Conclusions

Chapter 7 has considered a reduced order model of the vehicle dynamics which can be applied to both the helicopter flight simulator and the linear inverse simulation. This is because the helicopter flight simulator was difficult to pilot due to limitations of the linear helicopter model and the application of the controls in the flight simulator. The reduced order model is designed with careful consideration being given to the manoeuvre the user wishes to perform. The state parameters affected throughout the

duration of the manoeuvre are separated from those which will deviate little from their reference trim state, leaving a reduced order model which is still representative of the initial vehicle dynamics. The validity of the reduced order system is verified by considering the eigenvalues and periods of the remaining modes and comparing with the full system. An analysis of the ADS-33D slalom has been performed in Chapter 7, verifying that the reduced order linear inverse simulation, produces results consistent with the full system response.

Chapter 8

Identifying Pilot Parameters by Experiment

8.1 Introduction

A reduced order linear helicopter model for a lateral task was derived in Chapter 7. This model can be applied to the flight simulator described in Chapter 6 and the linear inverse algorithm discussed in Chapter 5. The main aim of the work, which is to demonstrate the necessity to incorporate pilot effect into the helicopter simulation for an initial handling qualities assessment, can now be addressed by determining the state and control time histories for a predefined lateral task using both simulation techniques. Chapter 8 therefore describes the experimental set-up procedure required for generating the data necessary to enable a handling qualities study. This includes selecting and mathematically defining the mission task such that the required Level 1 attitude quickness ratings are achieved and that the task can be replicated in the flight simulator. It is demonstrated that the slalom task considered to date does not exhibit Level 1 attitude quickness ratings and is unsuitable for a handling qualities analysis. The following section assesses variations of this task, illustrating how Level 1 attitude quickness ratings are unobtainable with a polynomial task definition but also highlights the problems which arise in the attitude quickness assessment when the task is defined using a piecewise modelling technique.

The task is selected with the aid of a final criterion, which is that the task must be realisable in the flight simulator by the human operator. This can be examined by determining the equalisation characteristics of the human operator, relating the primary controlled state variable in the task to the control input for the inverse simulation derived time histories. The HEC determined from the PPM considered in

Chapter 2 also provide an insight into how the operator performs the task and can even show how the pilot adapts to a new task. The final discussion in Chapter 8 relates again to the handling quality assessment by studying the pilot attack parameter.

8.2 Defining and Selecting a Mission Task Element

In order to attain meaningful results from the handling qualities analysis, a manoeuvre which portrays Level 1 handling characteristics, must first be defined according to the ADS-33 documents. As considered in Chapter 2, the slalom task performed over a distance of 608 metres with a maximum lateral distance of ±15.2 metres, when defined as either global or piecewise polynomial equation, does not yield the required Level 1 attitude quickness ratings. Consequently, the slalom task must be redefined mathematically so that the appropriate attitude quickness Levels are achieved or, a new task must be considered.

The approach adopted in reassessing the task was first to consider that the helicopter model employed in the flight simulator and the inverse simulation algorithm is linear. Therefore, valid only for small perturbations from trim. The large perturbations from trim required to complete the task are too great to be consistent with use in a linear helicopter model. Thus the task must be performed over a shorter period of time, whilst maintaining the same speed. This can be achieved either by shortening the manoeuvre distance or by performing only the first half of the task called the 'Lateral Jink'.

8.2.1 The Shortened Slalom Task

This task is essentially the same as the slalom considered throughout the text, however, the manoeuvre time has been reduced by decreasing the longitudinal manoeuvre distance by half to 304 metres, while keeping the maximum lateral distance the same as illustrated in Figure 8.1. Not only does this step reduce the

manoeuvre time to comply with the 'small angle' rule, but it also increases the aggression Level of the task by requiring larger and faster changes in roll angle. Figure 8.2 demonstrates the roll angle ϕ and roll rate p, generated using the linear inverse simulation algorithm for the global polynomial defined shortened slalom task. The plot illustrating ϕ, again demonstrates the smooth nature of the roll angle due to the smooth global polynomial manoeuvre definition, where the maximum roll angle has increased from five degrees in the 608x15 metres slalom to over thirty degrees in the shortened task. The roll attitude quickness parameters can again be calculated using the technique described in Section 2.3.2 and plotted on a quickness chart as illustrated in Figure 8.3. The quickness parameters attained show that compared to the 608x15 metre slalom, the attitude changes have increased as expected. However, the quickness parameters have remained approximately the same except for the first one which now exhibits Level 1 handling characteristics. The large change in the first quickness parameter is due to the fast roll rate required to give the initial roll angle for the task. The remaining parameters however are similar to those calculated for the original slalom because the increase in roll angle ϕ results in an increased roll rate. Thus the ratio of roll rate to roll angle has remained approximately the same.

Clearly this manoeuvre definition is again not satisfactory for a handling qualities assessment, therefore a piecewise definition may also be considered. This modelling technique is advantageous in this situation because the initial roll rate can be controlled such that Level 1 handling qualities are achieved. Figure 8.4 depicts one such piecewise slalom, where five individual piecewise sections are applied as a series of seventh order equations and straight lines of equal length to represent the flight path. Figure 8.5 then illustrates the roll angle ϕ and roll rate p for the Puma helicopter performing this task as predicted by the linear inverse algorithm. The plot shows that if this task to be completed, roll angles exceeding one hundred and fifty degrees and roll rates approaching five hundred degrees per second must be achieved. Although these large roll angles and roll rates are clearly not feasible in a helicopter, it should be noted that these parameters were calculated using a numerical integration routine and are subject to change if a smaller time step is applied in the algorithm. Even so, the maximum roll angle and roll rate required to perform this task in the

Puma helicopter at the chosen speed still prove to be unachievable, thus the shortened piecewise slalom model was discarded.

8.2.2 The Lateral Jink Manoeuvre

The Lateral Jink manoeuvre definition considers only the first half of the slalom task where, in the global polynomial case, the flight path can be defined by a fifth order polynomial equation, generating the flight path depicted in Figure 8.6. The state and control parameters are calculated from the inverse algorithm and the key parameters ϕ and p, can be viewed in Figure 8.7. From these time histories, the attitude quickness parameters can be calculated and are plotted in Figure 8.8.

This task can also be defined using a piecewise modelling technique. However, instead of attempting to define the flight path, the task this time is outlined by piecing together fifth order polynomial equations to represent the aircraft's lateral velocity. The maximum lateral velocity attained in the task is defined such that when integrated to give the flight path, the maximum lateral displacement required is found, in this case 15.2 metres, resulting in the piecewise flight path also depicted in Figure 8.6. An added advantage to the piecewise definition is that if the defined task does not yield Level 1 handling qualities, the time required to achieve the maximum or minimum acceleration, velocity or displacement, depending on how the task is defined, can be altered making the manoeuvre more or less aggressive as required. The velocity definition can be considered, as illustrated in Figure 8.9, to consist of five distinct phases

- The time required to reach the maximum velocity.
- The time required to slow down from the maximum velocity to zero.
- The time taken to fly along a straight line through the gate with zero lateral velocity.
- The time to reach the minimum (maximum negative) velocity.
- The time for returning to zero lateral velocity.

where the change in velocity is represented by [Leacock(2000)] as

$$v = \left[5\left(\frac{t}{t_1}\right)^5 - 15\left(\frac{t}{t_1}\right)^4 + 10\left(\frac{t}{t_1}\right)^3 \right] v_{\max} \qquad (8.1)$$

where t_1 represents the time for the manoeuvre segment. The equation can also be adjusted to represent a change in direction by making v negative.

Figure 8.7, which illustrates the state time histories for the polynomial defined lateral jink task also depicts the states ϕ and p for the velocity constrained piecewise task. The time taken to reach the maximum and negative maximum velocities has been selected such that the attitude quickness parameters are Level 1 as viewed in Figure 8.8. This point highlights the difference between the two approaches to manoeuvre modelling, whereby, if the piecewise definition is selected correctly, Level 1 handling qualities will be yielded. On comparison of the two roll angle time histories the more aggressive approach which must be adopted to perform this Level 1 task in relation to the polynomial defined task is clearly visible, where the larger roll angle is reached within the first second of the manoeuvre. It can also be seen from these plots that during the sections with constant lateral velocity there are transient oscillations in the time histories for the piecewise task. These cause uncharacteristic attitude quickness ratings due to the linear definition of the respective manoeuvre sections. The attitude quickness parameters representing the transient oscillation are visible for small changes in roll angle within the Level 1 ratings section. Verifying the suitability of the manoeuvre for a handling quality analysis therefore focuses on the larger changes in roll angle associated with a change in velocity or acceleration.

Although the piecewise lateral jink definition describes Level 1 handling qualities, a final test is performed before a task is flown in the flight simulator and further results presented. This is to ensure that the roll angle time history can be applied as the command signal of the MMCS and produce realistic HEC, i.e. the task is achievable by the pilot.

8.2.3 Calculation of Human Operator Equalisation Characteristics

The state and control time histories derived using the inverse algorithm were described in Chapter 5 as being the ideal state and control time histories for a task. This is because the command signal generated using this technique is without human operator limitations. The human equalisation characteristics derived from the PPM for a Helinv generated command signal represent the optimum achievable HEC for the task being performed without a human operator.

The lateral jink manoeuvre, like the slalom task described previously is primarily a single axis tracking task in the lateral axis, therefore the same assumptions can be used when deriving the transfer function representation of the vehicle dynamics by relating the roll angle to lateral cyclic. The vehicle dynamics are applied to the MMCS allowing the optimum pilot characteristics to be determined for the command signal time history, in this case the roll angle ϕ.

The optimisation technique applied for determining the HEC was chosen to be a constrained optimisation programme implemented in Matlab®. The form of the constrained optimisation utilised is known as Sequential Quadratic Programming (SQP) as discussed by Grace (1992). Each unknown parameter, in this case the equalisation characteristics (gain lead and lag), is assigned a range of values to be optimised, such as the range considered in Section 3.9.1 for each equalisation characteristic. Each range is then further split into a sequence of subsections. Essentially the process can be described as a method whereby the solution process proceeds by solving the sub-problem for each iteration. The unknown HEC are optimised for each iteration by finding the combination of equalisation characteristics that give the minimum mean square error between the system input and the system response. Table 8.1 demonstrates the human equalisation characteristics calculated for the polynomial and piecewise defined lateral jink and slalom manoeuvres at forty knots.

Table 8.1 Comparison of the Optimal Human Equalisation Characteristics For The Polynomial and Piecewise Defined Lateral Jink Task

	Error	Gain	Lead Time	Lag Time
Polynomial Lateral Jink	9.713	0.147	0.648	0.1
Piecewise Lateral Jink	53.02	0.0151	5.3	0.1
Polynomial Short Slalom	50.47	0.148	0.857	0.1

In the case of the piecewise lateral jink, the minimum error tended to the upper boundary of the lead time constant which was set at 5.3 seconds, suggesting that the lead time was still higher than this or possibly optimum equalisation characteristics could not be obtained. Although this large lead time exhibited Level 1 handling qualities, demonstrates that this highly aggressive task is beyond the limitations of the human operator when performed at forty knots in a Puma helicopter. According to McRuer & Krendel (1957), the operator gain should be between 0.1 and 2.5 seconds, although in extreme circumstances higher lead times have been recorded.

Although Level 1 handling qualities can only be obtained for this task with a highly aggressive mathematical definition, this task is not considered further for a handling quality analysis, as the human operator cannot adequately perform it. This then leaves only the two polynomial defined tasks, the short slalom and the lateral jink, which from Table 8.1 can be seen to exhibit similar gains. The error for the global polynomial, short slalom task, as expected, is much larger than that found for the global polynomial lateral jink case, as much larger roll angles must be achieved in the same period of time. The higher pilot lead time in the more difficult short slalom task, suggests that because the task is more aggressive than the lateral jink, more control input prediction is required by the pilot. Finally, the optimised pilot gains, which are a measure of the operators ability to respond to an error in the amplitude of a controlled variable, are approximately the same for both tasks. This result implies that although both tasks are flown with different control strategies, the operator is equally capable of responding to an error in the controlled variable.

8.2.4 Selecting a Suitable Mission Task for the Linear Helicopter Model

The preliminary human equalisation characteristics and attitude quickness parameters calculated for the tasks considered thus far do not meet suggested requirements for the manoeuvre definition. ADS-33D (1994) handling qualities analysis stipulates that Level 1 ratings must be realised for the task to be valid. These ratings are achieved from quick control inputs, resulting in a high attitude rate and large change in roll angle, which is contradictory to the small angle approximation rule applied in the linear helicopter model. It has also been demonstrated that the piecewise task requires operator characteristics which are unattainable. Thus a smooth global polynomial mission task definition, which does not provide Level 1 attitude quickness ratings is required if realistic HEC are to be found from the MMCS.

To achieve useable results, it is essential that the task can be piloted in the desktop flight simulator and operable human equalisation characteristics can be determined from the resulting time histories. The global polynomial shortened slalom task has been shown to be unsuitable for use in conjunction with a linear algorithm due to the small angle approximation. This is in sharp contrast with the level 1 HQR which require large changes in roll angle with a fast roll rate. The global polynomial lateral jink defined task however lends itself well to the stated requirements. Although it does not exhibit Level 1 HQR for all attitude quickness parameters, results are presented for this lateral task due to the unsuitable equalisation characteristics, or unsuitably large attitude changes of the other tasks considered.

8.2.5 Real Roll Attitude Quickness Calculation

Recall that the roll angle time history is applied as the command signal of the MMCS depicted in Figure 3.3 and the HEC then optimised. The output from the system can then be found which has the pilot effect on the command signal added as illustrated in Figure 8.10. If an attitude quickness assessment is to be accurately performed, the roll rate with added pilot effect is also required. This can be found simply by differentiating the roll angle time history with added pilot effect as illustrated in Figure 8.10. It is clear from these plots that the pilot model has introduced a delay into

the Helinv data, which is larger at the start of the task than in the middle and end sections. Figure 8.11 compares the roll attitude quickness parameters for the Helinv generated roll angle quickness chart in Figure 8.3, with the output from the MMCS for the same case. The effect of the optimal pilot limitations on the roll angle is evident, resulting in either a reduction in the net roll angle or a decrease in the attitude for the important 'navigation' quickness parameters. There is some discrepancy between the guidance parameters towards the top left of the graph, which can be explained by the different strategy adopted at the beginning of the task. This result suggests that although the main navigation quickness ratings for this task have remained approximately the same, smaller changes in roll angle are required by the pilot to achieve them due to the delay introduced at the beginning of the task.

So far, this chapter has provided the first complete example of the thesis main aim, which is to demonstrate how pilot model parameters can be used in an initial handling qualities assessment. A technique has been presented whereby pilot effect can be added to the linear inverse simulation output for any given MTE or linear helicopter model. The pilot effect on the attitude quickness ratings has been presented, demonstrating that the delay introduced by the pilot results in a smaller roll angle time history being required to successfully perform the task.

The next step in the analysis is the pilot attack calculation, however another problem arises at this point. Clearly two sets of control input time histories are required. Firstly the Helinv lateral cyclic and secondly, the MMCS output with additional pilot effect. This can only be achieved by finding the optimum HEC for the control input and the control input plus pilot effect. This is evidently not possible as different lead times will be forecast, rendering a pilot attack comparison invalid. Figure 8.12 however illustrates the lateral cyclic control and its derivative, calculated from Helinv, while Figure 8.13 shows the corresponding pilot attack chart. Due to the oscillatory nature of the control input predicted by Helinv, a series of attack parameters can be seen across the chart with rating 2.5. The main, first attack parameter however, can be seen at the top of the chart with rating 5 and eighteen percent stick displacement. It is also evident from Figure 8.12 that towards the end of the task lateral cyclic 'tails away' rather than returning to its trim position. This is because as the pilot nears the end of the task, lateral cyclic is applied in order to decrease the lateral velocity in meet the

specified end of manoeuvre criteria. The effect of this is also clearly visible in Figure 8.10 where the roll rate (p) is increased in order to roll the helicopter out of the turn, hence reducing lateral velocity.

8.3 Flight Simulator Set-up

Chapter 6 focuses on the development criteria for building the helicopter flight simulator, but does not demonstrate how the task should be included in order for the pilot to close the loop. When flying a lateral task such as the slalom or lateral jink, ADS-33D recommends that the pilot uses the runway to aid in flying the task, where the edges are the required lateral distances and the centre markings also reresent the task centreline. However, in the flight simulator the required flight path, defined by the same polynomial equation in the inverse algorithm, is plotted in conjunction with a series of gates representing the start and finish of the task and where the maximum lateral translation occurs. The flight path is plotted in the simulator, such that the start and end of the flight path line coincide with the start and finishing gates respectively, as illustrated in Figure 8.14. The maximum lateral distance is then achieved at the middle of the gate representing the maximum lateral distance. The three gates are each two metres wide, representing the maximum tolerable flight path deviation at these points. The pilot then attempts to fly the task by following the manoeuvre flight path.

8.4 The Reduced Order Helicopter Model Performing the Lateral Jink Task

A reduced order model was described in Chapter 7 for the slalom mission task element consisting of four states and two controls

$$\underline{x} = \begin{bmatrix} v & p & r & \phi \end{bmatrix}^T$$

$$\underline{u} = \begin{bmatrix} \theta_{1c} & \theta_{0tr} \end{bmatrix}^T$$

Like the slalom task, the lateral jink is primarily a lateral tracking task. Consequently, the same reduced order model may be applied in both the flight simulator and the inverse algorithm. It is not necessary at this point to reassess the reduced order helicopter model validation however, verification that the resulting time histories are still representative of the full linear model must be provided. Figure 8.15 compares the four states and two control time histories of the reduced order model with those of the full linear model. Clearly, as found previously with the slalom task, the reduced states are almost identical to the full system. As a result of the two longitudinal control inputs being constrained to their trim values there is a slight change in the control strategy, which again emphasises the cross coupling between the longitudinal and lateral helicopter modes, whereby in this case, a lag is introduced into the tail rotor collective.

It was also found that when the reduced order roll angle time history was applied as the command signal for the MMCS, HEC similar to those calculated using the full linear model were obtained. These results again are not presented here due to the previous model validation and the similarity between the full and reduced order roll angle time histories. The mission task element and vehicle dynamics may now be applied to the flight simulator discussed in Chapter 6.

8.5 Pilot Control Input Strategies For Flying The Lateral Jink in the Flight Simulator

"The single axis tracking task is to be performed by at least three pilots where at least two of the attitude quickness ratings must be similar if the task and results are to be valid" [ADS-33D (Anon.]

Three human operators who could offer varying degrees of experience, were asked to take part in the experiment with pilot A being the least experienced operator. Pilot A however is an experienced engineer but had the least flying time in the flight simulator flying the reduced order helicopter model through the prescribed task. The results listed as pilot B and pilot C were actually recorded for the same human operator but the results recorded as pilot C where after the pilot had been exposed to

the task for a greater period of time than as pilot B. The results for these two cases were recorded from the author flying the tasks. Finally pilot D was considered to be the most experienced operator with hands on piloting experience. Each pilot was required to fly the single axis lateral jink manoeuvre at thirty, forty and fifty knots a minimum of five times for each flight speed in the reduced order Puma helicopter model.

It is possible to perform this single axis tracking task using only lateral cyclic, tail rotor collective or indeed a combination of both as derived from the inverse algorithm. Clearly if the control strategy adopted by the pilot differs greatly from the optimal inverse simulation control time histories i.e. the pilot flies the task predominantly with one control, the results will not be comparable. This is demonstrated in Figure 8.16, which illustrates the forty knot roll angle time history recorded from linear inverse simulation when the task is performed using a combination of lateral cyclic and tail rotor collective, depicted in Figure 8.17. Also depicted in Figure 8.16 are the lateral cyclic and tail rotor collective roll angle time histories for a human operator performing the task using only one control and the control strategies plotted in Figure 8.17. From Figure 8.16 it is evident that the different control strategies adopted yield very different roll angle time histories. The lateral cyclic only task, where over eighty percent of the control is applied, is described as rolling to the left and then back to trim, whereas the tail rotor task produced roll angles in the opposite direction, requiring only small control inputs. This plot proves that if comparisons between the human operated flight simulator tasks and the inverse simulation generated time histories are to be made, the same control strategy must be adopted for both cases otherwise different tasks will have been flown. As Helinv cannot define tasks performed using only one control input, the task must be flown in the flight simulator using a combination of lateral cyclic and tail rotor collective.

8.6 Conclusions

Chapter 8 initially considered two tasks, the shortened slalom and the lateral jink, both of which may be defined mathematically using polynomial or piecewise

modelling techniques. The polynomial defined lateral jink task was chosen to be flown in the flight simulator, even though the task did not exhibit Level 1 handling qualities. This was simply because the piecewise defined tasks could not physically be flown by the pilot as uncharacteristically large roll angles and lead times are required. The shortened slalom task was realisable by the pilot in the flight simulator but was not selected due to the small angle approximation in the linear helicopter. Section 8.5 then considered three control strategies that may be employed by the pilot when flying the lateral jink task and why both techniques must employ the same control strategy. It was found that because Helinv can only predict flight data for the task when flown using a minimum of two control inputs, that the strategy involving lateral cyclic and tail rotor collective should be employed in the flight simulator.

Chapter 9

Comparison of Simulation Techniques - Pilot Model Parameters and Handling Qualities

9.1 Introduction

The aim of this chapter is to present an example of the work discussed throughout the thesis. A handling qualities study is performed on the data generated from the two simulation techniques, inverse simulation and a flight simulator, when flying the lateral jink task described in the previous chapter. The importance of correctly interpreting the task and how differences in control strategy effect the vehicle flight and HEC are considered, then the HEC derived for the range of pilots are presented. The handling qualities analysis then goes on to demonstrate the similarity between the results from the two simulation models, where conclusions can be drawn about the validity of the inverse model with incorporated pilot effect. The chapter finally reintroduces the multiple axis concept considered in Section 4.5, illustrating the difference between representing the vehicle dynamics in one control axis and two or more axes and the consequences for the handling qualities study.

9.2 Single Axis Analysis of Flight Simulator Results

The state and control time histories were recorded for each series of flights by all pilots throughout the prescribed flight speed range. The recorded roll angle time histories were then applied as the command signal to the MMCS to determine the pilot equalisation characteristics, where the vehicle dynamics are represented only by

the transfer function $\phi(s)/\theta_{lc}(s)$. These results are presented in Table 9.1 for the series of flights performed by pilot C at forty knots. The corresponding flight paths are recorded in Figure 9.1 and the roll angle time histories in Figure 9.2.

Table 9.1 Human Equalisation Characteristics for Pilot C Performing the Forty Knot Lateral Jink

Flight	Error	Gain	Lead	Lag
Linear Helinv	8.888	0.129	0.771	0.1
C_1	7.998	0.1674	0.654	0.1
C_2	9.896	0.152	0.762	0.1
C_3	12.293	0.126	1.099	0.1
C_4	10.686	0.11	1.279	0.1
C_5	9.766	0.14	0.968	0.1

The first noticeable result from Table 9.1 is that the optimisation errors, gains and leads are all of the same magnitude respectively, no definitive conclusions can be drawn about the pilots' learning process because there is no distinct pattern in the HEC. (Pilot C however, is 'experienced at piloting the task and if a less experienced operators characteristics were considered, some insight into the learning process should be obtainable). Figure 9.1 illustrates this by showing that the flight path for task C_1, where the first flight in the series, produces the most similar flight path and roll angle time histories to those generated from Helinv. The roll angle in Figure 9.2, however, shows that for this task, a large delay has been introduced in the first half of the task, which is not evident in the latter stages of the task, resulting in a high gain. The remaining attempts C_2 to C_5, all demonstrate similar flight paths and roll angle time histories for the first half of the task, where a large roll angle is required to reach the maximum lateral displacement. However, in the latter section different strategies are employed. This is clear in Figure 9.2, where, after the middle gate turn for C_3 and C_4, the pilot rolls back too early then attempts to correct this by slowing the roll rate reversal, resulting in high lead times. C_2, like task C_1 however, roll back to the left (positive to negative roll angle) after the middle section faster than Helinv, resulting in a lower lead time and a higher gain.

9.2.1 Comparison of HEC Effect on Helinv Output

Another interesting comparison that can be made between the optimum HEC and those calculated for an actual human operator, is to determine the effect of the actual human operators equalisation characteristics on the Helinv output. This has been illustrated in Figure 9.3, where the HEC for the first flight by pilot C were applied to the PPM in the MMCS to determine their effect on the output. The plot demonstrates that although the operators HEC differ from the optimum HEC, both the optimum and operator output produce similar roll angles. The operators HEC however, introduce an additional damped oscillation in the roll angle due to the decrease in the lead time constant.

9.2.2 Handling Qualities Assessment For Each Task Flown By Pilot C

The roll angle and roll rate time histories recorded from each task for pilot C can be subjected to a handling qualities assessment as described in Section 2.3.2, and plotted on an attitude quickness chart as illustrated in Figure 9.4. It is evident from this graph that each time pilot C flew the task, quickness parameters requiring larger attitude changes than those calculated for Helinv are recorded at the start of the task. This is in sharp contrast to the 'Helinv plus pilot effect' parameters presented in Chapter 8, Figure 8.10, however the remainder of the parameters follow the same predicted pattern.

The final step in the handling qualities assessment is a pilot attack calculation as considered in Section 2.6, which can be used to determine a pilots strategy. Figure 9.5 illustrates the attack parameters for Helinv and again for the series of missions recorded by pilot C. The attack parameters for the pilot tend to relate to vehicle guidance and stability rather than those predicted for Helinv, which suggest that the helicopter is 'navigated' through the task. It is also interesting to note that the pilot attitude changes, recorded in the quickness ratings which, are larger than Helinvs, result from small to medium stick displacements that are smaller than the Helinv control input. This is possibly due to the human operator controlling the task primarily with tail rotor as opposed to lateral cyclic as considered later in the chapter.

Although Table 9.1 and Figures 9.1 to 9.5 offer a great deal of insight into how the operator performed the series of flights, it is difficult to extract an overall assessment of the pilot skills or learning process. In this case no information can be extracted on the pilot learning process because there is no clear improvement on how the task was flown each time. Clearly though, differences in flight performance have been recorded making an overall pilot assessment difficult to achieve. As a result, it is not possible to represent the pilot by just one set of HEC. Thus in Section 9.3, the pilot is represented by the average error, gain lead and lag times. It should however be stressed that if a particular result differs greatly from the others, it should be discarded from the average calculation.

9.3 Single Axis Analysis of 'Averaged' Pilot Flight Simulator Results

The average gain lead and lag times were found for each series of flights, for each pilot and are presented in Tables 9.2 to 9.4.

Table 9.2 Human Equalisation Characteristics for 30 Knot Lateral Jink

Pilot	Error	Gain	Lead	Lag
Linear Helinv	3.191	0.141	0.702	0.1
A	6.253	0.116	1.007	0.1
B	5.255	0.1426	0.808	0.1
C	6.98	0.133	0.895	0.1
D	6.253	0.145	0.827	0.1

Table 9.3 Human Equalisation Characteristics for 40 Knot Lateral Jink

Pilot	Error	Gain	Lead	Lag
Linear Helinv	8.888	0.129	0.771	0.1
A	6.476	0.188	0.662	0.1
B	14.34	0.122	1.0524	0.1
C	10.127	0.139	0.952	0.1
D	9.712	0.133	1.066	0.1

Table 9.4 Human Equalisation Characteristics for 50 Knot Lateral Jink

Pilot	Error	Gain	Lead	Lag
Linear Helinv	25.650	0.107	1.005	0.1
A	11.048	0.175	0.754	0.1
B	22.106	0.118	1.33	0.1
C	20.279	0.111	1.304	0.1
D	17.453	0.087	1.752	0.1

Section 8.2.3 suggested that the HEC derived using inverse simulation were optimum. Hence the human operator gain should not exceed the Helinv gain, the lead time should not be less than that generated from inverse simulation and the pilot error should be greater than Helinv's. All the average pilot lead terms over the flight speed range examined for pilots B, C and D adhere to these criteria. The corresponding gains are generally the same as those calculated from Helinv. However, some cases such as pilot C at forty knots are slightly greater but still satisfactory, whereas the gains and lead times for pilot A clearly do not fit the previous definition.

It is also clear from the tables that as flight speed increases for Helinv, so too does the operator lead time whilst the gain decreases. This is due to the fact that as flight speed increases, the operator has less time, thus is less able to respond to an error in the controlled variable. if the pilot is less able to respond to an error in the controlled variable with increasing speed, it follows that in order to successfully perform the task, an increased prediction of the required control inputs is necessary, hence an increase in lead time. Finally Tables 9.1 to 9.4 demonstrate that the lag time has tended to the minimum boundary in each case. This is simply because the operator has applied the control inputs with a smooth transition, i.e. no oscillatory inputs are applied, causing a lag time constant to be introduced. However, in a more vigorous manoeuvre such as the piecewise lateral jink, lag times will inevitable be introduced by the human operator. Clearly the roll angle time histories generated from the polynomial defined lateral jink mission task element in Helinv are smooth, thus no lag time is introduced, for example, Figure 9.2 demonstrates smooth roll angle time

histories by pilot C, hence no lag time constant is introduced and it tends to its minimum boundary in the optimisation routine

It is interesting also at this point to assess the HEC relative to each other pilots assumed skill and experience. Pilot A, as stated, clearly does not fit into the hypothesis, as the operator gains are too high and the lead time too low. This suggests that the pilot adopts a control strategy that differs from Helinv. Pilot B is less experienced than pilot C, therefore it would be expected that C's gain should be greater. From Tables 9.2 to 9.4 however it is difficult to draw any definitive conclusions about this as only a narrow range of flight speeds has been considered, although the optimisation error has decreased across the flight speed range as expected because the pilot gains experience. Likewise, it is difficult to present statements about the 'assumed' most skilled operator, pilot D, simply because no clear patterns emerge in relation to increased flight speed or to the other pilots' results. It is therefore suggested that this could be further investigated by piloting the task over a wider flight speed envelope and also other tasks could be considered.

9.3.1 Pilot Strategy

A key parameter in assessing helicopter handling qualities is to be sure that each pilot fully understands the mission task under examination and how it is to be performed. In the case of an operator not fully comprehending the task requirements and constraints, the results generated may be akin to the pilot performing a completely different task. For this experiment the pilots were asked to fly the lateral jink task with the aid of visual cues, such as the required flight path actually being drawn in the simulator. Gates were also drawn representing points in the task which the pilot must pass through in order to reduce the risk of the pilot misinterpreting the instructions.

Preliminary results suggested that even with these visual cues, in some cases the pilots still adopt different control strategies whilst performing the task. This was counteracted by showing the pilots the control time histories derived from Helinv, and asking them to perform the task by attempting to memorise and follow this specific control strategy. Figure 9.6 demonstrates this by illustrating the state and control time

histories for pilot C before this additional constraint was applied and how it helped the pilot to perform the task in the manner required. The plots show that when the pilot initially flew the task, the strategy adopted was to use lateral cyclic only. However, when shown how the task was required to be flown, the operators changed their control strategy to fit that predicted by Helinv. Pilot A, even when shown the control strategy adopted by Helinv, performed the task by employing a different strategy. Figure 9.7 demonstrates this by comparing the flight path, states and controls recorded during the third flight by Pilot A, with the data recorded from pilot C. Although pilot C and pilot A in Figure 9.7, both closely follow the suggested flight path, both operators clearly perform the task in different ways, resulting in dissimilar sets of HEC. Pilot C applies almost exactly the same control strategy as Helinv, where a large pulse to the left in lateral cyclic is initially applied. Tail rotor collective then becomes the primary control input for the bulk of the task, where it is increased steadily for approximately one third of the manoeuvre. In order to decrease the lateral velocity of the helicopter, the tail rotor collective is decreased, then further reduced to bring the helicopter back to the task centreline. Finally, the tail rotor collective is returned to its trim position and a pulse in lateral cyclic applied to return the roll angle to its reference condition. It should be stressed that in the case under examination, heading is constrained to zero, thus application of the tail rotor would normally result in a change in heading ψ. However, here the lateral velocity and roll angle are its primary influences. Pilot A chooses to fly the task by applying what can be considered as step inputs in both control axis. Initially a long step is applied in lateral cyclic followed by an even longer step in tail rotor collective. The lateral cyclic input is reversed for approximately two seconds then returned to zero, while the tail rotor collective is decreased in two stages. Figure 9.7 also displays the state variable time histories, which demonstrate the differences in the roll angle time histories as a result of the contrasting control strategies employed. When the roll angle time histories are then applied to the MMCS, pilot C produces pilot characteristics similar to those described by Helinv, whereas pilot A's control strategy gives errors less than those predicted by Helinv with very high gains and low lead times.

This result can be interpreted in one of two ways. The first implies that for the lateral jink flight path defined in Helinv, the state and control time histories predicted by the

inverse algorithm are in fact not optimal. It must be remembered however, that the Helinv results are for the case of no human operator, i.e. theoretically the best possible strategy for piloting the task is implemented. It is therefore reasonable to suggest also that different operators will optimise their performance or equalisation characteristics by piloting the task using a control strategy which best suits that individual pilot, but which may not be the optimal control strategy predicted by inverse simulation. The gain and leads for pilot A also suggest that there is an optimal mission task flight speed for the human operator, where the gain reaches a maximum value and the lead time is minimised.

9.3.2 Pilot Input Adaptation

It was suggested in the introductory chapter that as the human operator becomes more proficient at flying a task, the pilot applies the control inputs with greater ease. This results in the optimisation error becoming smaller and the human equalisation characteristics therefore default towards those calculated for the Helinv derived time history. Figure 9.8 depicts the roll angle time history for pilot C for a flight that was included in the calculation of the average equalisation characteristics. Clearly this roll angle time history closely mimics that of the inverse simulation. However, an early attempt at performing the task by this operator as pilot B, with the same control strategy was recorded and is displayed with the latter manoeuvre time history as Figure 9.8. A sharp contrast between the control inputs and time histories is visible where the less experienced pilot did not accurately follow the predefined flight path due to a sub-optimal control strategy being adopted. In the early task the operator is seen to reach a peak roll angle twice as large as that recorded later by slowly increasing ϕ until the maximum lateral distance is almost reached. The inexperienced pilot then attempts to roll back to the other side, however, lateral cyclic is applied in the wrong direction and therefore a large tail rotor collective is required to maintain the required flight path. This inexperience causes the helicopter to have a negative roll angle throughout the task.

Table 9.5 Human Equalisation Characteristics for an Inexperienced Operator

Pilot	Error	Gain	Lead	Lag
Later Flight	9.896	0.152	0.654	0.1
Early Flight	16.94	0.092	1.947	0.151

Table 9.5 compares the equalisation characteristics for an early flight as pilot B with the results obtained when the operator is more experienced in flying the task. As pilot B gains experience and knowledge of the task and vehicle, the minimum optimisation error decreases towards that calculated from Helinv. It is also clear that the less experienced pilot B has introduced a lag component due to the operator applying large, oscillatory control inputs. The pilot gain, or the pilot's ability to respond to an error in the controlled variable, can be seen in the early flight case, to be less than that predicted by Helinv in Table 9.3. However, as operator experience increases so too does the gain. Conversely, the lead time constant is high for the inexperienced pilot and decreases with practice. The manner in which these latter two parameters behave is described in Chapter 4 as learning adaptation and input adaptation. As the human operator becomes more familiar with the system, they will learn about the response characteristics resulting in quicker detection of a problem hence a higher gain. The operator will also learn the pattern and thus be able to anticipate the control inputs, where a better ability to predict the control inputs results in a lower lead time.

9.4 Handling Qualities Assessment

A handling qualities assessment is next performed on the flight data presented from both simulation techniques via an attitude quickness analysis, followed by a pilot attack calculation. First, an attitude quickness assessment is performed for the flight case with pilot equalisation characteristics closest to the average for each pilot. This is because a handling qualities assessment cannot be made from an average roll angle time history for the series of flights by the pilots.

9.4.1 Attitude Quickness Calculation

Figure 9.9, Figure 9.10 and Figure 9.11 show the attitude quickness charts for the three speeds, thirty, forty and fifty knots respectively for the three pilots and the Helinv generated attitude quickness parameters. The first noticeable result from Figure 9.9 is the Helinv parameter in the top left corner of the chart. This attitude quickness parameter is due to the linear model resulting in a transient oscillation in the roll rate. The oscillation therefore corresponds to a very small change in the roll angle and thus gives an uncharacteristically large attitude quickness parameter. Further examination of the chart reveals that there are three distinguishable parameter groupings, each representing attitude quickness parameters for pilots B, C and D. The first grouping is in the bottom left hand corner of the chart relating to small changes in attitude. The second grouping defines slightly larger attitude changes between five and ten degrees. Finally, a third group can be differentiated in the bottom right of the chart, where the attitude change is greater than fifteen degrees per second which can be associated with larger or faster control inputs resulting in a large change in the vehicles flight path. It is also interesting to note that all the quickness parameter in each of the three groupings, for these three pilots, have approximately the same value. This suggests that the human operators piloted the task in a similar manner and that the recorded time histories are satisfactory for use in a handling qualities analysis. Pilot A, however, who has already been shown to adopt a different control strategy, again does not quite fit into the categorisation. It is evident from the chart that pilot A produces quickness parameters which fit into the second and third groupings, but none in the first set because larger roll angles are recorded throughout the task.

Close inspection of Figure 9.10 and Figure 9.11 reveals that the attitude quickness parameters for the four pilots fall into similar categories as described for the thirty knot case, suggesting that these mission task time histories are again suitable for a handling qualities assessment. Comparison of the three quickness charts also demonstrate that as the flight speed increases, the required change in roll attitude also increases for all pilots. A noticeable feature of this increased attitude change is that the attitude quickness parameters have not increased, but remained approximately the same. This is because as the flight speed increases, the mission time decreases. Therefore, the required roll attitude change becomes larger and faster while the ratio

of roll attitude to roll rate remains much the same. It should again be reiterated that these results do not meet Level 1 handling quality requirements as specified by ADS-33D. They only pass the attitude quickness assessment due to several constraints in the task definition as considered in Section 8.2.

9.4.2 Pilot Attack Calculation

The handling quality analysis may now be addressed using the pilot attack parameter introduced in Section 2.6, which relates the stick displacement to its derivative. The series of flights performed in the simulator, however, were performed using two control inputs, lateral cyclic and tail rotor collective. Thus, pilot attack can be calculated separately for both stick and pedal displacements. The analysis is performed again at forty knots for the reduced order linear inverse simulation result, in conjunction with each case for pilot C and also the task closest to the average for each pilot.

Only the forty knot pilot attack is be presented here because the attitude quickness assessment yielded results describing three similar groupings for each flight speed, hence certifying the task validation. Figure 9.12 illustrates the lateral cyclic stick displacement and derivative for the Helinv task and also for pilot B, while Figure 9.13 displays the corresponding lateral cyclic attack chart for the 'average' flight by all pilots. Section 2.6 considered that large net stick displacements were associated with vehicle navigation, large attack parameters and small stick displacements describe guidance, finally those in the bottom left hand corner simply represent vehicle stabilisation. Figure 9.13 demonstrates that none of the four pilots apply large stick displacements suggesting that the helicopter is guided through the task rather than navigated. For each pilot there are clearly some large attack parameters coincident with small stick displacements. As considered many of these are related to vehicle guidance however others are due to discontinuities in the linear model. These are especially evident in the case of pilot D. The lateral jink task may be described as a single axis tracking task, which in this case is not a highly aggressive manoeuvre. As a result, the human operator was expected to perform the task under the guidance

criteria rather than navigation, which is reserved for much more aggressive tasks requiring much larger changes in orientation.

As the task requires two control inputs, the attack parameters relating to the tail rotor collective have also been included. Figure 9.14 pictures the pedal displacement and derivative again for Helinv and Pilot C. Figure 9.15 displays the corresponding tail rotor attack chart for the five tasks performed by pilot C while Figure 9.16 shows the attack parameters for the 'average' case for all pilots at forty knots. The first important point to make about these attack charts is that a problem with the tail rotor control axis in the flight simulator did not allow the control a smooth transition when increased or decreased. This resulted in uncharacteristic and unrepresentative peaks in η_p and its derivative $\dot{\eta}_p$ which translated into attack parameters up to the value of three hundred. As these higher parameters are not a feature of the real system they have been omitted from the attack chart. Otherwise, the attack parameters for the pilot tail rotor input can be seen to be of the same order of magnitude as the lateral cyclic attack chart, confirming that for the flight, each control input influences the state time histories to the same extent and that no one control dominates the task.

9.5 Multiple Axis Tracking Task Discussion

The two control inputs required to perform the task, lateral cyclic and tail rotor collective, were considered in the previous section where pilot attack charts could be plotted separately for both controls. If the task is to be flown with two controls, a problem materialises when determining the HEC from the PPM. The problem is that the command signal, in this case the roll angle ϕ, is optimised with respect to the control input which causes the change in the state parameters. The transfer function representation of the vehicle dynamics is also derived from this relationship and as two controls are applied for this task, two optimisations are required. The first relates roll angle to lateral cyclic and the second relates the roll angle to the tail rotor collective. The resulting sets of equalisation characteristics will clearly have different pilot gains and lead times for the different axis because, although both inputs contribute significantly to the vehicle control, they are applied with different

strategies. However, in order to analyse the overall task, it is necessary to model the helicopter such that only one set of HEC is produced, which describe the overall pilot contribution.

Although the lateral jink, like the ADS-33D defined slalom task, can be described as a single axis tracking task, the operator is still required to apply more than one control input to perform the task due to the cross-coupling between the longitudinal and lateral axes of the helicopter. This is a widely recognised problem and has been tackled with innovations such as specially adapted automatic flight control systems which apply the control inputs from three axes, allowing the pilot to concentrate on the task at hand by applying only the primary control input. This type of AFCS has not been employed in the flight simulator thus another technique for representing the vehicle dynamics is considered as described in Section 4.5. Again as in Section 8.4, results are presented for each of the five tasks flown by pilot C and also the case nearest the average HEC parameters for each of the pilots.

9.5.1 Estimation of Multiple Control Vehicle Pilot Model Parameters for Pilot C

Table 9.6 presents the HEC for the multiple control representation of the vehicle dynamics, for each task flown by pilot C.

Table 9.6 Optimum Equalisation Characteristics For the Flights by Pilot C

Flight	Error	Gain	Lead	Lag
Linear Helinv	11.359	0.132	0.598	0.1
C_1	10.4942	0.1499	0.7075	0.1
C_2	12.4874	0.1522	0.6058	0.1
C_3	13.4304	0.1409	0.8000	0.1
C_4	12.2586	0.1264	0.9094	0.1
C_5	12.6336	0.1436	0.7562	0.1

The first noticeable result from Table 9.6 is that the errors are larger than for the single control axis optimisation, which is clearly as expected, as the pilot's attention is

divided between the two control inputs. The gains have remained approximately the same as expected as it was hypothesised at the beginning that the pilot operates with only one gain and a different lead time for each axis. This statement is reinforced when considering that the lead time constants have decreased for all cases other than C_1.

9.5.2 Estimation of Averaged Multiple Control Vehicle Pilot Model Parameters for All Pilots

Tables 9.7, 9.8 and 9.9 present the average optimised equalisation characteristics for each of the pilots when the vehicle dynamics are represented as described in Section 4.5.

Table 9.7 Multiple Control Human Equalisation Characteristics for 30 Knot Lateral Jink

Pilot	Error	Gain	Lead	Lag
Linear Helinv	3.397	0.138	0.578	0.1
A	9.645	0.151	0.825	0.1
B	8.263	0.136	0.676	0.1
C	6.606	0.146	0.636	0.1
D	7.638	0.147	0.629	0.1

Table 9.8 Multiple Control Human Equalisation Characteristics for 40 Knot Lateral Jink

Pilot	Error	Gain	Lead	Lag
Linear Helinv	11.359	0.132	0.598	0.1
A	8.804	0.181	0.517	0.1
B	17.754	0.139	0.738	0.1
C	12.261	0.143	0.756	0.1
D	11.743	0.155	0.689	0.1

Table 9.9 Multiple Control Human Equalisation Characteristics for 50 Knot Lateral Jink

Pilot	Error	Gain	Lead	Lag
Linear Helinv	32.875	0.120	0.684	0.1
A	15.49	0.174	0.551	0.1
B	28.665	0.158	0.529	0.1
C	24.839	0.149	0.661	0.1
D	21.088	0.135	0.706	0.1

Again, the errors are larger than for the single control axis optimisation, which is clearly as expected. The gains on the whole have stayed approximately the same, however, the average lead time for each pilot has decreased. Different conclusions can thus be drawn from these tables compared with those in Section 9.3. Pilot A (least experienced) again produces results similar to those found previously except for the thirty knot case. Here the error and lead time are much higher than those recorded by any other operator, suggesting that A did in fact struggle to perform the task. This statement is reinforced when considering the gain and lead for the remaining flight speeds. As with the single axis case, pilot A's gain is seen to be larger and the lead smaller for the forty knot case than the other two presented. This suggests that instead of pilot A finding the task increasingly difficult to pilot, there is a preferred or optimal flight speed for this operator somewhere in the region of forty knots. Pilot D displays similar characteristics.

Pilots C and B (same operator with different experience levels) again describe the suggested hypothesis that pilot C with more experience has a lower error than pilot B. Comparison of the gains calculated for these two pilots also reveals that throughout the flight speed range the gains are very similar. The Gain of pilot B (inexperienced pilot C) unlike pilot A, increases with flight speed, however, as the operator became more experienced and recorded data as pilot C, the gains remain similar. This therefore raises the question does a pilot operate with a constant gain when controlling a specific attitude angle? This question has not been addressed in this work but is suggested as being a possible topic for future work.

9.6 Conclusions

The handling qualities analysis performed using the pilot attack parameter demonstrates that each pilot performed the lateral jink manoeuvre simply by guiding the helicopter through the task. However, if the task was more aggressive, pilot attack parameters representing navigation rather than control would have been displayed. The attack charts also demonstrate that this task was flown using two controls and that the task was not monopolised by only either of the control inputs. It has also been demonstrated that it is imperative to include both in the equalisation pilot characteristics estimation or inaccurate results are attained. It should however be stressed that this does not affect the handling qualities analysis as only the dominant attitude angle or control inputs are required.

Chapter 10

Research Conclusions

10.1 Introduction

The final chapter presents a summary not only of the main aims of the work described in Chapter 1, but also a review of individual objectives achieved throughout the project and recommendations for future work. Before this however, it is worthwhile reiterating the main aim stated in Chapter 1. The work presented aimed to develop a desktop tool, which allows pilot effect to be incorporated into the inverse simulation output to improve model fidelity for an initial helicopter handling qualities assessment. The remainder of the chapter is split into three sections. Firstly the individual objectives pertaining to the overall aim are presented followed by a discussion of the main aim. Finally a discussion on recommended future work is included.

10.2 Thesis Objectives

The addition of pilot effect to the inverse simulation output centres on the MMCS, where each element in the system is tailored to a specific set of requirements. Clearly one of the most critical aspects of the work is the pilot model selected for the assessment. As the human operator is the limiting factor in the control system, it was important to select a model which could provide pilot information when performing a tracking task. The quasi-linear model selected, the Precision Pilot Model, encompasses these requirements where the pilot can be described as a series of gain

and phase characteristics. The PPM has thus proven to be an invaluable tool for determining the pilot effect on the input command signal.

Like the pilot, the vehicle must also be modelled to a high standard. If either pilot or helicopter model are not fully representative, the model becomes invalid. A linear HGS model was presented in Chapter 4 which is well established in the engineering community. The state space format of the model allows the vehicle dynamics to be determined as a transfer function, relating a controlled variable to the primary control input. This vehicle representation may be adequate for fixed wing aircraft however due to complex cross-coupling terms between the longitudinal and lateral modes in the helicopter, this description proves to be inadequate for a handling qualities assessment as more than one control input is required. A method whereby this can be achieved was demonstrated whereby the transfer function relating each control to the dominant attitude are included in parallel to one another.

The command signal is generated from two simulation techniques, inverse simulation and conventional forward simulation. Inverse simulation has been proven to generate state and control time histories that can be used in a handling qualities assessment, consisting of three components. A mathematical manoeuvre definition, split into equal time intervals, which initiates a time marching algorithm. This in turn calls a helicopter model to execute the predefined flight path. Chapter 5 demonstrates the non-linear algorithm, validated by Thomson & Bradley (1990), and a linearised version. The linear algorithm employs a linear helicopter model for generating the state and control time histories and functions in exactly the same manner as the non-linear model. This algorithm has been validated by comparison with the full non-linear Helinv package and was found to emulate almost exactly the non-linear results.

Chapter 6 considered that to derive flight data using a helicopter flight simulator, a flight simulator incorporating all the features stated would have to be developed as an appropriate PC based simulator was not available commercially at the time. The criteria on which this flight simulator is based make the simulator 'unique', allowing exactly the same helicopter model as that employed in inverse simulation to be piloted through exactly the same task. The flight simulator, due to hardware limitations, was

restricted to three control inputs thus only a reduced order helicopter model could be simulated accurately.

This is particularly important when assessing the vehicle response in any one particular axis. It allows a dynamic analysis of the longitudinal or lateral modes without the complex cross-coupling terms, making it easier to identify the vehicle modes. The reduced order model is only applicable if representative of the full system. It was shown in the thesis that, for a longitudinal tracking task, the helicopter can be represented by four state variables and two control inputs when flown at a constant speed. This model may be applied to both the inverse algorithm and the flight simulator, again allowing a true comparison between simulation techniques.

Before a mathematically defined mission task element is applied to either simulation technique, verification that the task exhibits Level 1 handling qualities is required. It was demonstrated that smooth global polynomial defined tasks tend to exhibit substandard handling qualities, whereas several piecewise models resulted in a transient oscillation in the flight path due to a numerical integration error. The co-ordinates for the predefined mission task flight path, can be extracted from the inverse algorithm and applied to the helicopter flight simulator to ensure that the operator pilots exactly the same task as Helinv.

10.3 General Conclusions

A review of a questionnaire based, subjective handling qualities was presented, demonstrating the advantages of identifying any deficiencies early in the aircraft design stage. This work by Cooper & Harper led to the development of an objective assessment technique considered in the ADS document series through pilot attack ratings. The objective method was illustrated by demonstrating the compatibility of inverse simulation and forward simulation to a handling qualities assessment, suggesting that both are important in the early assessment of handling qualities.

Inverse Simulation has been shown to be a powerful tool when replicating flight test data by manoeuvring precisely along a predefined flight path, suggesting that the

control time histories generated are in fact the ideal control inputs. Helinv however does not employ a pilot model thus the pilot workload calculation reveals that the Helinv outputs relate only to vehicle guidance. It is therefore advantageous to correct this data by adding the pilot effect to the control time histories, by optimising the equalisation characteristics in the PPM. The optimised HEC are a measure of pilot behaviour, however these parameters can be related to the pilot workload and/or optimal pilot equalisation characteristics to determine how well the manoeuvre was performed in relation to the optimal flight test case.

With pilot effect being incorporated into the inverse simulation output, it is possible to determine the optimum pilot parameters for the task and compare with those calculated from the pilot based, flight simulator recorded results. The pilot parameters describe the pilot behaviour during the task but they can also be used to determine performance. In essence it has been demonstrated that it is possible to relate the optimum equalisation characteristics for each pilot to the corresponding attitude quickness and attack charts.

10.4 Recommendations for Future Work

i) Further Development of the Linear Helicopter Flight Simulator

It is evident that the application of the linear helicopter flight simulator is limited to cases where a maximum of only three control inputs can be applied. It would therefore be advantageous if this problem could be overcome allowing a full linear helicopter model to be implemented. Several more enhancements to the flight simulator could be made to increase realism such as the incorporation of noise and a higher fidelity automatic flight control system.

ii) Incorporate Non-Linear Helicopter Model

Although the linear helicopter model incorporated in the flight simulator has been proven to replicate the non-linear model, it is limited in the flight simulator to performing tasks at a constant velocity. If tasks such as the quick-hop are to be

accurately replicated a model that allows large changes in velocity and attitude are necessary. Therefore, a flight simulator based on the non-linear HGS model is required.

iii) Consideration of Longitudinal Tasks

The thesis only considers one lateral task, the slalom/lateral-jink. However, a wide range of tasks have been defined in the Helinv algorithm which can also be flown in the flight simulator if the suggested improvements are made. A handling qualities assessment on the corresponding flight test data would then allow a catalogue of pilot ability and vehicle handling qualities over a range of mission tasks and flight speeds.

iv) Pilot Effect on Different Tasks and Aircraft

Although there is scope for analysis of further mission task elements, another approach would be to perform the same task or tasks in different helicopters to determine whether pilot characteristics varied for different vehicles, or if they remain approximately the same for any given pilot. This can also be applied to other tasks to find out if a pilots gain remains constant when controlling specific attitudes.

v) Application of Multi-Axis Pilot Models

The man-machine control system with PPM is used to determine the optimum HEC relating the primary state variable to the dominant control input. A technique has also been demonstrated for relating the primary state parameter to two control inputs. However, although equalisation characteristics can be calculated for each state, the pilot operates with only one lead time and a gain for each control axis. This merits a further analysis of multiple axis pilot modelling to determine pilot characteristics for the task incorporating the full vehicle state matrix, rather than just the primary controlled variable.

10.5 Concluding Remarks

The research described in this dissertation has demonstrated that linear modelling, of inverse simulation and a helicopter flight simulator, can be used to generate flight test data at an early design stage for use in a handling qualities assessment. As a result, the inverse simulation generated time histories with added pilot effect can be directly compared with flight test data recorded from the validated helicopter flight simulator. This primarily involves comparisons between pilot response and vehicle handling qualities. It should be reiterated that the aim was not to assess helicopter handling qualities, but to develop a desktop tool for including the pilot effect in inverse simulation models to increase the overall model fidelity. This has been successfully achieved enhancing the understanding of the pilot effect on the state and control time histories and pilot workload.

Appendix I

Puma Data File

Puma Airframe Mass/Inertia Information

Aircraft mass	m	5806	kg
Moments of Inertia	I_{xx}	9638	kgm^2
	I_{yy}	33240	kgm^2
	I_{zz}	25889	kgm^2
	I_{xz}	-2226	kgm^2
Centre of Gravity location	x_{cg}	-0.2	m
	y_{cg}	0	m
	z_{cg}	-0.675	m

Rotor Data : Main Rotor

Number of Blades	N	4	
Blade Radius	R	7.489	m
Hinge Offset	e	3.87	%
Lag Damper		14.15	Nm/rad/s
Nominal Rotorspeed	W	27	rad/s

Rotor Data : Tail Rotor

Number of Blades	*N*	5	
Blade Radius	*R*	1.518	m
Hinge Offset	*e*	7.2	%
Lag Damper		50	Nm/rad/s
Nominal Rotorspeed	*W*	137	rad/s

Appendix II

Stability and Control Augmentation System (SCAS)

The Stability and Control Augmentation System (SCAS) is one part of the Automatic Flight Control System (AFCS) applied through a series of actuators alongside autopilot functions. The following mathematical description of the SCAS was first presented by Padfield (1981), where each of the controls is discussed in terms of the primary control linkage and the interlinks with main rotor collective.

A2.1 Pitch and Roll Channels

If a pilot wishes to achieve a manoeuvre in pure pitch or roll, coupled control inputs are required as the phase lag between cyclic pitch and blade flap is less than 90 degrees. Although the phase lag varies throughout the flight speed envelope, a single mixing is usually selected as a compromise to all flight conditions, modelled by

$$\begin{bmatrix} \theta_{1s} \\ \theta_{1c} \end{bmatrix} = \begin{bmatrix} \cos\psi_f & \sin\psi_f \\ -\sin\psi_f & \cos\psi_f \end{bmatrix} \begin{bmatrix} \theta^*_{1s} \\ \theta^*_{1c} \end{bmatrix} \tag{A2.1}$$

where,

θ_{1s} and θ_{1c} are the longitudinal and lateral cyclic pitch *after* mixing, that is the actual rotor blade pitch displacements.

θ^*_{1s} and θ^*_{1c} are the longitudinal and lateral cyclic pitch *before* mixing.

ψ_f is the cyclic mixing or phase angle (usually 8 →10 degrees).

Before mixing between the longitudinal and lateral cyclic occurs, the pilot and components of θ^*_{1s} and θ^*_{1c} are passed through an actuation element (such as hydraulic actuators) which can be represented as a first order lag. This however is a crude approximation to a complicated servo-elastic system and is in the form of

$$\theta^*_{1s} = \frac{\theta^*_{1sp} + \theta^*_{1sa}}{1 + \tau_{c1} s} \tag{A2.2}$$

$$\theta^*_{1c} = \frac{\theta^*_{1cp} + \theta^*_{1ca}}{1 + \tau_{c2} s} \tag{A2.3}$$

where,

θ^*_{1sa} and θ^*_{1ca} are the longitudinal and lateral flight control system inputs.

θ^*_{1sp} and θ^*_{1cp} are the longitudinal and lateral pilot control inputs.

τ_{c1} and τ_{c2} are the longitudinal and lateral time constants.

The longitudinal and lateral cyclic channel contribution from the pilot can be written in the form

$$\theta^*_{1sp} = g_{1s0} + g_{1s1}\eta_{1s} + (g_{sc0} + g_{sc1}\eta_{1s})\eta_c \tag{A2.4}$$

$$\theta^*_{1cp} = g_{1c0} + g_{1c1}\eta_{1c} + (g_{cc0} + g_{cc1}\eta_{1c})\eta_c \tag{A2.5}$$

where,

g_{1s0}, g_{1s1}, g_{sc0}, g_{sc1}, are gains and offsets in the longitudinal channel.

g_{1c0}, g_{1c1}, g_{cc0}, g_{cc1}, are gains and offsets in the lateral channel.

η_c, is the collective lever input and η_{1s}, η_{1c}, are the longitudinal and lateral cyclic inputs.

Finally the stabiliser input can be written as:

$$\theta^*_{1sa} = k_\theta \theta + k_q q + (\eta_{1s} - \eta_{1s0}) k_{1s} \tag{A2.6}$$

$$\theta^*_{1ca} = k_\phi \phi + k_p p + (\eta_{1c} - \eta_{1c0}) k_{1c} \quad \text{(A2.7)}$$

where,

k_θ, k_q, k_{1s} are the proportional feedback, derivative feedback and feedforward gains respectively and

η_{1s0} is the reference longitudinal trim position ($0 \leq \eta_{1s} \leq 1$);

k_ϕ, k_p,k_{1c} are the proportional feedback, derivative feedback and feedforward gains respectively and

η_{1c0} is the reference longitudinal trim position ($0 \leq \eta_{1c} \leq 1$);

A2.2 Yaw Channel

In a similar way the pilot and autostabiliser commands are passed through an actuator, giving the relationship:

$$\theta^*_{0tr} = \frac{\theta^*_{0trp} + \theta^*_{0tra}}{1 + \tau_{c3} s} \quad \text{(A2.8)}$$

The pilot contribution to the yaw channel is modelled using a coupling of the main and tail rotor collective:

$$\theta^*_{0trp} = g_{0tr0} + g_{g0tr1} \eta_{ct} \quad \text{(A2.9)}$$

where,

g_{0tr0}, g_{0tr1}, are gearing constants

η_{ct} is the cable length which is a linear relationship between pedal and collective lever positions

$$\eta_{ct} = g_{ct0}(1 - \eta_p) + (1 - 2g_{ct0})\eta_c \quad \text{(A2.10)}$$

where

η_p is the pedal displacement by the pilot ($0 \leq \eta_p \leq 1$)

The autostabiliser contribution to the yaw channel can be written as

$$\theta^*_{0tra} = k_\varphi(\varphi - \varphi_h) + k_r r \tag{A2.11}$$

φ_h is the heading adjustable by the pilot.

A2.3 Heave Channel

Finally the main rotor collective input can be expressed as

$$\theta^*_0 = \frac{\theta^*_{0p} + \theta^*_{0a}}{1 + \tau_{c4} s} \tag{A2.12}$$

where the pilot contribution to the collective channel is

$$\theta^*_{0p} = g_{c0} + g_{c1}\eta_c \tag{A2.13}$$

and the stabiliser contribution is given by

$$\theta^*_{0a} = k_g \Delta_n \tag{A2.14}$$

where,

$$\Delta_n = 1 + \frac{a_z}{g} \tag{A2.15}$$

k_g is the accelerometer feedback gain,

a_z is the heave axis acceleration measured by the accelerometer,

g is the acceleration due to gravity.

Each initial control displacement can now be calculated for a given vehicle and trimmed flight speed from the SCAS, using Puma parameters and trim values derived by the linearised HGS model.

Appendix III

Helicopter Generic Simulation (HGS)

A3.1 Overview of Model

The HGS model was derived by Thomson (1992) from a conventional simulation model developed by the Royal Aircraft Establishment [Padfield (1981)]. The model employs the well established non-linear rigid body equations as given in Chapter 4, equations (4.3 a → f), where the rate of change of the attitude angles are related to the body axes angular velocities by equations (4.3 g → i).

The defining characteristics for any rigid body for which the Euler equations are applied are the aerodynamic forces and moments. These can be split into their constituent components, which for the helicopter, consists of the main rotor *R*, tail rotor *TR*, fuselage *f*, tailplane *tp* and the fin *fn*, resulting in the following aerodynamic force and moment expressions

$$\begin{aligned} X &= X_R + X_{TR} + X_f + X_{tp} + X_{fn} \\ Y &= Y_R + Y_{TR} + Y_f + Y_{tp} + Y_{fn} \\ Z &= Z_R + Z_{TR} + Z_f + Z_{tp} + Z_{fn} \\ L &= L_R + L_{TR} + L_f + L_{tp} + L_{fn} \\ M &= M_R + M_{TR} + M_f + M_{tp} + M_{fn} \\ N &= N_R + N_{TR} + N_f + N_{tp} + N_{fn} \end{aligned} \qquad \text{(A3.1)}$$

The complex aerodynamic forces and moments can be determined by considering each component starting here with the main rotor.

A3.2 The Main Rotor Model

As HGS employs a rotor disc model, the assumption that only the steady components calculated effect the vehicle dynamics, allowing the rotor forces and moments to be determined over the entire rotor disc. The initial step in determining the forces and moments of the helicopter rotor blades is to calculate the aerodynamic and inertial loads on an individual blade element then integrate the elemental loads across the blade span.

The external forces and moments applied to the helicopter causes the axes system (which is fixed to the aircraft cg) to move with varying translational (U, V, W) and rotational (P, Q, R) velocity components. If $\underline{i}$, $\underline{j}$, $\underline{k}$ are unit vectors along the x, y, z axes respectively then that the linear translational velocity and acceleration of the cg of the helicopter is given by

$$V_{cg} = U\underline{i}_{bod} + V\underline{j}_{bod} + W\underline{k}_{bod} \tag{A3.2}$$

$$a_{cg} = \dot{U}\underline{i}_{bod} + \dot{V}\underline{j}_{bod} + \dot{W}\underline{k}_{bod} \tag{A3.3}$$

The corresponding rotational velocity and acceleration in body axes are

$$\underline{\omega}_{bod} = P\underline{i}_{bod} + Q\underline{j}_{bod} + R\underline{k}_{bod} \tag{A3.4}$$

$$\underline{\alpha} = \frac{\partial \underline{\omega}_{bod}}{\partial t} = \dot{P}\underline{i}_{bod} + \dot{Q}\underline{j}_{bod} + \dot{R}\underline{k}_{bod} \tag{A3.5}$$

As the aim here is to determine the blade element velocity and acceleration relative to the blade, the rotor parameters must be found relative to the rotor hub and then transformed to the blade element axes via the following transformations

- Body to hub axes (transformed through shaft angle
- Hub to shaft axes (transformed through azimuth angle)
- Shaft to blade element axes (transformed through flap angle)

Where the velocity, acceleration and angular velocity in blade axes are given by

$$\begin{aligned}\underline{V}_{hub/bl} &= \left[-U_{hub}\cos\Psi + V_{hub}\sin\Psi - \beta W_{hub}\right]\underline{i}_{bl} \\ &+ \left[-U_{hub}\sin\Psi - V_{hub}\cos\Psi\right]\underline{j}_{bl} \\ &+ \left[\beta\left(-U_{hub}\cos\Psi + V_{hub}\sin\Psi\right) + W_{hub}\right]\underline{k}_{bl}\end{aligned} \tag{A3.6}$$

$$\begin{aligned}\underline{a}_{hub/bl} &= \left[-\underline{a}_{hub/x}\cos\Psi + \underline{a}_{hub/y}\sin\Psi - \beta\underline{a}_{hub/z}\right]\underline{i}_{bl} \\ &+ \left[-\underline{a}_{hub/x}\sin\Psi - \underline{a}_{hub/y}\cos\Psi\right]\underline{j}_{bl} \\ &+ \left[\beta\left(-\underline{a}_{hub/x}\cos\Psi + \underline{a}_{hub/y}\sin\Psi\right) + \underline{a}_{hub/z}\right]\underline{k}_{bl}\end{aligned} \tag{A3.7}$$

$$\begin{aligned}\underline{\omega}_{hub/bl} &= \left[-p_{hub}\cos\Psi + q_{hub}\sin\Psi - \beta\left(r_{hub} - \Omega\right)\right]\underline{i}_{bl} \\ &+ \left[\dot{\beta} - p_{hub}\sin\Psi - q_{hub}\cos\Psi\right]\underline{j}_{bl} \\ &+ \left[\beta\left(-p_{hub}\cos\Psi + q_{hub}\sin\Psi\right) + \left(r_{hub} - \Omega\right)\right]\underline{k}_{bl}\end{aligned} \tag{A3.8}$$

The absolute velocity of a point p, a distance r_b from the centre of rotation of the rotor blade can be written as

$$\underline{V}_{p/bl} = \underline{V}_{hub/bl} + \left(\underline{\omega}_{bl} \times r_{p/H}\right) \tag{A3.9}$$

where

$$r_{p/H} = r_b\,\underline{i}_{bl}$$

Substituting equation (A3.6) in to the above expression then gives the velocity at a point on the blade as

$$\underline{V}_{p/bl} = \underline{V}_{x/bl}\,\underline{i}_{bl} + \underline{V}_{y/bl}\,\underline{j}_{bl} + \underline{V}_{z/bl}\,\underline{k}_{bl} \tag{A3.10}$$

The absolute acceleration of a point p in local blade axes can be defined in a similar manner as

$$\underline{a}_{p/bl} = \underline{a}_{hub/bl} + \left(\underline{\alpha}_{bl} \times r_{p/H}\right) + \underline{\omega}_{bl} \times \left(\underline{\omega}_{bl} \times r_{p/H}\right) + 2\underline{\omega}_{bl} \times \frac{d}{dt} r_{p/H} \quad \text{(A3.11)}$$

Again, equation (A3.6) can be substituted into this expression to yield

$$\underline{a}_{p/bl} = \underline{a}_{x/bl}\underline{i}_{bl} + \underline{a}_{y/bl}\underline{j}_{bl} + \underline{a}_{z/bl}\underline{k}_{bl} \quad \text{(A3.12)}$$

Equation (A3.10) and equation (A3.12) are fundamental to the rotor model, as it is now possible to determine expressions for blade loads off which the HGS model assumes there are two of acting on a blade element.

A3.2.1 Rotor Aerodynamic Forces

The normal and tangential components of lift and drag can be expressed as

$$f_{z/bl} = -L\cos\Phi - D\sin\Phi \quad \text{(A3.13)}$$

$$f_{y/bl} = D\cos\Phi - L\sin\Phi \quad \text{(A3.14)}$$

From the assumption that the tangential airflow over the blade element U_T is much greater than the perpendicular velocity U_P, the angle of attack of the blade element is small such that $L\cos\Phi >> D\sin\Phi$, and from 2D aerodynamic theory the lift and drag coefficients are given by

$$f_{z/bl} = -\frac{1}{2}\rho c a_0 \left(U_T^2\theta + U_P U_T\right) dr_b \quad \text{(A3.15)}$$

$$f_{y/bl} = \frac{1}{2}\rho c a_0 \left(\frac{\delta}{a_0} U_T^2 - U_P U_T \theta - U_P^2\right) dr_b \quad \text{(A3.16)}$$

The total forces acting on the rotor blade are then determined by integrating the elemental forces along the blade span. Assuming that the rotor blade of length R, with root cut out e, where e is expressed as a fraction of the blade span, the rotor forces and moments can be calculated from the normalised rotor coefficients

$$C_{z/bl} = -\frac{1}{2} s a_0 \frac{1}{b} \int_0^{1-e} \left(\bar{U}_T^2 \theta + \bar{U}_P \bar{U}_T \right) d\bar{r}_b \tag{A3.17}$$

$$C_{y/bl} = \frac{1}{2} s a_0 \frac{1}{b} \int_0^{1-e} \left(\frac{\delta}{a_0} \bar{U}_T^2 - \bar{U}_P \bar{U}_T \theta - \bar{U}_P^2 \right) d\bar{r}_b \tag{A3.18}$$

where the rotor solidity is $s = \dfrac{bc}{\pi R}$

and the normalised radial blade position is given by $\bar{r}_b = \dfrac{r_b - eR}{R}$.

The integration of the coefficients in equations (A3.17) & (A3.18) with respect to $\bar{r}_b$ are relatively simple as the equations can be arranged into polynomial functions of $\bar{r}_b$. The resulting expressions obtained in powers of $cos\psi$ and $sin\psi$ giving the following expressions for the total blade aerodynamic coefficients

$$\begin{aligned} C_{Z_A} &= -\frac{1}{2b} s a_0 \left(C_{Z_{A0}} + \sum_{n=1}^{\infty} (C_{Z_{Anc}} \cos\psi + C_{Z_{Ans}} \sin\psi) \right) \\ C_{Y_A} &= \frac{1}{2b} s a_0 \left(C_{Y_{A0}} + \sum_{n=1}^{\infty} \left(C_{Z_{Anc}} \cos\psi + C_{Z_{Ans}} \sin\psi \right) \right) \end{aligned} \tag{A3.19}$$

A3.2.2 Rotor Inertial Forces

The inertial forces acting on the blade element of length dr_b can be given by

$$dX_{i/bl} = -m_0 \underline{a}_{x/bl} dr_b \quad dY_{i/bl} = -m_0 \underline{a}_{y/bl} dr_b \quad dZ_{i/bl} = -m_0 \underline{a}_{z/bl} dr_b \tag{A3.20}$$

Making the relevant substitutions, equation (A3.12) gives the blade inertial forces as

$$X_{i/bl} = \left(\underline{a}_{hub/x}\cos\Psi - \underline{a}_{hub/y}\sin\Psi + \beta\underline{a}_{hub/z}\right)m_b + \left(\underline{\omega}_y^2 + \underline{w}_z^2\right)M_\beta$$

$$Y_{i/bl} = \left(\underline{a}_{hub/x}\sin\Psi + \underline{a}_{hub/y}\cos\Psi\right)m_b - \left(\dot{\underline{\omega}}_z + \underline{\omega}_y\underline{\omega}_z\right)M_\beta \qquad \text{(A3.21)}$$

$$Z_{i/bl} = \left[\beta\left(\underline{a}_{hub/x}\cos\Psi - \underline{a}_{hub/y}\sin\Psi\right) - \underline{a}_{hub/z}\right]m_b - \left(\underline{\omega}_x\underline{\omega}_z - \dot{\underline{\omega}}_y\right)M_\beta$$

where

the blade mass is given by $m_b = \int_{eR}^{R} m_0 dr_b$

the blade moment of mass is given by $M_\beta = \int_{eR}^{R} m_0 r_b dr_b$

and $\underline{\omega}_{x,y,z}$ are the angular velocity components of the blade element in the blade axes.

These equations can be expanded by including the blade angular velocities and accelerations, and the blade flap angle as functions of the heading angle. The resulting equations can then be non-dimensionalised by dividing through by the term $\rho(\Omega R)^2\pi R^2$ to give the inertial coefficients

$$C_{X_i} = C_{X_{i0}} + C_{X_{i1c}}\cos\Psi + C_{X_{i1s}}\sin\Psi$$

$$C_{Y_i} = C_{Y_{i0}} + C_{Y_{i1c}}\cos\Psi + C_{Y_{i1s}}\sin\Psi \qquad \text{(A3.22)}$$

$$C_{Z_i} = C_{Z_{i0}} + C_{Z_{i1c}}\cos\Psi + C_{Z_{i1s}}\sin\Psi$$

A3.2.3 The Total Rotor Forces

The total rotor blade forces can be obtained through the summation of the aerodynamic and inertial forces to give the coefficients in component form as

$$C_{X/bl} = C_{X_0} + C_{X1c/bl}\cos\Psi + C_{X1s/bl}\sin\Psi$$

$$C_{Y/bl} = C_{Y_0} + C_{Y1c/bl}\cos\Psi + C_{Y1s/bl}\sin\Psi \qquad \text{(A3.23)}$$

$$C_{Z/bl} = C_{Z_0} + C_{Z1c/bl}\cos\Psi + C_{Z1s/bl}\sin\Psi$$

where $C_{X_0} = C_{X_{I0}}$, $C_{Y_0} = \frac{sa_0}{2b} C_{Y_{A0}} + C_{Y_{I0}}$ etc.

Recall that the vehicle equations of motion are defined with respect to the body axes while the blade element loading is determined with respect to the blade axes, therefore the blade element loading must be transformed back to the body axes. This is achieved in exactly the opposite manner of the previous transformation, that is, the blade forces are transformed from blade to shaft axes and from shaft to hub axes. During the transformation it is again assumed that only the steady terms contribute to the rotorcraft dynamics, hence the periodic terms that are a function of blade azimuth can be neglected. The final transformation is then from hub to body axes through the rotor shaft angle γ_s. The main rotor contribution to the external forces can now be given by

$$X_R = \rho(\Omega R)^2 \pi R^2 \left[C_{X/hub}\cos\gamma_s - C_{Z/hub}\sin\gamma_s\right]$$

$$Y_R = \rho(\Omega R)^2 \pi R^2 \left[C_{Y/hub}\right] \qquad \text{(A3.24)}$$

$$Z_R = \rho(\Omega R)^2 \pi R^2 \left[C_{X/hub}\sin\gamma_s + C_{Z/hub}\cos\gamma_s\right]$$

A3.2.4 Rotor Moments

The flapping model incorporated in the HGS model assumes the rotor to consist of rigid blades hinged at the hub with a stiffness in flap, modelled by a torsional spring of stiffness K_β. The total moments acting on a single rotor blade are determined by summing the elemental inertia and aerodynamic moments over the span and equating

them to the restoring moment at the hub due to blade flap, hence the roll, pitch and yaw hub moments acting at the cg in body axes form are

$$\begin{aligned} L_R &= L_{hub}\cos\gamma_s - N_{hub}\sin\gamma_s + h_R Y_R \\ M_R &= M_{hub} - h_R X_R + x_{cg} Z_R \\ N_R &= L_{hub}\sin\gamma_s + N_{hub}\cos\gamma_s + x_{cg} Y_R \end{aligned} \tag{A3.25}$$

After some algebra manipulation as described by C. Taylor (1995) the blade flapping can be expressed as

$$\begin{aligned} \mathrm{B}_i'' + \left[\lambda_\beta^2 + \frac{\overline{M}_\beta R}{I_\beta}\left(\eta_x\cos\Psi_i - \eta_y\sin\Psi_i\right)\right]\beta_i = \\ 4n_\beta \int_0^{1-e}\left(\overline{U}_T^2\theta + \overline{U}_T\overline{U}_P\right)\left(\overline{r}+e\right)d\overline{r}_b \\ + \frac{\overline{M}_\beta R}{I_\beta}\eta_z + 2\left[\left(\frac{q'_{hub}}{2} + \overline{p}_{hub}\right)\cos\Psi_i + \left(\frac{p'_{hub}}{2} + \overline{q}_{hub}\right)\sin\Psi_i\right] \end{aligned} \tag{A3.26}$$

where expressions for the normalised flap frequency λ_β, the blade flapping moment of inertia I_β and the blade inertia number N_β are given by

$$\lambda_\beta^2 = \frac{K_\beta}{I_\beta\Omega^2} + 1 \qquad I_\beta = \int_{eR}^{e} m_0 r_b^2 dr_b \qquad N_\beta = \frac{\rho c a_0 R^4}{8 I_\beta}$$

Other terms evident in equation (A3.26) are given as

$$\mathrm{B}_i'' = \frac{d^2\beta_i}{d\Psi^2} \qquad q'H = \frac{\dot{q}H}{\Omega^2} \qquad p'H = \frac{\dot{p}H}{\Omega^2}$$

This equation can be used to describe the flapping motion of an individual blade, however as the flapping model in HGS requires the flapping motion to be described in multi-blade co-ordinates.

A3.2.5 The Multi-blade Transform

In HGS, equation (A3.26) is solved by applying the multi-blade transformation, which effectively converts the individual blade angles β_i (i=1→n) into a multi-blade co-ordinates where β_0 is the coning angle, β_{1s} and β_{1c} are the longitudinal and lateral flapping angles and β_d is the differential coning angle. By applying the multi-blade transformation for a four blade rotor, the individual blade angles $\beta_i = \begin{bmatrix}\beta_1 & \beta_2 & \beta_3 & \beta_4\end{bmatrix}^T$ can be determined as follows

$$\beta_i = \underline{L}_\beta \beta_M \tag{A3.27}$$

where

$$\underline{L}_\beta = \begin{bmatrix} 1 & -1 & \cos\Phi & \sin\Phi \\ 1 & 1 & \sin\Phi & -\cos\Phi \\ 1 & -1 & -\cos\Phi & -\sin\Phi \\ 1 & 1 & \sin\Phi & \cos\Phi \end{bmatrix}$$

$$\beta_M = \begin{bmatrix}\beta_0 & \beta_d & \beta_{1s} & \beta_{1c}\end{bmatrix}^T$$

Incorporating the multi-blade transformation into the flapping equation and expressing the resulting periodic equation in non-periodic form allows the flapping equation to be written as

$$\beta_M'' + C_{M_0} + \beta_M' + D_{M_0}\beta_M = h_{M_0} \tag{A3.28}$$

where the matricies C_{M_0}, D_{M_0} and h_{M_0} are obtained by substituting for successive values of ψ_i for each blade from the equation

$$\Psi_i = \Psi - (i-1)\frac{\pi}{2}$$

hence the resulting expressions are lengthy and the reader is referred to Thomson (1992) for the full set of equations.

Equation (A3.28) can be solved for the multi-blade angles, however the solution is often simplified by assuming quasi-steady blade flapping. This assumption implies that the blade flapping dynamics are decoupled from the fuselage dynamics and therefore have little effect on the forces and moments applied to the rotor or fuselage. The quasi-linear blade flapping motion then becomes

$$\beta_M = D_{M_0}^{-1} h_{M_0} \tag{A3.29}$$

which can be solved for the vector β_M due to its algebraic nature to give the blade flap angles at a discrete point in time.

A3.3 HGS Tail Rotor Model

The modelling of the tail rotor is essentially the same as for the main rotor, the exception being that the tail rotor hub is assumed to be rigid so that no blade flapping occurs. The rotor blades are assumed to be of constant chord, root cut out and vary linearly with blade twist. The rotor inflow representation is again of the same form however, the inertial forces and moments are assumed small and therefore neglected. The rotor force and moment coefficients were evaluated using Mathematica and neglecting terms higher than zero order and first harmonic terms are

$$C_{ZTR/trbl} = -\frac{1}{2} s_{TR} a_{0TR} \left(C_{Z_0 TR/trbl} + C_{Z_{1c} TR/trbl} \cos\Psi_{TR} + C_{Z_{1s} TR/trbl} \sin\Psi_{TR} \right)$$

$$C_{YTR/trbl} = -\frac{1}{2} s_{TR} a_{0TR} \left(C_{Y_0 TR/trbl} + C_{Y_{1c} TR/trbl} \cos\Psi_{TR} + C_{Y_{1s} TR/trbl} \sin\Psi_{TR} \right) \quad \text{(A3.30)}$$

$$C_{QTR/trbl} = -\frac{1}{2} s_{TR} a_{0TR} \left(C_{Q_0 TR/trbl} + C_{Q_{1c} TR/trbl} \cos\Psi_{TR} + C_{Q_{1s} TR/trbl} \sin\Psi_{TR} \right)$$

Neglecting periodic terms and de-normalising, the moment components due to the offset off the tail rotor hub forces can be added to the tail rotor moments to give the force and moment contribution of the tail rotor in body axes as

$$X_{TR} = \rho\left(\Omega_{TR} R_{TR}\right)^2 \pi R_{TR}^2 C_{XTR/trh}$$

$$Y_{TR} = \rho\left(\Omega_{TR} R_{TR}\right)^2 \pi R_{TR}^2 C_{ZTR/trh} \quad \text{(A3.31)}$$

$$Z_{TR} = \rho\left(\Omega_{TR} R_{TR}\right)^2 \pi R_{TR}^2 C_{YTR/trh}$$

$$L_{TR} = h_{TR} Y_{TR}$$

$$M_{TR} = -\rho\left(\Omega_{TR} R_{TR}\right)^2 \pi R_{TR}^3 C_{QTR/trh} + \left(x_{cg} + l_{TR}\right) Z_{TR} - h_{TR} X_{TR} \quad \text{(A3.32)}$$

$$N_{TR} = -\left(x_{cg} + l_{tr}\right) \dot{Y}_{TR}$$

where $C_{XTR/trh}$, $C_{YTR/trh}$, $C_{ZTR/trh}$ and $C_{QTR/trh}$ are the tail rotor force and moment coefficients in the tail rotor hub axes. The terms x_{cg} and l_{tr} are the distances to the centre of gravity and tail rotor hub from the fuselage reference point respectively.

A3.4 The Fuselage Model

The aerodynamic forces and moments generated by the fuselage are calculated from look-up tables of aerodynamic coefficients as functions of angle of attack α or sideslip angle β, which are derived from wind tunnel tests and are denoted by C_{Xf}, C_{Yf}, C_{Zf}, C_{Lf}, C_{Mf} and C_{Nf}.

The force coefficients in the x and z-axes and the moment coefficient in the y-axis are functions of the angle of attack while the remainder are dependent on the sideslip angle. The wind tunnel data in the look-up tables is measured relative to the fuselage reference point just below the hub and therefore the moments due to this offset must be accounted for resulting in the following force and moment coefficients

$$\begin{aligned} X_f &= \rho(\Omega R)^2 \pi R^2 C_{Xf} \\ Y_f &= \rho(\Omega R)^2 \pi R^2 C_{Yf} \\ Z_f &= \rho(\Omega R)^2 \pi R^2 C_{Zf} \end{aligned} \tag{A3.33}$$

$$\begin{aligned} L_f &= 0 \\ M_f &= \rho(\Omega R)^2 \pi R^3 C_{Mf} + x_{cg} Z_f \\ N_f &= \rho(\Omega R)^2 \pi R^3 C_{Nf} + x_{cg} Y_f \end{aligned} \tag{A3.34}$$

A3.5 The Fin and Tailplane Models

The fin and tailplane coefficients are C_{Yfn} and C_{Ztp} respectively, where the coefficients are determined in a similar manner to the fuselage, although here as functions of the fin sideslip angle and the angle of incidence of the tailplane. The contribution of the fin surface area S_{fn} and the tailplane surface area S_{tp} are hence required in the overall force and moment expressions given by

Fin		*Tailplane*	
$X_{fn} = 0$		$X_{tp} = 0$	
$Y_{fn} = \rho(\Omega R)^2 S_{fn} C_{Yfn}$		$Y_{tp} = 0$	
$Z_{fn} = 0$	(A3.35)	$Z_{tp} = \rho(\Omega R)^2 S_{tp} C_{Ztp}$	(A3.36)
$L_{fn} = Y_{fn} h_{fn}$		$L_{tp} = 0$	
$M_{fn} = 0$		$M_{tp} = Z_{tp}(x_{cg} + l_{tp})$	
$N_{fn} = Y_{fn}(x_{cg} + l_{fn})$		$N_{tp} = 0$	

where l_{fn} is the distance from the fuselage reference point to the fin centre of pressure, h_{fn} is the height of the fin above the fuselage datum, l_{tp} is the distance of the tailplane behind the reference point and finally h_{tp} is the height of the tailplane above the fuselage datum.

Appendix IV

Inverse Simulation - The Helinv Algorithm

A4.1 Introduction

This appendix aims to present a comprehensive discussion of the algorithm employed in the inverse simulation package (Helinv), where the dynamic system response for a predetermined flightpath is simulated as illustrated in equation (5.5). The output of the system y is specified by the trajectory of the vehicle cg in terms of the longitudinal, lateral and vertical position with respect to an earth fixed axes x_e, y_e and z_e. Using this rationale, it is clear that the inverse algorithm has the six rigid body non-linear equations of motion

$$\dot{U} = -(WQ - VR) + \frac{X}{m} - g\sin\Theta \tag{A4.1a}$$

$$\dot{V} = -(UR - WP) + \frac{Y}{m} + g\cos\Theta\sin\Phi \tag{A4.1b}$$

$$\dot{W} = -(VP - UQ) + \frac{Z}{m} - g\cos\Theta\cos\Phi \tag{A4.1c}$$

$$L = I_{xx}\dot{P} - I_{xz}\dot{R} + QR(I_{zz} - I_{yy}) - PQI_{xz} \tag{A4.1d}$$

$$M = I_{yy}\dot{Q} + RP(I_{xx} - I_{zz}) + (P^2 - R^2)I_{xz} \tag{A4.1e}$$

$$N = I_{zz}\dot{R} - I_{xz}\dot{P} + PQ(I_{yy} - I_{xx}) + QRI_{xz} \tag{A4.1f}$$

in conjunction with a seventh rotor speed degree of freedom given by

$$\Omega = \ddot{Q}_E \tau_{e1} \tau_{e2} + \left(\tau_{e1} + \tau_{e3}\right)\dot{Q}_E + Q_E - K_3\left(\Omega - \Omega_{idle} + \tau_{e2}\dot{\Omega}\right) \qquad \text{(A4.1g)}$$

with which to solve the four unknown controls and three Euler attitude angles. In order to obtain a unique solution a further constraint must be applied, which, when considering helicopter control, can be applied as either a heading or a side slip constraint, leaving the vector of unknowns as

$$\underline{u} = \left[\Phi \quad \Theta \quad \theta_0 \quad \theta_{1s} \quad \theta_{1c} \quad \theta_{0tr} \quad \Omega\right] \qquad \text{(A4.2)}$$

The technique focused on throughout the thesis is the constrained side slip case and is again considered here for consistency, where the side slip velocity and acceleration are defined as

$$V = V_f \sin\beta \qquad \text{(A4.3)}$$

$$\dot{V} = \dot{V}_f \sin\beta + \dot{\beta} V_f \cos\beta \qquad \text{(A4.4)}$$

where V_f is the flight path velocity and $\dot{\beta}$ is the rate of change of side slip. The side slip velocity can also be determined from the transformation of the velocity components in the earth axes to the body axes given by

$$V = \left[\begin{matrix} m_1 \dot{X}_e & m_2 \dot{Y}_e & m_3 \dot{Z}_e \end{matrix}\right]^T \qquad \text{(A4.5)}$$

where

$m_1 \sin\Phi \sin\Theta \cos\Psi - \cos\Phi \cos\Psi$

$m_2 = \sin\Phi \sin\Theta \sin\Psi + \cos\Phi \cos\Psi$

$m_3 = \sin\Phi \cos\Theta$

Equation (A4.5) can be rewritten in the form

$$a\cos\Psi + b\sin\Psi + c = 0 \tag{A4.6}$$

where

$$a = \dot{X}_e \sin\Phi\sin\Theta + \dot{Y}_e \cos\Phi$$
$$b = -\dot{X}_e \cos\Phi + \dot{Y}_e \sin\Phi\sin\Theta$$
$$c = \dot{Z}_e \sin\Phi\cos\Theta - V$$

This equation can be solved for ψ using the Newton-Raphson method provided Φ and Θ are known. When all the required flight parameters have been calculated from the input manoeuvre data, the inverse simulation can proceed.

A4.2 The Inverse Algorithm

The basic problem of the Helinv algorithm is the solution of the six equations motion in conjunction with the rotorspeed equation. The seven equations of motion with seven unknowns in the Helinv algorithm can be rearranged to give

$$f_1(\Phi \quad \Theta \quad \theta \quad \theta_0 \quad \theta_{1s} \quad \theta_{1c} \quad \Omega) = -m(\dot{U} + WQ - VR) + X - mg\sin\Theta = 0$$
$$\vdots$$
$$f_7(\Phi \quad \Theta \quad \theta \quad \theta_0 \quad \theta_{1s} \quad \theta_{1c} \quad \Omega) = \ddot{Q}_E \tau_{e1}\tau_{e2} + (\tau_{e1} + \tau_{e3})\dot{Q}_E + Q_E - K_3(\Omega - \Omega_{idle} + \tau_{e2}\dot{\Omega}) = 0$$

The inverse algorithm starts the solution process by providing an initial guess of the vector $\underline{u}$. It then proceeds to calculate the rates of the unknown attitudes $\dot{\Phi}$ and $\dot{\Theta}$ by numerical differentiation. This allows the unsteady terms in the equations to be calculated, converting the vehicle equations of motion into a set of non-linear equations. The Newton-Raphson iterative technique is used to provide a better estimate of the unknown vector $\underline{u}$. As the output vector $\underline{y}$ expresses the desired flight path in the form of a manoeuvre time history, the inverse algorithm is cast in a time marching form and solves the equations of motion at each point on the flight path.

A4.2.1 Evaluation of body Attitude Angles and Rates

Initial guesses of the vehicle pitch and roll attitudes are made at the start of each iteration j of the Newton-Raphson iterative scheme. Considering only the pitch attitude Θ, the initial estimate is given by

$$\Theta_{i,j} = \begin{cases} \Theta_e & m=1, k=1 \\ \Theta_{i-1} & m=1 \\ \Theta_{i,j-1} & m\rangle 1 \end{cases} \qquad \text{(A4.7)}$$

For the first iteration at each time point i in the trajectory, it is evident that the previous value i-1 is used as an initial estimate. Also for the first iteration at time t=0, the estimate of pitch assumes a predetermined trim value Θ_e, where the roll angle Φ and the rotorspeed Ω are treated in a similar manner. Using numerical differentiation it is then possible to determine the first and second derivatives of pitch attitude with respect to time

$$\dot{\Theta}_{i,j} = \frac{\Theta_{ij} - \Theta_{i-1}}{t_i - t_{i-1}}$$
$$\ddot{\Theta}_{i,j} = \frac{\dot{\Theta}_{ij} - 2\dot{\Theta}_{i-1} - \dot{\Theta}_{i-2}}{\left(t_i - t_{i-1}\right)^2} \qquad \text{(A4.8)}$$

The roll attitude and rotorspeed derivatives can thus be evaluated in a similar manner.

A4.2.2 Evaluation of body Translational Velocities and Accelerations

The vehicle body axes velocities are evaluated by a series of transformations of the earth fixed axes X_e, Y_e and Z_e, via the Euler attitude angles. This transformation is the transpose of that implied in chapter 5, equation (5.2) where the output y is related to

the system state vector $\underline{x}$ via the function g, thus the vehicle translational velocities for the j^{th} iteration of the time point i can be found from

$$\begin{bmatrix} U \\ V \\ W \end{bmatrix}_{i,j} = \begin{bmatrix} l_1 & l_2 & l_3 \\ m_1 & m_2 & m_3 \\ n_1 & n_2 & n_3 \end{bmatrix} \begin{bmatrix} \dot{X}_e \\ \dot{Y}_e \\ \dot{Z}_e \end{bmatrix}_i \tag{A4.9}$$

where l_1, l_2 and l_3 are the direction cosines. The rotorcraft body axes accelerations can be found by differentiating equation (A4.9) to give

$$\begin{bmatrix} \dot{U} \\ \dot{V} \\ \dot{W} \end{bmatrix}_{i,j} = \begin{bmatrix} l_1 & l_2 & l_3 \\ m_1 & m_2 & m_3 \\ n_1 & n_2 & n_3 \end{bmatrix} \begin{bmatrix} \ddot{X}_e \\ \ddot{Y}_e \\ \ddot{Z}_e \end{bmatrix}_i + \begin{bmatrix} \dot{l}_1 & \dot{l}_2 & \dot{l}_3 \\ \dot{m}_1 & \dot{m}_2 & \dot{m}_3 \\ \dot{n}_1 & \dot{n}_2 & \dot{n}_3 \end{bmatrix} \begin{bmatrix} \dot{X}_e \\ \dot{Y}_e \\ \dot{Z}_e \end{bmatrix}_i \tag{A4.10}$$

where $(\dot{l}_1, \dot{l}_2, \ldots\ldots, \dot{n}_3)$ are the derivatives of the direction cosines with respect to time and can be rewritten as

$$\dot{l}_1 = -\dot{\Theta}_{i,j} \sin\Theta_{i,j} \sin\Psi_i + \dot{\Psi}_i \cos\Theta_{i,j} \cos\Psi_i \text{ etc.} \tag{A4.11}$$

A4.2.3 Evaluation of Body Rotational Velocities and Accelerations

The vehicle rotational angular velocities about the body fixed axes set for the i^{th} time point and j^{th} iteration of the Newton-Raphson scheme can be determined by rearranging equation (5.2) to give

$$\begin{aligned} p_{i,j} &= \dot{\Phi}_{i,j} - \dot{\Psi}_i \sin\Theta_{i,j} \\ q_{i,j} &= \dot{\Theta}_{i,j} \cos\Phi_{i,j} + \dot{\Psi}_i \cos\Theta_{i,j} \sin\Phi_{i,j} \\ r_{i,j} &= \dot{\Psi}_{i,j} \cos\Theta_{i,j} \cos\Phi_{i,j} - \dot{\Theta}_{i,j} \sin\Phi_{i,j} \end{aligned} \tag{A4.12}$$

Which can be differentiated to give

$$\dot{P} = \ddot{\Phi} - \ddot{\Psi}_i \sin\Theta - \dot{\Psi}_i \dot{\theta} \sin\Theta$$

$$\dot{Q} = \ddot{\Theta}\cos\Phi - \dot{\Theta}\dot{\Phi}\sin\Phi + \ddot{\Psi}_i \cos\Theta\sin\Phi + \dot{\Psi}_i\left(-\dot{\Theta}\sin\Theta\sin\Phi + \dot{\Phi}\cos\Theta\cos\Phi\right) \quad \text{(A4.13)}$$

$$\dot{R} = \ddot{\psi}_i \cos\Theta\cos\Phi - \ddot{\Theta}\sin\Phi - \dot{\Theta}\dot{\Phi}\cos\Phi + \dot{\Psi}_i\left(-\dot{\Theta}\sin\Theta\cos\Phi - \dot{\Phi}\cos\Theta\sin\Phi\right)$$

where the subscript i,j has been neglected from $\dot{P},\dot{Q},\dot{R},\Phi,\dot{\Phi},\Theta,\dot{\Theta}$, in equation (A4.13) for simplicity but its importance should not be forgotten.

A4.2.4 Determination of Vehicle External Forces and Moments

With estimates of all the states, it is possible to determine the external forces and moments as considered in the following appendix. Once the net contribution of individual forces and moments generated by the components of the helicopter are found, all the information required to derive the latest error vector will have been obtained.

A4.2.5 Updating the Control Estimate

The Newton-Raphson iterative scheme employed in the inverse simulation algorithm has the following structure

$$\begin{bmatrix} \Phi \\ \vdots \\ \vdots \\ \Omega \end{bmatrix}_{i,j+1} = \begin{bmatrix} \Phi \\ \vdots \\ \vdots \\ \Omega \end{bmatrix}_{i,j} - \begin{bmatrix} \left(\frac{\partial F_1}{\partial \Phi}\right)_{i,j} & \cdots\ \cdots & \left(\frac{\partial F_1}{\partial \Omega}\right)_{i,j} \\ \vdots & & \vdots \\ \vdots & & \vdots \\ \left(\frac{\partial F_7}{\partial \Phi}\right)_{i,j} & \cdots\ \cdots & \left(\frac{\partial F_7}{\partial \Omega}\right)_{i,j} \end{bmatrix}^{-1} \begin{bmatrix} F_1(\Phi\ \ \Theta\ \ \theta_0\ \ \theta_{1s}\ \ \theta_{1c}\ \ \theta_{0tr}\ \ \Omega) \\ \vdots \\ \vdots \\ F_7(\Phi\ \ \Theta\ \ \theta_0\ \ \theta_{1s}\ \ \theta_{1c}\ \ \theta_{0tr}\ \ \Omega) \end{bmatrix} \quad \text{(A4.14)}$$

This allows new estimates of the unknown variables to be made whereby the Helinv algorithm iterates until the error functions are within a prescribed tolerance. The Jacobian elements are calculated by numerical differentiation such that

$$\left(\frac{\partial F_1}{\partial \Phi}\right)_{i,j} = \frac{F_1(\Phi + \delta\Phi, \Phi, \ldots, \Omega)_{i,j} - F_1(\Phi - \delta\Phi, \Phi, \ldots, \Omega)_{i,j}}{2\delta\Phi} \tag{A4.15}$$

for small perturbations of Φ and $\delta\Phi$. Once the Jacobian has been evaluated it is inverted using a standard matrix inversion. Following this a better estimate of the unknowns can be determined from equation (A4.14) and the steps repeated until the desired convergence. When the control, attitude and rotorspeed parameters are determined for the i^{th} time point, the algorithm steps forwards one point, repeating the process for the duration of the manoeuvre.

Appendix V

Linear Helinv - Constrained Heading

The linearised equations of motion when expressed in state space form

$$\dot{\underline{x}} = \mathbf{A}\underline{x} + \mathbf{B}\underline{u} \tag{A5.1}$$

can be used to describe the unconstrained motion of the helicopter by rewriting them in such a way that they represent the inverse of the problem. The state vector is split into unconstrained parameters and those strongly influenced by the constraints. The flightpath is defined as a function of time therefore so are the velocities by differentiation, hence u, v, and w must be strongly influenced. Finally as the tail rotor strongly influences the heading ψ giving $\underline{x}_1$ the vector of constraint influenced states and $\underline{x}_2$ the vector of unconstrained states

$$\underline{x}_1 = \begin{bmatrix} u & v & w & r \end{bmatrix}^T \qquad \underline{x}_2 = \begin{bmatrix} p & q & \theta & \phi \end{bmatrix}^T \tag{A5.2}$$

The linearised equation (A5.1) can then be rewritten by restructuring the system and control matrices as suggested by Houston and Caldwell (1984a &1984b)

$$\begin{bmatrix} \dot{\underline{x}}_1 \\ \dot{\underline{x}}_2 \end{bmatrix} = \begin{bmatrix} \mathbf{A}_{11} & \mathbf{A}_{12} \\ \mathbf{A}_{21} & \mathbf{A}_{22} \end{bmatrix} \begin{bmatrix} \underline{x}_1 \\ \underline{x}_2 \end{bmatrix} + \begin{bmatrix} \mathbf{B}_1 \\ \mathbf{B}_2 \end{bmatrix} \begin{bmatrix} \underline{u} \end{bmatrix} \tag{A5.3}$$

On expansion this gives

$$\underline{\dot{x}}_1 = \mathbf{A}_{11}\underline{x}_1 + \mathbf{A}_{12}\underline{x}_2 + \mathbf{B}_1\underline{u} \tag{A5.4}$$

$$\underline{\dot{x}}_2 = \mathbf{A}_{21}\underline{x}_1 + \mathbf{A}_{22}\underline{x}_2 + \mathbf{B}_2\underline{u} \tag{A5.5}$$

Solving equation (A5.4) for the control vector assuming $\boldsymbol{B}_1$ to be non-singular

$$\underline{u} = \mathbf{B}_1^{-1}\left[\underline{\dot{x}}_1 - \mathbf{A}_{11}\underline{x}_1 - \mathbf{A}_{12}\underline{x}_2\right] \tag{A5.6}$$

Substituting (A5.6) into (A5.5) allows the unconstrained states to be expressed in terms of the constraint influenced states

$$\underline{\dot{x}}_2 = \left[\mathbf{A}_{22} - \left(\mathbf{B}_2\mathbf{B}_1^{-1}\right)\mathbf{A}_{12}\right]\underline{x}_2 + \left[\left(\mathbf{A}_{21} - \left(\mathbf{B}_2\mathbf{B}_1^{-1}\right)\mathbf{A}_{11}\right)\underline{x}_1 + \left(\mathbf{B}_2\mathbf{B}_1^{-1}\right)\underline{x}_1\right] \tag{A5.7}$$

The linear solution requires the unconstrained states $\underline{x}_2$ to be expressed in terms of the constraints $\underline{f}_c$. However the strongly influenced states $\underline{x}_1$ are a function of both $\underline{x}_2$ and $\underline{f}_c$ as is apparent on examination of the linearised Euler transformation

$$\begin{bmatrix} u \\ v \\ w \end{bmatrix} = \begin{bmatrix} L_{1_0} & L_{2_0} & L_{3_0} \\ M_{2_0} & M_{2_0} & M_{3_0} \\ N_{1_0} & N_{2_0} & N_{3_0} \end{bmatrix} \begin{bmatrix} \dot{x} \\ \dot{y} \\ \dot{z} \end{bmatrix} + \begin{bmatrix} L_{1_d} & L_{2_d} & L_{3_d} \\ M_{1_d} & M_{2_d} & M_{3_d} \\ N_{1_d} & N_{2_d} & N_{3_d} \end{bmatrix} \begin{bmatrix} \theta \\ \phi \\ \psi \end{bmatrix} \tag{A5.8}$$

where the direction cosines are given by

$$L_1 = \cos\Theta\cos\Psi \qquad L_2 = \cos\Theta\sin\Psi \qquad L_3 = -\sin\Theta$$

$$M_1 \sin\Phi\sin\Theta\cos\Psi - \cos\Phi\sin\Psi \qquad M_2 = \sin\Phi\sin\Theta\sin\Psi + \cos\Phi\cos\Psi \qquad M_3 = \sin\Phi\cos\Psi$$

$$N_1 = \cos\Phi\sin\Theta\cos\Psi + \sin\Phi\sin\Psi \qquad N_2 = \cos\Phi\sin\Theta\sin\Psi - \sin\Phi\cos\Psi \qquad N_3\cos\Phi\cos\Theta$$

The yaw velocity is given by the kinematic expression

$$R = \dot{\Psi}\cos\Theta\sec\Phi - Q\tan\Phi \tag{A5.9}$$

Which when linearised gives

$$r = \dot{\psi}\cos\theta_e \sec_e - q\tan\Phi_e \tag{A5.10}$$

Combining and rearranging (A5.8) and (A5.10) gives

$$\underline{x}_1 = \mathbf{T}_1\underline{\dot{f}}_c + \mathbf{T}_2\underline{f}_c + \mathbf{T}_3\underline{x}_2 \tag{A5.11}$$

where

$$\mathbf{T}_1 = \begin{bmatrix} L_{1_0} & L_{2_0} & L_{3_0} & 0 \\ M_{1_0} & M_{2_0} & M_{3_0} & 0 \\ N_{1_0} & N_{2_0} & N_{3_0} & 0 \\ 0 & 0 & 0 & \dfrac{\cos\Theta_e}{\cos\Phi_e} \end{bmatrix} \quad \mathbf{T}_2 = \begin{bmatrix} 0 & 0 & 0 & L_{3_d} \\ 0 & 0 & 0 & M_{3_d} \\ 0 & 0 & 0 & N_{3_d} \\ 0 & 0 & 0 & 0 \end{bmatrix} \quad \mathbf{T}_3 = \begin{bmatrix} 0 & 0 & L_{1_d} & L_{2_d} \\ 0 & 0 & M_{1_d} & M_{2_d} \\ 0 & 0 & N_{1_d} & N_{2_d} \\ 0 & -\tan\Phi_e & 0 & 0 \end{bmatrix}$$

The linearised transformation of Earth fixed to body fixed axis accelerations is given by

$$\begin{bmatrix} \dot{u} \\ \dot{v} \\ \dot{w} \end{bmatrix} = \begin{bmatrix} L_{1_0} & L_{2_0} & L_{3_0} \\ M_{2_0} & M_{2_0} & M_{3_0} \\ N_{1_0} & N_{2_0} & N_{3_0} \end{bmatrix} \begin{bmatrix} \ddot{x} \\ \ddot{y} \\ \ddot{z} \end{bmatrix} - \begin{bmatrix} W_e q - V_e r \\ U_e r - W_e p \\ V_e p - U_e q \end{bmatrix} \tag{A5.12}$$

Differentiating (A5.10) gives the yaw acceleration

$$\dot{r} = \ddot{\psi}\cos\Theta_e \sec\Phi_e - \dot{q}\tan\Phi_e \tag{A5.13}$$

Combining and rearranging equations (A5.12) and (A5.13) gives

$$\dot{\underline{x}}_1 = \mathbf{T}_1\underline{\ddot{f}}_c + \mathbf{T}_4\dot{\underline{x}}_2 + \mathbf{T}_5\underline{x}_2 + \mathbf{T}_6\underline{x}_1 \tag{A5.14}$$

where

$$\mathbf{T}_4 = \begin{bmatrix} 0 & 0 & 0 & 0 \\ 0 & 0 & 0 & 0 \\ 0 & 0 & 0 & 0 \\ 0 & -\tan\Phi_e & 0 & 0 \end{bmatrix} \quad \mathbf{T}_5 = \begin{bmatrix} 0 & -W_e & 0 & 0 \\ W_e & 0 & 0 & 0 \\ -V_e & U_e & 0 & 0 \\ 0 & 0 & 0 & 0 \end{bmatrix} \quad \mathbf{T}_6 = \begin{bmatrix} 0 & 0 & 0 & V_e \\ 0 & 0 & 0 & -U_e \\ 0 & 0 & 0 & 0 \\ 0 & 0 & 0 & 0 \end{bmatrix}$$

Substituting for $\underline{x}_1$ from (A5.11) gives

$$\dot{\underline{x}}_1 = \mathbf{T}_1 \ddot{\underline{f}}_c + \mathbf{T}_4 \dot{\underline{x}}_2 + \left[\mathbf{T}_5 + \mathbf{T}_6\mathbf{T}_3\right]\underline{x}_2 + \mathbf{T}_6\mathbf{T}_1 \dot{\underline{f}}_c + \mathbf{T}_6\mathbf{T}_2 \underline{f}_c \qquad \text{(A5.15)}$$

Finally equations (A5.11) and (A5.15) can be substituted into (A5.7) giving

$$\begin{aligned} \dot{\underline{x}}_2 = &\left[I - \mathbf{B}_2\mathbf{B}_1^{-1}T_4\right]^{-1}\left\{\mathbf{A}_{22} - \mathbf{B}_2\mathbf{B}_1^{-1}\left(\mathbf{A}_{12} - \mathbf{T}_5\right) + \left(\mathbf{A}_{21} - \mathbf{B}_2\mathbf{B}_1^{-1}\left(\mathbf{A}_{11} - \mathbf{T}_6\right)\right)\mathbf{T}_3\right\}\underline{x}_2 + \\ &\left[I - \mathbf{B}_2\mathbf{B}_1^{-1}\mathbf{T}_4\right]^{-1}\left\{\left[\mathbf{B}_2\mathbf{B}_1^{-1}\mathbf{T}_4\right]\ddot{\underline{f}}_c + \left[\left(\mathbf{A}_{21} - \mathbf{B}_2\mathbf{B}_1^{-1}\left(\mathbf{A}_{11} - \mathbf{T}_6\right)\right)\mathbf{T}_1\right]\dot{\underline{f}}_c\right\} + \\ &\left[I - \mathbf{B}_2\mathbf{B}_1^{-1}\mathbf{T}_4\right]^{-1}\left\{\left[\left(\mathbf{A}_{21} - \mathbf{B}_2\mathbf{B}_1^{-1}\left(\mathbf{A}_{11} - \mathbf{T}_6\right)\right)\mathbf{T}_2\right]\underline{f}_c\right\} \end{aligned}$$

The unconstrained states are now expressed in terms of the constraints. This solution can be simplified to

$$\dot{\underline{x}}_2 = \mathbf{A}_c\underline{x}_2 + \mathbf{B}_c\underline{u}_c \qquad \text{(A5.16)}$$

where

$$\mathbf{A}_c = \left[I - \mathbf{B}_2\mathbf{B}_1^{-1}\mathbf{T}_4\right]^{-1}\left\{\mathbf{A}_{22} - \mathbf{B}_2\mathbf{B}_1^{-1}\left(\mathbf{A}_{12} - \mathbf{T}_5\right) + \left[\mathbf{A}_{21} - \mathbf{B}_2\mathbf{B}_1^{-1}\left(\mathbf{A}_{11} - \mathbf{T}_6\right)\right]\mathbf{T}_3\right\}$$

$$\mathbf{B}_c = \begin{bmatrix} \left[I - \mathbf{B}_2\mathbf{B}_1^{-1}\mathbf{T}_4\right]^{-1}\mathbf{B}_2\mathbf{B}_1^{-1}\mathbf{T}_1 \\ \left[I - \mathbf{B}_2\mathbf{B}_1^{-1}\mathbf{T}_4\right]^{-1}\left(\mathbf{A}_{21} - \mathbf{B}_2\mathbf{B}_1^{-1}\left(\mathbf{A}_{11} - \mathbf{T}_6\right)\right)\mathbf{T}_1 \\ \left[I - \mathbf{B}_2\mathbf{B}_1^{-1}T_4\right]^{-1}\left(\mathbf{A}_{21} - \mathbf{B}_2\mathbf{B}_1^{-1}\left(\mathbf{A}_{11} - \mathbf{T}_6\right)\right)\mathbf{T}_2 \end{bmatrix}^T$$

$$\underline{u}_c = \begin{bmatrix} \ddot{\underline{f}}_c \\ \dot{\underline{f}}_c \\ \underline{f}_c \end{bmatrix} \qquad \underline{f}_c = \begin{bmatrix} x \\ y \\ z \\ \psi \end{bmatrix} \qquad \underline{x}_2 = \begin{bmatrix} p \\ q \\ \theta \\ \phi \end{bmatrix}$$

Chapter 1 Figures

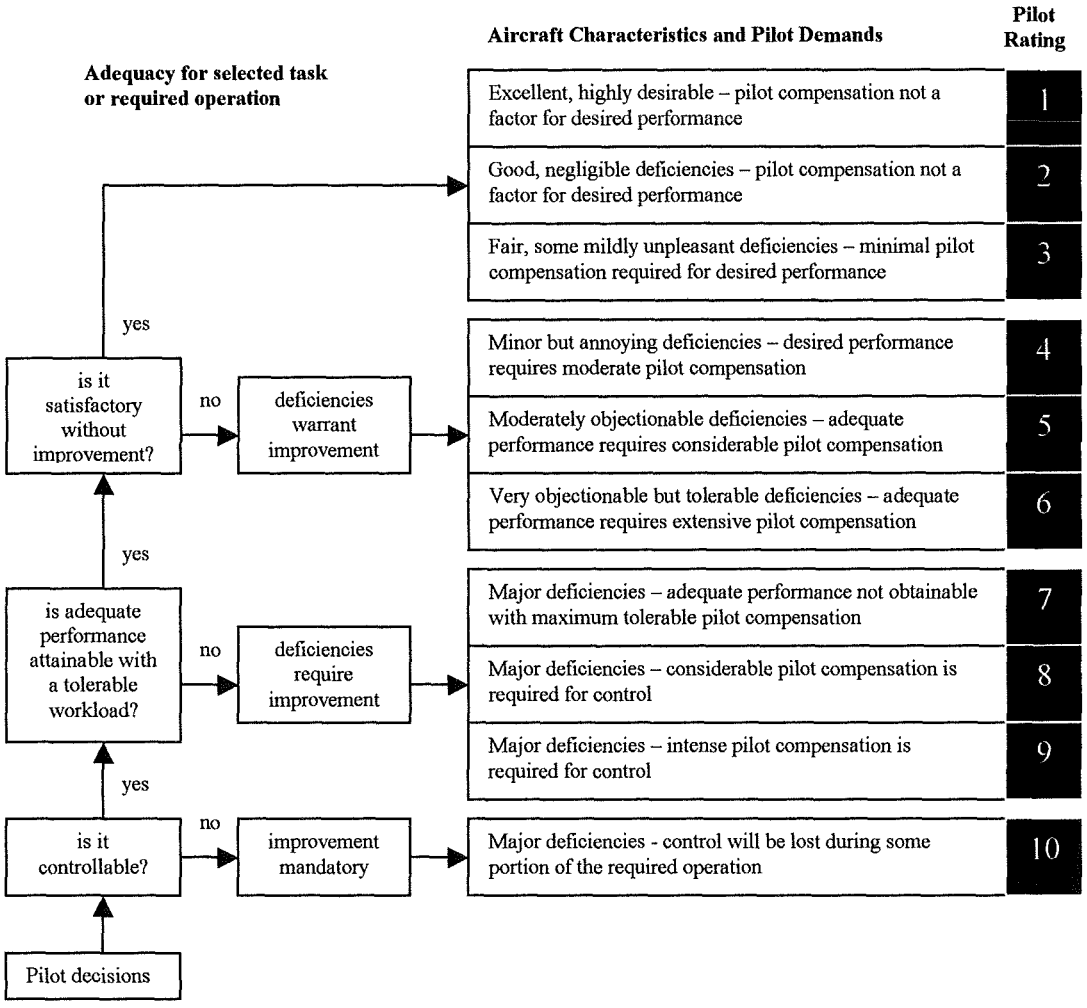

Figure 1.1 The Cooper-Harper Handling Qualities Rating Scale [Padfield 1998]

Pilot..... MTE..... Config.....

RATING	**1**	**3**	**3**	**4**	**5**
TASK CUES	Excellent	Good	Fair	Poor	Inadequate
AGRESSION	Minimal	Low	Moderate	High	Maximum
TASK PERFORMANCE	Clearly within desired performance limits	Desired performance marginally	Clearly within adequate performance limits	Adequate performance marginally	Adequate performance not achieved
TASK WORKLOAD	Low	Moderate	Considerable	Extensive	Intolerable
SYSTEM CHARACTERISTICS	Satisfactory or better	Minor but annoying deficiencies	Moderately objectionable deficiencies	Objectionable but tolerable deficiencies	Major deficiencies, controllable
Heli + Control Law	**1**	**2**	**3**	**4**	**5**
Inceptor	**1**	**2**	**3**	**4**	**5**

HQR		1	2	3	4	5	6	7	8	9	10
HQR/Subphases		Transition/Acquisition				Tracking					
Influencing factors						--	-	0	+	++	
Vehicle and control law	Primary response, stability, Coupling effects due to inceptor or H/C, Vehicle limits										
Inceptor	Ergonomics, Mechanical and Control char. Sensitivity										
Cues	Outside visual cues, Instruments (HUD), Acceleration cues										
comments											

Figure 1.2 Pilot Questionnaire [Leacock (2000)]

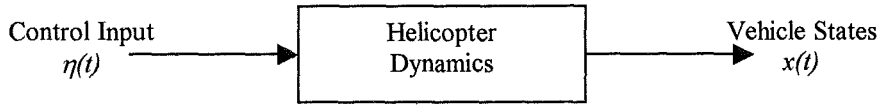

Figure 1.3 Forward Simulation

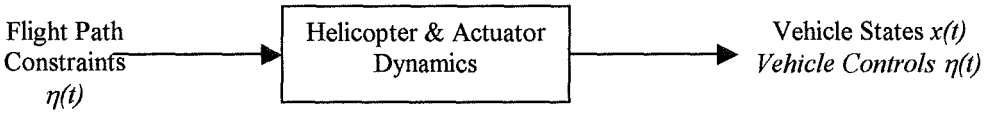

Figure 1.4 Inverse Simulation

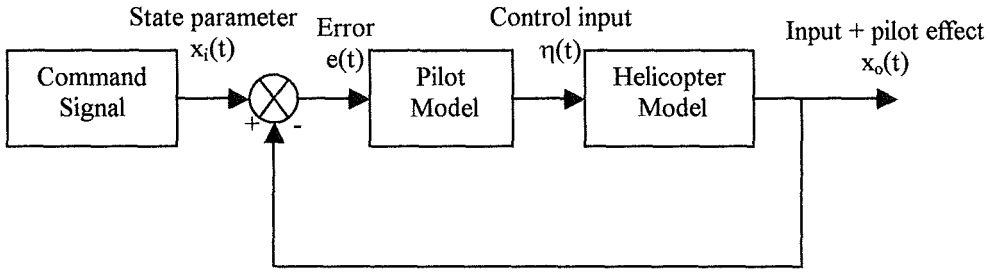

Figure 1.5 Man-Machine Control System

Chapter 2 Figures

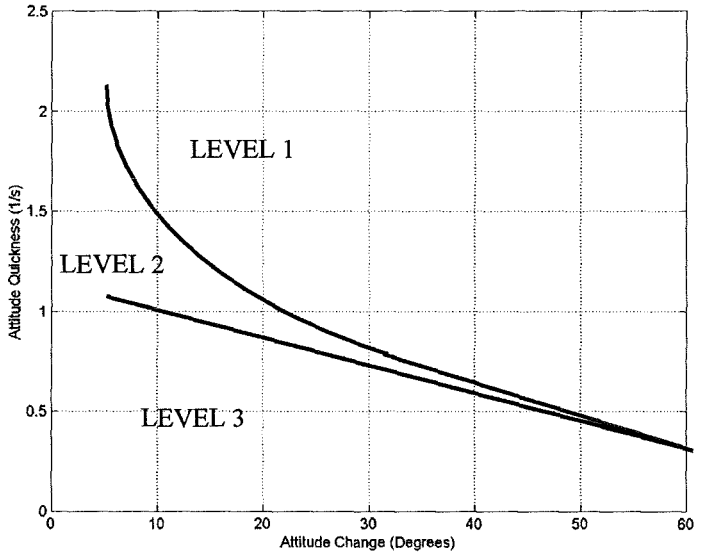

Figure 2.1a Roll Attitude Quickness, Target Acquisition and Tracking [ADS-33D (1994)]

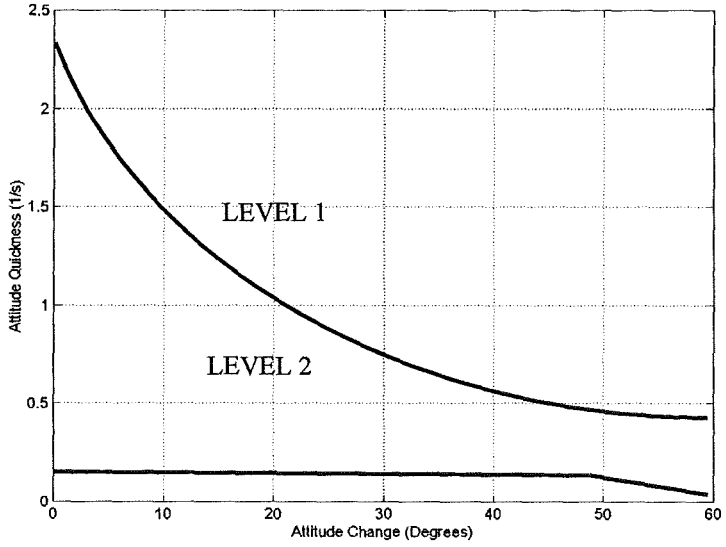

Figure 2.1b Roll Attitude Quickness Chart, All Other MTEs [ADS-33D (1994)]

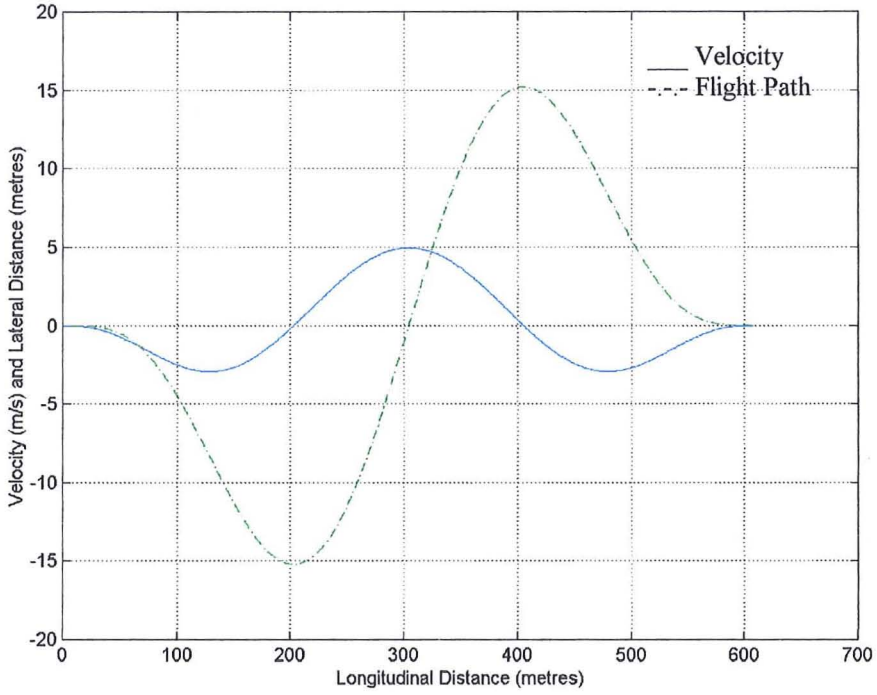

Figure 2.2 Slalom Flight Path Generated using a Smooth Global Polynomial with Velocity Constraints

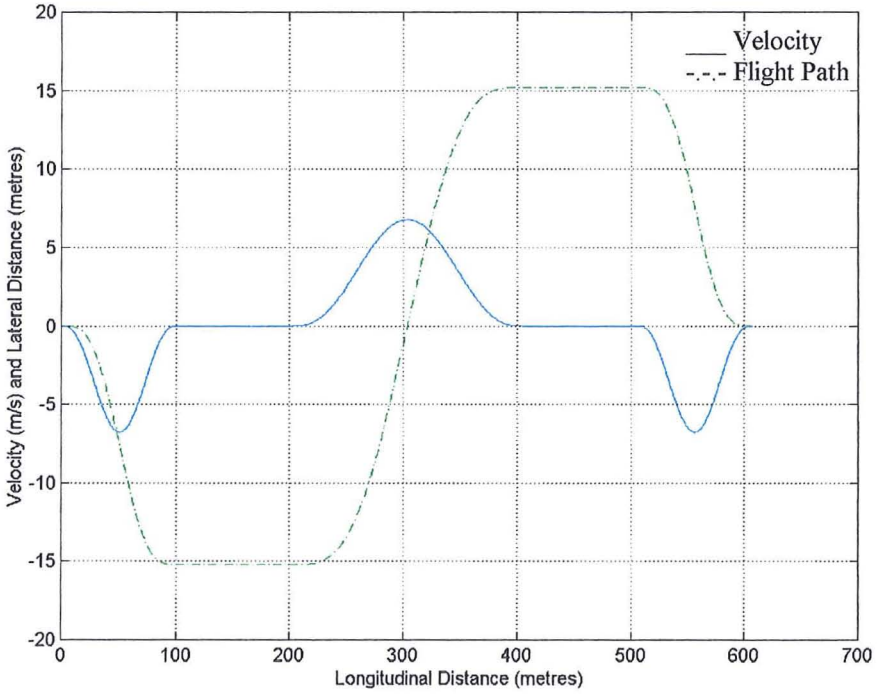

Figure 2.3 Slalom Flight Path Generated using a Piecewise Technique with Velocity Constraints

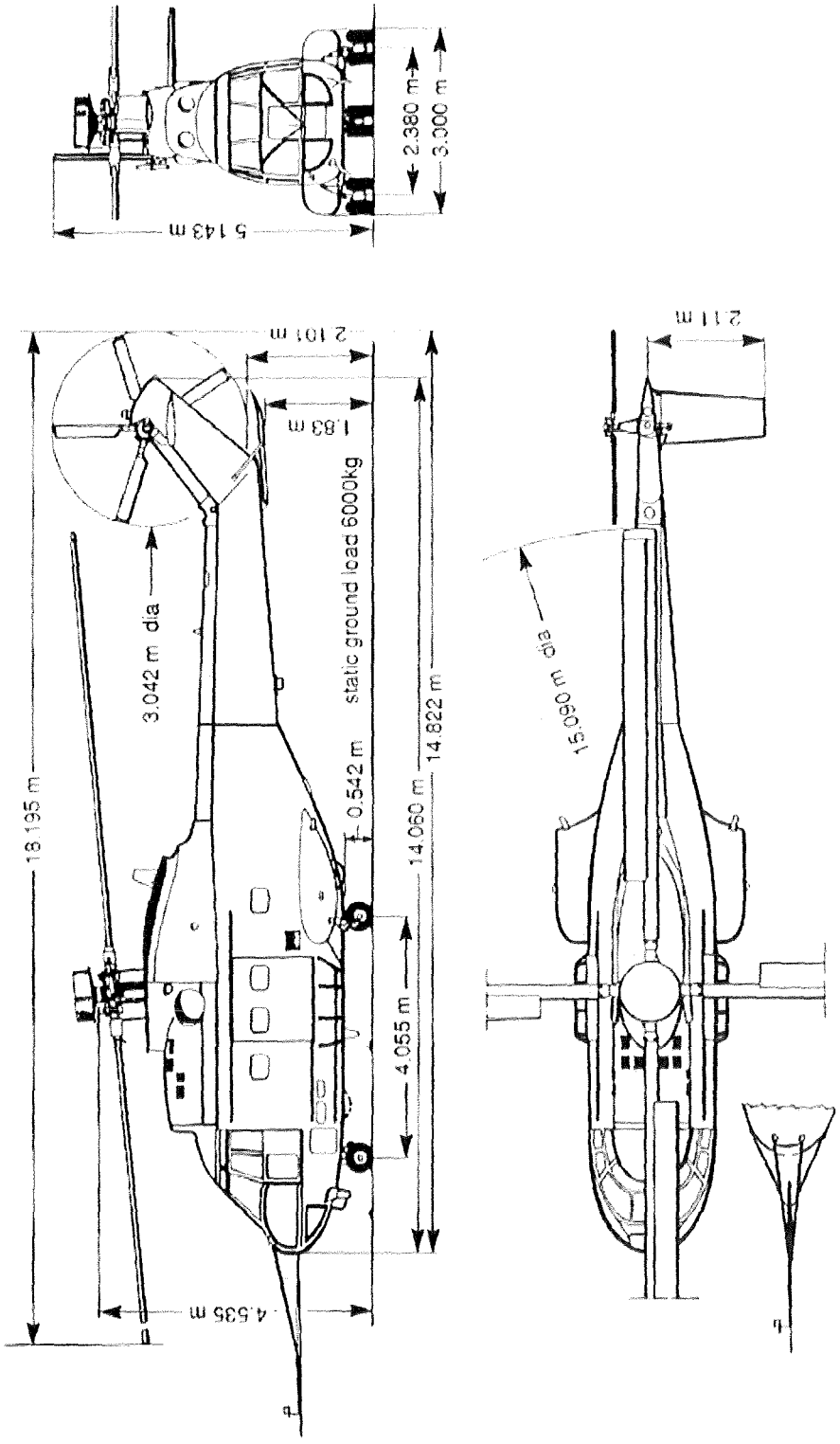

Figure 2.4 The Puma Helicopter [Reproduced from Padfield (1996)]

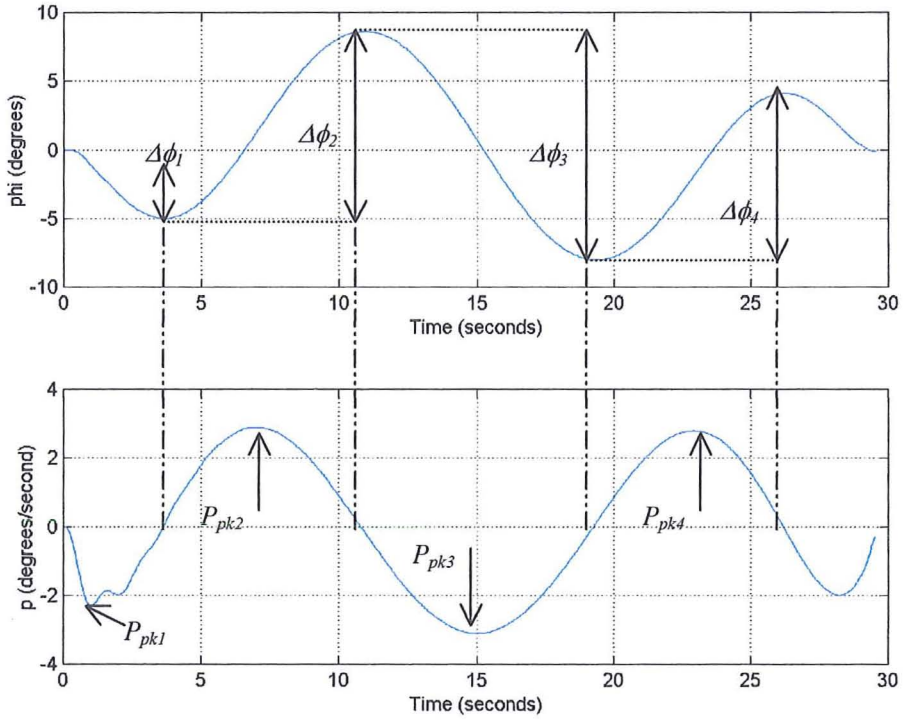

Figure 2.5 Roll and Roll Rate Time Histories Attitude for Polynomial Defined Slalom Performed at 40knots in a Puma Helicopter

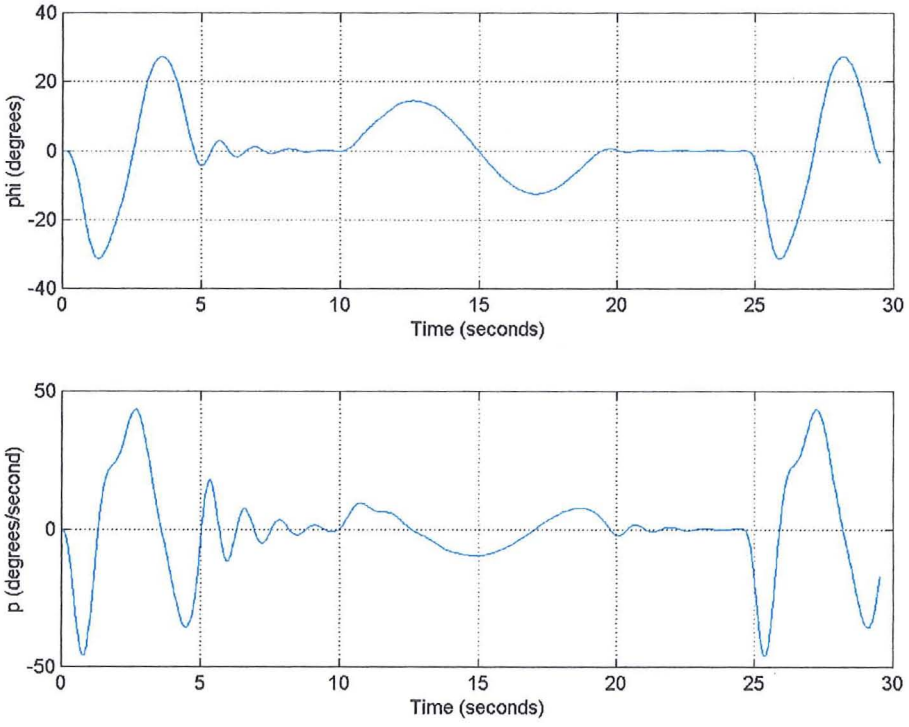

Figure 2.6 Roll and Roll Rate Time Histories for Piecewise Defined Slalom Performed at 40knots in a Puma Helicopter

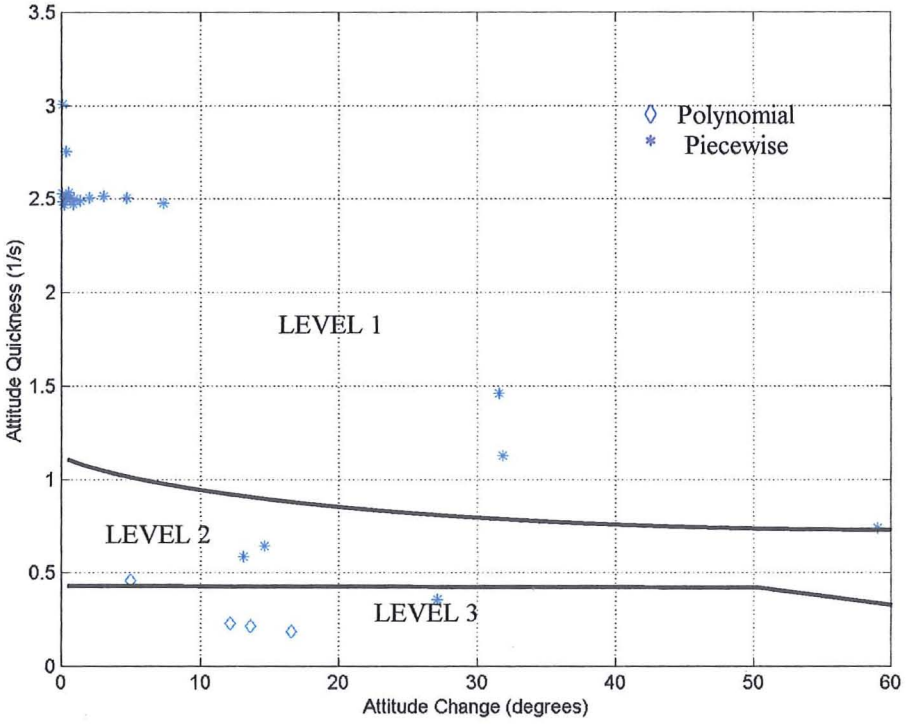

Figure 2.7 Corresponding Roll Attitude Quickness Chart

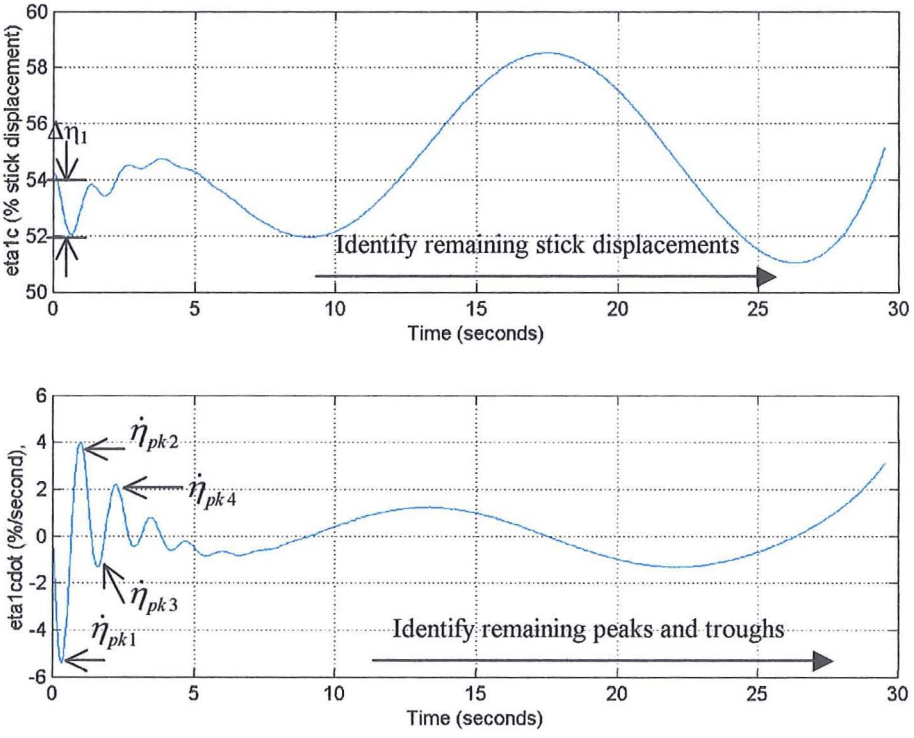

Figure 2.8 Lateral Stick Displacement and Derivative For Polynomial ADS Slalom Mission Task Performed in a Puma at 40knots

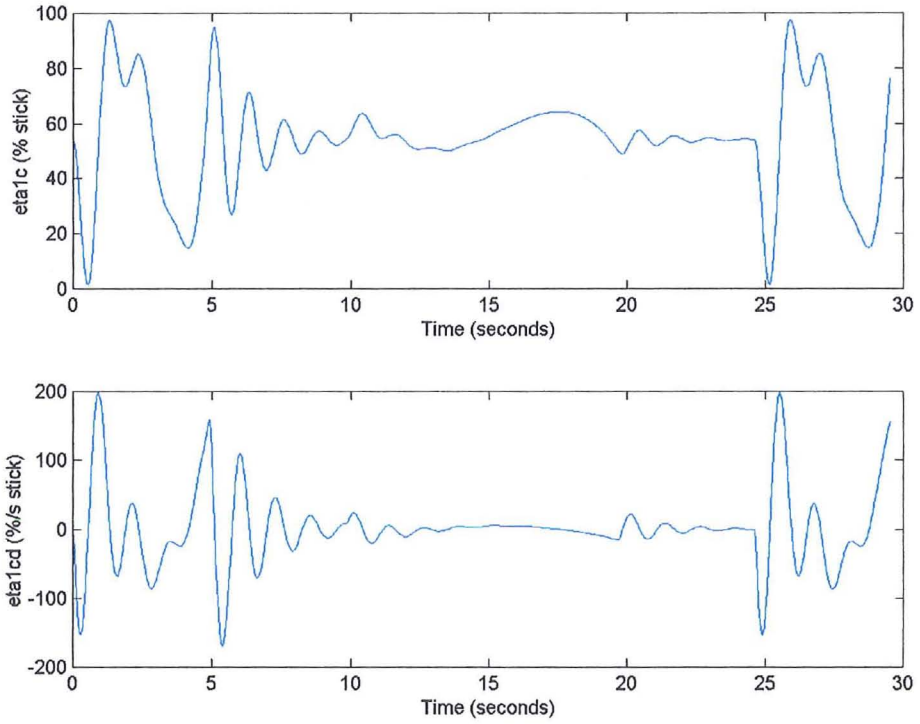

Figure 2.9 Lateral Stick Displacement and Derivative For piecewise ADS Slalom Mission Task Performed in a Puma at 40knots

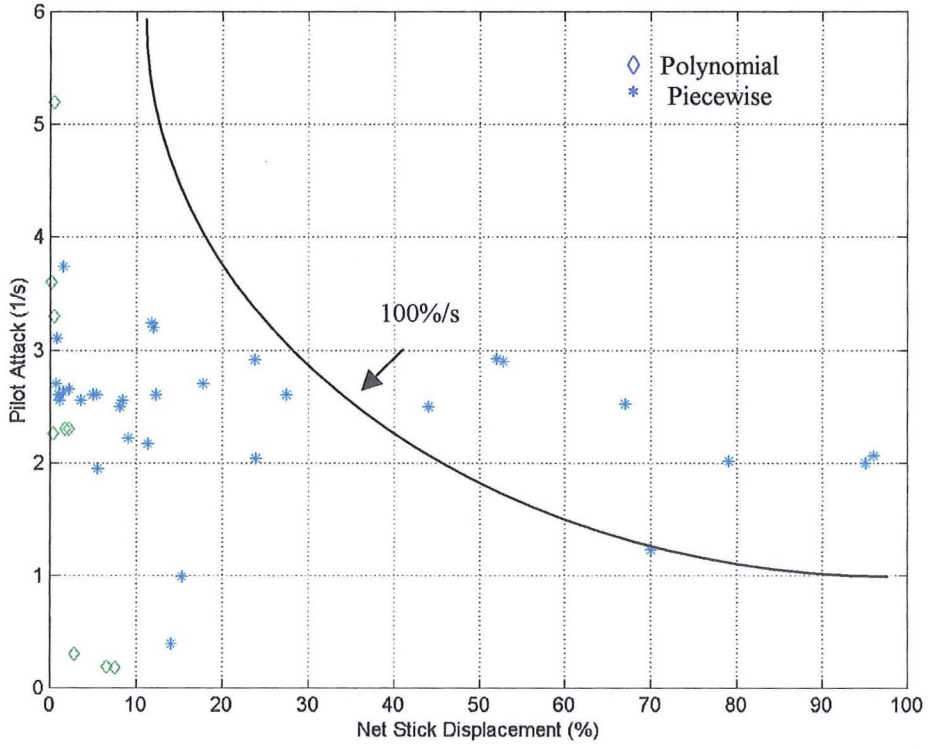

Figure 2.10 Corresponding Pilot Attack Chart

Chapter 3 Figures

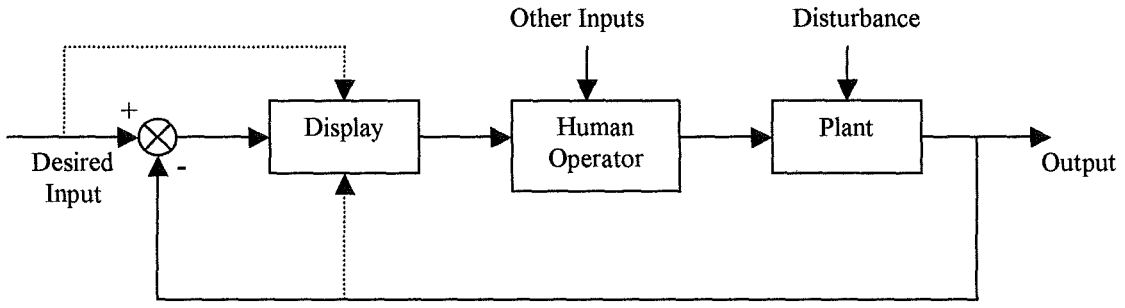

Figure 3.1 Basic Man-Machine Control System

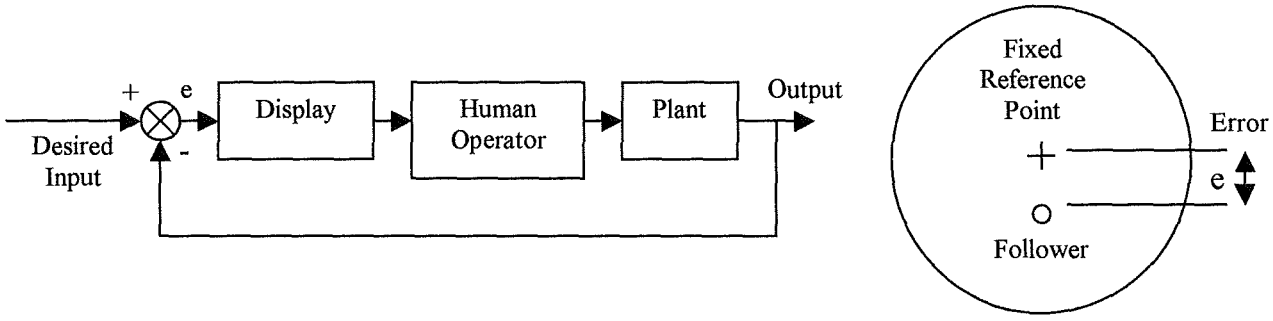

Figure 3.2a Compensatory Tracking Task and Display

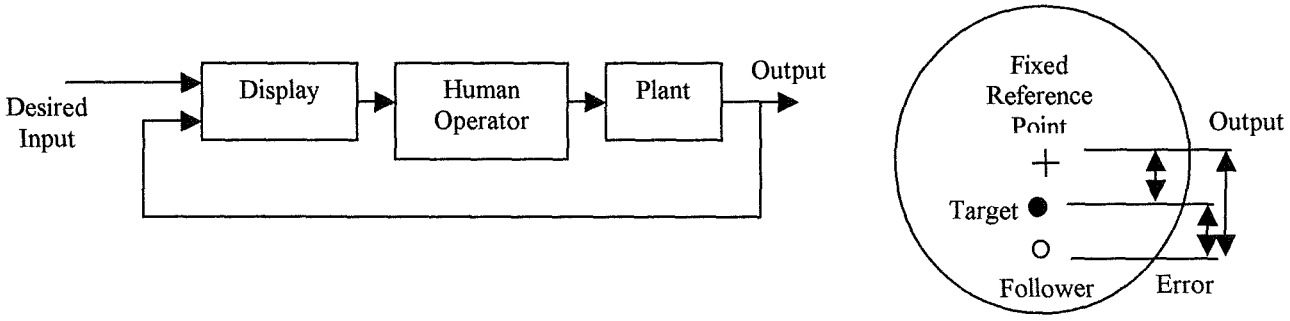

Figure 3.2b Pursuit Tracking Task and Display

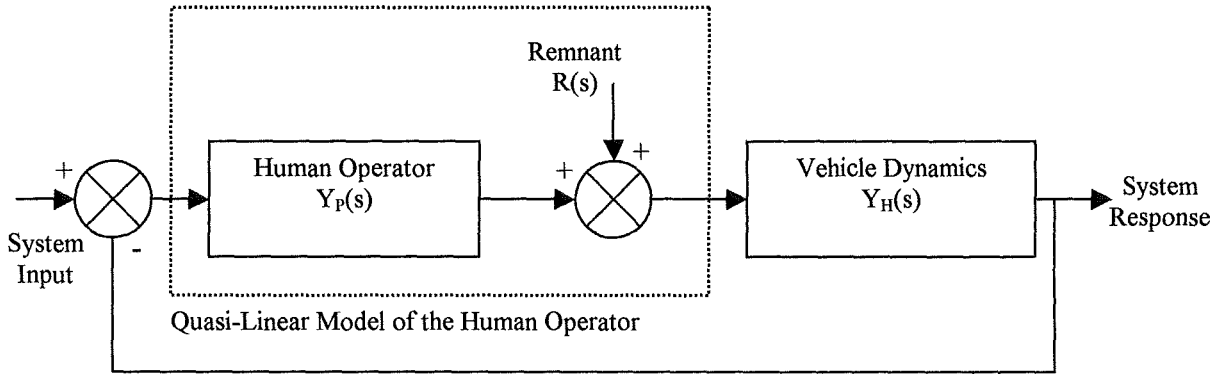

Figure 3.3 A Quasi-Linear Model of the Human Operator

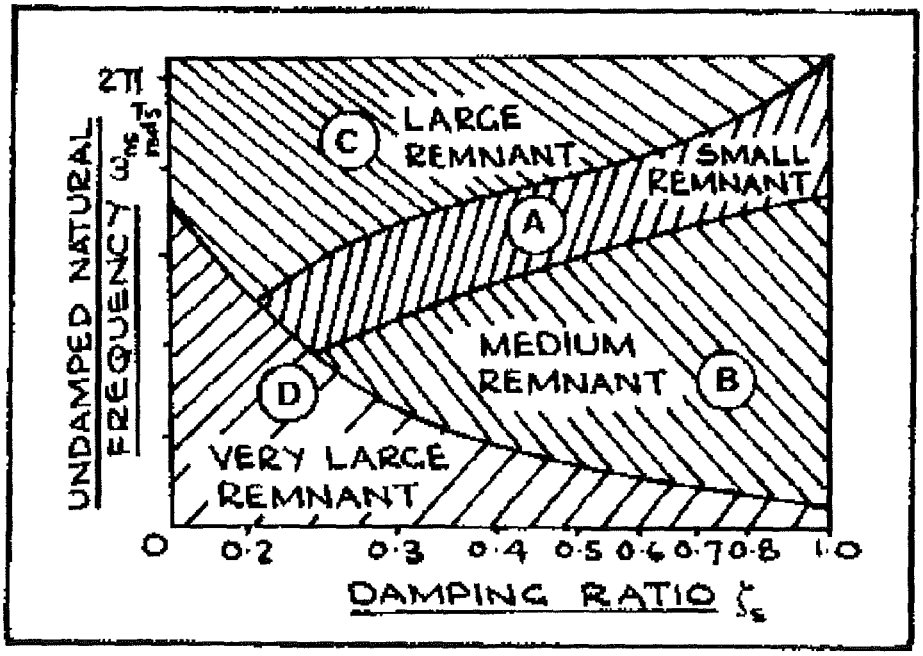

Figure 3.4 Remnant Differences with Variations in the Parameters off the Short Pitch Transfer Function of an Aircraft as Pictured by Sutton (1990)

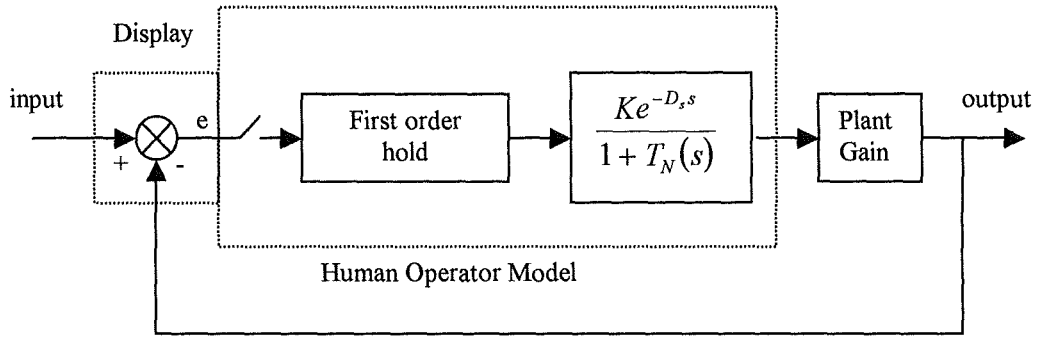

Figure 3.5 A Sampled Data Model of the Human Operator (Bekey 1962)

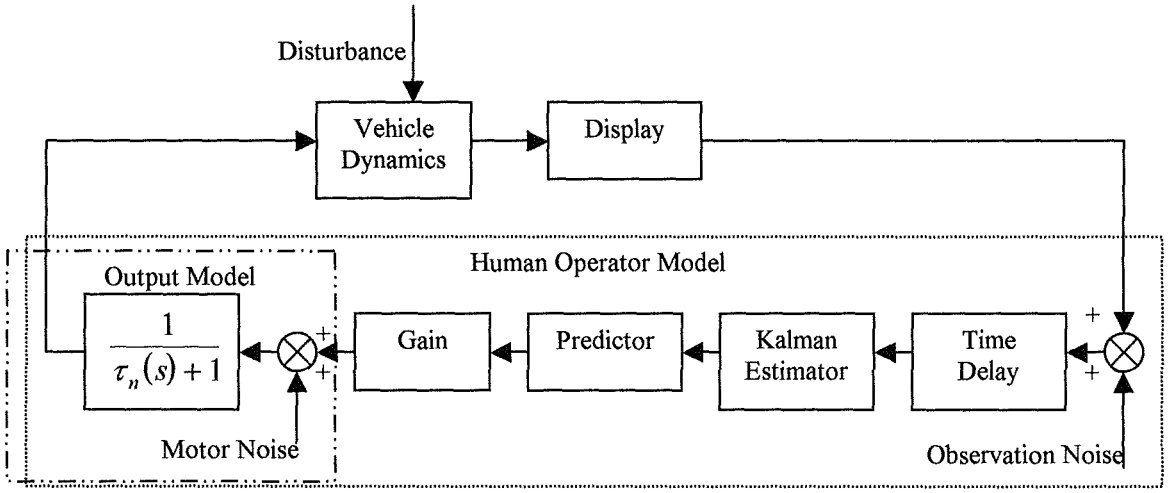

Figure 3.6 An Optimal Control Model of the Human Operator (Kleinman 1962)

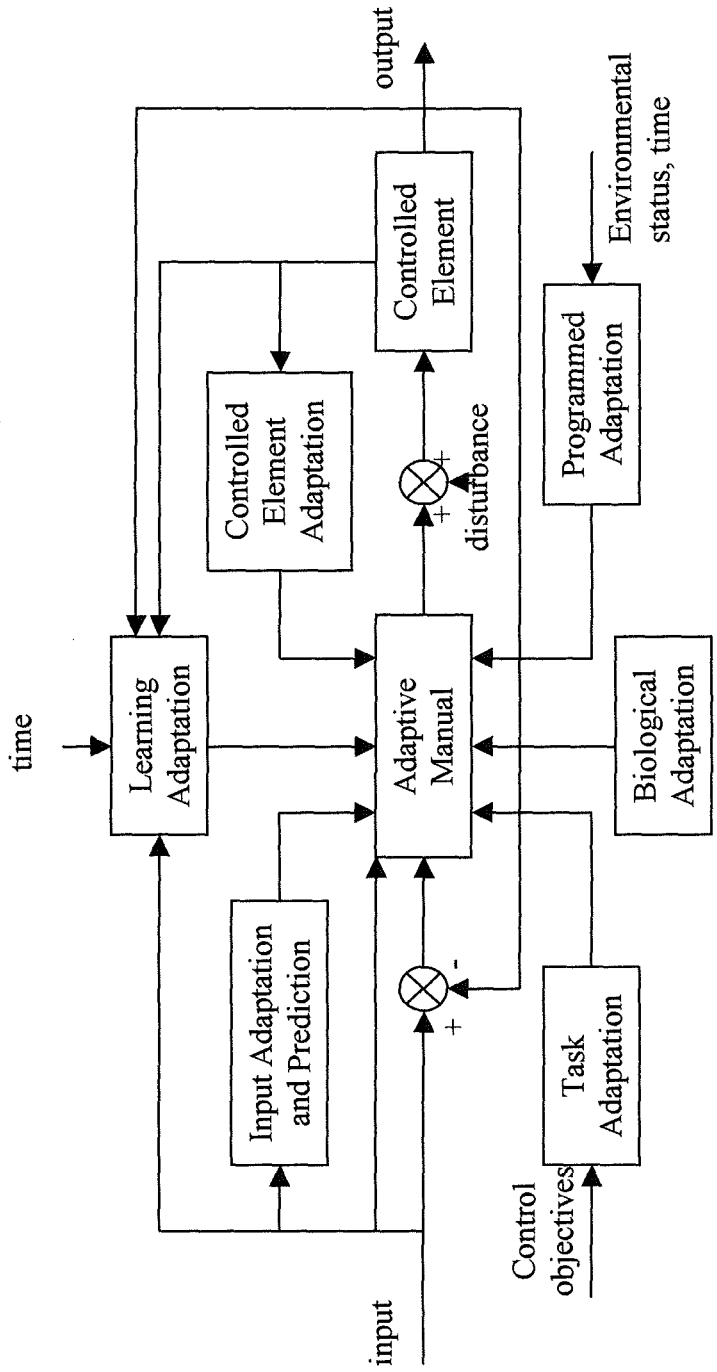

Figure 3.7 The Main Adaptive Characteristics of the Human Operator in a Manual Control Task (Young 1969)

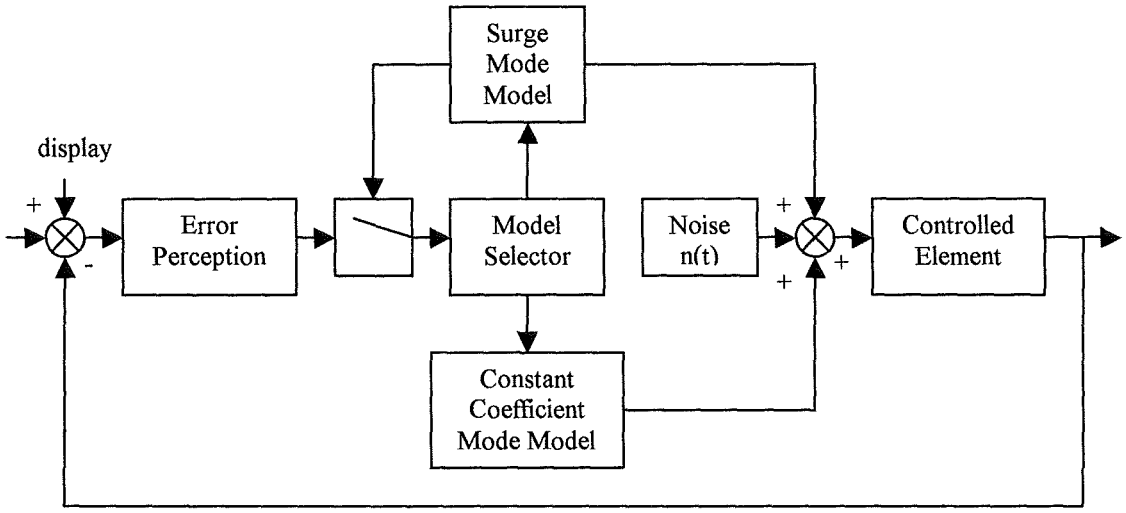

Figure 3.8 A Block Diagram of Costello's Surge Model (Costello 1968)

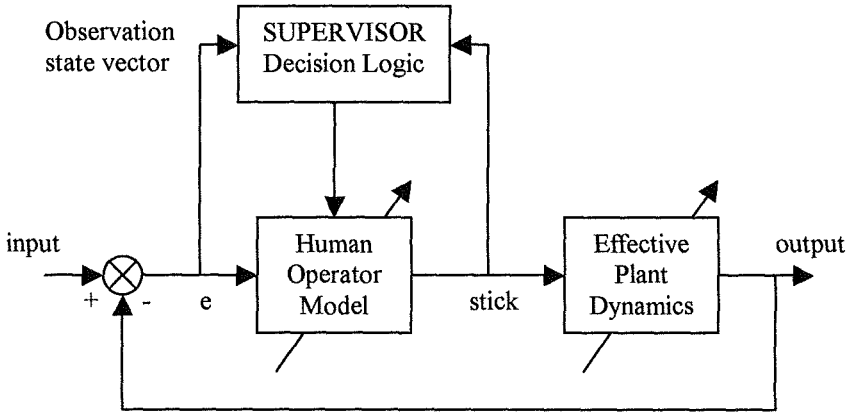

Figure 3.9 A Block Diagram of the Adaptive Model (Phatak & Bekey 1969)

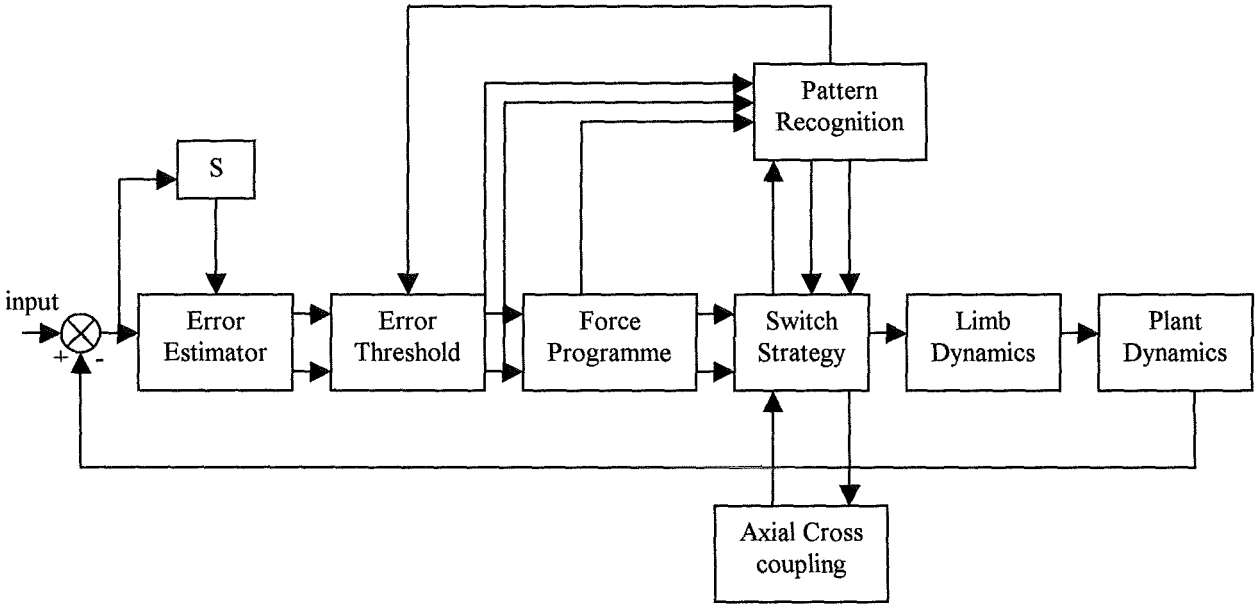

Figure 3.10 A Block Diagram of the Adaptive Model (Gilstad & Fu 1971)

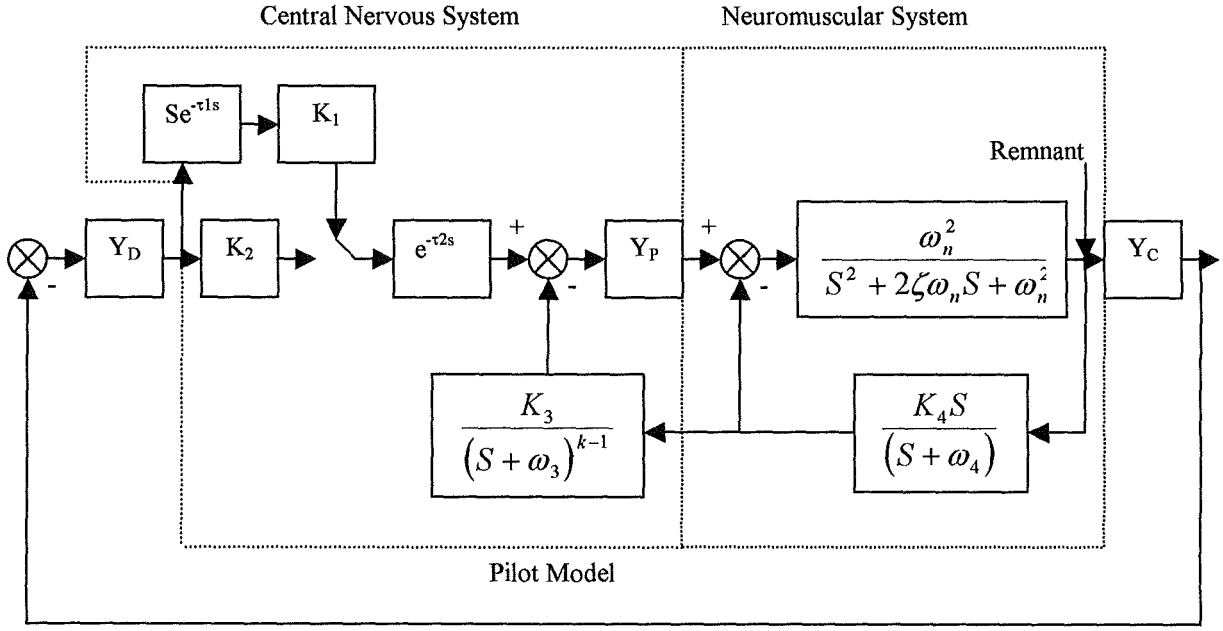

Figure 3.11 The Structural Pilot Model (Hess 1980

Chapter 4 Figures

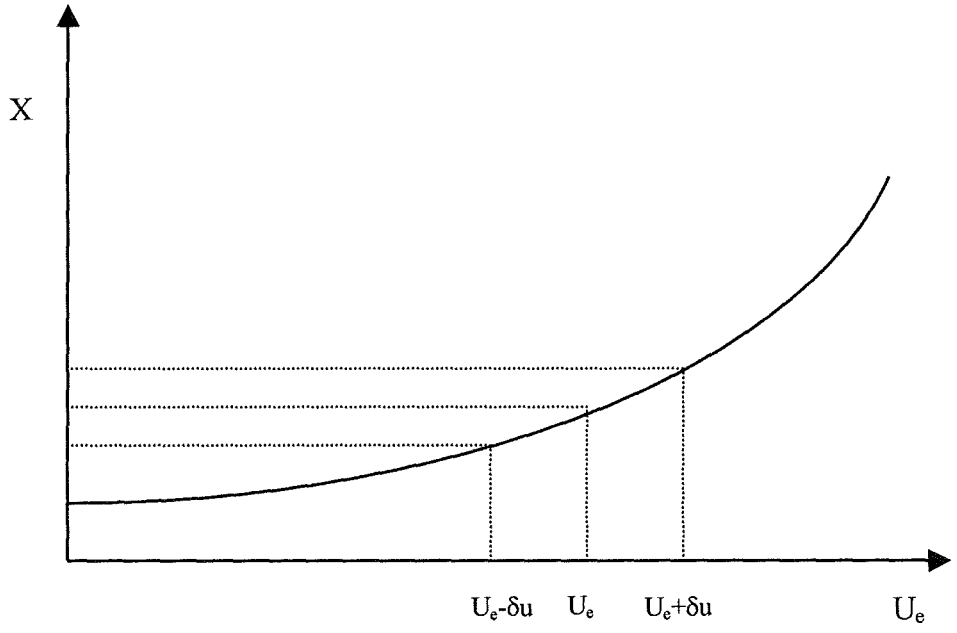

Figure 4.1 Numerical differentiation Technique Employed in Determining the Stability Derivatives

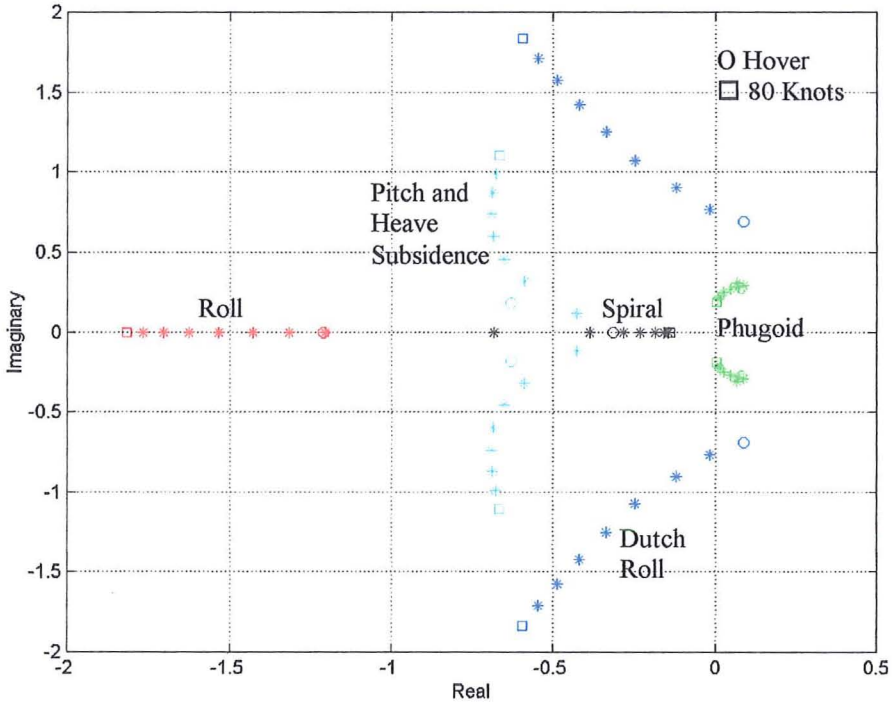

Figure 4.2 Loci of Puma Eigenvalues from Hover to 80 Knots

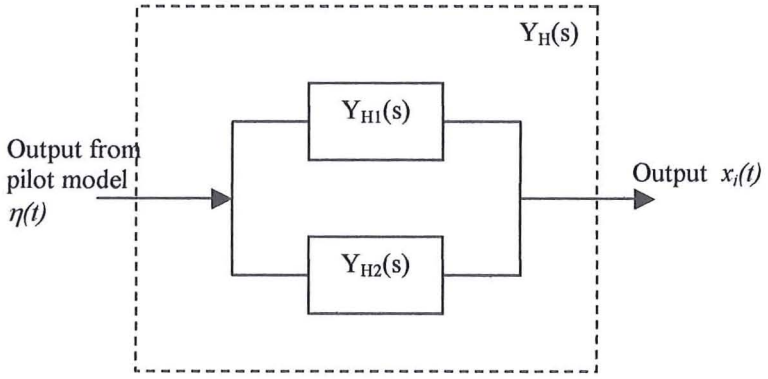

Figure 4.3 Multiple Control Axis Plant Dynamics Representation

Chapter 5 Figures

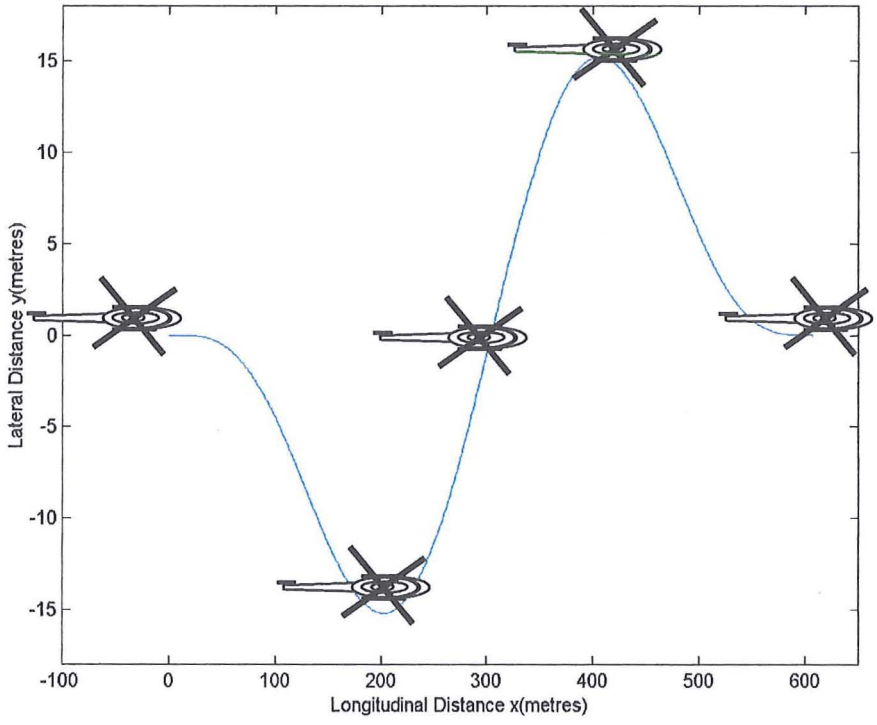

Figure 5.1 ADS-33D Slalom with Constrained Heading

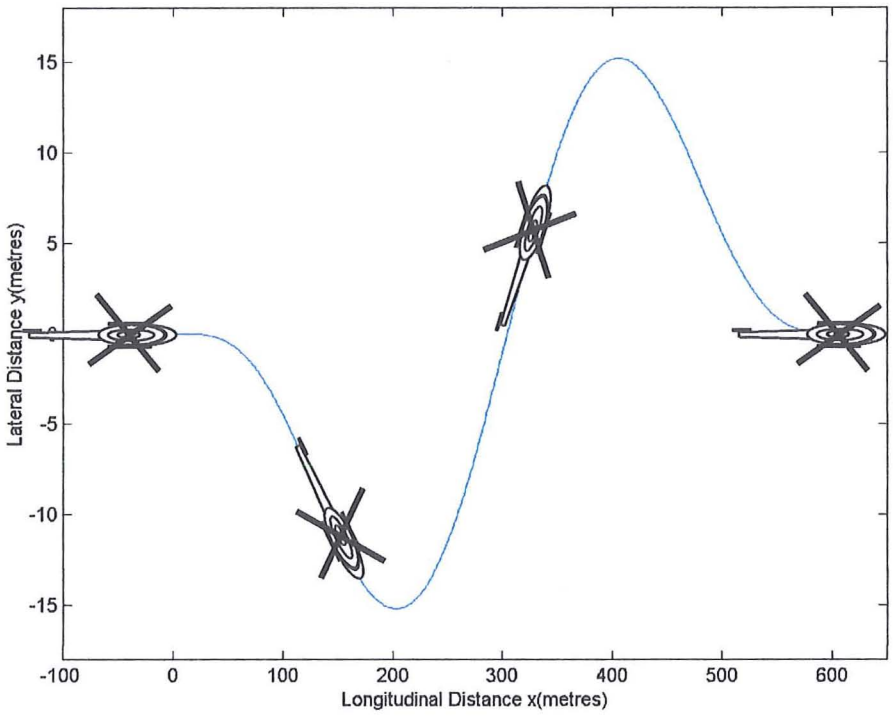

Figure 5.2 ADS-33D Slalom with Constrained Sideslip

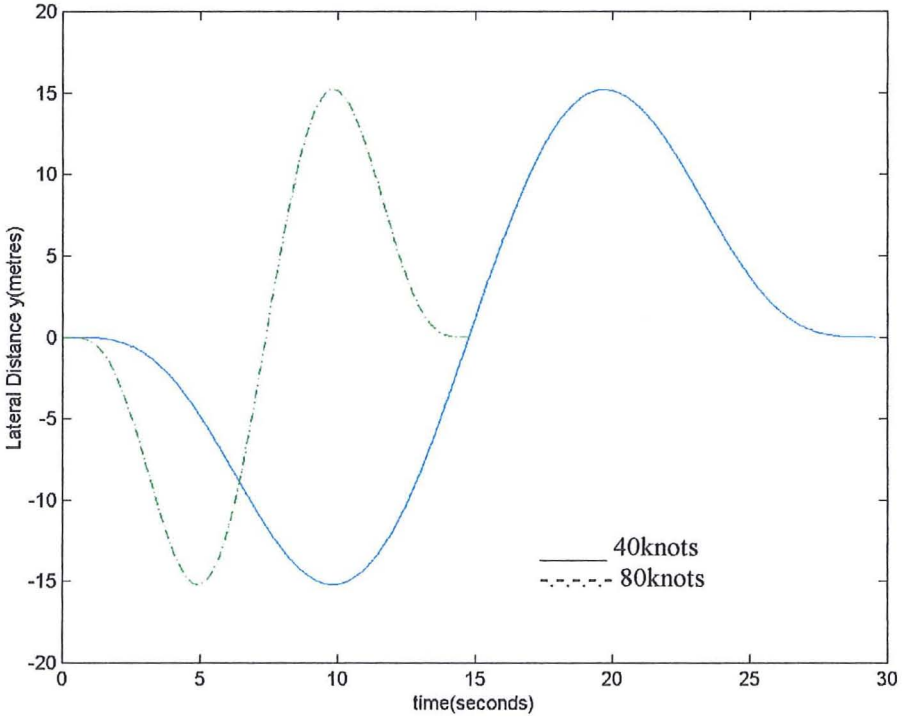

Figure 5.3 ADS-33D Slalom Lateral Translation at 40 & 80 Knots

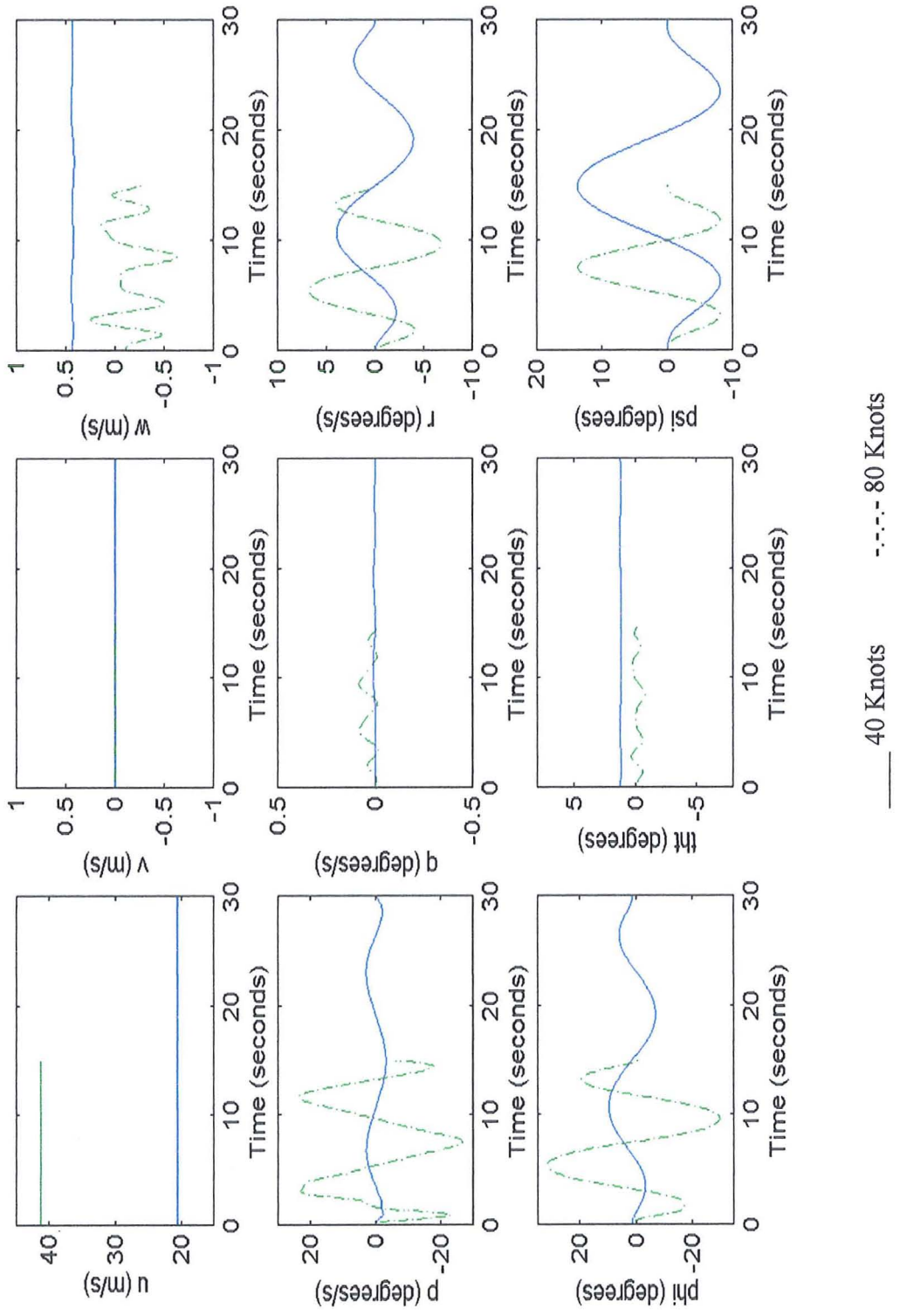

Figure 5.4 Helinv Predicted State Parameter Time Histories for 40 & 80 Knot Slalom with Constrained Sideslip

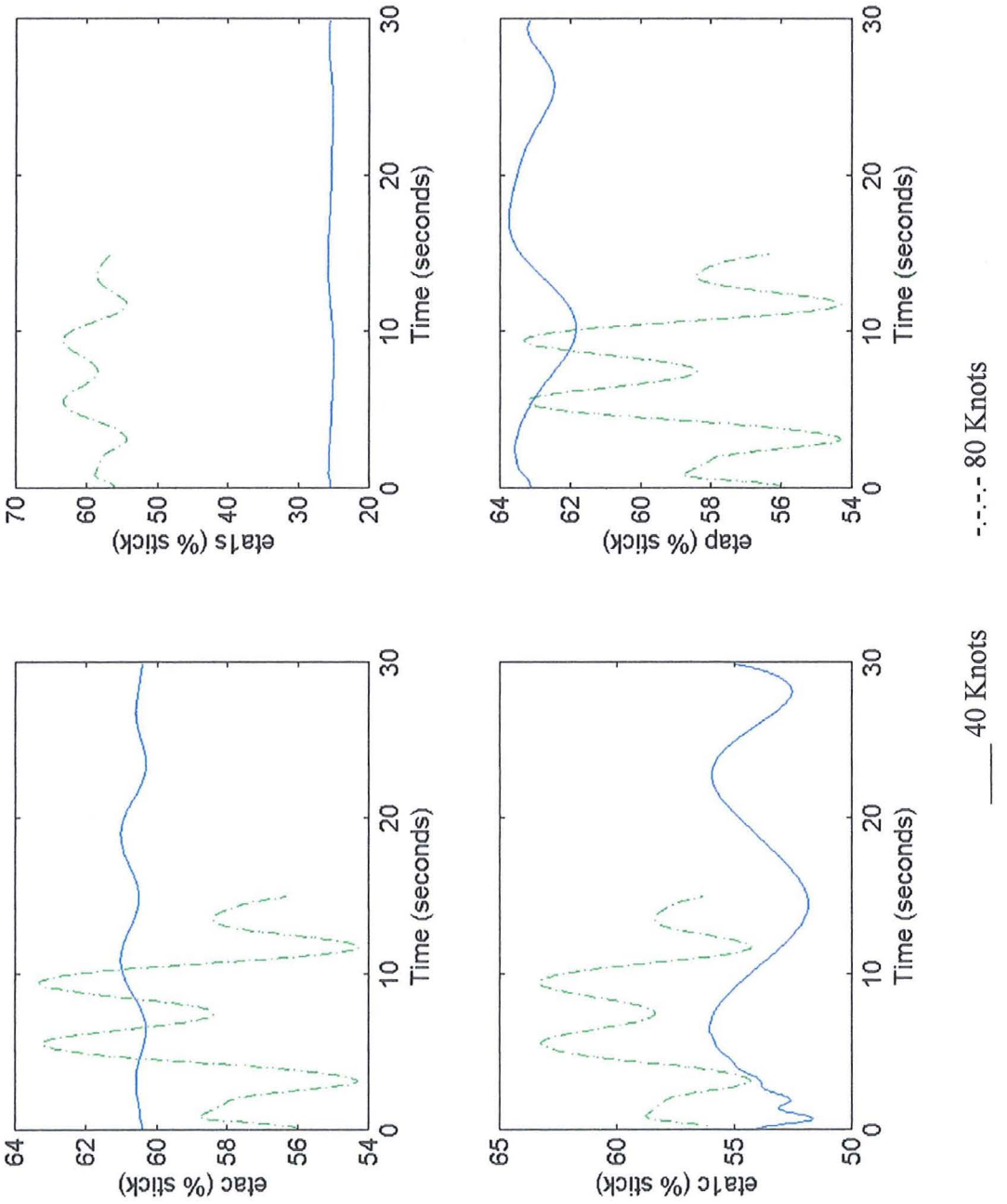

Figure 5.5 Helinv Predicted Control Parameter Time Histories for 40 & 80 Knot Slalom with Constrained Sideslip

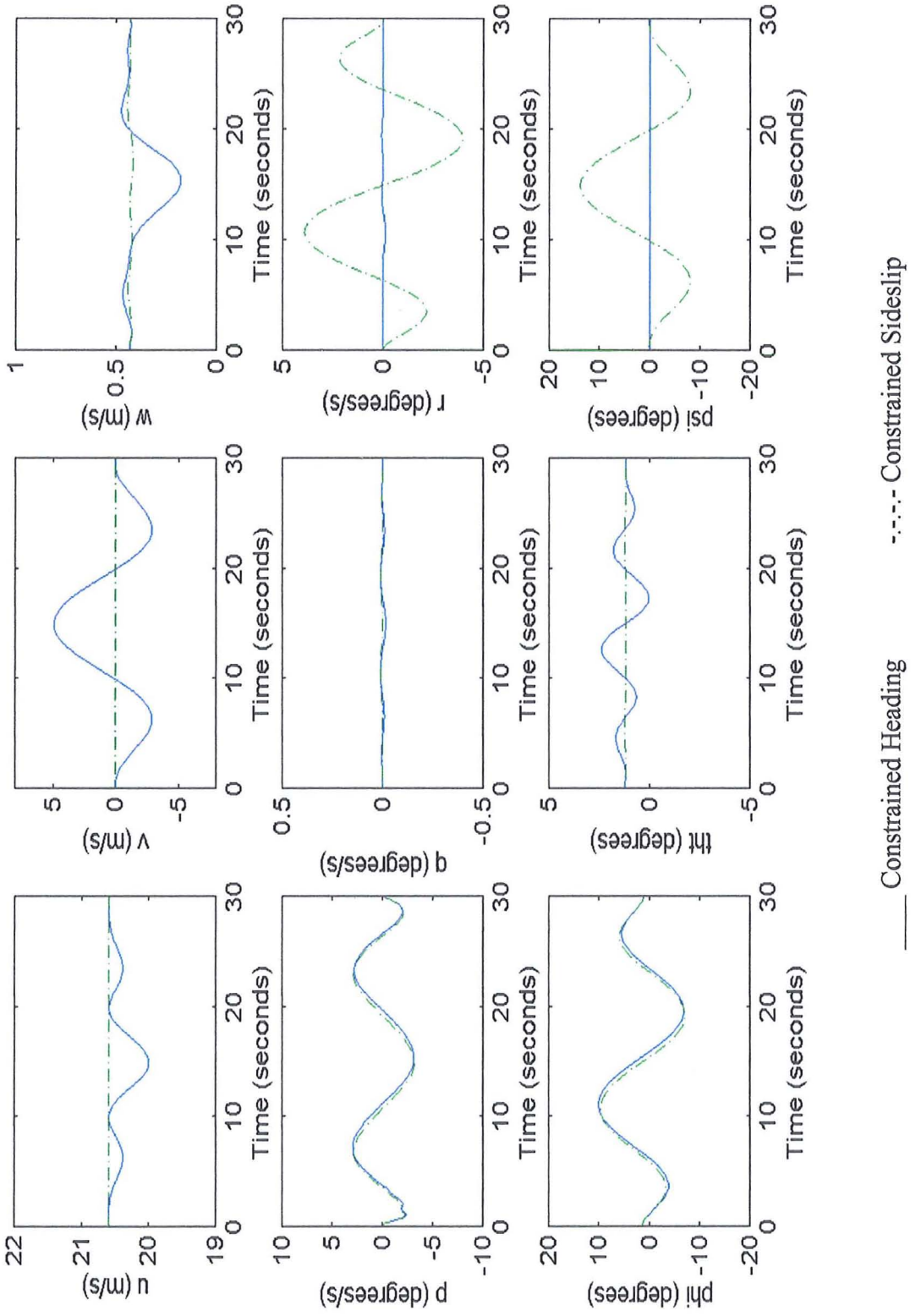

Figure 5.6 Comparison of Helinv Predicted State Parameter Time Histories for 40 Knot Slalom with Constrained Heading and Constrained Sideslip

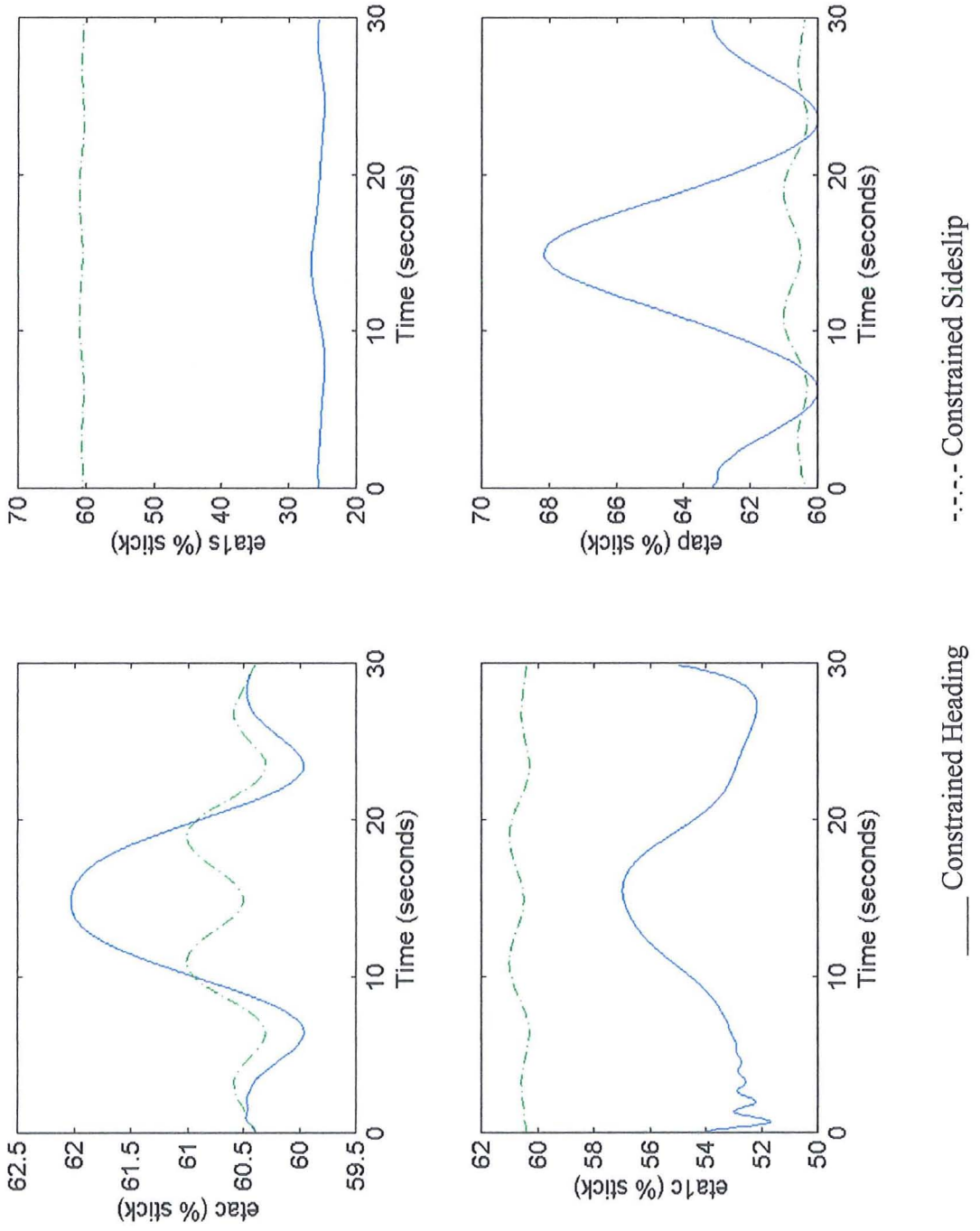

Figure 5.7 Comparison of Helinv Predicted Control Parameter Time Histories for 40 Knot Slalom with Constrained Heading and Constrained Sideslip

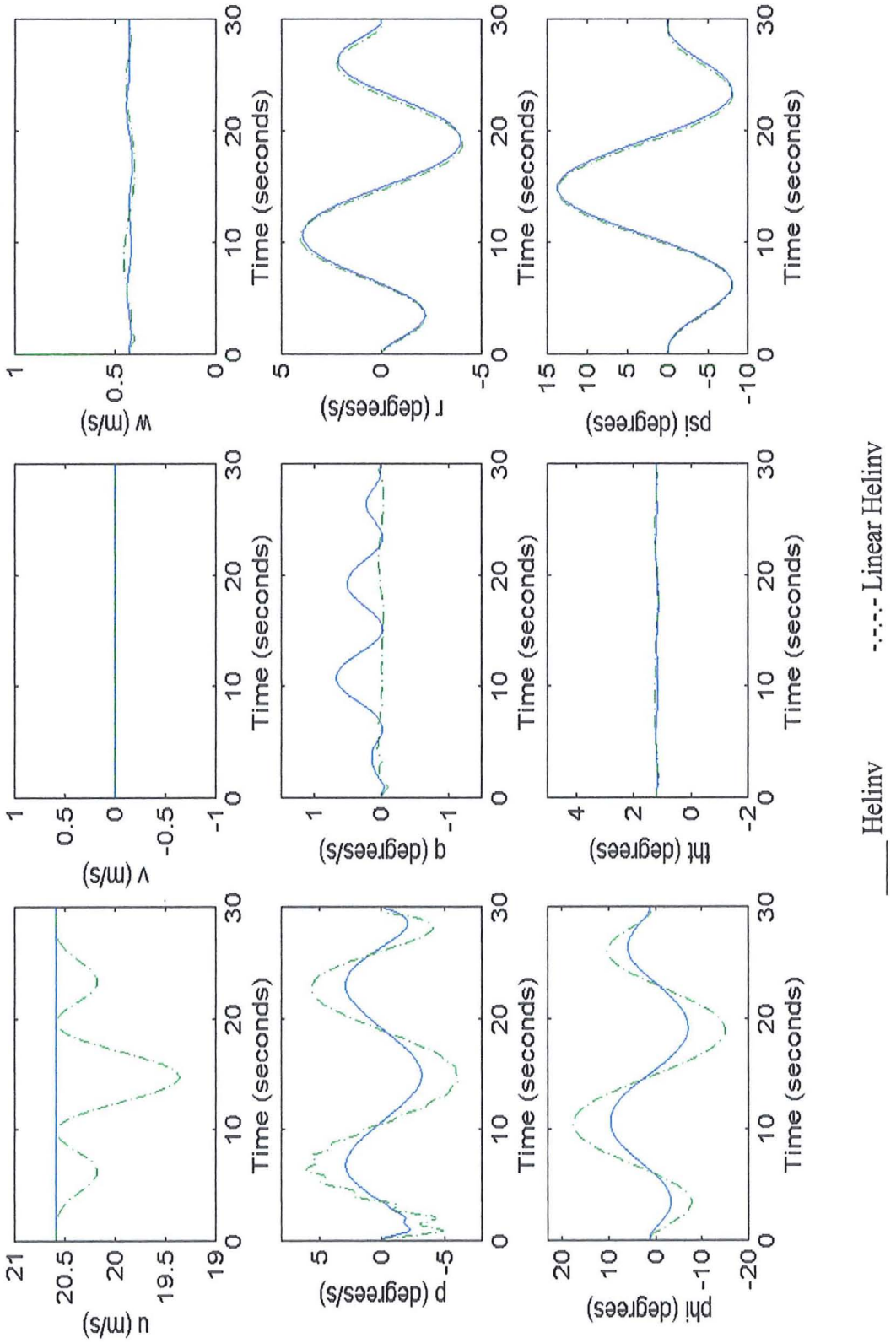

Figure 5.8 Comparison of Helinv and Linear Helinv Predicted State Parameter Time Histories for 40 Knot Slalom with Constrained Sideslip

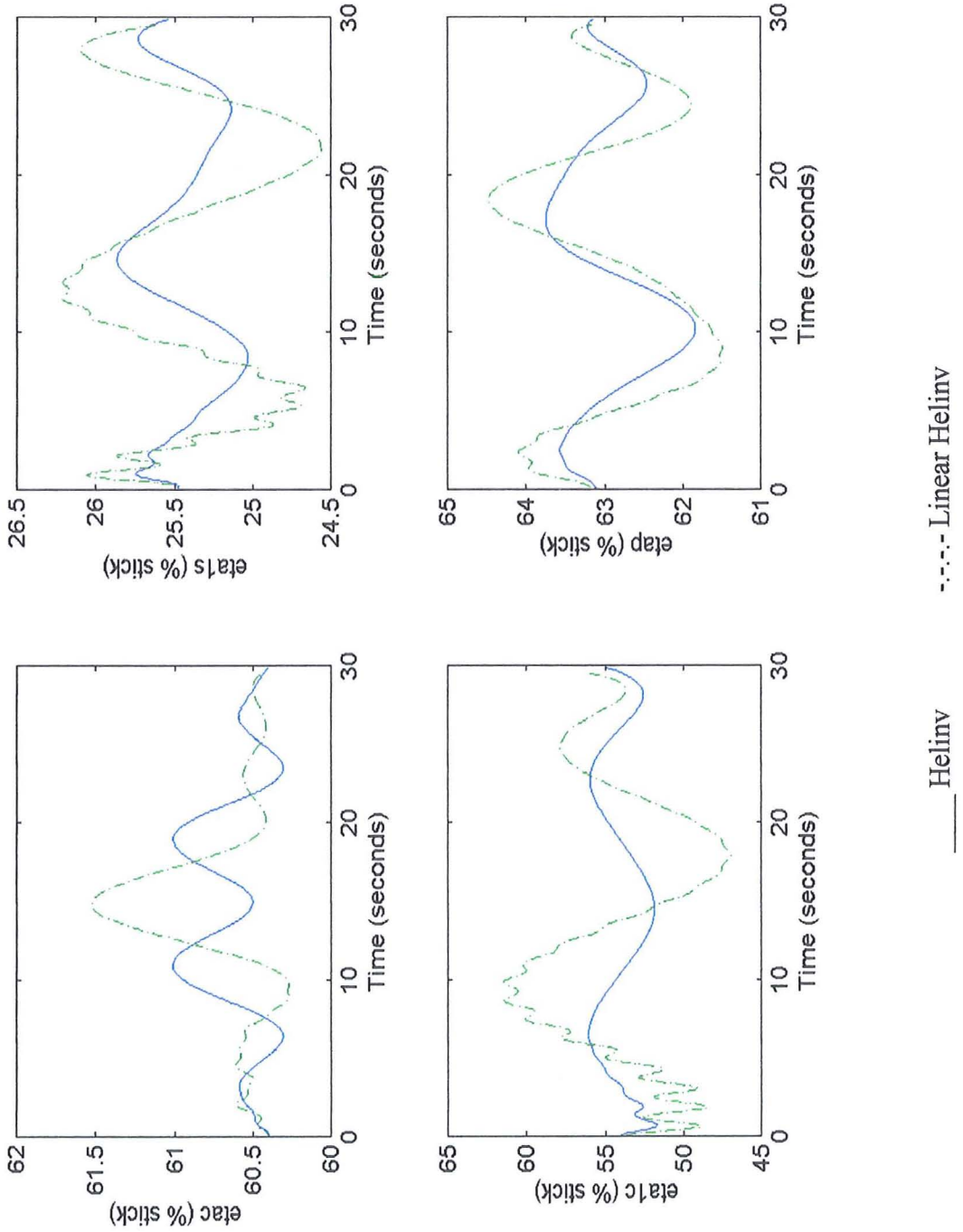

Figure 5.9 Comparison of Helinv and Linear Helinv Predicted Control Parameter Time Histories for 40 Knot Slalom with Constrained Sideslip

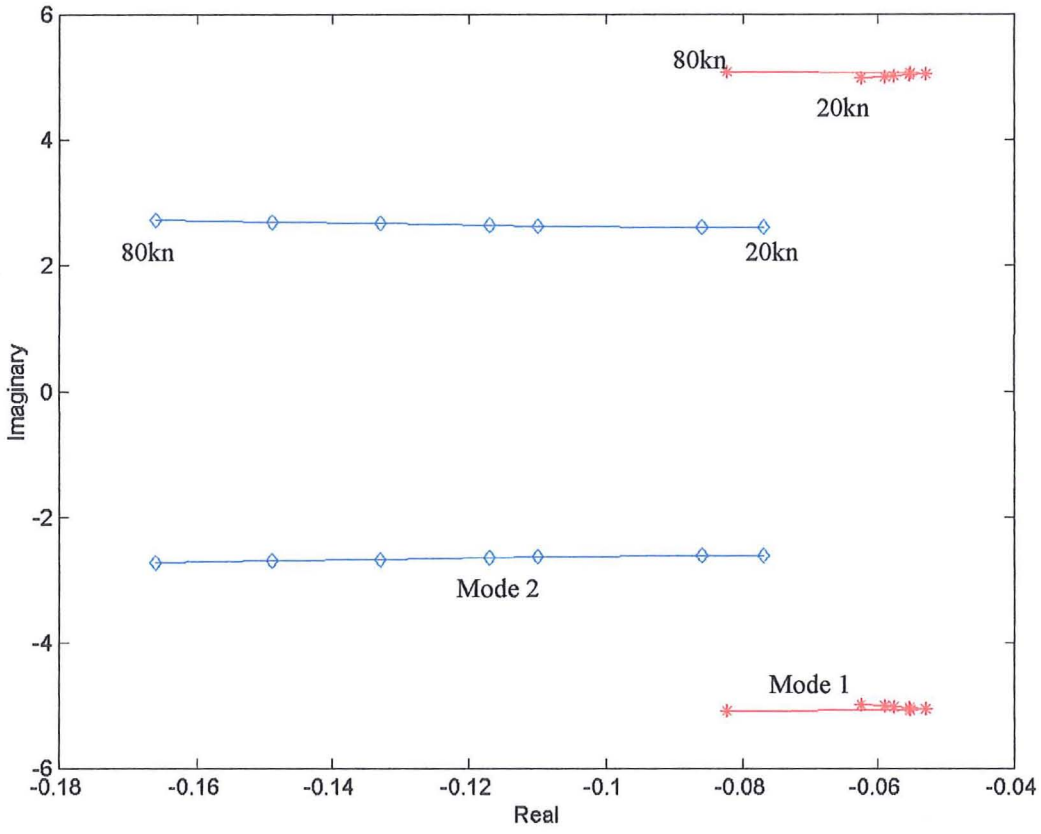

Figure 5.10 Root Locus Plots of Oscillatory Modes of Puma Helicopter in Constrained Flight

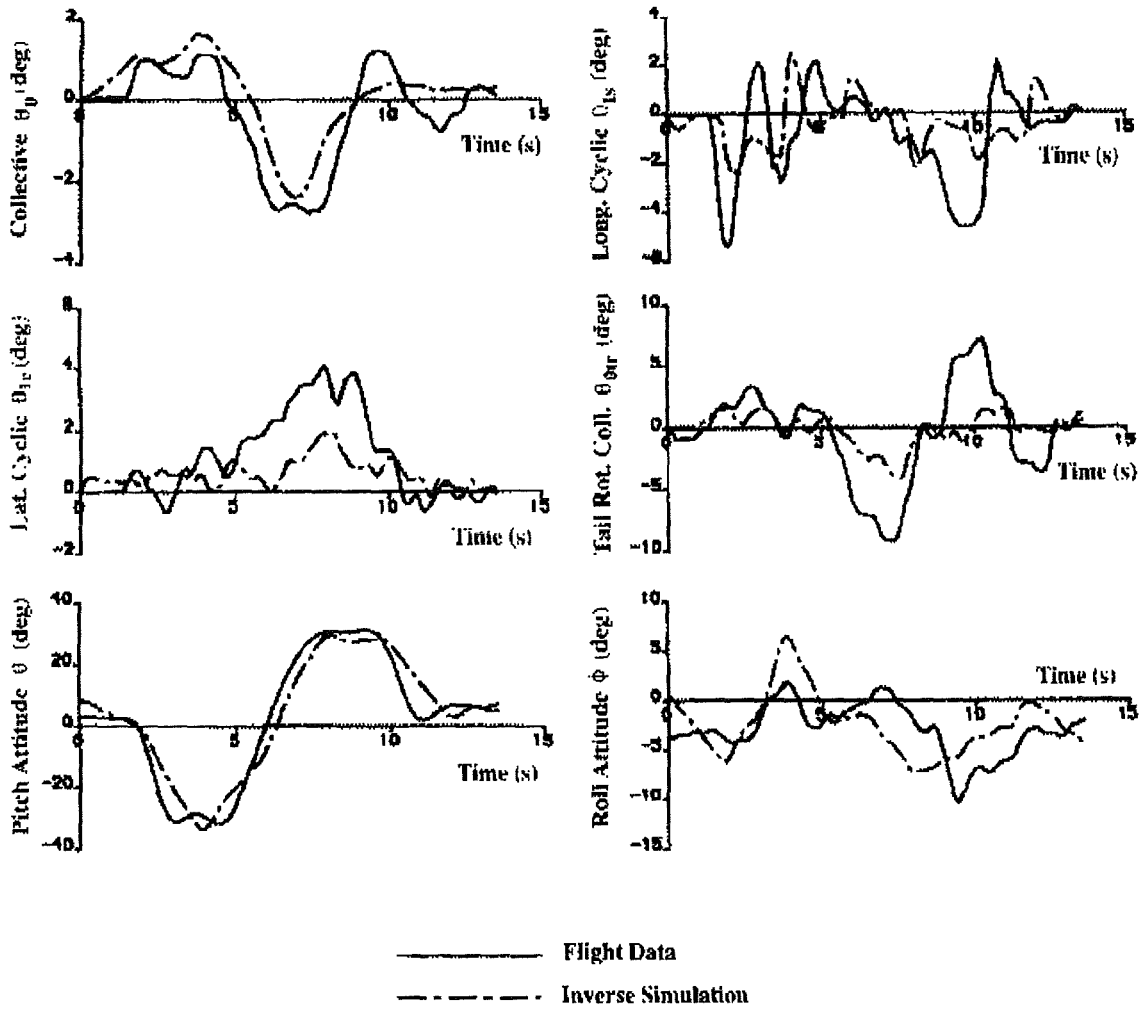

Figure 5.11 Comparison of Flight Data and Inverse Simulation Results for a 'Quick-Hop' Manoeuvre [Thomson & Bradley (1997)]

Chapter 6 Figures

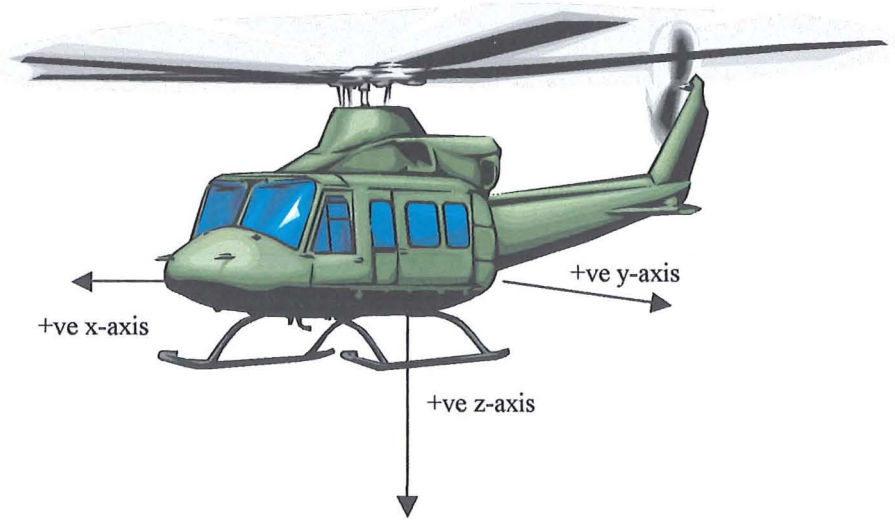

Figure 6.1 Aircraft Frame of Reference

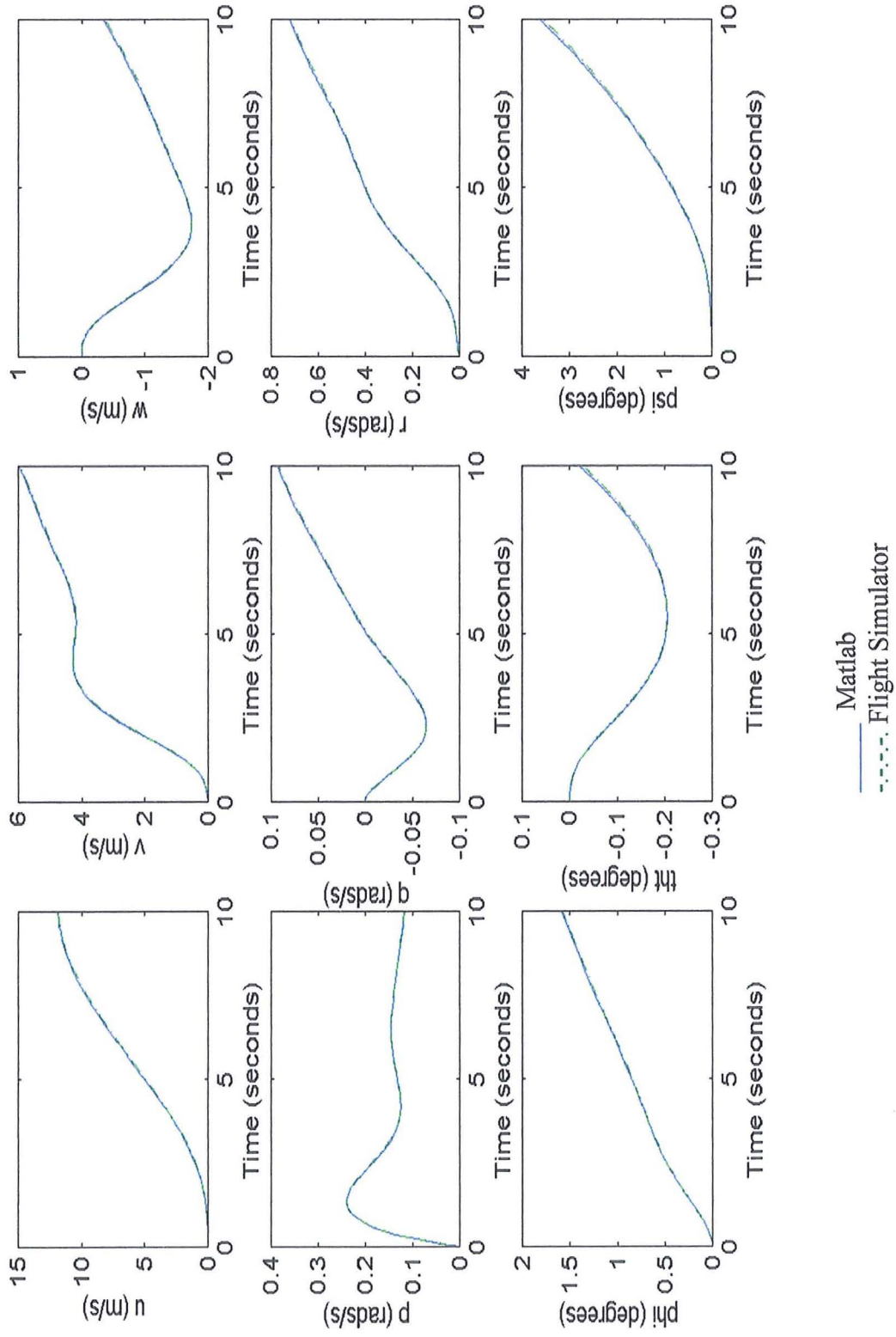

Figure 6.2 Response of a Puma to a One Degree Step Input in Lateral Cyclic at 40 Knots

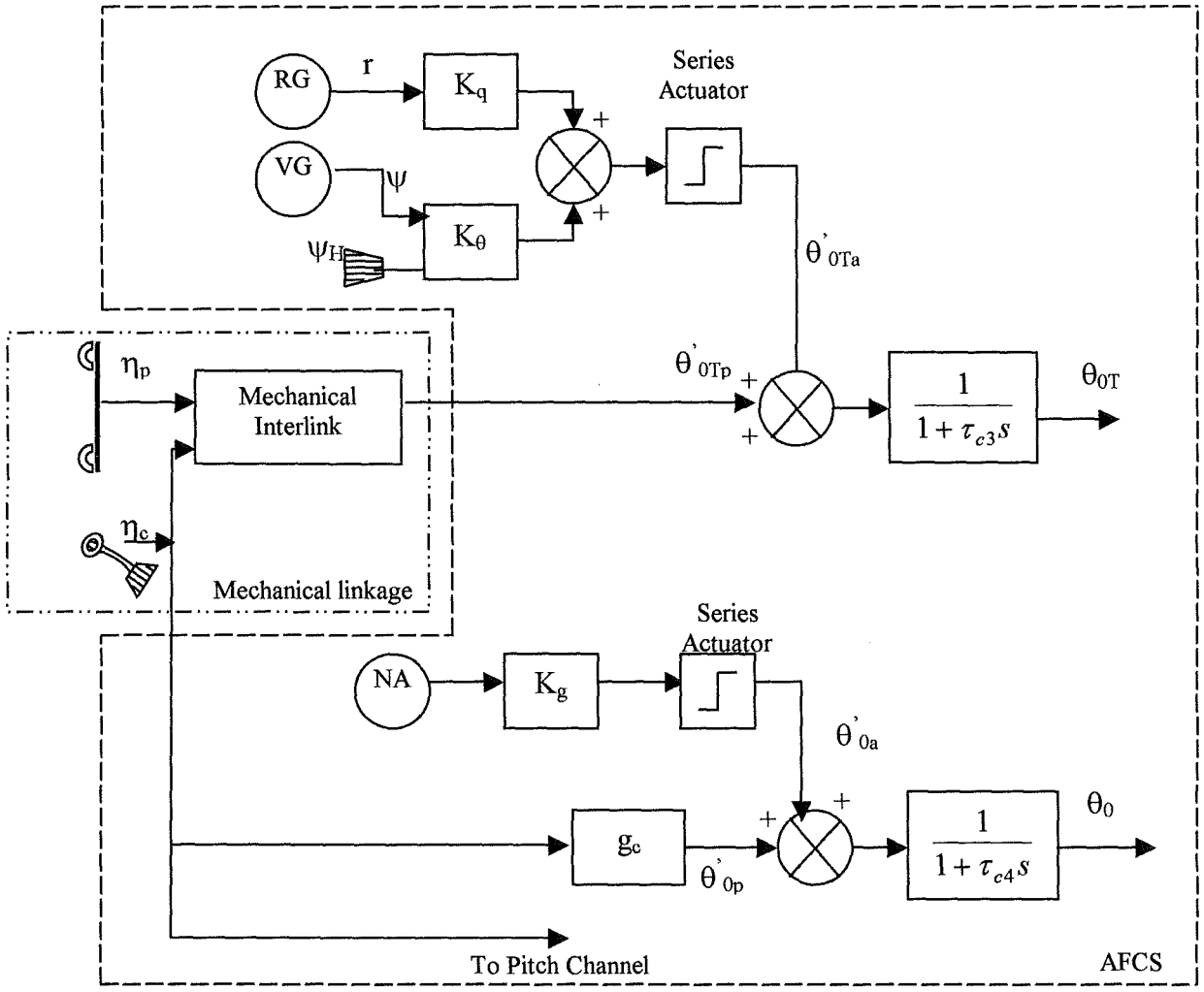

Figure 6.3a Schematic of a Helicopter Flight Control System [Padfield (1996)]

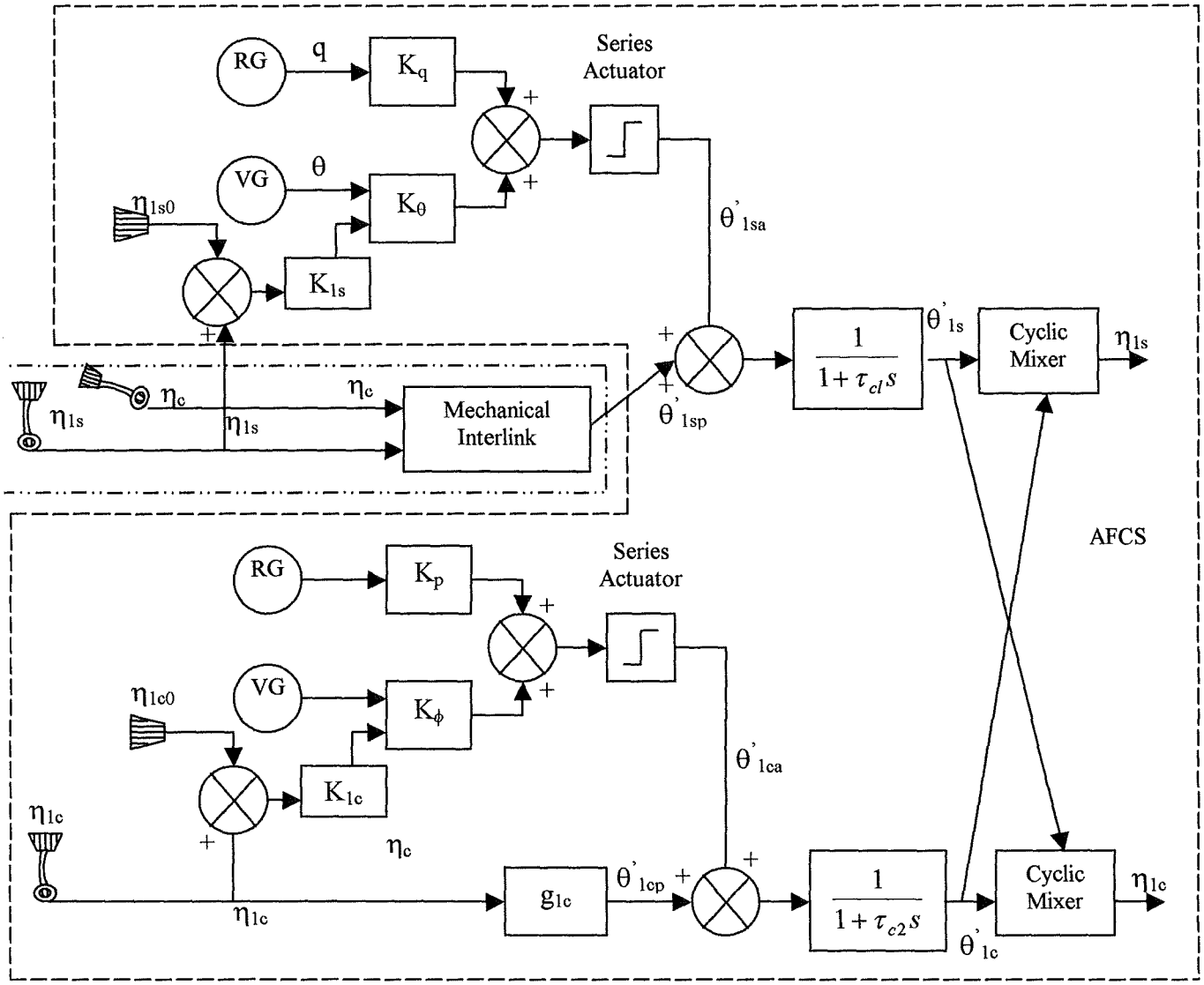

Figure 6.3b **Schematic of Pitch and Roll Control in a Helicopter Flight Control System [Padfield (1996)]**

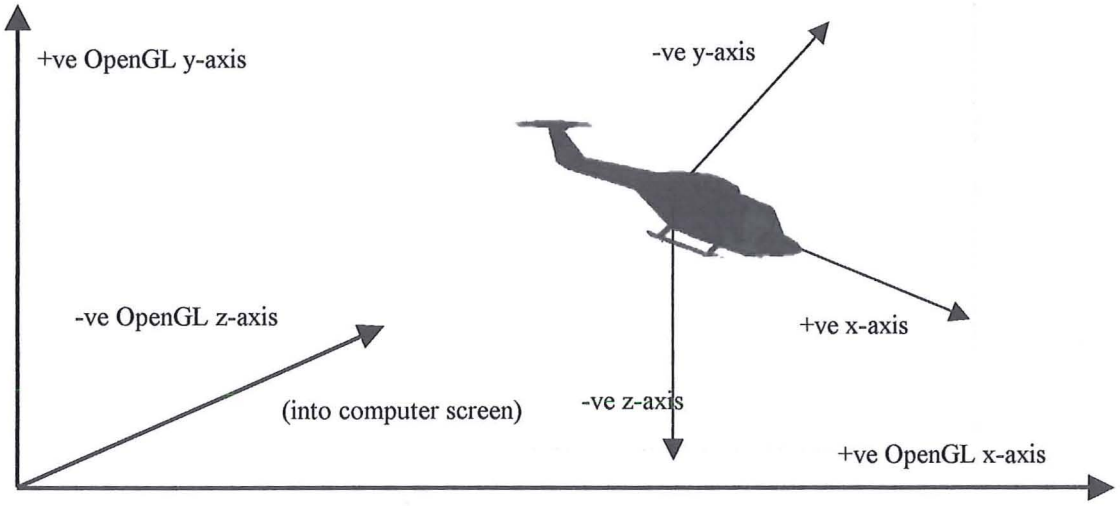

Figure 6.4 Open Graphics Libraries and Aircraft Frames of Reference

Figure 6.5 Lynx Helicopter Model

Figure 6.6 Screenshot from Helicopter Flight Simulator Cockpit

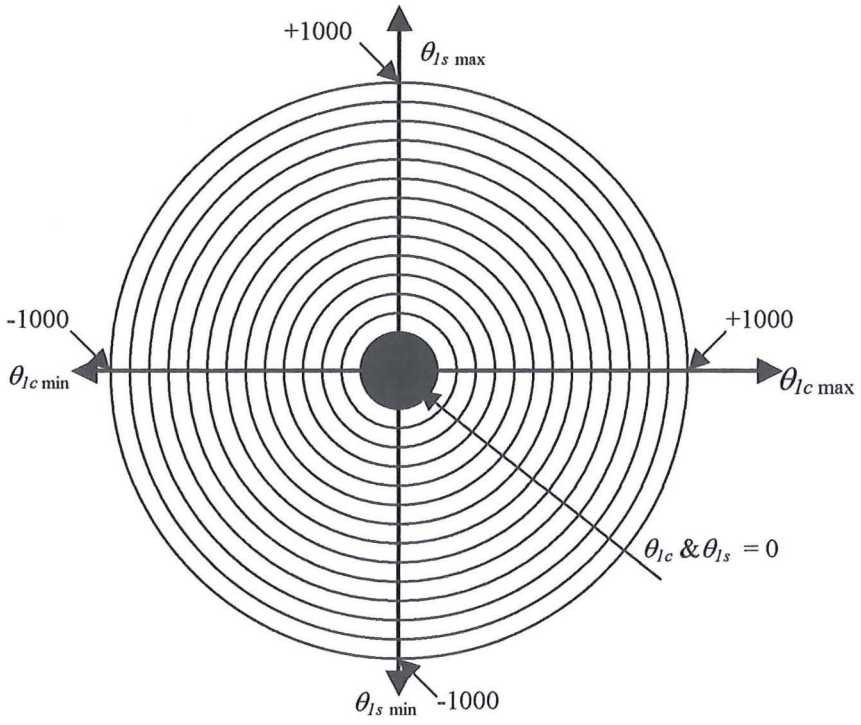

Figure 6.7 Joystick Calibration for Longitudinal and Lateral Cyclic

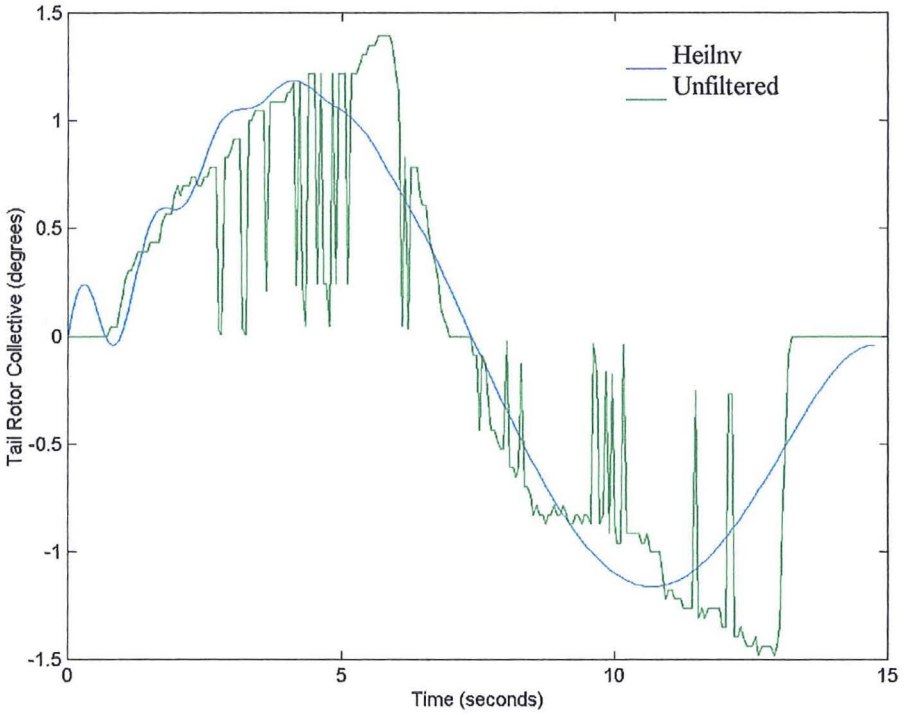

Figure 6.8 Helinv and Unfiltered Flight Simulator Tail Rotor Collective for 40 Knot Slalom

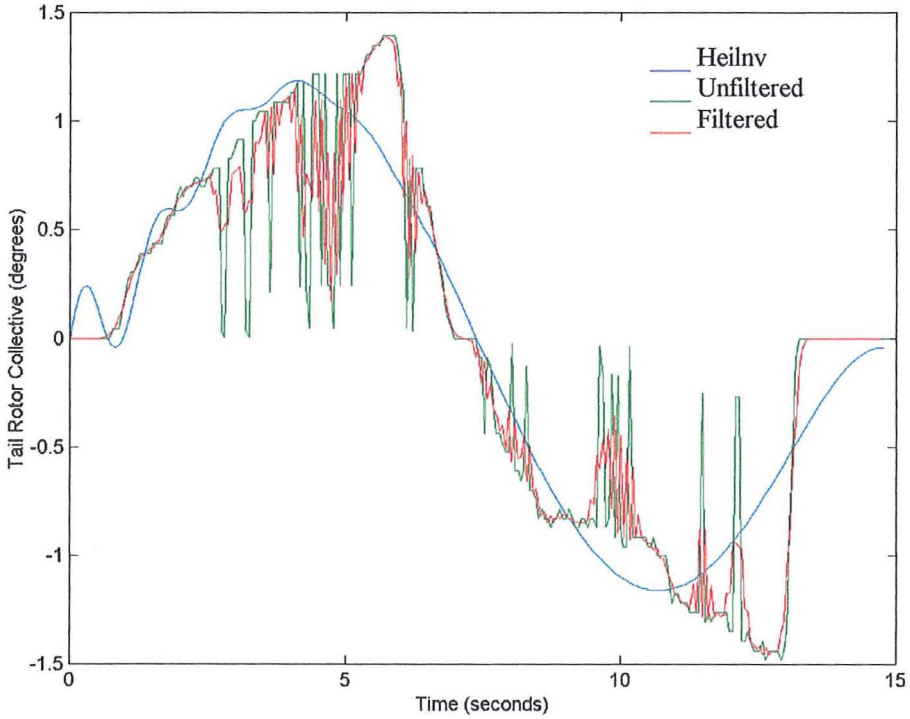

Figure 6.9 Helinv and Filtered Flight Simulator Tail Rotor Collective for 40 Knot Slalom

Chapter 7 Figures

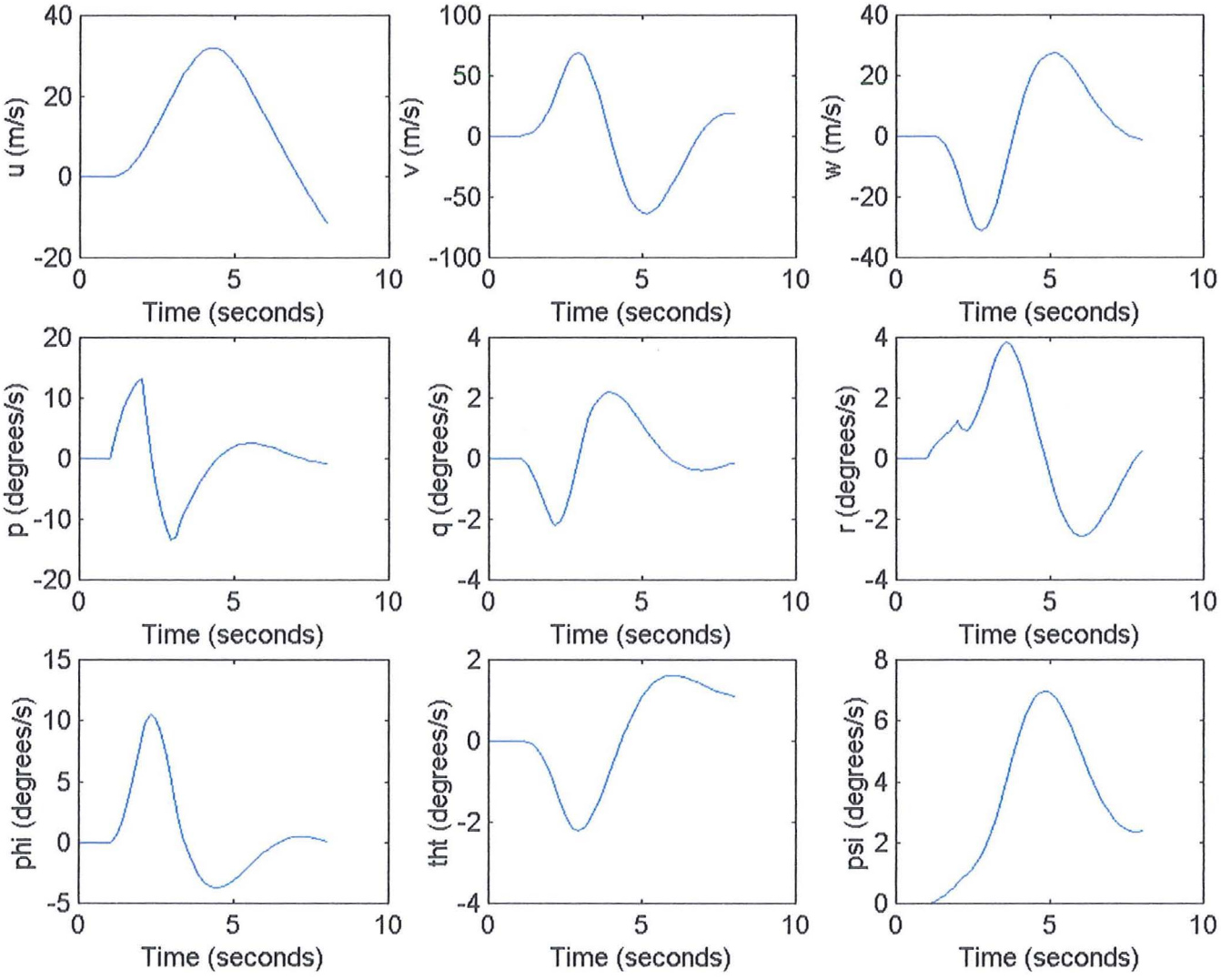

Figure 7.1 Puma System Response to a One Degree Doublet Input in Lateral Cyclic

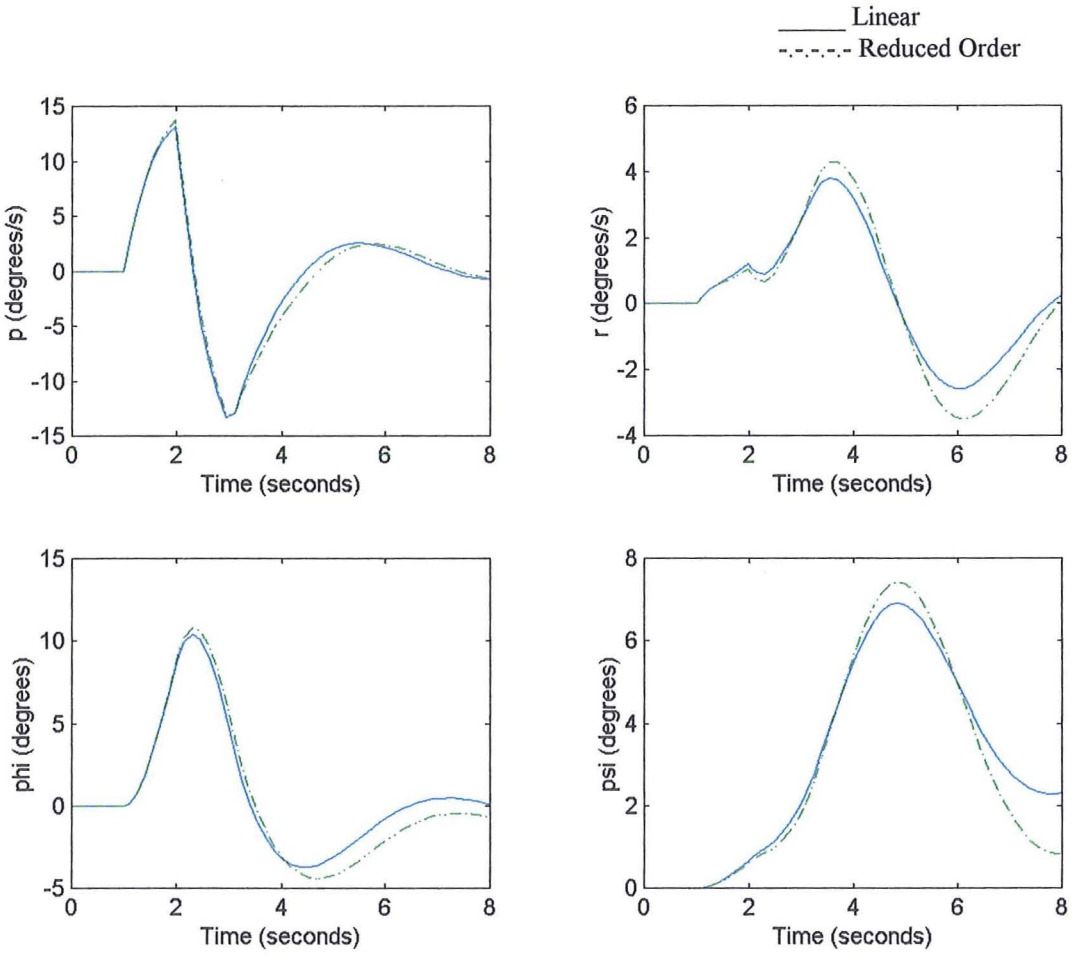

Figure 7.2 Comparison of Full and Reduced Order System Response to a One Degree Doublet input in Lateral Cyclic

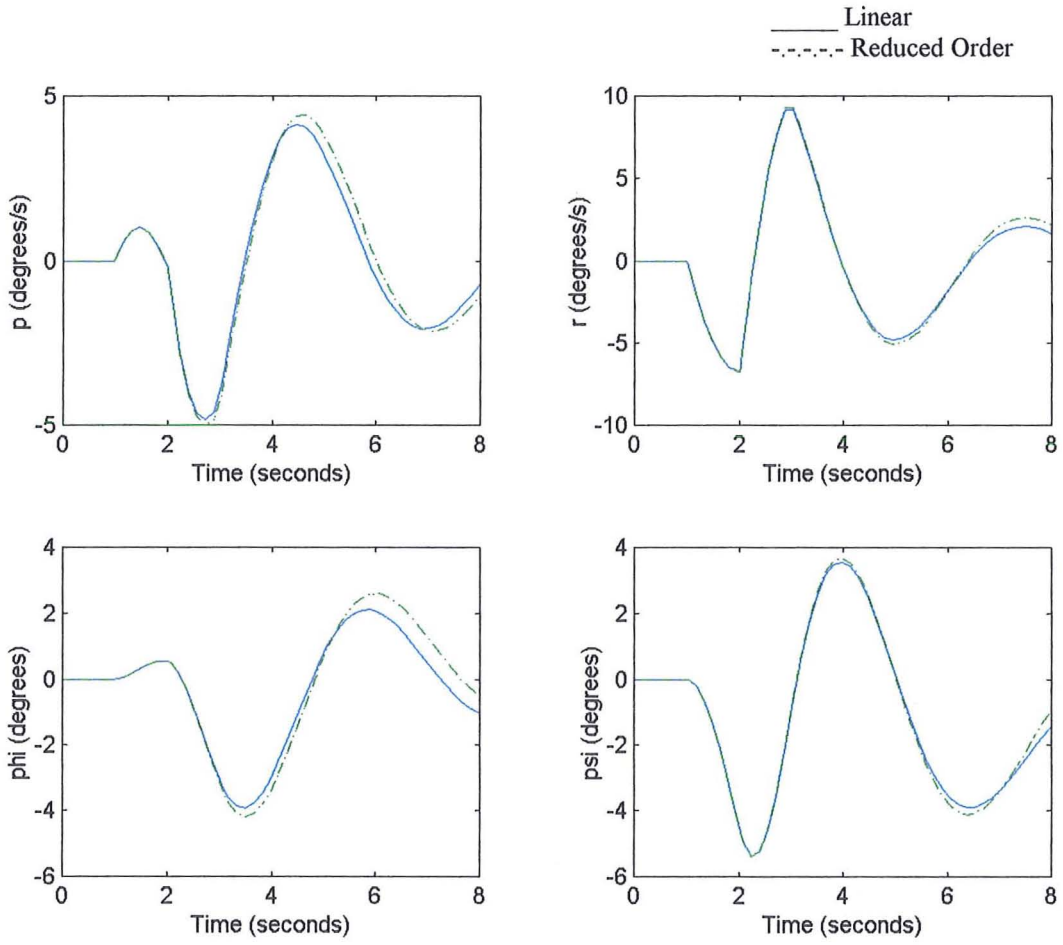

Figure 7.3 Comparison of Full and Reduced Order System Response to a One Degree Doublet input in Tail Rotor Collective

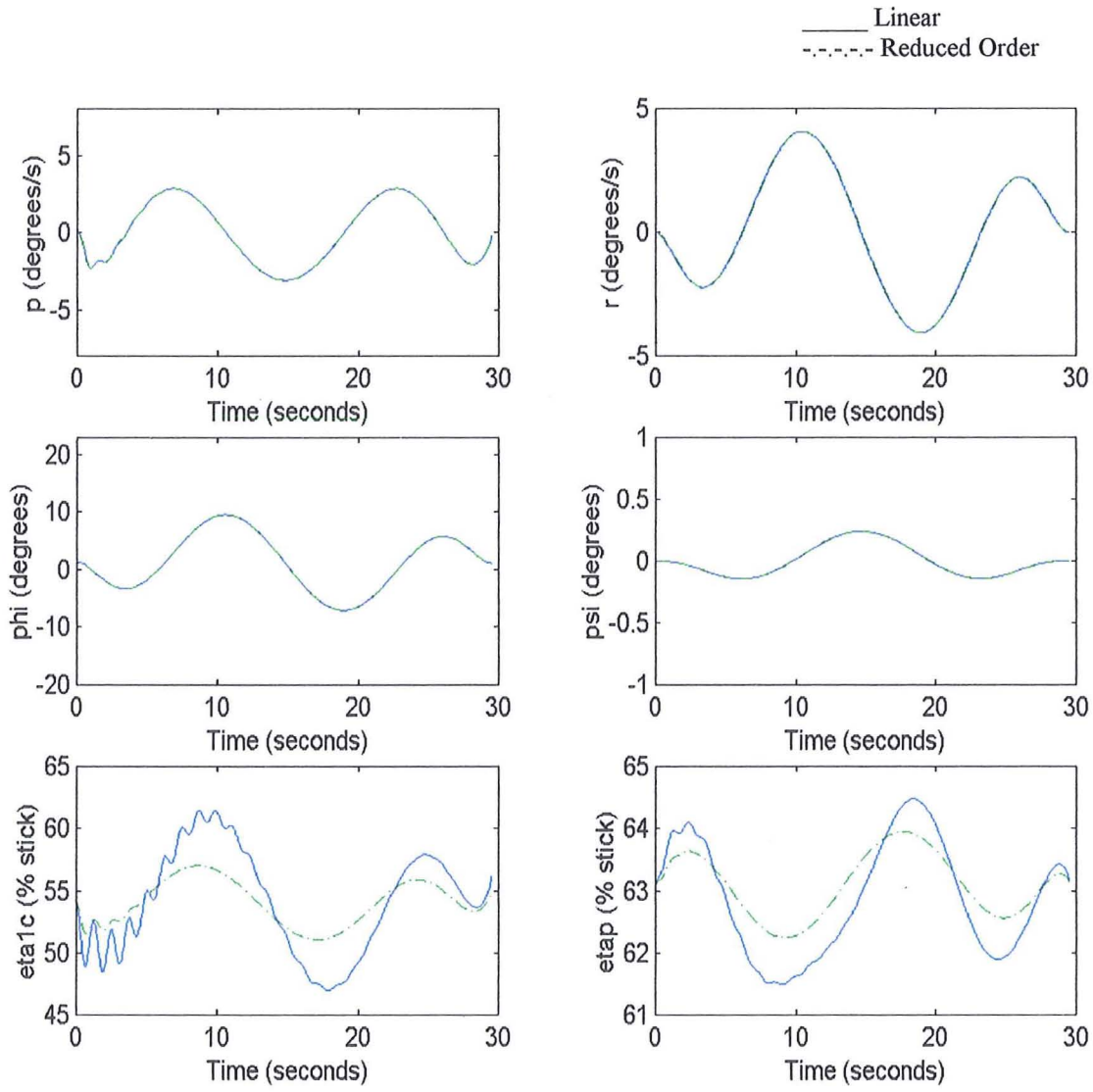

Figure 7.4 Forty Knot Slalom State and Control Time Histories Derived Using Linear and Reduced Order Linear Inverse Simulation

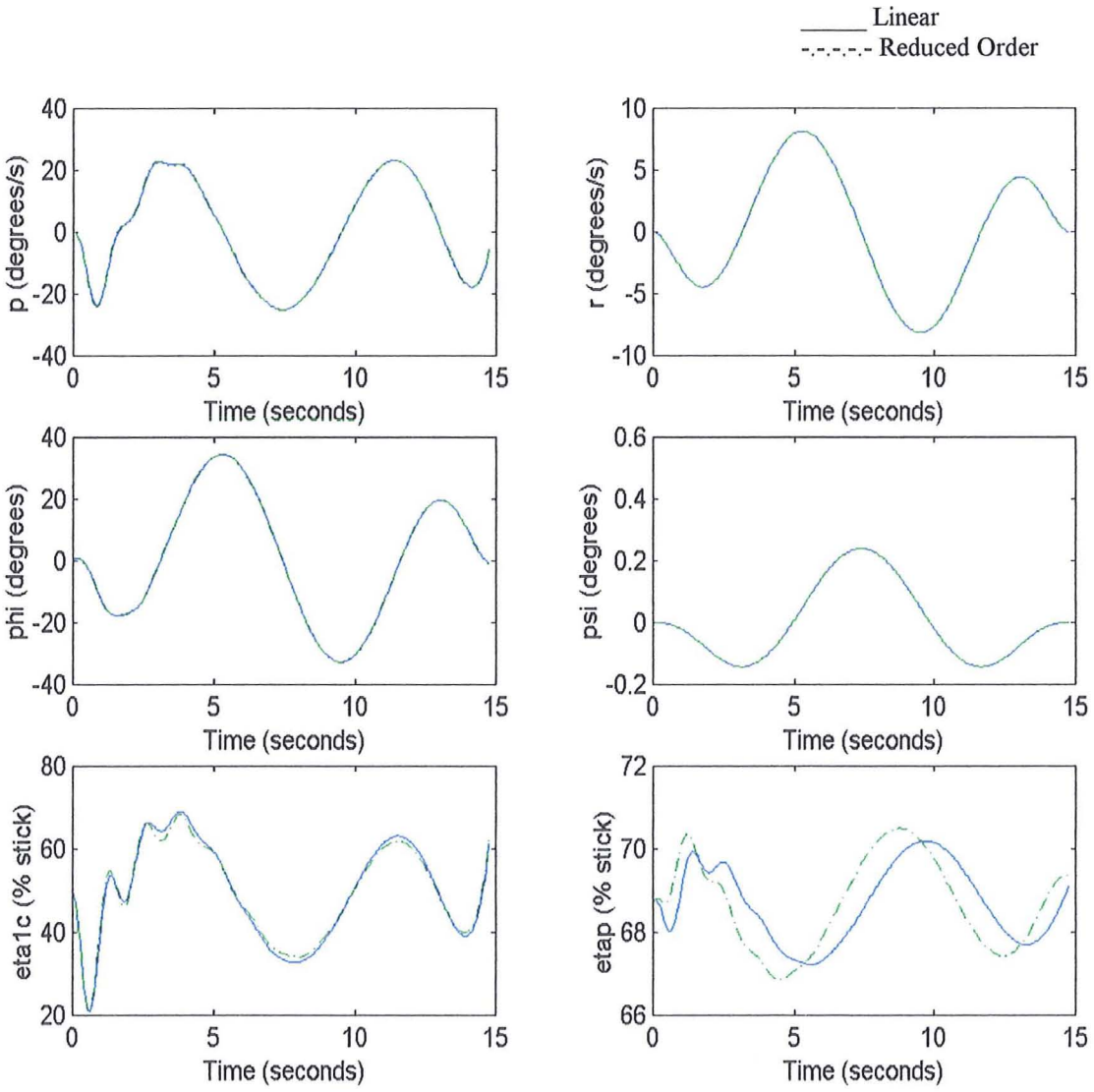

Figure 7.5 Eighty Knot Slalom State and Control Time Histories Derived Using Linear and Reduced Order Linear Inverse Simulation

Chapter 8 Figures

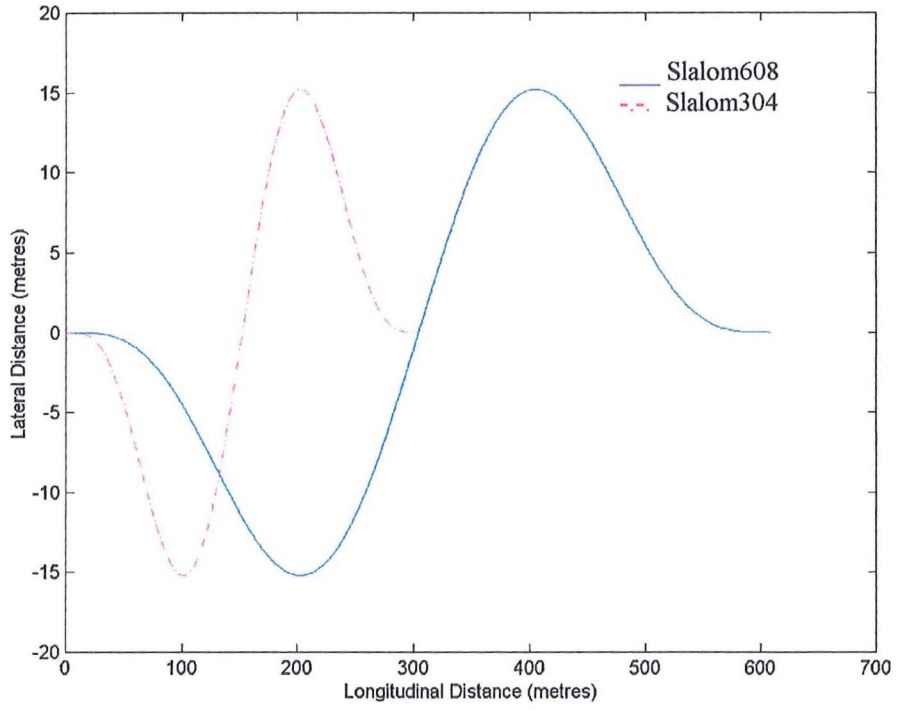

Figure 8.1 Comparison of Polynomial Defined Full and Shortened Slalom Flight Path

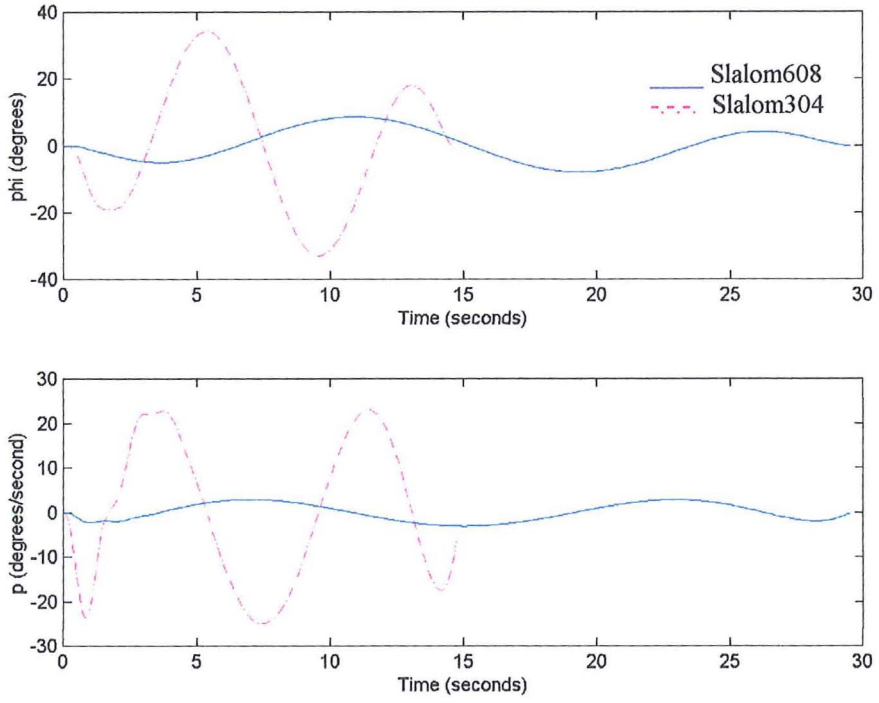

Figure 8.2 Roll and Roll Rate Time Histories for 304x15m and 608x15m Polynomial Slalom Performed at 40knots in a Puma Helicopter

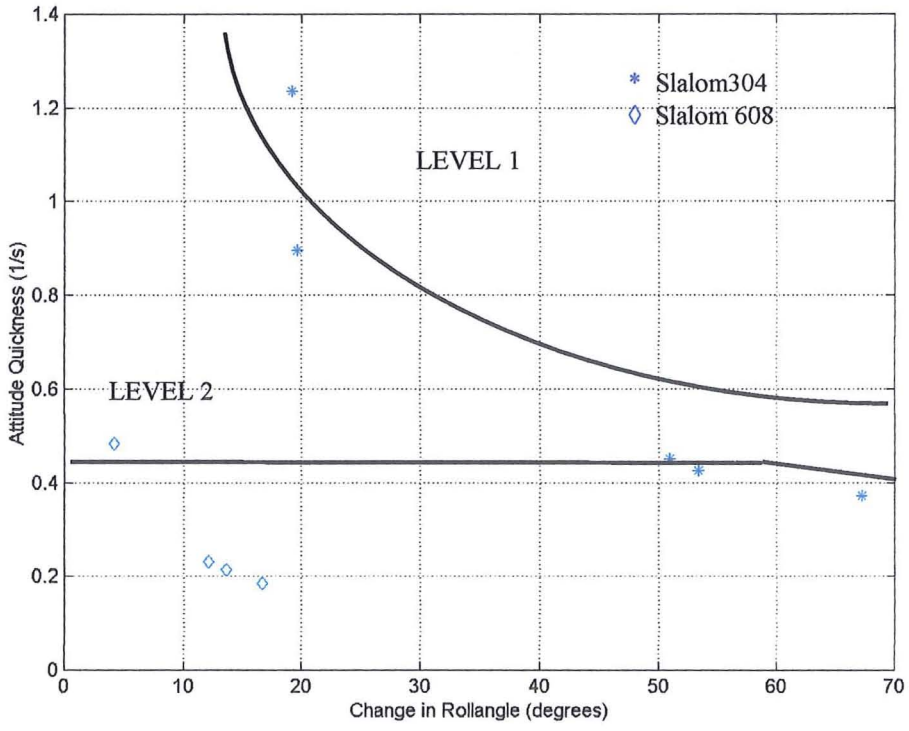

Figure 8.3 Corresponding Roll Attitude Quickness Chart

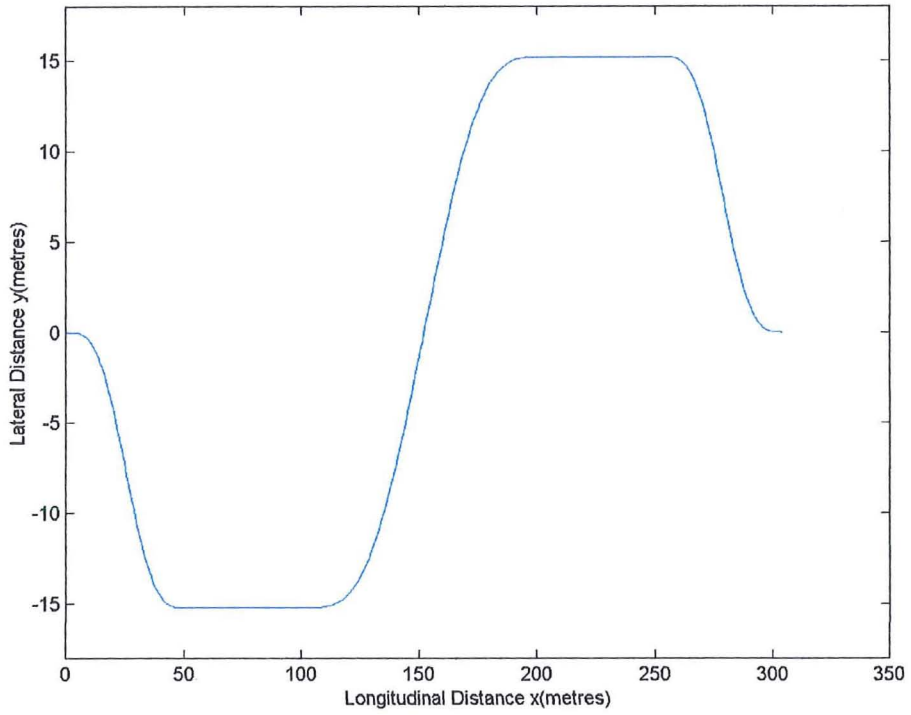

Figure 8.4 Piecewise Defined Shortened Slalom Flight Path

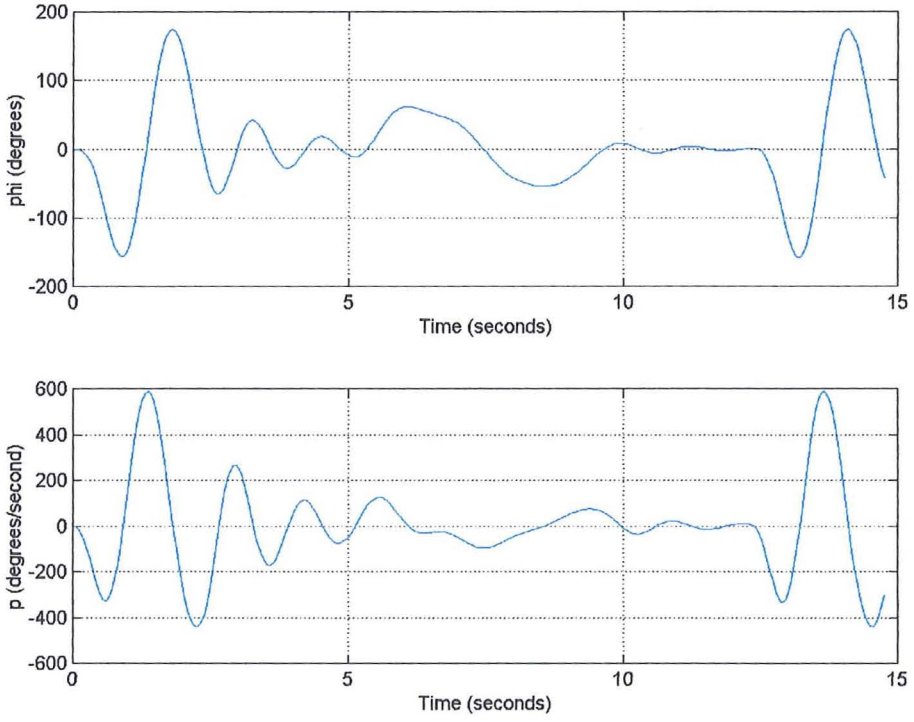

Figure 8.5 Roll and Roll Rate Time Histories for 304x15m Piecewise Slalom Performed at 40 Knots in a Puma Helicopter

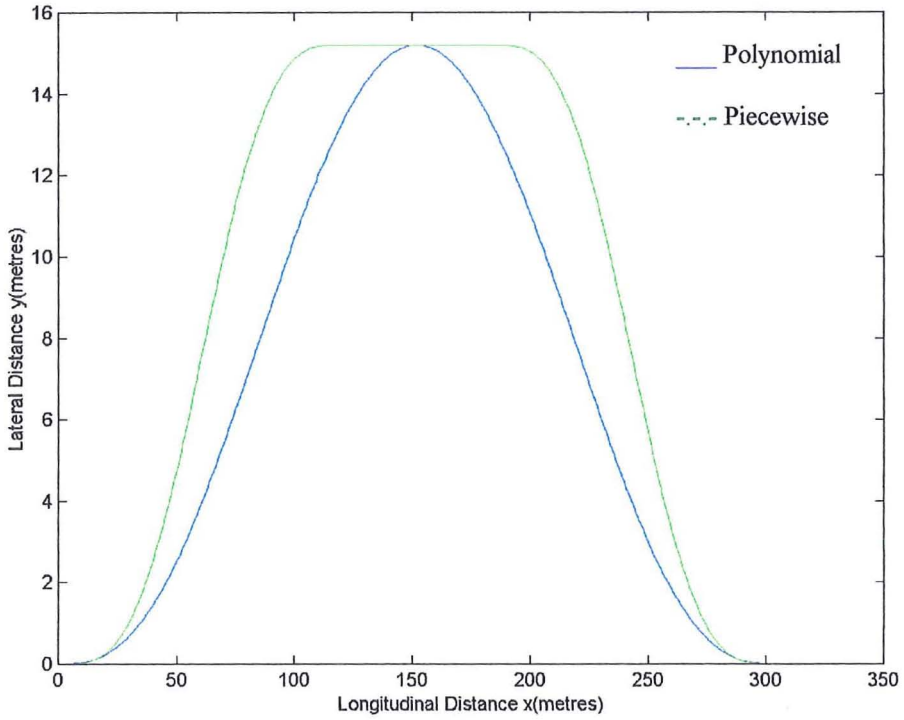

Figure 8.6 Piecewise and Polynomial Defined Lateral Jink Flight paths

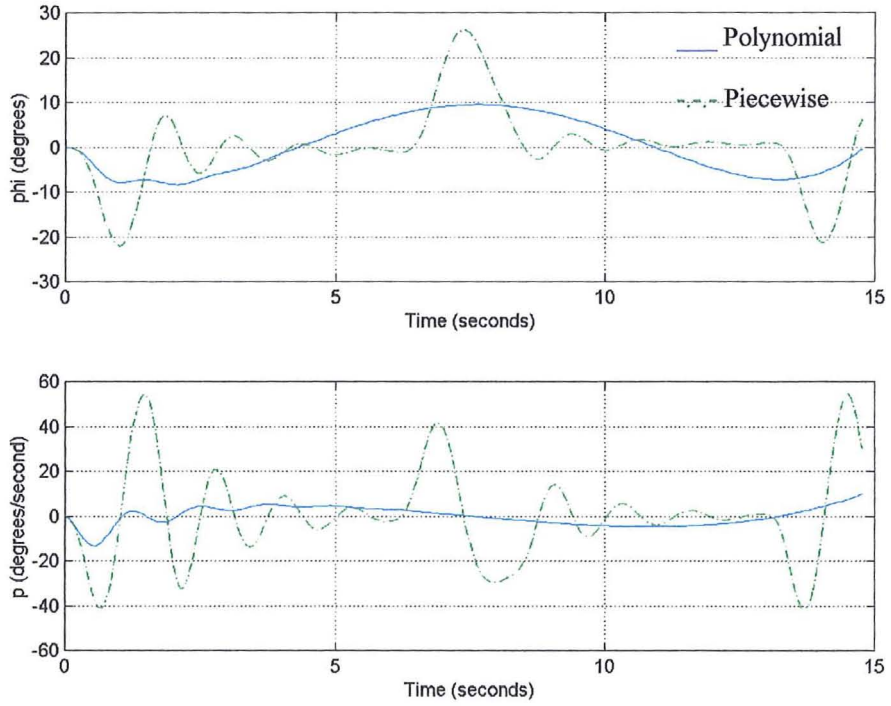

Figure 8.7 Roll and Roll Rate Time Histories for 304x15m Polynomial and Piecewise Lateral Jink Performed at 40knots in a Puma Helicopter

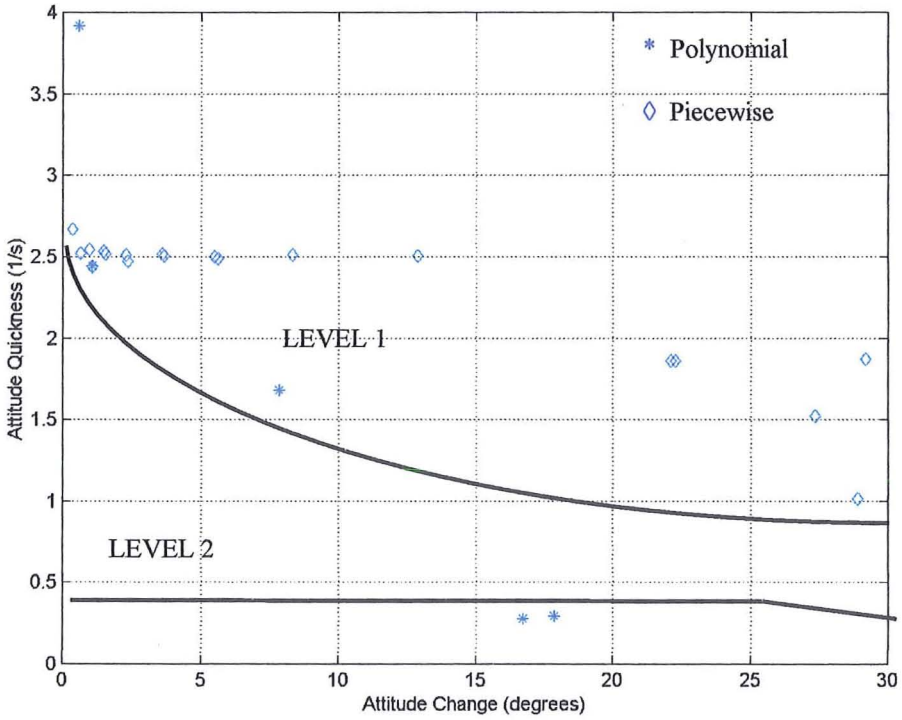

Figure 8.8 Corresponding Roll Attitude Quickness Chart

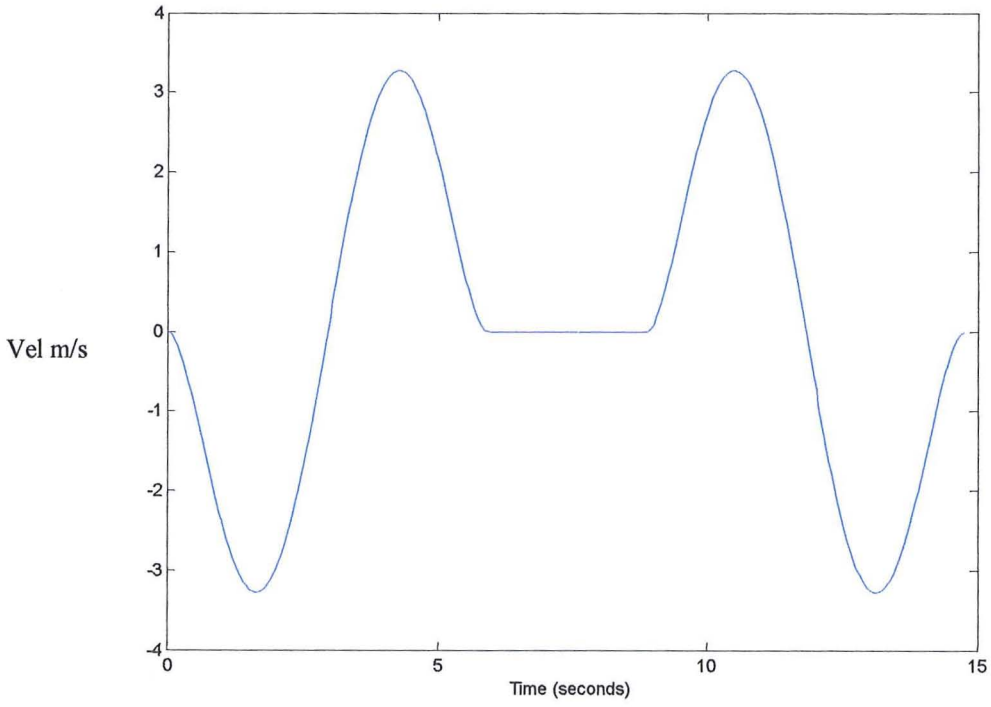

Figure 8.9 Polynomial Lateral Jink Manoeuvre Velocity Profile

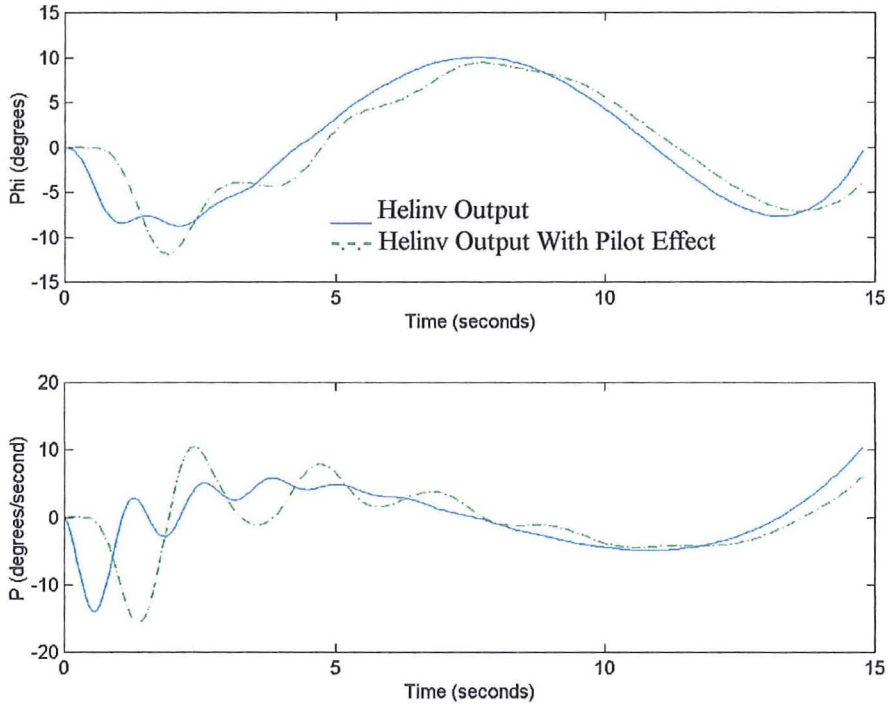

Figure 8.10 Helinv Derived State Time Histories With Added Pilot Effect

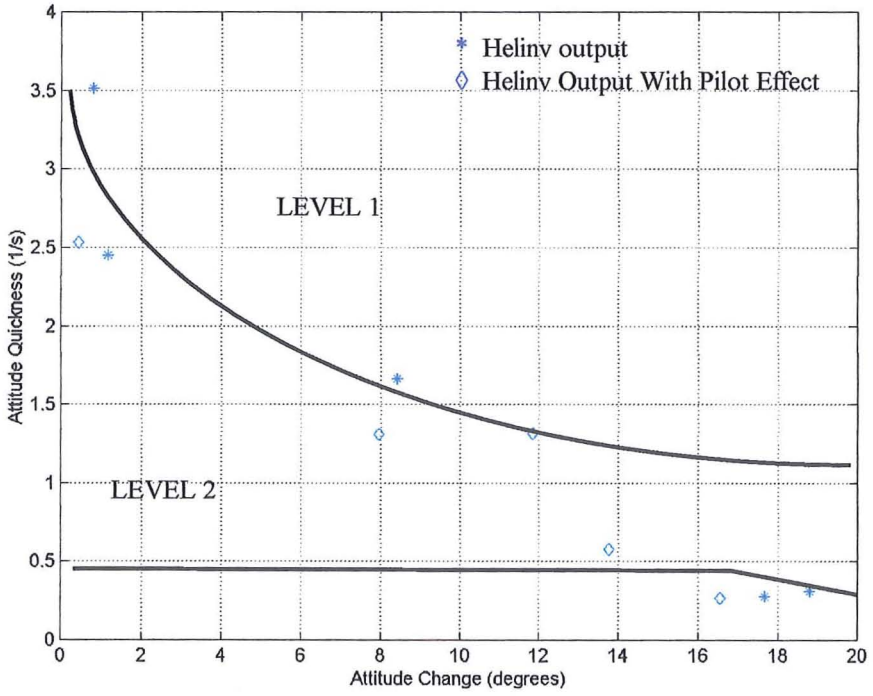

Figure 8.11 Corresponding Attitude Quickness Chart

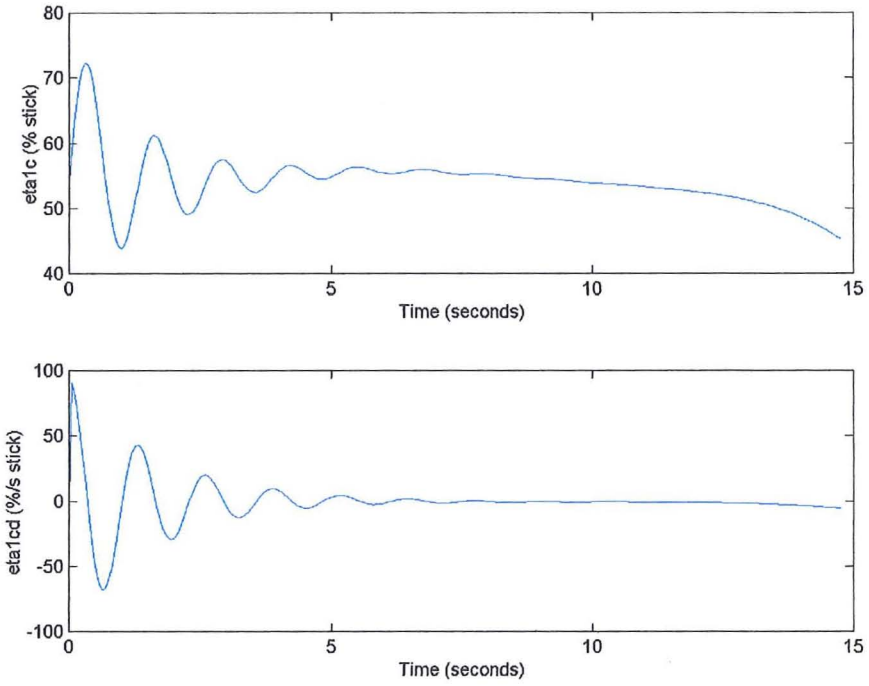

Figure 8.12 Helinv Derived State Time Histories With Added Pilot Effect

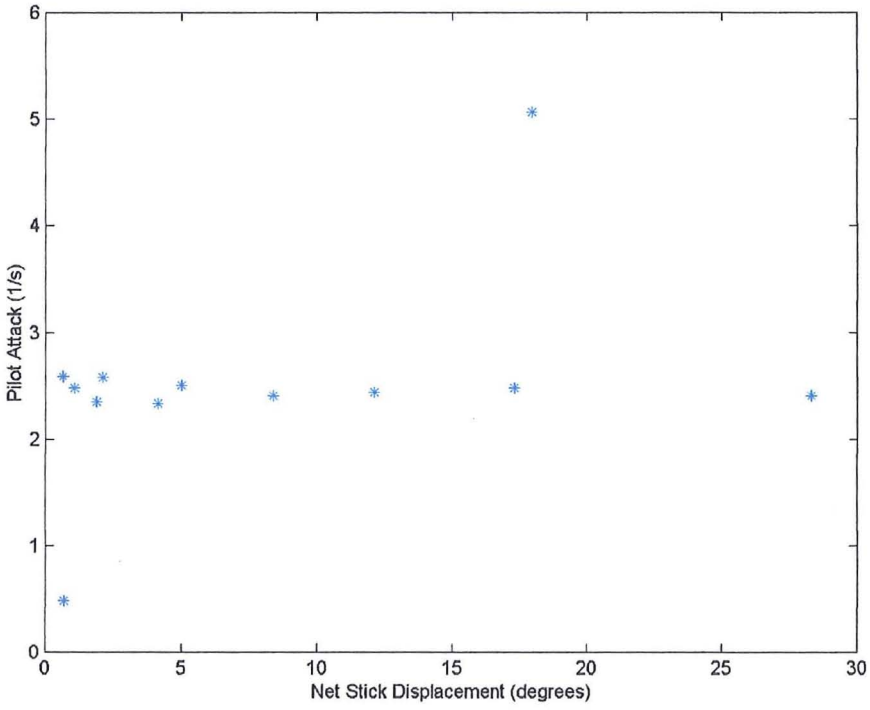

Figure 8.13 Corresponding Pilot Attack Chart

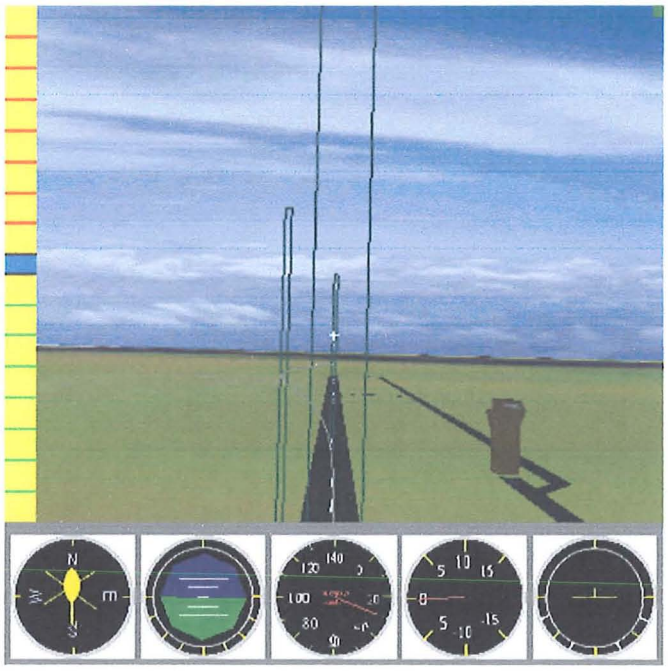

Figure 8.14 Mission Task Flight Path Representation in The Flight Simulator

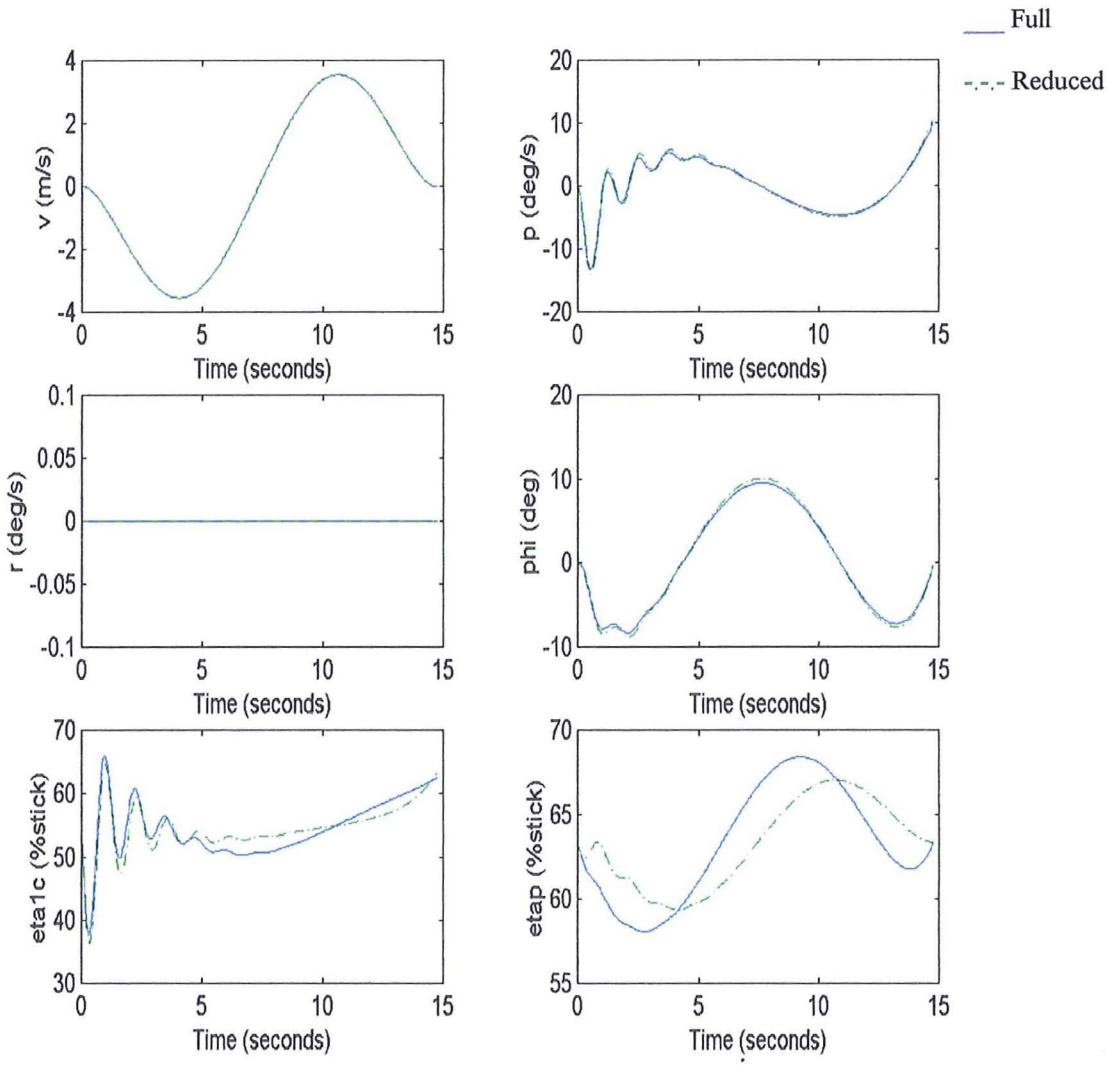

Figure 8.15 Comparison of Full and Reduced Order Lateral Jink State and Control Time Histories Derived Using Inverse Simulation

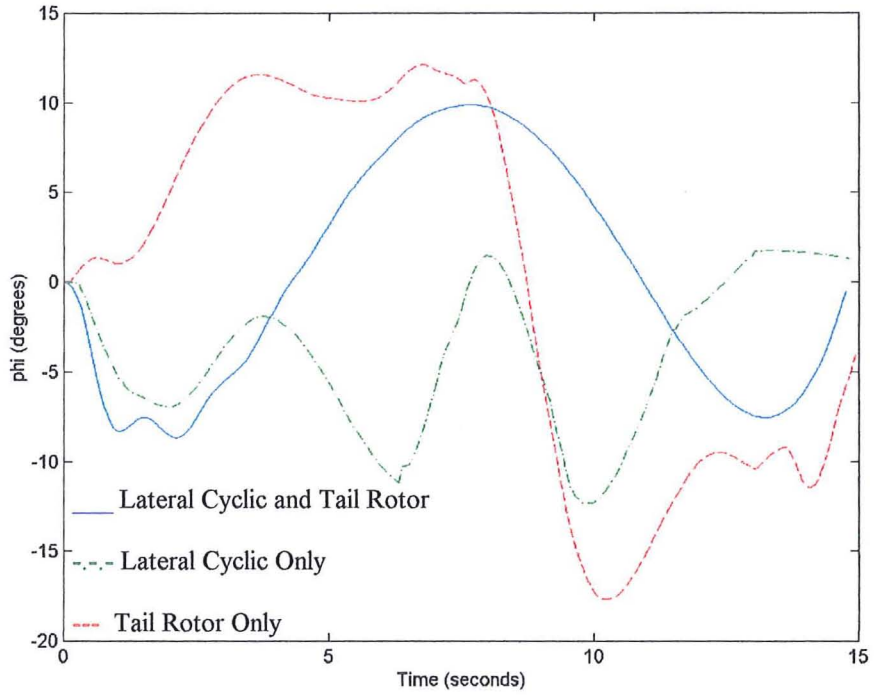

Figure 8.16 Roll Time History for the Lateral Jink Flown Using Lateral Cyclic Only, Tail Rotor Collective Only and a Combination of Both

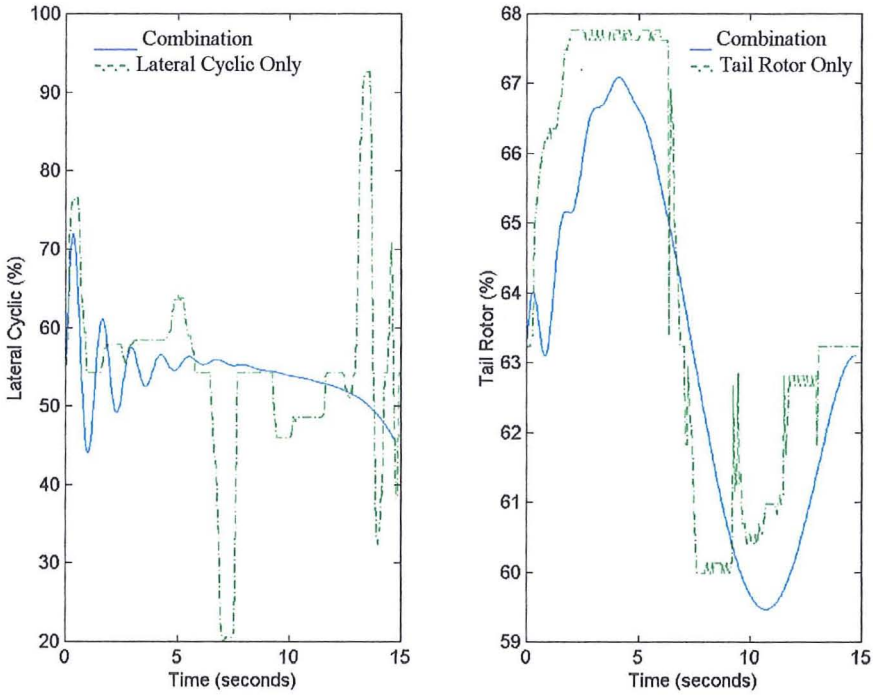

Figure 8.17 Control Inputs For Lateral jink Task When Flown With Lateral Cyclic Only, Tail Rotor Collective Only and a Combination of Both

Chapter 9 Figures

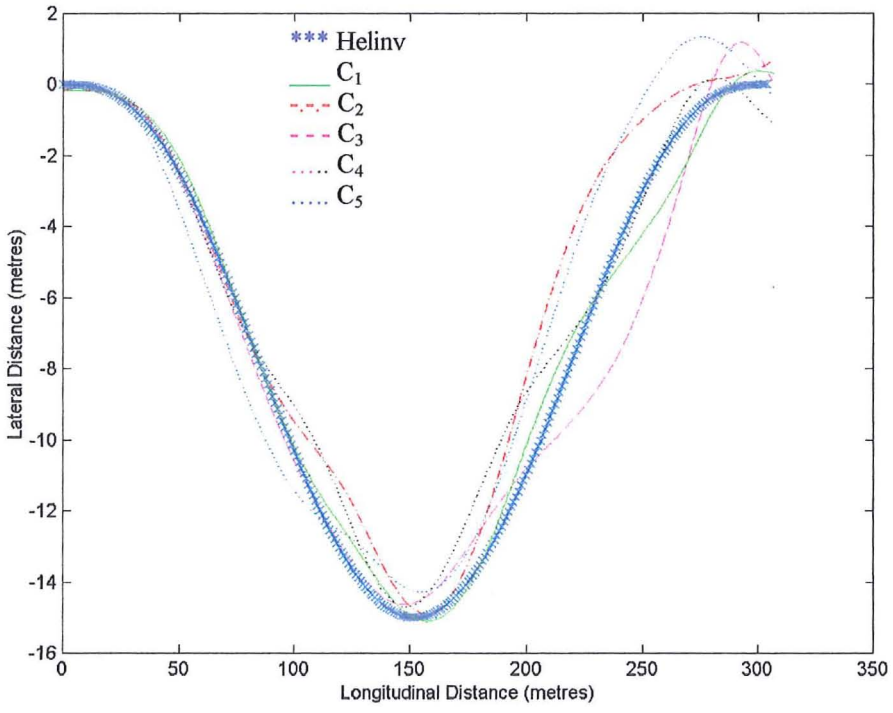

Figure 9.1 Roll angle Time Histories for Helinv and The Series of Flights Performed by Pilot C

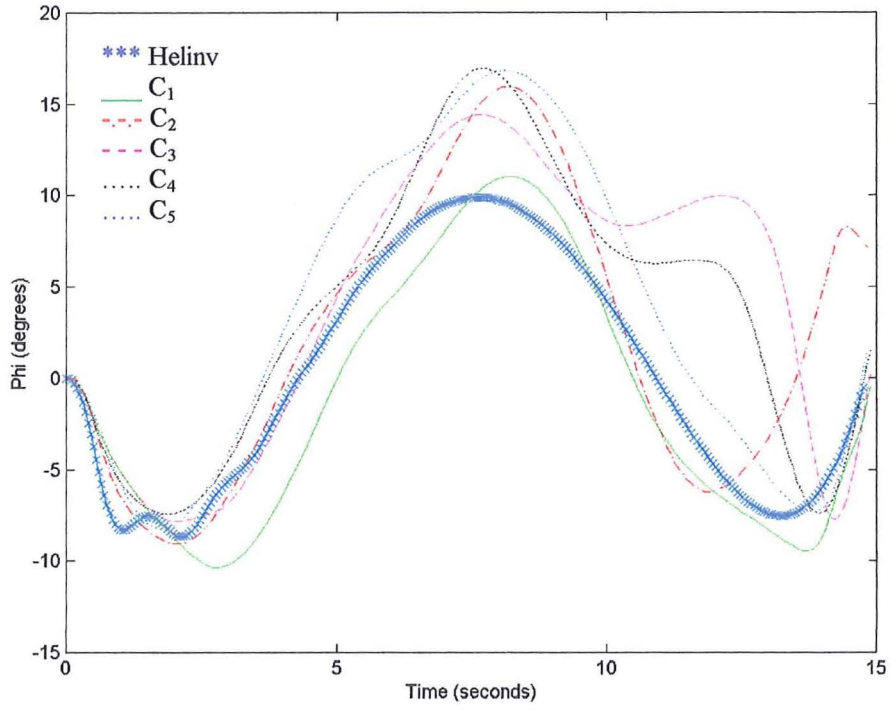

Figure 9.2 Roll angle Time Histories for Helinv and The Series of Flights Performed by Pilot C

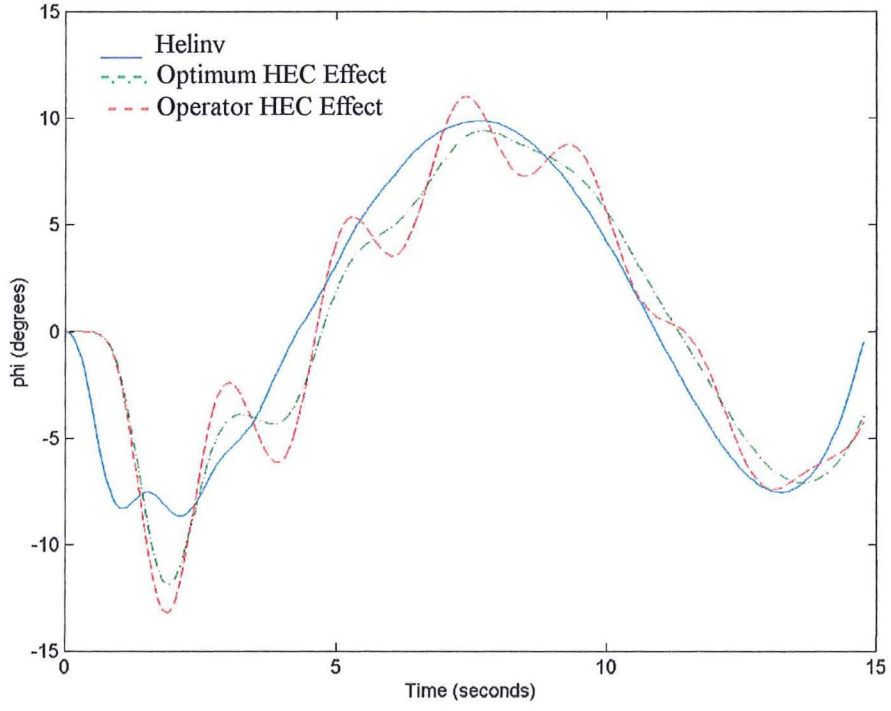

Figure 9.3 Optimum and Operators HEC Effect On Helinv Roll angle Time Histories

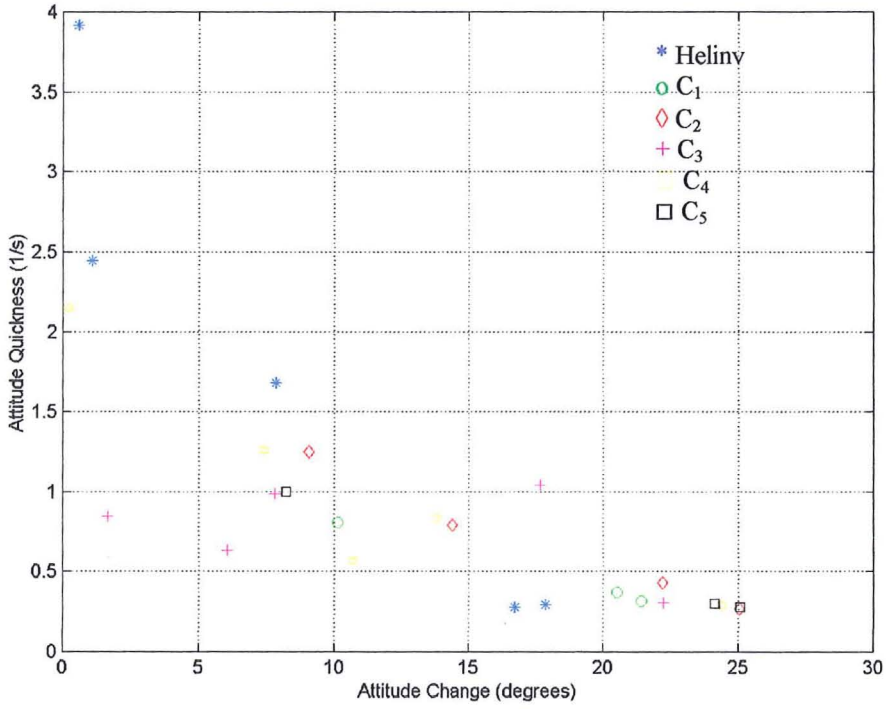

Figure 9.4 Attitude Quickness Charts For The Series of Flights Performed by Pilot C

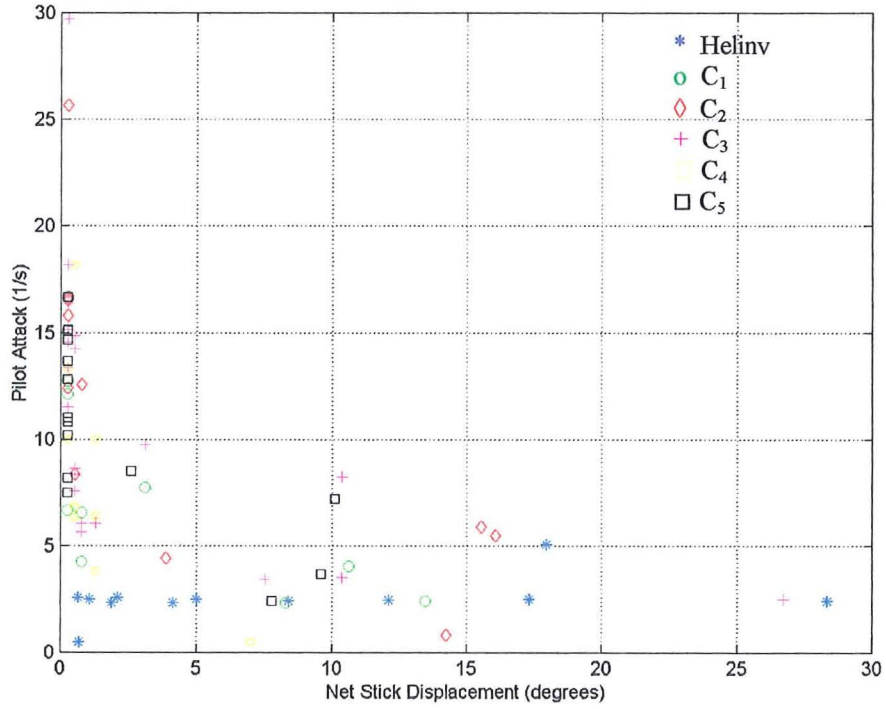

Figure 9.5 Pilot Attack Charts For Helinv and The Series of Flights Performed by Pilot C

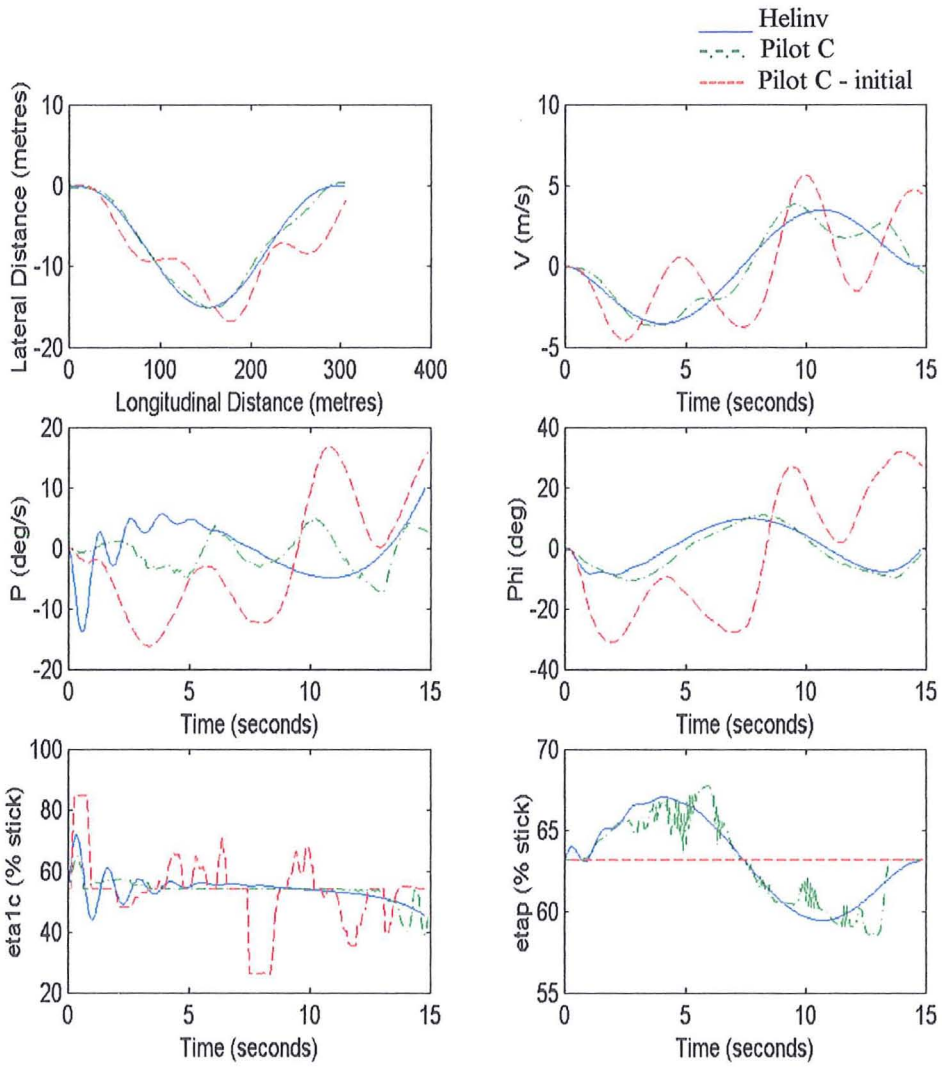

Figure 9.6 Comparison of a Pilot C Time History with a Helinv Generated Time History For the Lateral Jink Task

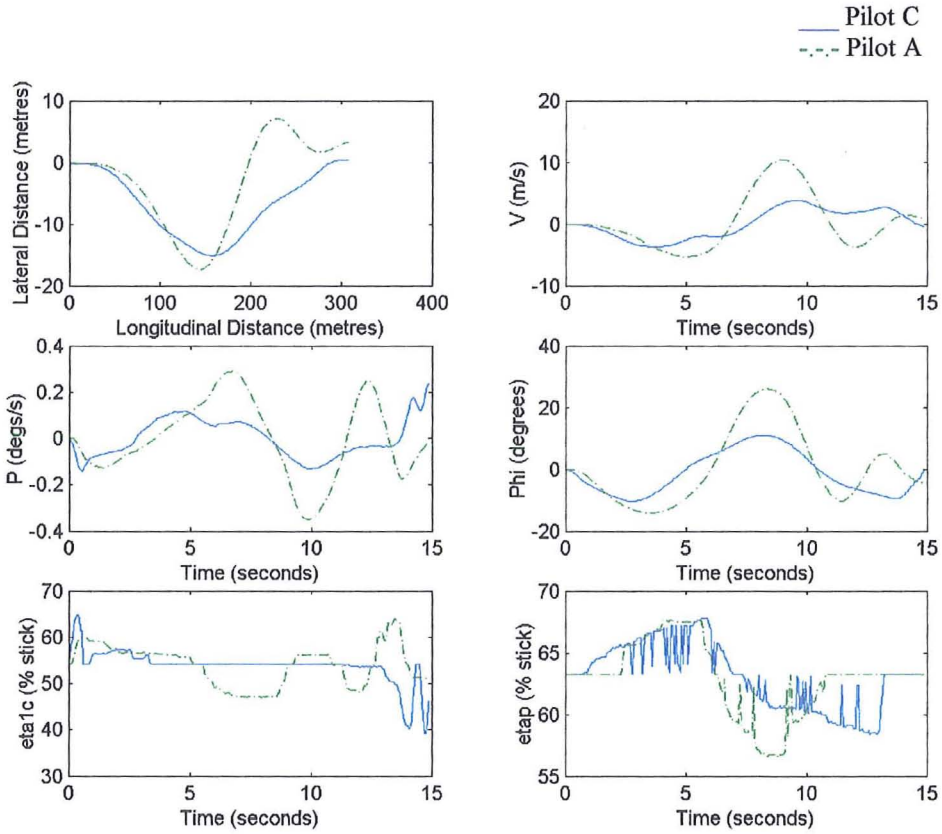

Figure 9.7 Comparison of Pilot C and Pilot A with Helinv Generated Time Histories

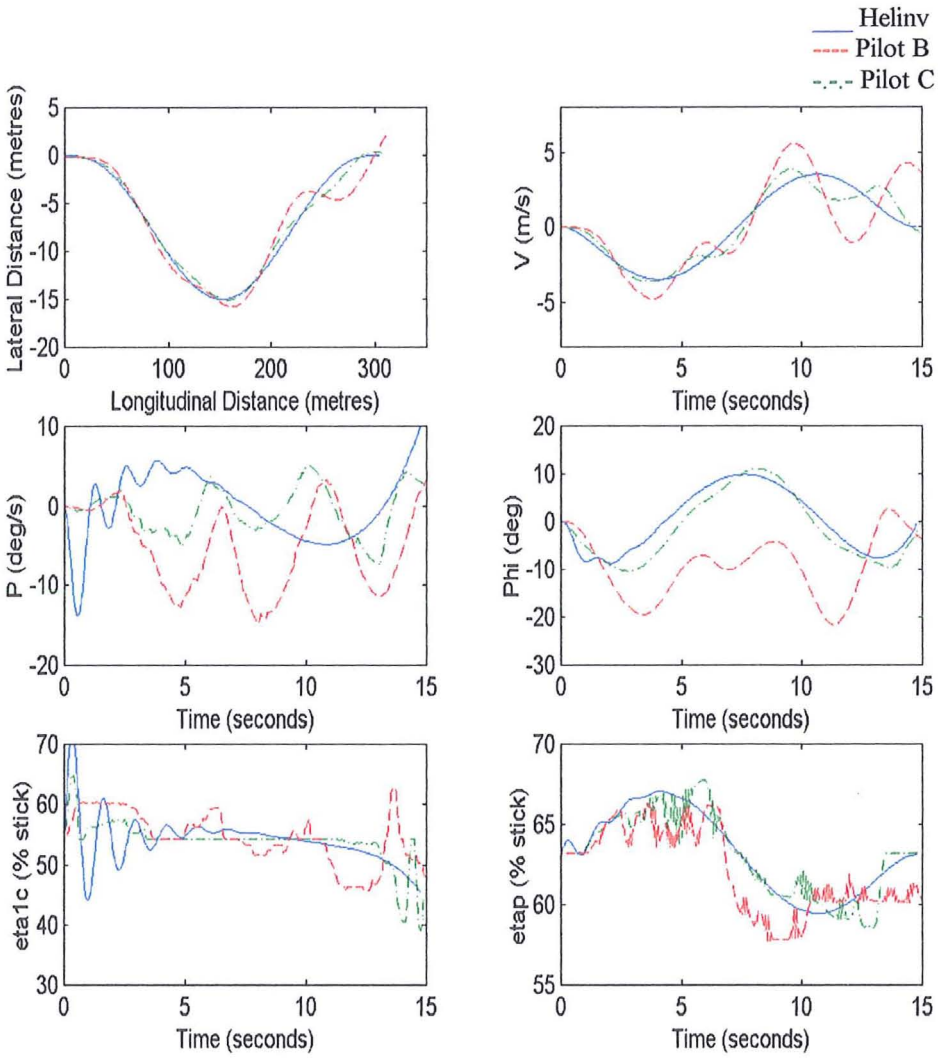

Figure 9.8 Comparison of Pilot B with Helinv and Pilot C Time Histories For the Lateral Jink Manoeuvre

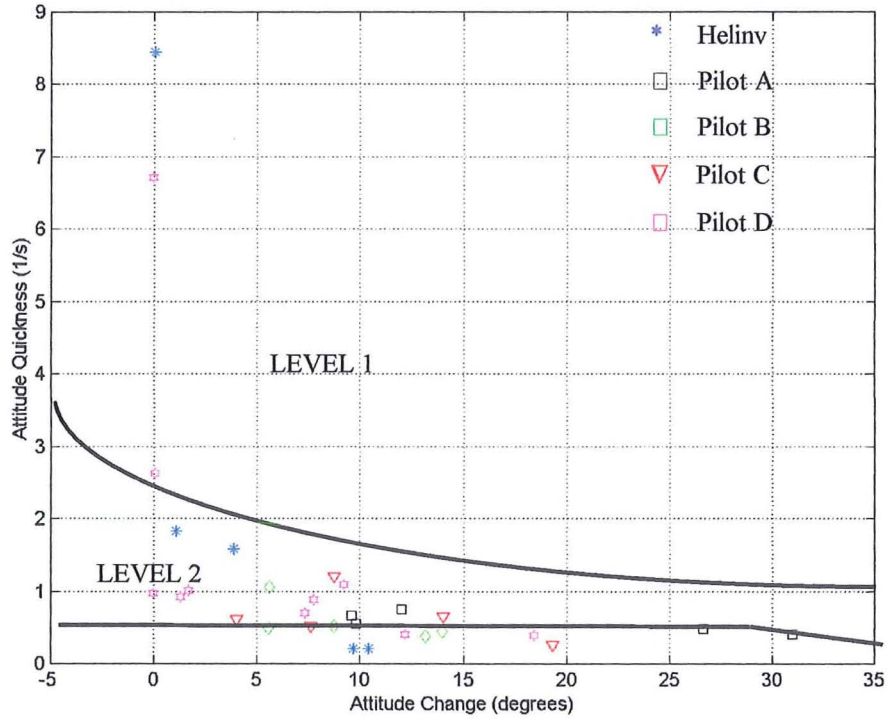

Figure 9.9 30 Knot Attitude Quickness Chart

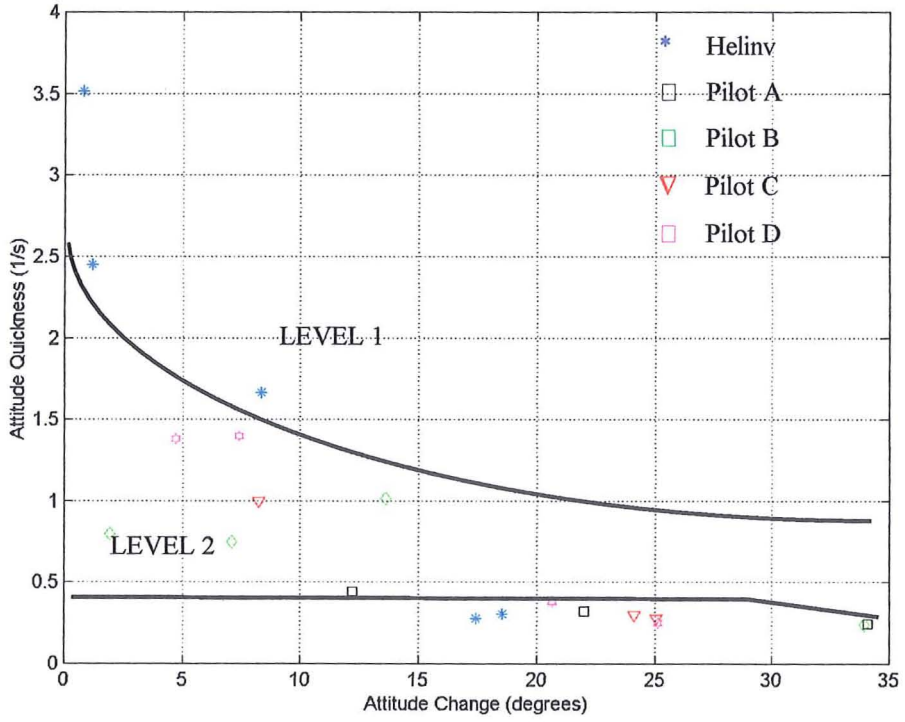

Figure 9.10 40 Knot Attitude Quickness Chart

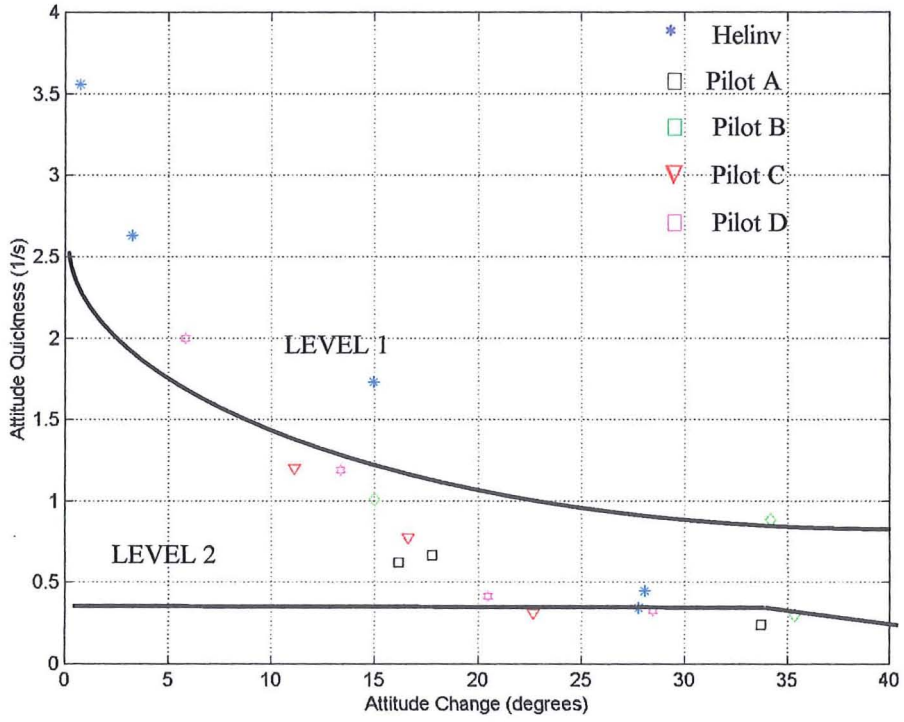

Figure 9.11 50 Knot Attitude Quickness Chart

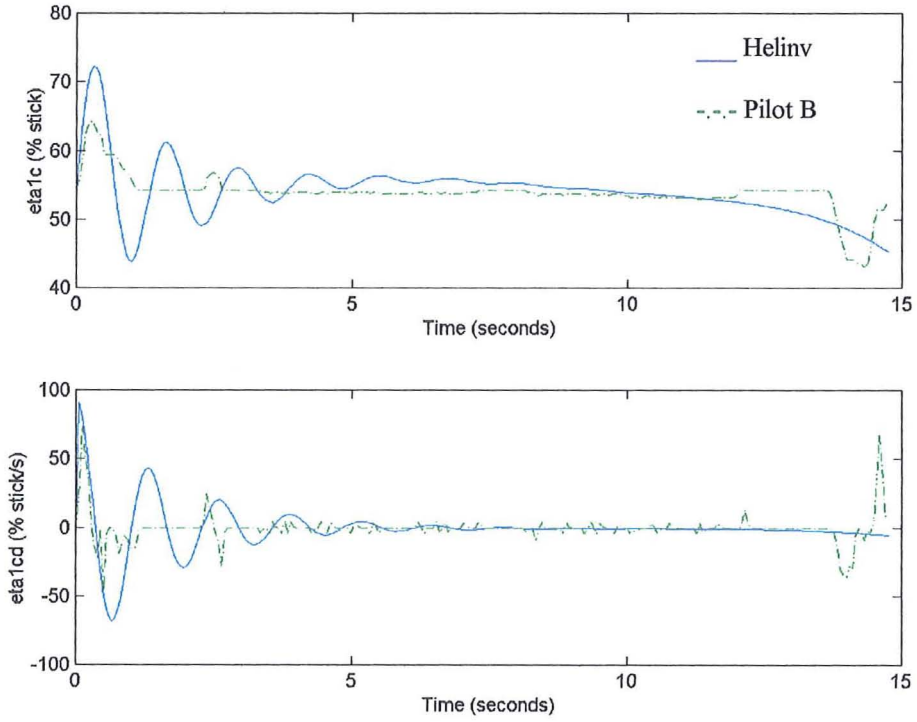

Figure 9.12 40 Knot Helinv and Pilot B Lateral Cyclic stick Displacement and Derivative

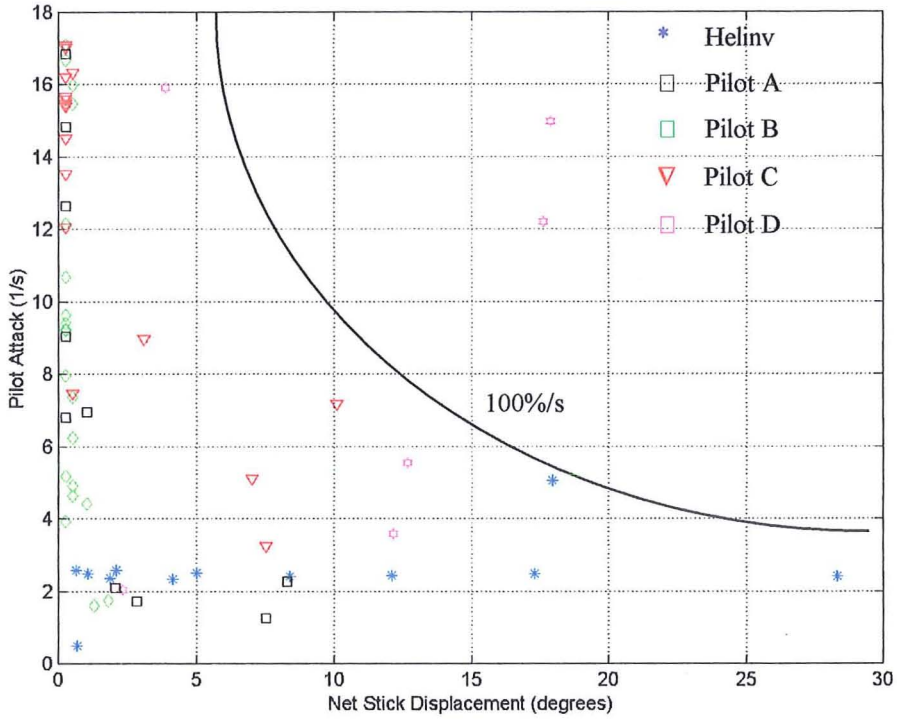

Figure 9.13 40 Knot Lateral Cyclic Pilot Attack Chart

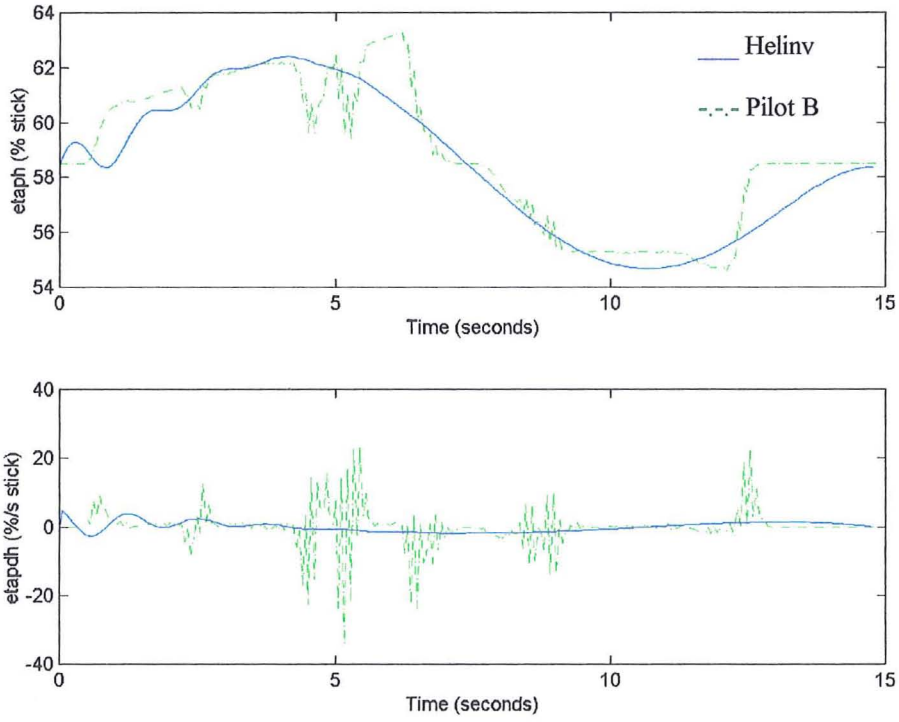

Figure 9.14 40 Knot Helinv and Pilot C Tail Rotor Collective Displacement (above) and Derivative (lower)

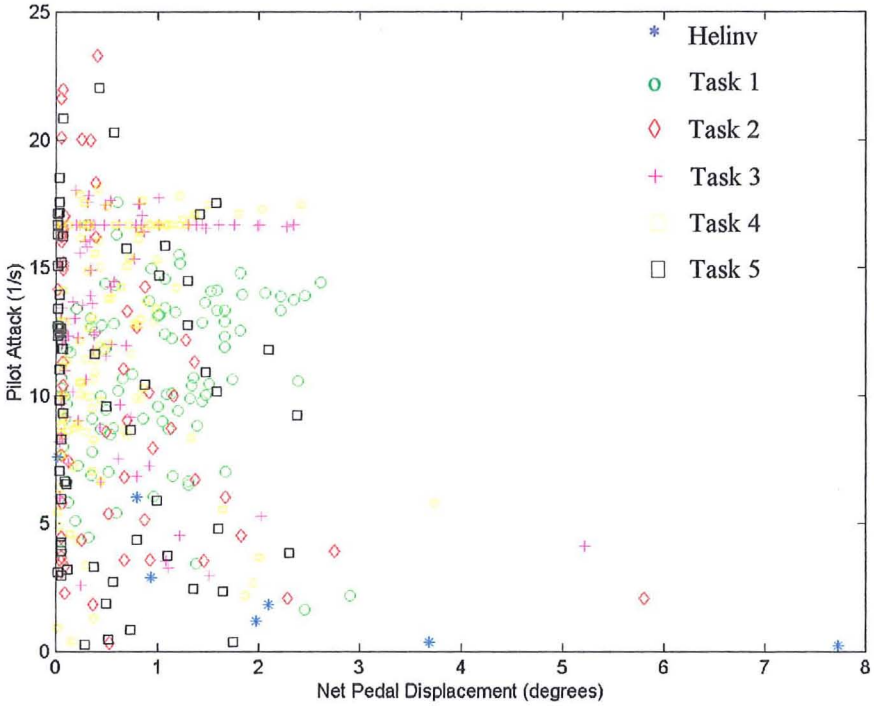

Figure 9.15 Tail Rotor Collective Pilot Attack Charts For Helinv and The series of Flights Performed by Pilot C at 40 Knots

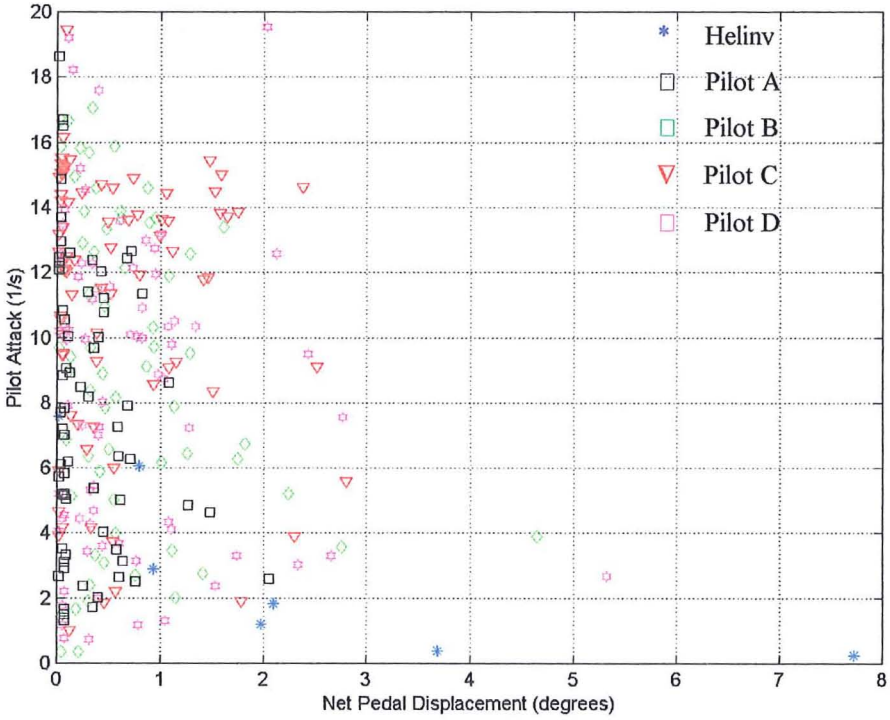

Figure 9.16 40 Knot Tail Rotor Collective Pilot Attack Chart

References

Anon., "Aeronautical Design Standard ADS-33D. Handling Qualities Specifications for Military Rotorcraft." United States Army Aviation and Troop Command, St. Louis, Mo., Directorate for Engineering, July 1994.

Anon., "Aeronautical Design Standard ADS-33E. Handling Qualities Specifications for Military Rotorcraft." United States Army Aviation and Troop Command, St. Louis, Mo., Directorate for Engineering, July 1996.

Anon,. "Helicopter flying and Ground Handling Qualities; General Requirements for: Mil-H-8501", 1961.

Anon., Military Specification, "Flying Qualities of Piloted Airplanes", MIL-F-8785B (ASG), 1969.

Anon., Defence Standard, "Design and Airworthiness Requirements for Service Aircraft", 00-970, Vol. 2, 1984.

Anon., "Rotor System Identification." AGARD lecture Series 178, NATO, 1991

Anon., UK Def Stan 00-970, "Design and Airworthiness Requirements for Service Rotorcraft", Vol. 2, Rotorcraft, Book 1, 1984.

Babister, A.W., "Aircraft Dynamic Stability and Response." Pergamon Press, 1981.

Bates, J., Tompkins. T., "Practical Visual C++6." Que Corporation, MacMillan Computer publishing. 1999.

Bekey, G. A., "The Human Operator as a Sampled Data System". IRE Transactions on Human Factors in Electronics, pp 43-51, September, 1962.

Cameron, N., "Preliminary Investigation into the use of Inverse Simulation for Pilot Modelling". Aerospace Engineering, University of Glasgow. 1999.

Charlton, M. T., Howell, S. E., Padfield, G. D., Jones, J. G., Bradley, R., Macdonald, C., Thomson, D. G., Leacock, G. R., "A Methodoly for the Prediction of Pilot Workload and the Influence of Effectiveness in RotorCraft Mission Tasks", Paper 5, 24th ERF, Marseilles, September 1998.

Chen, C. "A New Look at Transfer Function Design", Proc, IEEE, 59, No. 11, Nov. 1971.

Cooper, G. E., Harper, R. P., "The use of Pilot Rating and Evaluation of Aircraft Handling Qualities", NASA TN D-5153, April 1969.

Costello, R. G., "The Surge Model of the Well Trained Human Operator in Simple Manual Control", IEEE Trans on Man-Machine Systems, MMS- 9, No. 1, 1968.

Gerlach, O.H., "Developments in Mathematical Models of Human Pilot Behaviour." Aeronautical Journal, pp293-305, 1977.

Craik, K. J. W., "Theory of the Human Operator in Control Systems, The operator as an Engineering System", Brit J Psychol, Vol. 38, pp 56-61, 1947.

Elkind, J.I., " Characteristics of Simple Manual Control Systems". MIT, Lincoln lab, Tech report 111, April 1956.

Elkind, J. I., Kelly, J. A., Payne, R. A., "Adaptive Characteristics of the Human Operator in Systems having Complex Dynamics", Human Factors in Engineering, 1964.

Gillon, G., "Preliminary Development of a basic Flight Simulator." Final Year Project, University of Glasgow, 1995.

Gilstad, D.W., Fu, K.S., "Two-Dimensional Adaptive Model of a Human Controller Using Pattern Recognition Techniques. IEEE trans, SMC-1, No. 3, July 1971.

Giltrap, J.A., "Dynamic Graphics for the visualisation of a Manoeuvring Aircraft." Final Year Project, University of Glasgow, 1995.

Grace, A., "Optimisation Toolbox for use with MATLAB", The Math Works Inc., November 1992.

Hess, R. A., "A Model Based Theory for Analysing Human Control Behaviour." Advances in Man-Machine Systems Research, vol.2, 1985 p129-175.

Hess, R. A., "A Model for Human Use of Motion Cues in Vehicular Control." Journal of Guidance, Control and Dynamics, 13, pp476-482, 1990.

Hess, R. A., "Structural Model of the adaptive Human Pilot." Journal of Guidance and Control, Volume 3. No 5., Sept-Oct 1980, pp 416-423.

Hess, R. A., "Theory for Aircraft Handling Qualities Based Upon a Structural Pilot Model." Journal of Guidance and Control, Volume 12. No 6, Nov-Dec 1989, pp 792-797.

Hess, R. A., "Unified Theory for Aircraft Handling Qualities and Adverse Aircraft-Pilot Coupling." Journal of Guidance, Control and Dynamics. Vol. 20, No. 6. Nov-Dec 1997, pp 1141-1148.

Hess, R.A., Chan, K.K., "Preview Pilot Control Model for Near Earth Manoeuvring Helicopter Flight." Journal of Guidance, Control and Dynamics, 11, pp 146-152, 1988.

Hess, R.A., Gao, C., Wang, S.H., "Generalized Technique for Inverse Simulation Applied to Aircraft Manoeuvres." Journal of Guidance, Control and Dynamics, Vol. 14, No. 5, 1991, pp920-926.

Hess, R.A., Yousefpor, M., "analysing the Flared Landing Task with Pitch-Rate Flight Control Systems." Journal of Guidance, Control and Dynamics, Vol. 15,No. 3 pp768-774.

Hess, R.A., Zeyada, Y., "Modelling and Simulation for Helicopter Task Analysis", American Helicopter Society Forum, Washington DC, 2001.

Houston, S.S., Caldwell, A.E., "A Computer Based Study of Helicopter Agility, Including the Influence of an Active Tailplane". Tenth European Rotorcraft Forum, August, 1984.

Howell, S. E., "Preliminary Results From Flight and Simulation Trials to Investigate Pilot Control and Workload in Slalom Manoeuvres", Flight Management and Control Department, DERA, December 1995.

Howell, S. E., Charlton, M. E., "Trial Specification for AFS Simulation Trial TWIN3", Draft Version, Flight Management and Control Department, DERA, November 1997.

Johnson, W., "Helicopter Theory", Dover Publications, 1980.

Kelley, C. R., "Manual and Automatic Control", John Wiley & sons, New York, 1968.

Key, D. L., "A New Handling Qualities Specification for U.S. Military Rotorcraft", Helicopter Handling Qualities and Flight Control, RaeSoc, London 1988.

Kilgard, M.J. "The OpenGL Utility Toolkit (GLUT) Programming Interface", API Version 3, Silicon Graphics, Inc. 1996.

Kleinman, D. L., "A Control Theoretic Approach to Manned-Vehicle Systems Analysis", IEEE trans Automatic Control, AC-16, pp 824-832, 1971.

Kreifeldt, J. G,. "A sampled Data Pursuit Tracking Model". IEEE Transactions on Human Factors in Electronics, pp 65-73, September, 1965.

Leacock, G. R., "Helicopter Inverse Simulation for Workload and Handling Qualities Estimation", PhD. Thesis, University of Glasgow, 2000.

Magdelano, R.E., McRuer, D.T., Moore, G.P., "Small Perturbation Dynamics of the Neuromuscular System in Tracking Tasks." NASA report CR-1212.

MATLAB Reference Guide. The Math Works Inc. 1992.

McDonnell, J.D., "Pilot Rating Techniques For the Estimation and Evaluation of Handling Qualities", AFFDL TR-68-76, Systems technology, inc., Dec 1968.

M^{c}Ruer, D.T., Jex, H.R., "A review of Quasi-Linear Pilot Models". IEEE Transactions on Human Factors in Electronics, pp 231-246, September 1967.

M^{c}Ruer, D.T., Krendel, E.S., "Dynamic Response of the Human Operator". Wright Patterson AFB, Ohio, Tech. Report 56 – 524, October 1957.

M^{c}Ruer, D.T., Krendel, E.S., "Mathematical Models of Human Pilot Behaviour". AGARD-AG-188, January 1974.

Nomoto, K,. "Some Aspects of Simulator Studies on Ship Handling", PRADS-International Symposium on Practical Design in Ship Building, Tokyo, pp202-310, October 1977.

Padfield, G.D., "Helicopter Flight Dynamics", Blackwell Science. 1996.

Padfield, G.D., Jones, J.P., Charlton, M.T., Howell, S.E., Bradley, R "Where Does the Workload go when the Pilot Attacks the Manoeuvre" paper 83, 20th ERF October, 1994.

Pausder, H,J. Jordan, D., "Handling Qualities Evaluation of Helicopters with Different Stability and Control Characteristics". Vertica, Vol. 1, 1976, pp 125 – 134.

Pausder, H. J.,Von Grünhagen, W., "Handling Qualities Evaluation for Highly Augmented Helicopters", Unknown Source.

Phatak, A.V., Bekey, G.A., "A Model of the Adaptive Behaviour of the Human Operator in Response to a Sudden Change in Control System", IEEE Trans on Man-Machine Systems, Vol-MMS-10, No. 3, Nov. 1969.

Press, W.H., Teukolsky., S.A., Vetterling, W.T., Flannery, B.P., "Numerical Recipes in C, The art of Scientific Computing, Second Edition.", Cambridge University Press, 1995.

Rutherford, S., "Simulation Techniques for the study of the Manoeuvring of Advanced Rotorcraft Configurations." Ph,D. Thesis, University of Glasgow, 1997.

Sheridan, T. B., "Forty Five Years of Man-Machine Systems: History and Trends, Design and Evaluation of Control Systems, Varese, Italy, September 1985.

Sheridan, T.B., Ferrell, W.R., "Remote Manipulative Control With Transmission Delay", IEEE Trans on Human Factors in Electronics, Sept 1963, p25-29.

Smith, R. H., "A theory for Handling Qualities with Applications to MIL-F-8785B." Air Force Flight Dynamics Lab. 1976, pp 75-119.

Sutton, R.," Modelling Human Operators in Control Systems Design". Research Studies Press Ltd. John Wiley & Sons. 1990.

Taylor, C., "The Development of a Simulation Technique For the Analysis of Helicopter Offshore Operations", Ph.D. Thesis, University of Glasgow, 1995.

Teukolsky, Vetterling, Flannery, "Numerical Recipes in C". 1995.

Thomson, D.G., "The Development and Verification of an Algorithm for Helicopter Inverse Simulation". Vertica, Vol. 14, No. 2, May 1990.

Thomson, D.G., Bradley, R., "Improved Methodology For Inverse Simulation". Journal of the American Helicopter Society, p79-86, June 1996.

Thomson, D.G., Bradley, R., "Mathematical Definition of Helicopter Maneuvers". Journal of the American Helicopter Society, p307-309, June 1997.

Thomson, D.G., Bradley, R., "Prediction of the Dynamic Characteristics of Helicopters in Constrained Flight". Aerospace Engineering, University of Glasgow, 1989.

Thomson, D.G., Bradley, R., "The Principles and Practical Application of Helicopter Inverse Simulation." Simulation Practice and Theory, Journal of the Federation of European Simulation Societies. 1998 p47-70.

Thomson, D. G., Bradley, R., "The use of Inverse Simulation for Preliminary Assessment of Helicopter Handling Qualities." Aeronautical Journal of the Royal Aeronautical Society. Aug-Sept 1997, pp. 287-293.

Thomson, D. G., Leacock G. R., "Helicopter Handling Qualities Studies Using Pilot Modelling and Inverse Simulation." 54th Annual Forum, American Helicopter Society Washington DC. 1998. pp. 1325-1336.

Tustin, A., "An Investigation of the Operator's Response in Manual Control of a Power Driver Gun". Metropolitan-Vickers Electrical Co. Limited, Sheffield, CS Memo no169, 1944.